Investigating ion dyshomeostasis in Niemann-Pick disease type C, both *in vitro* and *in vivo*

Emily Maguire
Ph.D. 2017

Summary

This thesis investigated ion dyshomeostasis within Niemann-Pick disease type C (NPC), a neurodegenerative lysosomal storage disease. Chapter 3 characterizes newly discovered lysosomal Zn^{2+} storage in NPC, and identifies a novel function for the NPC1 protein as a lysosomal Zn^{2+} transporter. Zn^{2+} accumulation appears responsible for some lipid storage within NPC, and treating cells with the Zn^{2+} chelator phytic acid corrects downstream NPC phenotypes. Chapter 4 investigates Ca^{2+}-modulating therapies for treating NPC. These include tanganil, demonstrated in a recent case study to ameliorate ataxia within NPC patients, and which works by increasing cytosolic Ca^{2+} to overcome the NPC lysosomal Ca^{2+} signaling defect. The importance of this Ca^{2+} signaling defect in NPC can be seen both in the aforementioned beneficial effects of Ca^{2+} modulating therapies and when looking at NPC-like lipid storage and reduced neuronal Ca^{2+} spikes observed following treatment of zebrafish with an inhibitor of lysosomal Ca^{2+} signaling, Ned-19 (Chapter 5). In addition, Chapter 5 describes the generation and characterization of NPC zebrafish treated with inhibitors of npc1 (U18666A, 1NMP) and microinjected with *npc1*-morpholino. These models accurately recapitulate human NPC phenotypes (characteristic lipid storage, behavioural defects) and can be used to test emerging NPC therapies *in vivo* (e.g. phytic acid, tanganil). Finally, Chapter 6 explores how different formulations of curcumin, which correct NPC phenotypes both *in vitro* and *in vivo* via Ca^{2+} modulation, have reduced effect and can exacerbate storage in cells when combined with lipid vectors. Having described studies into both Ca^{2+} and Zn^{2+} dyshomeostasis in NPC, a new 2-armed pathogenic cascade was hypothesized whereby early dyshomeostasis of lysosomal Ca^{2+} and Zn^{2+} generates all downstream NPC phenotypes. Combination therapies with Ca^{2+} modulators (e.g. tanganil) and Zn^{2+} chelators (e.g. phytic acid) may provide the best option to treat this complex disease, and require testing both *in vitro* and *in vivo*.

Acknowledgements

Firstly, thanks to both the NPRF and NPDG-UK, for funding my project alongside other invaluable NPC research, and for everything else they do for the Niemann-Pick community. You' re smashing it! Next, I'd like to thank my supervisor Emyr, for his constant stream of good ideas which allowed me to generate such interesting data, and for helping me learn how to be a proper-scientist. Helen as well, for all the support she has provided me over the years, and Arwyn, for providing such useful advice on my previous reports. Thanks to Kim for helping set up the zebrafish facility and teaching me all the techniques required; without your help the entire fish chapter would not have been possible! Thanks also to Jo, my co-supervisor, for always making time for me, helping me with anything and everything. Your support was so important to me, and I know we will stay in touch.

Thanks to all the collaborators I worked with throughout my PhD. Including those from the labs of Daniella Riccardi (Cardiff Uni) and Richard Webb (Cardiff Met). And for Luke and the many summer & placement year students over the years for their experimental contributions to this thesis.

Throughout my PhD I have met so many awesome people, both within the lab and outside of it, and this has been what's really made it such a fantastic experience! I'm going to miss everyone and I'm sure you will all go on to do great things. The constants have been Luke, Camille and Emily. We have struggled along together but the end is in sight! Don't panic! And of course my family, always there for me and who have always been very supportive of my 'cancer research'. Somewhat less constant has been the boyfriends. But my favorite one so far is Josh, who doesn't like acknowledgements sections because he thinks they're soppy, but who I'm going to acknowledge anyway.

Abbreviations

1NMP	1-(1-naphthylmethyl)-piperazine	IP$_3$R	Inositol 1,4,5-triphosphate receptor
AAV9	Adeno-associated virus serotype 9	JP	JetPei DNA transfection reagent
AM	Acetyoxymethyl ester	LacCer	Lactosylceramide
AMPAR	Alpha-amino-3-hydroxy-5-methyl-4-propionic acid receptor	LDL	Low density lipoprotein
ASM	alpha-amino-3-hydroxy-5-methyl-4-propionic acid receptor	LSD	Lysosomal storage disease
BBB	Blood brain barrier	M6P	Mannose-6-phosphate
BCA	Bicinchoninic acid	MCU	Mitochondrial calcium uniporter
BHK	Baby hamster kidney	MLIV	Mucolipidosis type IV
BMP	Bis(monoacylglycero)phosphate	MLSA1	Mucolipin synthetic agonist 1
BSA	Bovine serum albumin	MO	Morpholino
CaSR	Extracellular Ca^{2+}-sensing receptor	MPSII	Mucopolysaccharidosis type II
CaV	Voltage-gated Ca^{2+} selective channels	MT	Metallothionein
CAX	Ca^{2+}/H$^+$ exchanger	NAADP	Nicotinic acid adenine dinucleotide phosphate
CD	Crohn's disease	NCKX	Na$^+$/Ca^{2+}-K$^+$ exchanger
CDE	Clathrin dependent endocytosis	NCX	Na$^+$/Ca^{2+} exchanger
CHO	Chinese hamster ovary	NHEJ	Non-homologous end joining
CICR	Ca^{2+}-induced Ca^{2+}-release	NPA	Niemann-pick type A
CIE	Clathrin independent endocytosis	NPB	Niemann-pick type B
CNS	Central nervous system	NPC	Niemann-pick type C
CRISPR	Clustered regularly interspaced short palindromic repeats	PAβN	Phe-Arg β-naphthylamide dihydrochloride
CtxB	Cholera toxin B subunit	PBS	Phosphate buffered saline
CYP	Cytochrome P450	PFA	Paraformaldehyde
DMEM	Dulbecco's modified eagle's medium	PKA	Protein kinase A
DMSO	Dimethyl sulfoxide	PKC	Protein kinase C
dpf	Days post fertilization	PMCA	Plasma membrane Ca^{2+} ATPase
ENU	N-ethyl-N-nitrosourea	PS	Phosphatidylserine
ER	Endoplasmic reticulum	QPCR	Quantitative polymerase chain reaction

FPS	Frames per second	RND	Resistance nodulation cell division
FU	Fluorescence units	ROS	Reactive oxygen species
GalCer	Galactosylceramide	RyR	Ryanodine receptor
GalNac	N-acetylgalactosaminyl	SERCA	Sarco-/endoplasmic reticulum Ca^{2+} ATPase
GFP	Green fluorescent protein	TALEN	Transcription activator-like effector nucleases
GlcCer	Glucosylceramide	TILLING	TILLING Targeting induced local lesions in genomes
GPCR	G-protein coupled receptor	TLC	Thin layer chromatography
GPN	Gly-phe β-naphylamide	TPC	Two-pore channel
GSL	Glycosphingolipid	TRP	Transient receptor potential ion channel
HBSS	Hank's balanced salt solution	UDCA	Ursodeoxycholic acid
HEK	Human embryonic kidney	VFTD	Venus flytrap domain
HF	Human fibroblast	WT	Wild-type
hpf	Hours post fertilization	YFP	Yellow fluorescent protein
HPβCD	Hydroxypropyl-β-cyclodextrin	YSL	Yolk syncytial layer
hr	Hour	ZFN	Zinc finger nuclease
HSP70	Heat shock protein 70	ZIP	Zn^{2+} import protein
IBD	Inflammatory bowel disease	ZnT	Zn^{2+} transporter protein
IP$_3$	Inositol 1,4,5-triphosphate	β-hex	β-hexosaminidase

List of figures

List of tables

List of appendices

Table of contents

Chapter 1: General Introduction

1.1 The endocytic system

Cells take-in extracellular lipids, ligands and plasma membrane proteins via endocytosis. Internalization is balanced by other endosomal pathways which return many of these materials to the plasma membrane. The dynamics of these processes help determine plasma membrane composition, which in turn influences nutrient uptake, cell adhesion and junction formation, cell migration, cytokinesis, cell polarity and signal transduction (Grant and Donaldson, 2009). The dynamics of this process, alongside information on the various characteristics of the different organelles involved, can be seen in figure 1.1.

Clathrin dependent endocytosis (CDE) and clathrin independent endocytosis (CIE) are the two major mechanisms by which endocytosis takes place (Grant and Donaldson, 2009). The most well studied of these two mechanisms is CDE, which occurs following recognition of specific cytoplasmic domains of plasma membrane proteins by adaptor proteins, allowing packaging into clathrin-coated vesicles and transport into the cell (Grant and Donaldson, 2009). Known CDE cargo proteins include receptors for iron-bound transferrin and low-density lipoprotein (LDL) (Grant and Donaldson, 2009). In addition, numerous forms of CIE exist, and these include caveolar endocytosis which facilitates the transport of glycosphingolipids (GSLs) and some viruses, as well as phagocytosis and macropinocytosis (Mayor and Pagano, 2007). Whilst CDE relies on specific adaptor proteins to select cargo, these are not found with CIE, and therefore how cargo is selected for transport is largely unknown (Mayor and Pagano, 2007). One theory follows observations that divergent forms of CIE appear reliant on free cholesterol, proteins and lipids residing in sphingolipid rich plasma membrane 'lipid rafts' (Mayor and Pagano, 2007). For one, fluorescent analogs of GSLs appear to cluster in membrane microdomains prior to internalization by calveolae (Singh et al., 2003, Puri et al., 2001, Sharma et al., 2004), whilst a non-natural analogue that does not cluster in membrane microdomains is not internalized via this mechanism (Singh et al., 2006). This suggests that some CIE cargo is identified by association with lipid microdomains at the plasma membrane.

Following either CDE or CIE, endocytosed material is first delivered to early endosomes where cargo is sorted depending on whether it is to be recycled back to the plasma membrane or targeted to the lysosome for degradation (Jovic et al., 2010). Early endosomes, characterized by the expression of a small-GTP binding protein known as Rab5 (Jovic et al., 2010), are tubular, multi-vesicular compartments located in the cell periphery (Gruenberg, 2001). This structure facilitates sorting; with cargo destined for recycling often clustering within tubular domains which proceed to bud off into

recycling vesicles, and material to be degraded found within multivesicular elements (Mellman, 1996). The slightly acidic pH (~6) of early endosomes, maintained by an ATP-driven proton pump, can allow dissociation of receptors from their ligands (Jovic et al., 2010). This mechanism promotes recycling of the LDL-receptor to the plasma membrane whilst LDL is targeted to the lysosome for degradation (Goldstein et al., 1979). Ca^{2+} is taken up into early endosomes via endocytosis, although within ~5 minutes of entry endosomal acidification causes Ca^{2+} to rapidly leak out of these organelles, in a manner dependent on initial Ca^{2+} concentration. This suggests that H^+ intake into endosomes is balanced by Ca^{2+} exit via endosomal Ca^{2+} channels, or, alternatively, that Ca^{2+} is required for the opening of other endosomal ion channels (e.g. K^+ or Cl^-) which facilitate charge compensation (Gerasimenko et al., 1998).

Overtime, early endosomes accumulate ligands destined for lysosomal degradation, and eventually lose their ability to fuse with endocytic vesicles, signaling their maturation into late endosomes (Dunn and Maxfield, 1992). New sorting early endosomes are continuously formed to replace those that have undergone maturation into late endosomes (Dunn and Maxfield, 1992). Late endosomes, characterized by the expression of Rab7 (Poteryaev et al., 2010), move along microtubules to achieve a perinuclear localization and begin to acidify (pH ~5) prior to fusion with lysosomes (Hu et al., 2015), which will be discussed in the next section. Both homotypic fusion of late endosomes and heterotypic fusion of endosomes and lysosomes appears dependent on Ca^{2+} release from these organelles (Luzio et al., 2007).
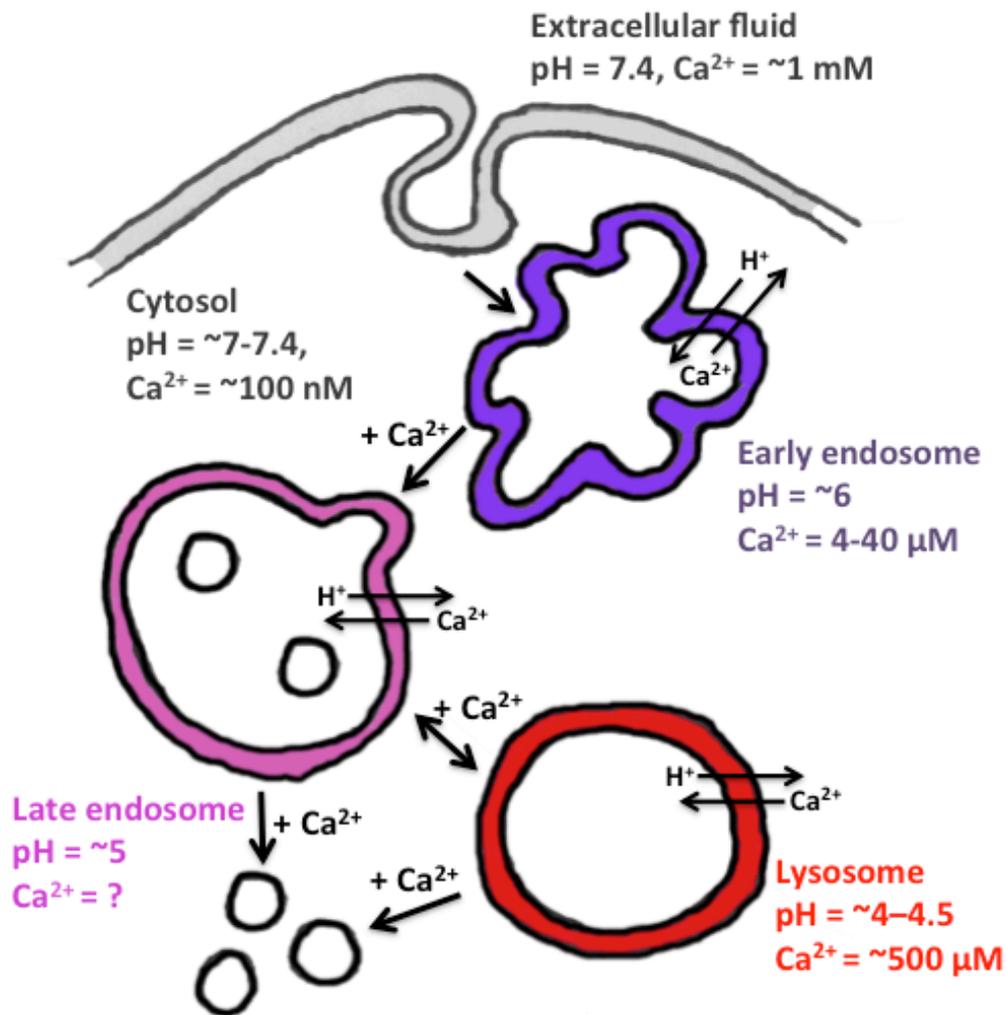
Figure 1.1. Schematic of the endocytic system within eukaryotic cells. Each organelle displays characteristic pH and Ca^{2+} conditions. Ca^{2+} is transported into early endosomes following endocytosis and uptake of extracellular fluid. Acidifcation of these organelles then proceeds to reduce Ca^{2+} content. A proton dependent mechanism next acts to fill both late endosomes and lysosomes with Ca^{2+}. The endo-lysosomal Ca^{2+} store plays a key role regarding endocytic transport and fusion (image adapted from (Lloyd-Evans *et al.,* 2010))

1.2 The lysosome

Lysosomes, first characterized by Christian De Duve in 1954 (de Duve, 1983) are membrane bound organelles containing a wide range of acid hydrolases; facilitating their essential role in cellular recycling. Many endocytosed proteins and lipids are targeted for degradation within the lysosome, where complex molecules can be broken down, and their components reused. Lysosomal enzymes are synthesized in the endoplasmic reticulum (ER) prior to transport to the Golgi apparatus were they acquire a mannose-6-phosphate (M6P) tag. This tag is recognized by M6P-receptors which facilitate their transport to lysosomes (Gary-Bobo et al., 2007). Macromolecules degraded and recycled by

lysosomes include LDL derived cholesterol, GSLs, sphingomyelin, sphingosine, and bis(monoacylglycero)phosphate (BMP) (Cooper, 2000).

To protect against self-digestion, this organelle can be seen to contain a carbohydrate rich glycocalyx (Neiss, 1984), which acts to sequester the numerous acid hydrolases from the rest of the cytoplasmic components (Fukuda, 1991). BMP acts as another key component of the endo-lysosomal membrane, promoting fission and fusion events whilst acting as a cofactor for several important lysosomal enzymes (Gallala and Sandhoff, 2011). These acidic organelles maintain their pH using a proton-pumping V-type ATPase, which utilizes ATP in order to pump protons into the lysosome lumen (Mindell, 2012). Alongside the upmost importance of the lysosome regarding recycling, this organelle has numerous other roles. For one, lysosomal exocytosis plays a key role in membrane repair following exposure to Ca^{2+} ionophores and pore-forming toxins (Divangahi et al., 2009, Jaiswal et al., 2002, Rodriguez et al., 1997). Furthermore, the lysosome has been shown to act as an important cellular Ca^{2+} store with key roles in signaling (Galione and Churchill, 2002).

1.3 Lysosomal storage diseases

The fundamental importance of the lysosome is seen when observing the 70 genetic LSDs (Cox and Cachon-Gonzalez, 2012). These disorders, typically inherited as autosomal recessive traits (~1/5000 live births), arise following loss of function of soluble lysosomal enzymes, non-enzymatic lysosomal proteins, or non-lysosomal proteins that impinge on lysosomal function. Resulting dyshomeostasis leads to copious cellular pathologies alongside progressive storage of undegraded materials within the lysosome. LSDs are often classified according to the biochemical nature of the primary accumulating substrate, for example, mucopolysaccharidoses are named following primary accumulation of mucopolysaccharides, and display a broad clinical spectrum regarding severity of symptoms, progression and age of onset. Symptoms often affect both central nervous system (CNS) and visceral function (Vitner et al., 2010).

LSDs act as a highly important area of study. Firstly, these diseases have devastating effects both on sufferers and their families, as well as putting significant pressure on healthcare services. This alone makes research into both mechanism and novel therapeutics vital. Furthermore, whilst individually rare, LSDs have a combined birth frequency of over 1/7500 (Meikle et al., 1999) and manifest as the most prevalent cause of pediatric neurodegenerative disease (Jalanko and Braulke, 2009). Also, as well as greatly improving the lives of many LSD sufferers, research into LSDs has greatly enhanced our understanding of basic cellular homeostasis involving lysosomes and endocytosis. In

addition, numerous links of LSDs to more common human diseases have been emerging in recent years (Herbert et al., 2015, Maxfield, 2014, Shachar et al., 2011).

Despite differences in both symptom development and storage profiles, LSDs often display similarities when looking at biochemical, cellular and clinical features. Common mechanisms of cellular pathogenesis include Ca^{2+} dyshomeostasis, oxidative stress, chronic inflammation, altered lipid trafficking, defective autophagy, ER stress and activation of the unfolded protein response, and autoimmune disease. Overlapping mechanisms of pathogenesis observed among different LSDs means that therapies developed could be widely applied to treat multiple diseases (Vitner et al., 2010).

1.4 Niemann-Pick type C (NPC) disease

NPC disease is a rare (~1/90,000 living births (Wassif et al., 2016)) autosomal recessive inherited neurodegenerative LSD. NPC belongs to the Niemann-Pick group of lipidoses along with Niemann-Pick A (NPA) and Niemann-Pick B (NPB), both of which are characterized by a primary defect in acid sphingomyelinase (ASM), the degradative enzyme of the lipid sphingomyelin (Schuchman and Wasserstein, 2016). Despite manifesting as a highly heterogeneous disease with variable age of onset and progression (Yerushalmi et al., 2002, Imrie et al., 2007, Wassif et al., 2016), NPC patients often present with ataxia and dementia following both neurological and visceral degeneration, and symptoms culminate in a reduced life expectancy (Sevin et al., 2007). Characteristic degeneration of cerebellar Purkinje neurons (Higashi et al., 1993), which causes the above mentioned ataxia, alongside oxidative stress (Fu et al., 2010) and inflammation (Baudry et al., 2003) form common features of this disorder. Other symptoms include vertical supranuclear gaze palsy, dysarthria, cognitive defects, hepatosplenomegaly, psychiatric disorders, dysphagia and cataplexy (Sevin et al., 2007). Occasionally, patients may also present with coagulation and platelet changes such as thrombocytopenia, anemia and petechial rash (Del Principe et al., 1971, Spiegel et al., 2009), inflammatory bowel disease/Crohn's-like symptoms (Schwerd et al., 2016, Jolliffe and Sarkany, 1983, Steven and Driver, 2005) and reduced liver function (Patterson et al., 2012).

1.5 NPC gene/protein defects

Whilst most LSDs are monogenic, NPC occurs following mutations in either NPC1 (~95% of cases (Scriver, 1995)) or NPC2 genes. The NPC1 gene is located on chromosome 18q11 (Carstea et al., 1993) and encodes a 13-transmembrane domain 1278 amino acid protein (Carstea et al., 1997) residing within the limiting membrane of late endosomes and lysosomes (Ioannou, 2005, Babalola et al., 2007). This protein is currently of unknown function but it is known to be able to bind cholesterol at the

luminal N terminus (Infante et al., 2008). At least 58 mutations have been described in NPC patients (Park et al., 2003). Recently, NPC1 has been found essential for EBOLA virus infection, allowing the virus to fuse with the lysosomal membrane and escape from late endosomes following infection (Carette et al., 2011, Cote et al., 2011).

The NPC2 gene is located on chromosome 14q24.3 (Naureckiene et al., 2000) and encodes a soluble lysosome lumen cholesterol binding protein of 132 amino acids. Dysfunction of either gene results in identical phenotypes, therefore it is likely that they act either in a common cellular pathway or upon the same downstream target (Sleat et al., 2004). Topological prediction for NPC1 can be seen in Figure 1.2.

1.6 NPC lipid storage & cellular pathogenesis

NPC disease is characterized by a highly complex storage material within lysosomes following progressive accumulation of multiple classes of lipids (Lloyd-Evans et al., 2008, te Vruchte et al., 2004). These lipids include cholesterol, sphingomyelin, numerous GSLs, the sphingolipid catabolic product sphingosine, (Lloyd-Evans et al., 2008) and the endo-lysosome specific phospholipid BMP (Chevallier et al., 2008). Alongside storage, a profound block in the endocytic pathway at the level of the late endosome can be observed with limited fusion between lysosomes and late endosomes, autophagic vacuoles or phagosomes (Lloyd-Evans et al., 2008, Ko et al., 2001, Mayran et al., 2003). How trafficking defects and lipid storage lead to neurodegeneration is largely unknown.
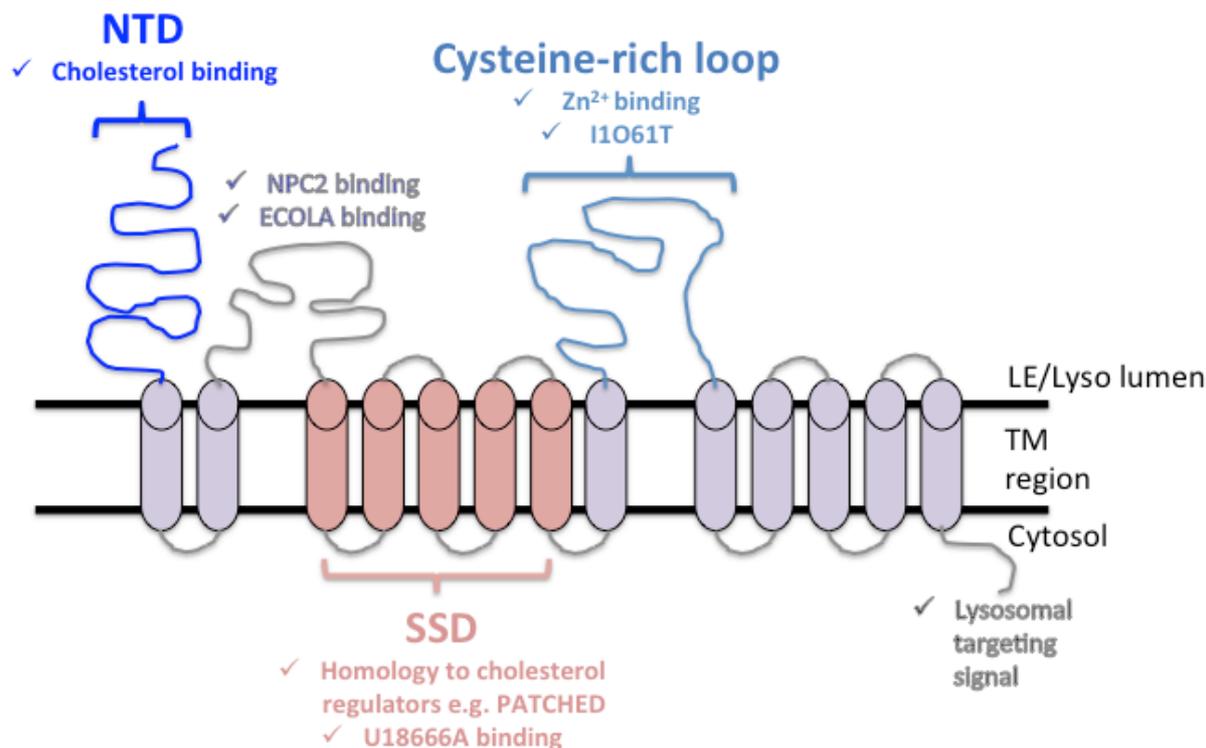
Figure 1.2: Predicted topological structure of NPC1. NTD = N-terminal domain, SSD = sterol sensing domain, TM = transmembrane, LE = late endosome, Lys = lysosome. Cholesterol, NPC2, U18666A, EBOLA and Zn^{2+} binding sites are shown, alongside the location of the most common NPC causing mutation, I1061T, and the lysosomal targeting signal. Adapted from Lloyd-Evans and Platt 2010.

1.7 Deciphering NPC1 protein function: history of NPC disease

In order to investigate how genetic defects in *NPC1* and *NPC2* result in storage and neurodegeneration within patients, the precise function of the NPC1 protein must first be deciphered.

Following initial characterization of NPC as a primary sphingomyelin storage disease by Crocker *et al.,* in 1958 (Crocker and Farber, 1958), ideas regarding the classification of NPC disease have fluctuated greatly. In 1966 a key role for sphingomyelin was dismissed (Brady et al., 1966), and by 1984 NPC was reclassified as a lactosylceramide (LacCer) storage disease (Elleder et al., 1984). This idea was revised in 1972 (Dawson, 1972) and concurrently work completed by Peter Pentchev *et al* 1985 (Pentchev et al., 1985) suggested NPC as a disorder associated with defective LDL cholesterol recycling. The identification of the gene in 1997 further strengthened the possibility that NPC disease was a cholesterol lipidosis by highlighting sequence similarity between NPC1 and mediators of cholesterol regulation and synthesis including SCAP, SREBP, PATCHED and HMG CoA reductase (Carstea et al., 1997). Most recently, Li *et al.,* 2016 (Li et al., 2016) published the crystal structure of a large fragment of NPC1, with the potential to aid future characterization.

To this day, the function of the NPC1 protein, and how loss of function results in cellular pathology, remains a highly disputed subject within the field following contradicting lines of evidence and conflicts of interest.

1.8 Classical cascade: NPC as a primary cholesterol storage disease

Development of the classical NPC cascade, with cholesterol acting as the primary storage material, arose in 1985 (Pentchev et al., 1985), and can be seen in Figure 1.3. Within this model, cholesterol redistribution was suggested to result in downstream storage of other materials following major roles of this lipid regarding trafficking of sphingolipids along the endocytic pathway (Puri et al., 1999). However, numerous lines of evidence exist against NPC as a primary cholesterol storage disease. Arguments for and against NPC as a primary cholesterol storage disease are contrasted in Table 1.

For	Against
• Within peripheral diseased tissues cholesterol shows the greatest fold elevation of all NPC lipids (Butler et al., 1993) • *Depletion of LDL within NPC cell culture medium can correct both cholesterol and GSL storage (Salvioli et al., 2004) • Both NPC1 and NPC2 are able to bind cholesterol (Infante et al., 2008)	• No net increase in CNS cholesterol is seen (Karten et al., 2003), despite a key neurological phenotype • LDL does not only contain cholesterol: also contains ceramide (Lightle et al., 2003) and traces of GSLs (Garner et al., 2001) (see*) • There exists no evidence that purified full-length NPC1 directly transports cholesterol (Lloyd-Evans and Platt, 2010) • Cyclodextrin does not enter the CNS but does correct it (Pontikis et al., 2013), therefore cannot be beneficial by direct interaction with lipids • At least one NPC1 independent endosomal cholesterol efflux pathway already exists (Aye et al., 2009) • No clinical benefit is seen when testing the use of cholesterol-lowering therapies, and also when looking at the effects of NPC-null/LDL receptor-null double knock out mice (Patterson et al., 1993, Somers et al., 2001, Erickson et al., 2000) • Variant NPC disease shows no storage of LDL-derived cholesterol, whilst still displaying characteristic sphingolipid

	trafficking defects alongside clinical symptoms (Sun et al., 2001)
	• SLOS patients display a deficiency in the cholesterol synthesis enzyme DHCR7, leading to a reduction in cholesterol levels and increase in cholesterol precursors. Despite this defect in cholesterol synthesis, patient cells display an NPC-like phenotype when grown in cholesterol-free culture conditions (Wassif et al., 2002)
	• Treatment with the approved NPC drug miglustat results in reduced GSL synthesis whilst having no affect on cholesterol levels (te Vruchte et al., 2004)
	• Various therapies (e.g. curcumin (Lloyd-Evans et al., 2008), increasing Rab expression (Narita et al., 2005), Vitamin E (Xu et al., 2012b)) can rescue the cholesterol transport defect in NPC1 null cells without targeting cholesterol storage directly
	• Addition of sphingosine to healthy cells can induce NPC phenotypes whereas overloading with free cholesterol cannot (Roff et al., 1991)

Table 1.1 Arguments for and against cholesterol being the primary storage material in NPC. NPC = Niemann-pick type C, CNS = central nervous system, LDL = low density lipoprotein, GSL = glycosphingolipid, SLOS = Smith-Lemli-Opitz syndrome, DHCR7 = 7-dehydrocholesterol reductase.

1.9 Other NPC lipids

1.9.1 Glycosphingolipids (GSLs)

GSLs, including glucosylceramide (GlcCer), LacCer, and the gangliosides GM2 and GM3, show the greatest net elevation within the NPC patient brain (te Vruchte et al., 2004, Zervas et al., 2001). These lipids may be stored as a consequence of altered cellular trafficking (Lloyd-Evans et al., 2008), or alternatively following impaired breakdown (Salvioli et al., 2004). Disrupted saposin activity following accumulation of cholesterol and sphingomyelin within the lysosome may also result in GSL storage (Kolter and Sandhoff, 2005). Saposins are heat stable glycoproteins which activate lysosomal hydrolases involved in the breakdown of sphingolipids (Kishimoto et al., 1992). These molecules display optimal activity within BMP populated inner lysosomal membranes under low cholesterol

conditions. Altered environments within NPC cells may consequently hinder function (Kolter and Sandhoff, 2005).

One line of evidence suggesting GSLs as a major driver of NPC pathogenesis arose following observations that storage within other disorders (e.g. Tay-Sachs, Sandhoff disease (GM2), and GM1 gangliosidosis), resulted in severe neuropathology (Sandhoff and Harzer, 2013). This hypothesis was reconsidered however when NPC1 mice were crossed with mice lacking the polypeptide N-acetylgalactosaminyl (GalNac) transferase, producing offspring unable to produce numerous complex gangliosides (including GM1 and GM2) (Liu et al., 2000). Despite reduced GSLs however, no improvement of NPC phenotypes was seen in these mutants, suggesting minimal involvement of these lipids regarding pathogenesis (Gondre-Lewis et al., 2003). These mice were still able to produce GSLs such as GlcCer and LacCer however; therefore these neutral lipids may still play a role regarding pathology. Within the NPC1/ GalNac double mutant, reduction in gangliosides was accompanied by a reduction in cholesterol (Gondre-Lewis et al., 2003). This result demonstrates how cholesterol accumulation lies downstream of GSL increase.

Despite above arguments, when discussing the importance of gangliosides within NPC disease, positive effects of the iminosugar *N*-butyl-deoxynojirimycin (miglustat) must also be considered (Zervas et al., 2001, Ko et al., 2001). This glucose analog acts as an inhibitor of ceramide-specific glucosyltransferase, which catalyzes the first step in GSL biosynthesis (Platt et al., 1994). Acting as the only currently approved therapy for NPC patients (Lachmann et al., 2004), miglustat provides some improvement regarding both delayed disease onset (Zervas et al., 2001) and cellular trafficking abnormalities (Lachmann et al., 2004).

1.9.2 Sphingomyelin

Accumulation and mislocalization of the lipid sphingomyelin (Lloyd-Evans et al., 2008) alongside reduced activity (Elleder and Smid, 1985) and mislocalization of the sphingomyelin catabolic enzyme acid sphingomyelinase (ASM) (Tamura et al., 2006) can be observed within NPC1 disease cells, and both of these factors likely contribute towards pathogenesis (Lloyd-Evans and Platt, 2010). Characteristic ASM inhibition explains why this disease was initially entitled Niemann-Pick type C: Niemann-pick types A and B both arise following initial ASM defects (Ginzburg and Futerman, 2005).

Sphingomyelin storage within NPC cells may arise following abnormal post-translational alterations in ASM, leading to reduced activity and therefore reduced sphingomyelin breakdown (Reagan et al., 2000). An alternative hypothesis suggests that decreased protein kinase C (PKC) activity in NPC1 following sphingosine storage directly results in increased sphingomyelin; phosphorylation of

ASM via PKC has been shown to regulate enzyme activity (Zeidan and Hannun, 2007, Rodriguez-Lafrasse et al., 1997). Alterations in levels or functionality of BMP within NPC null cells may also regulate ASM activity: BMP has been shown to act as essential cofactor in the interaction between ASM and sphingomyelin (Kolter and Sandhoff, 2005, Linke et al., 2001).

Adding sphingomyelinase to cellular plasma membranes results in a release of free cholesterol; this suggests a close biophysical relationship between these two lipids (Abi-Mosleh et al., 2009). The above experiment also demonstrates how cholesterol storage and mislocalization may arise following sphingomyelin dyshomeostasis, with sphingomyelin acting as a molecular trap for cholesterol (and vice versa) (Lloyd-Evans and Platt, 2010). Furthermore, similarly to cholesterol, sphingomyelin storage is not observed within NPC1 disease brain (Karten et al., 2002).

1.9.3 Bis(monoacylglycero)phosphate (BMP)

BMP is another lipid shown to markedly increase within both NPC1 and NPC2 deficient cells (Chevallier et al., 2008), often within internal membranes of disease related multivesicular storage bodies (Karten et al., 2009). Within healthy cells, this lipid can be found primarily within late endosomes and lysosomes were, under the control of Alix/AlP1, it is able to regulate fission and fusion of the multivesicular endosome membrane (Chevallier et al., 2008).

Despite observed increase of this phospholipid within diseased cells, addition of exogenous BMP to NPC null results in partial reversion to wild-type phenotypes (Chevallier et al., 2008). As previously discussed, BMP performs essential roles regarding activation of hydrolases involved in the lysosomal degradation of GSLs (Kolter and Sandhoff, 2005), as well as acting as a cofactor for the ASM enzyme during sphingomyelin breakdown (Kolter and Sandhoff, 2005, Linke et al., 2001). Bearing this in mind, it appears as if modifications to BMP, rather than decreased availability, result in downstream storage of GSLs and sphingolipids within NPC.

Storage of BMP is likely to arise following characteristic endocytic trafficking defects observed in NPC (Lloyd-Evans et al., 2008, Ko et al., 2001, Mayran et al., 2003).

1.10 Current cascade: NPC1 as a sphingosine transporting RND permease?

Following cholesterol controversy, a new NPC cascade was proposed (Figure 1.3). This cascade used growing evidence suggesting NPC1 as a resistance-nodulation cell-division (RND) permease transporter (Tseng et al., 1999, Davies et al., 2000). RND permeases are frequently observed within

gram-negative bacteria, where they function to transport lipophilic drugs, detergents, bile salts, fatty acids, metal ions and dyes out of the cytosol (Davies et al., 2000).

As an RND permease, it was proposed that NPC1 could be acting to transport the detergent-like molecule sphingosine, with sphingosine thereby acting as the primary NPC lipid following inhibition (Lloyd-Evans and Platt, 2010). This sphingoid base acts as a backbone for the formation of sphingolipids such as sphingomyelin, and is released following breakdown in the lysosome. This lipid then requires a transporter to facilitate its egress from the lysosome following its net positive charge (Lloyd-Evans and Platt, 2010). Sphingosine exists as an important cellular metabolite and signaling lipid in animal cells; acting as a potent inhibitor of PKC, Ca^{2+} channels, cell cycle progression and a mediator of apoptosis (Betto et al., 1992, Bottega et al., 1989, Kagedal et al., 2001, Lloyd-Evans et al., 2003, Werneburg et al., 2002).

Initial evidence for a key role of sphingosine arose following observations that levels of this lipid increase up to 12-fold in peripheral areas of NPC patients; namely in the liver and spleen (te Vruchte et al., 2004). Furthermore, a 4-fold increase of this lipid is observed within the NPC patient brain (te Vruchte et al., 2004). Moreover, in contrast to other NPC lipids, addition of sphingosine to healthy cells at a concentration equivalent to that found in diseased cells results in an NPC phenotype (Roff et al., 1991). Finally, following treatment of healthy cells with the well-known NPC1 inhibitor U18666A (Lu et al., 2015), sphingosine acts as the first lipid elevated, followed by defective endocytosis and consequent secondary storage of lipids (Lloyd-Evans et al., 2008). Early storage highlights sphingosine as an upstream event following inactivation of NPC1.

Following its elevation within diseased cells, sphingosine appears to inhibit Ca^{2+} store filling via an unknown mechanism, thereby reducing late-endosomal/lysosomal Ca^{2+} levels (Lloyd-Evans et al., 2008, Lloyd-Evans and Platt, 2010). Within healthy cells, late-endosomal/lysosomal Ca^{2+} signaling mediates both vesicular release and late-endosomal/lysosome fusion (Pryor et al., 2000), and these stores are then expected to refill via Ca^{2+} influx channels on the lysosomal membrane (Christensen et al., 2002, Gerasimenko et al., 1998), although the exact nature of these import systems is currently unknown. By impeding above Ca^{2+} signaling pathways, sphingosine mediated Ca^{2+} dyshomeostasis results in the dramatic trafficking defects observed within NPC cells (Lloyd-Evans and Platt, 2010). Enhancing PKC activity using Phorbol 12-myristate 13-acetate results in increased vimentin-associated endocytic transport via Rab9 and a reduction in cholesterol storage (Walter et al., 2009). Consequently, endocytic defects may also emerge following previously discussed sphingosine-mediated PKC inhibition (Rodriguez-Lafrasse et al., 1997). PKC can also act to regulate Ca^{2+} channels; therefore we cannot discount the possibility that PKC inhibition caused by sphingosine primarily accounts for the lysosomal Ca^{2+} defect in NPC (Yazaki et al., 2015).

A) Classical cascade

NPC mutation

↓

↑Cholesterol

↓

Disease

B) Current cascade

NPC mutation

↓

↑Sphingosine

↓

↓Lysosomal Ca^{2+}

↓

Endocytosis defects

↓

↑Lipid

↓
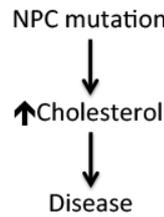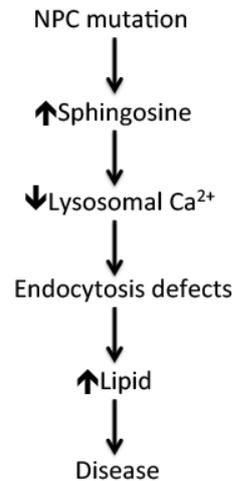
Disease

Figure 1.3 Potential NPC1 pathogenic cascades. A) The classic NPC cascade whereby NPC1 acts as a cholesterol transporter: mutation leads directly to cholesterol storage within lysosomes and disease symptoms. B) The current NPC cascade: NPC1 acts as a sphingosine transporter. Defects lead to initial sphingosine storage within lysosomes, Ca^{2+} signalling and endocytosis defects, and finally lipid storage and disease. Adapted from Lloyd-Evans *et al.,* (2008).

1.11 NPC1: Homology to other proteins

Whilst NPC1 currently remains of unknown function, comparison to other proteins shows various homologies.

Firstly, NPC1 sequence shares 23% sequence identity (35% within the carboxyl terminal) when compared with the membrane receptor Patched (Park et al., 2003). Upon Patched binding to cholesterol-modified sonic hedgehog, the G-protein coupled receptor (GPCR) Smoothened is released, resulting in activation of numerous downstream signaling cascades (Burglin, 2008). Hypothetically, NPC1 could also act to transduce signals via this pathway, with loss of function altering signaling homeostasis (Lloyd-Evans and Platt, 2010).

Following sequence alignments against the RND permease AcrB, found in *Escherichia coli*, NPC1 has recently been proposed as the only known mammalian RND permease (Scott and Ioannou, 2004). Further evidence for an RND permease function of NPC1 arose when the protein demonstrated the ability to transport acriflavine, a known RND permease substrate (Davies et al., 2000). Acting as an RND permease, it was suggested that NPC1 could act to regulate lysosomal content of endogenous amines (Kaufmann and Krise, 2008), for example the sphingoid base sphingosine as previously discussed (Lloyd-Evans and Platt, 2010). Similarly to other bacterial RND permeases, NPC1 could potentially transport numerous substances, not just sphingosine, thereby rendering NPC disease even

more complex than first thought. For one, NPC1 has previously been implicated in clearance of both the anti-cancer drug daunorubicin and dextran molecules from cells (Gong et al., 2006).

Alongside various similarities across proteins, orthologs of the NPC1 protein show high evolutionary conservation across species (Malathi et al., 2004). This was demonstrated when it was shown that the yeast orthologue of *NPC1*, *ncr1*, is able to compensate for NPC1 deficiency when expressed in mammalian cells (Malathi et al., 2004). Furthermore, within yeast, ncr1 is found on the vacuolar membrane (Malathi et al., 2004), with the vacuole having been shown functionally equivalent to the eukaryotic lysosome (Patel and Cai, 2015). Given high conservation regarding both sequence and location, studies into the role of ncr1 within yeast may provide further clues to deciphering NPC1 function. Current research suggests against a cholesterol transport function of ncr1 following observation that during ergosterol autotrophic conditions sterols are neither internalized by nor trafficked through the yeast vacuole (Schulz and Prinz, 2007). However, a, sphingolipid transport function of ncr1 was hypothesized when it was shown that point mutations in the sterol sensing domain resulted in a primary sphingolipid trafficking phenotype (Malathi et al., 2004).

1.12 Therapeutics available for the treatment of NPC

The rarity and relative lack of understanding of this disorder means therapeutic options for NPC are limited. Currently, *N*-butyldeoxynojirimycin, or miglustat, acts as the only approved therapy for NPC (Lyseng-Williamson, 2014), although hydroxypropyl-β-cyclodextrin (HPβCD), arimoclomol, curcumin and gene therapy are currently being investigated. More information about curcumin can be found in Chapter 6.

1.12.1 Miglustat

Miglustat acts as an inhibitor of GSL synthesis via inhibition of GlcCer synthase, and was previously developed as a therapy for glycosphingolipidoses such as Gaucher disease (Cox et al., 2000). Patients with Gaucher disease show a primary defect in GSL metabolism, leading to progressive storage of these moieties within lysosomes (Scriver, 1995). As previously discussed, GSL storage can also be observed within NPC (te Vruchte et al., 2004, Zervas et al., 2001).

Zervas *et al.,* 2001 demonstrated how NPC mice treated with this iminosugar display reduced GSL accumulation alongside delayed onset of symptoms and increased lifespan. Additionally, work by Lachmann *et al.,* (2004) showed how this substrate reduction therapy is able to correct lipid trafficking defects observed within NPC patients.

In 2007 the results of a small clinical trial in the UK and USA indicated beneficial effects of miglustat in arresting multiple components of NPC disease pathology (Patterson et al., 2007). Subsequently, miglustat has been approved worldwide (apart from in the USA) for use in NPC patients. It is at present the only approved therapy. Early treatment appears to significantly retard disease onset and progression. However, despite beneficial effects observed, miglustat is far from a curative treatment for this disease (Lyseng-Williamson, 2014).

Hung *et al.,* (2014) determined that miglustat is unable to correct disrupted metal homeostasis in NPC patients (Hung et al., 2014). Furthermore, miglustat treatment does not correct cholesterol phenotypes, suggesting this accumulation may also present as an upstream effect (te Vruchte et al., 2004). Discussed limitations of this therapy prompted the development of curcumin and cyclodextrin as potential treatments for NPC.

1.12.2 Hydroxypropyl-β-cyclodextrin (HPβCD, cyclodextrin)

Allopregnanolone was found deficient in NPC patients, prompting work by Griffin *et al.,* 2004 where they treated $Npc1^{-/-}$ mice with this neurosteroid, solubilized in 20% hydroxypropyl-β-cyclodextrin (HPβCD). NPC mice presented with significant improvements regarding both lifespan and neuropathology (Griffin et al., 2004). Subsequent experiments however demonstrated how injection of the cyclodextrin vehicle alone could account for the vast majority of the improvement seen (Davidson et al., 2009). Since this discovery, intracisternal injection of HPβCD in feline models of NPC has been shown to delay cerebellar degeneration and purkinje cell loss whilst reducing lipid accumulation and increasing life expectancy (Vite et al., 2015). Several clinical trials are currently taking place investigating the effects of HPβCD in human patients (Garcia-Robles et al., 2016, Matsuo et al., 2013, Maarup et al., 2015).

Cyclodextrins are membrane-impermeant cyclic oligosaccharides. Despite widespread use of these molecules both *in vitro* and *in vivo* to manipulate cholesterol levels (Zidovetzki and Levitan, 2007, Davis and Brewster, 2004), mechanism of action against NPC pathology is currently unknown. One view suggests this molecule is able to sequester cholesterol within its hydrophobic core (Davis and Brewster, 2004). Another hypothesizes that HPβCDs induce lysosomal exocytosis by damaging the plasma membrane, thereby releasing storage materials and decreasing cell stress (Chen et al., 2010). Nonetheless, the question that remains is how this molecule can correct neurological phenotypes, despite an inability to cross the blood brain barrier (BBB) (Pontikis et al., 2013). Brain endothelial cells are in close contact with astrocytes at the BBB, and Ca^{2+} signals can be propagated across these cells bidirectionally via gap-junctions (Braet et al., 2001). For this reason, a potential capacity of HPβCD to

restore NPC Ca^{2+} signaling, thereby partially correcting both trafficking and lipid storage, has been suggested (Goike and Lloyd-Evans *et al.* unpublished observation).

Despite potential benefits of this therapy, toxic effects regarding both hearing and hair-cell death have recently been proposed to occur following HPβCD treatment of feline and mouse NPC models (Crumling et al., 2012, Ward et al., 2010, Vite et al., 2015).

1.12.3 Arimoclomol

Arimoclomal acts as a heat shock protein-based therapy currently being tested in a 2/3 clinical trial with 46 NPC patients (Kirkegaard et al., 2016).

Molecular chaperones of the heat shock protein 70 (HSP70) family protect pathologically challenged cells via direct interaction with lysosomes (Kirkegaard et al., 2010, Nylandsted et al., 2004). HSP70 binding to BMP stabilizes the interaction of this lipid with numerous lysosomal enzymes, preventing degradation of the enzymes and increasing their activity (Kirkegaard et al., 2010). For one, increased BMP binding to ASM improves breakdown of sphingomyelin to ceramide, therefore preventing lysosomal aggregation, membrane permealization and stress-induced cell death found in numerous LSDs (Kirkegaard et al., 2010, Nylandsted et al., 2004, Petersen and Kirkegaard, 2010, Guicciardi et al., 2004, Micsenyi et al., 2013). Furthermore, HSP70 has recently been found to enhance the proper folding and activity of mutant NPC1 proteins. Combined, these results demonstrate potential dual benefits of HSP70 based therapies in NPC. Indeed, treating NPC1 mice with recombinant HSP70 both reduced lipid storage and improved neurological phenotypes (Kirkegaard et al., 2016).

Despite benefits observed in the mouse model, HSP inducers such as rHSP70 have been known to stress cells, discouraging there use in a chronic condition like NPC. Bearing this in mind, Kirkegaard *et al.,* (2016) instead performed studies on NPC mice treated with arimoclomol, a small-molecule orally available coinducer of the HSP70 system. Arimoclomal was seen to cross the blood-brain barrier in NPC mice in order to reduce storage and improve motor function. Beneficial effects of arimoclomol have also been observed *in vitro*, with treatment reducing lysosomal expansion and lipid storage in NPC patient fibroblasts (Kirkegaard et al., 2016).

1.12.4 Gene therapy

Whilst still in development, gene therapy to specifically increase levels of functional NPC1 within patients holds great promise for the treatment of NPC.

This method was first investigated for its use to treat NPC disease following observations that expressing wild-type NPC1 under either a prion (Loftus et al., 2002), neuron (Lopez et al., 2011) or glial (Borbon et al., 2012a) specific promoter prevents neurodegeneration and extends the lifespan of $Npc1^{-/-}$ mice. Recently, Chandler *et al.,* (2017) utilized an adeno-associated virus serotype 9 vector (AAV9) to increase levels of Npc1 in $Npc1^{-/-}$ mice. This resulted in increased Purkinje cell survival, improved motor deficits, reduced cholesterol storage, and an extended lifespan (Chandler et al., 2017).

1.13 Inhibitors of NPC1

Using inhibitors of NPC1 to generate disease phenotypes in wild-type cells and organisms provides tremendous benefit regarding the study of NPC disease. For one, inhibiting NPC1 to induce NPC in macrophages and checking phenotypes at various time points allowed deduction of the order of the pathogenic cascade (Lloyd-Evans et al., 2008). Four substances are currently known to induce an NPC-like phenotype: U18666A (Lu et al., 2015), Phe-Arg β-naphthylamide dihydrochloride (PAβN) (Lloyd-Evans *et al.,* unpublished observation), 1-(1-naphthylmethyl)-piperazine (1NMP) (Lloyd-Evans *et al.,* unpublished observation), and sphingosine (Roff et al., 1991). U18666A is a cationic amphiphile known to generate an NPC phenotype by binding and directly inhibiting NPC1 (Lu et al., 2015), whilst 1NMP and PAβN act as RND permease inhibitors (Schumacher et al., 2006, Lomovskaya et al., 2001, Renau et al., 1999), therefore inhibiting the only known mammalian RND permease, NPC1. The fact that we observe NPC phenotypes following treatment with RND permease inhibitors further implicates NPC1 as a member of this family of transporters. Finally, as previously discussed, sphingosine acts as the only NPC lipid that results in an NPC-like phenotype when added to cells at a physiologically relevant concentration (Roff et al., 1991), highlighting this storage as an early disease phenotype.

1.14 Aims of this thesis

The function of NPC1, mutated in ~95% of NPC patients, remains unknown. This project utilized *in vitro* and *in vivo* models to further characterize the function of NPC1, decipher the pathogenic cascade that occurs following mutation and to uncover novel therapeutics designed to target upstream stages of this cascade, namely the observed acidic-store Ca^{2+} defect and lysosomal Zn^{2+} storage.

Chapter 2 describes materials and methods used throughout the thesis; methods specific for each results chapter can be found at their start.

Chapter 3 investigates lysosomal Zn^{2+} storage in NPC, a novel function for NPC1 as a lysosomal Zn^{2+} transporter, and Zn^{2+} chelators (e.g. phytic acid) as potential treatments for NPC.

Chapter 4 looks to characterize the effects of previously investigated and novel Ca^{2+} modulators on the NPC cellular phenotype. Ca^{2+} modulators have previously been shown to overcome the lysosomal Ca^{2+} defect in NPC, thereby preventing endocytosis defects and lipid storage.

Chapter 5 demonstrates the development and characterization of a zebrafish model of NPC: providing insight into the NPC cascade and allowing rapid evaluation of novel therapeutics *in vivo*.

Chapter 6 examined the effects of various curcumin nutraceuticals on NPC glia. Several NPC patients began taking curcumin supplements following work by Lloyd-Evans *et al.,* 2008 demonstrating beneficial effects of curcumin in the mouse, but observations of toxicity *in vitro* suggested the need for further study.

Chapter 7 concludes the thesis with a general discussion, including implications of the findings outlined in this thesis for future NPC therapy and a greater understanding of the pathogenic cascade.

Chapter 2: General Materials & Methods

Unless otherwise stated, all reagents were from Sigma-Aldrich. For all methods not shown here, see chapter specific methods.

2.1 Cell culture

Glia (mouse astrocytes) were primary cells cultured by Dr E Lloyd-Evans from wild-type $Npc1^{+/+}$ (wild-type) and $Npc1^{-/-}$ (NPC1-null) mice (Lloyd-Evans et al., 2008). Glia were grown as monolayers in a humidified incubator at 37°C and 5% CO_2 in complete Dulbecco's Modified Eagle's medium (DMEM). Flasks (T75s with 75ml total volume and T25s with 25ml total volume) were used for maintenance and chamber slides (ibidi), 24-well plates (Greiner), and coated 96-well plates (Greiner) were used for treatments and assays. Other cells used include chinese hamster ovary (CHO), baby hamster kidney (BHK) and human fibroblasts (see Chapter 3 for more detailed methods on these cell types).

2.2 Microscopy

All cell microscopy was performed using an inverted Zeiss Colibri LED widefield fluorescence microscope with a high-speed monochrome charged coupled device (CCD) Axiocam MRm camera and Axiovision 4.7 software. All images were taken using a 40x oil magnification lens. For imaging of fixed cells, cells were grown and treated on acid washed glass coverslips in 24-well plates and fixed and stained as described below. The coverslips were mounted on glass slides using Mowiol mounting medium (Mowiol 4-88, Calbiochem). For live imaging (including Ca^{2+} imaging), cells were grown and treated in chamber slides (ibidi), stained as described below and imaged directly. For live Zn^{2+} staining and fixed BMP/sphingomyelin staining (Chapter 3), lysosomal Ca^{2+} imaging (Chapter 4), and live and fixed imaging of zebrafish (Chapter 5) see chapter specific methods.

2.3 Treatment with inhibitors of NPC1 (U18666A & 1NMP)

U18666A is a cationic amphiphile known to generate an NPC phenotype by binding and directly inhibiting NPC1 (Lu et al., 2015) and 1-(1-naphthylmethyl)-piperazine (1NMP) is an RND permease inhibitor, acting to inhibit the only identified mammalian RND permease, NPC1 (Schumacher et al., 2006, Lomovskaya et al., 2001). For more information about using U18666A and 1NMP these to induce an NPC1 phenotype in cells (Chapter 3) and zebrafish (Chapter 5) please see chapter specific methods.

2.4 Fixed cell staining

2.4.1 Fixing cells in paraformaldehyde (PFA)

Glia grown on glass coverslips were washed once with phosphate buffered saline (PBS), and incubated with 4% paraformaldehyde (PFA, Taab) at room temperature for 5 minutes. Cells were then washed once with complete medium, then washed twice more in PBS and stored at 4°C.

2.4.2 Cholesterol staining using filipin

Cholesterol was visualized using filipin (filipin complex from *Streptomyces filipinenses*), a naturally fluorescent antibiotic that specifically binds cholesterol (Bornig and Geyer, 1974). PFA-fixed glia were incubated in complete DMEM with 187.5μg/ml filipin at room temperature for 30 minutes, then washed 3 times in PBS. Excitation/Emission = 360/480nm.

2.4.3 GM1 fixed staining using Alexa Fluor 488-CtxB

Ganglioside GM1 was visualized using Alexa Fluor 488-Cholera toxin B subunit (CtxB) (Svennerholm, 1976). PFA-fixed glia were incubated in blocking buffer (PBS with 1% bovine serum albumin (BSA) and 0.1% saponin) with 2.5μg/ml Alexa Fluor 488-CtxB at 4°C overnight, then washed 3 times in PBS. Excitation/Emission = 495/519nm.

2.4.4 Hoescht nuclear staining

A blue fluorescent hoescht 33258 pentahydrate (bis-benzimide) nuclear stain was sometimes used to help identify stained glia. PFA-fixed cells were incubated in PBS with 2μg/ml hoescht (Invitrogen) at room temperature for 10 minutes, then washed 3 times in PBS. Excitation/Emission = 361/497nm.

2.5 Live cell staining

2.5.1 Lysotracker green staining for lysosomes

Glia grown in ibidi chamber slides were washed once in complete Hank's Balanced Salt Solution (HBSS + 1mM HEPES pH7.2m 1mM CaCl$_2$, 1mM MgCl$_2$) prior to incubation with Lysotracker green (Invitrogen, 200nM in HBSS), which loads specifically into lysosomes, for 15 minutes at 37°C. Cells were then washed twice in complete HBSS and imaged live. For more information about using Lysotracker in zebrafish, see Chapter 5 specific methods. Excitation/Emission = 504/511nm.

2.5.2 Ca^{2+} imaging using Fura-2 AM

Elevation in cytoplasmic Ca^{2+} following the addition of various drugs (MLSA1, δ-tocopherol, CGS21680, acetyl-X-leucine, and curcumin nutraceuticals) was measured using the cell permeable Ca^{2+} indicator Fura-2AM (ThermoFisher Scientific) with an excitation at 360 and 380nm and emission at 525nm. Ca^{2+} release was calculated ratiometrically between emissions of 360 and 380nm. Cells in ibidi chamber slides were washed once in cold medium with 1% BSA. Following the wash, cells were incubated for an hour at <16°C with 5µM Fura-2AM in complete DMEM with 1% BSA and 0.025% Pluronic F127. The Fura-2AM solution was then removed and the cells were left for 10 minutes in complete HBSS to allow esterases within cells to cleave the acetoxymethyl ester (AM) group on the probe, which would otherwise inhibit fluorescence. Cells were then washed twice with complete HBSS and imaged live.

2.6 Thin layer chromatography (TLC)

Relative lipid species across samples were compared using a thin later chromatography (TLC) method. Chapter-specific modifications can be found within individual methods sections.

2.6.1 Bicinchoninic acid (BCA) protein assay to determine amount of protein in a sample

Treated and untreated *Npc1$^{+/+}$* and *Npc1$^{-/-}$* glia were harvested from T75 flasks and pelleted by centrifugation at 159xg for 5 minutes. The cell pellets were then homogenized using three rounds of freeze-thaw followed by 20 strokes in a dounce 30 homogenizer. For details on homogenization of zebrafish see Chapter 5 specific methods. Following homogenization, the BCA protein assay was performed as per the manufacturers instructions. Absorbance was read using a TECAN absorbance microplate reader at 570nm wavelength.

2.6.2 Lipid extraction

Lipids were extracted using the method described in Neville *et al.,* (2004) (Neville et al., 2004) with modifications required for zebrafish extractions (see Chapter 5).

Aliquots of the homogenates equal to 1mg were taken from all the samples. The samples were made up to equal volumes in MilliQ water before extracting lipids by adding 5 times the original volume of chloroform:methanol 1:2 (Fisher) which solubilizes lipids. The samples were then left on a roller overnight at 4°C. Following this incubation, samples were centrifuged at 1429xg for 5 minutes and the supernatant was collected prior to the addition of 4 parts the original volume of PBS and chloroform. The samples were then vortexed and left to settle to give a clear phase separation, allowing for the

upper aqueous phase to be removed and discarded. The remaining organic lipid-containing phase was dried down under a stream of nitrogen using a nitrogen evaporator.

2.6.3 Thin layer chromatography (TLC) separation of lipids

Following lipid extraction, TLC was performed as described by Maue *et al.,* 2012 (Maue et al., 2012). The samples were re-suspended in 50µl chloroform:methanol 1:1 solution before being vortexed and sonicated for 10 minutes. 15µg of polar lipid standard (Avanti Polar Lipids) was also dried down under nitrogen prior to re-suspension in chloroform:methanol 1:1. The samples were then applied to 1cm lanes at the bottom of a silica gel HPTLC plate (Merck Millipore) alongside the polar lipid standard. Loaded plates were then ran in a pre-equilibrated TLC tank containing one of 2 mobile phases until the solvent mobile front was approximately 1cm from the top of the silica gel plate. Mobile phases where made up to chloroform:MeOH:H_2O ratios of either 65:25:4 for better visualization of phospholipids (or for separation of curumin supplements alone, see Chapter 6) or 80:10:1 (Chapter 6).

2.6.4 Developing of the silica gel TLC plate

Once taken out of the TLC tanks the plates were dried using a hairdryer for 10 minutes. The plates were then sprayed until saturation with dH_2O plus 1% sulphuric acid (Fisher) and 0.1% orcinol. Following spraying, the saturated plates were developed following gradual warming up to 100°C.

When developed, the plates were scanned in greyscale in order to obtain the integrated greyscale values using the gel analysis plugin in ImageJ. Greyscale values were then used to calculate the area under the curve for each band in order to compare band density (representing amount of lipid) between the different samples.

2.7 Image analysis: thresholding and distribution analysis

Following staining with various fluorescent probes, staining intensity was quantified using thresholding. Using ImageJ, the brightness for one set of images, representing one treatment category (usually untreated *Npc1*$^{-/-}$ astrocytes), was adjusted so that a particular percentage of cells were visible, and this percentage was recorded as number of bright cells. Other images of different treatment categories (e.g. *Npc1*$^{+/+}$, *Npc1*$^{-/-}$ + U18666A etc) then had their brightness adjusted to the same amount as the first category, and percent visible cells (bright cells) were calculated. This allowed comparison of probe intensity across sets of images. Following quantification of several repeats, statistical analysis was performed on the percentages.

Distribution analysis was performed to highlight differences in cellular phenotypes following staining with Zinquin, FluoZin3-AM or filipin.

2.8 Statistical analysis

Results were analyzed for statistical significance using T-tests (for comparison of the means of 2 groups) or ANOVA using a Dunnet's multiple comparisons posthoc test (for comparison of the means of more than 2 groups) carried out using GraphPad Prism 7.0a software.

Chapter 3: NPC1 Zn^{2+} phenotype, NPC1 as a Zn^{2+} transporter & treatment of this Zn^{2+} phenotype with chelators

3.1 Introduction

Recently, evidence has emerged suggesting lysosomal Zn^{2+} storage as a key phenotype in NPC1 disease. We therefore decided to investigate this phenotype, as well as potential therapies to combat Zn^{2+} storage, further.

3.1.1 Zn^{2+} as an essential trace element

Zn^{2+} acts as a highly regulated, essential trace element within healthy cells; functioning within proteins as structural components, as well as acting as cofactors for over 300 enzymes with roles regulating numerous essential cellular processes (Takeda, 2000).

Cellular Zn^{2+} is regulated by a large variety and number of regulatory proteins: in fact, between 3 and 10% of all proteins in the mammalian genome are suspected to bind Zn^{2+} (Vallee and Falchuk, 1993). Among these, highly important regulators include 10 ZnTs (Zn^{2+} transporter proteins) which mediate transport from the cytosol to the lumen of intracellular organelles or out of the cell (Liuzzi and Cousins, 2004), 14 ZIPs (Zn^{2+} importing proteins) which mediate influx at the plasma membrane and efflux from intracellular organelles (Liuzzi and Cousins, 2004) and 4 isoforms of MTs (metallothioneins) which are Zn^{2+} buffering proteins (Vallee, 1995, Maret and Vallee, 1998). ZnT, ZIP and MT expression is highly regulated in response to changing levels of Zn^{2+} (Ghoshal and Jacob, 2001, Cousins et al., 2006).

Cells are predicted to contain intracellular Zn^{2+} stores, although their exact location is unknown. ZnT2 is known to pump Zn^{2+} into lysosomes (Mocchegiani et al., 2010), however, in lysosomal proteomics, no known Zn^{2+} transporter has been discovered that could potentially be pumping Zn^{2+} out (Chapel et al., 2013). One study did claim that they had found ZIP8 on lysosomes in T-cells (Aydemir et al., 2009): however, the antibody used is known to be non-selective (Lloyd-Evans communication), therefore confounding results.

Zn^{2+} displays key roles regarding synaptic transmission, with several glutamatergic terminals showing enrichment of Zn^{2+} exceeding 1mmol/L within glutamate containing synaptic vesicles. Following its release from synapses, this ion generates both dampening and stimulatory effects on assorted inhibitory and excitatory neurons (Frederickson et al., 2000).

3.1.2 Zn^{2+} and neurological disease

Zn^{2+} dyshomeostasis can be seen within numerous neurological disorders. Firstly, accumulation of Aβ plaques acts as a pathological hallmark of Alzheimer's disease (Terry and Katzman, 1983). These plaques have been shown to bind Zn^{2+} with high affinity (Bush et al., 1994b, Bush et al., 1994a), and absence of synaptic Zn^{2+} has been shown to reduce plaques by 20% (Lee et al., 2002). Furthermore, in Parkinson's disease, Zn^{2+} accumulation can be seen within affected dopaminergic neurons and other patient tissues (Dexter et al., 1991, Hozumi et al., 2011). NPC1 and Alzheimer's disease share many disease-related molecular pathways including accumulation of Aβ plaques, tau pathology and cholesterol storage (Malnar et al., 2014). Furthermore, lysosomal Zn^{2+} accumulation is observed within NPC1 cells and mouse brain (Figure 3.1, Lloyd-Evans *et al.,* unpublished observation). These observations suggest Zn^{2+} dyshomeostasis as a potential cause of the neurological decline observed in NPC.

3.1.3 Zn^{2+}, reactive oxygen species (ROS) and apoptosis

Zn^{2+} appears to promote neuronal apoptosis through various mechanisms, and this is likely to impact on pathologies of numerous neurological disorders presenting with Zn^{2+} dyshomeostasis. For one, both cytosolic and inter-mitochondrial Zn^{2+} dyshomeostasis can potentially interfere with mitochondrial function and ultimately culminate in cell death (Sensi et al., 2000, Dineley et al., 2005, Sensi et al., 1999, Malaiyandi et al., 2005). Furthermore, through PKC (Noh et al., 1999), nicotinamide adenine dinucleotide phosphate (NADPH) (Kim and Koh, 2002), and neuronal nitric oxide synthase (Kim and Koh, 2002) activation, increased Zn^{2+} levels result in elevated ROS and superoxide generation. Increased ROS can be highly toxic to cells as these molecules advocate fragmentation of DNA (Wiseman and Halliwell, 1996), lipids (Bruckdorfer, 1998), and matrix components (Tiku et al., 1999). These highly aggressive molecules promote oxidative changes to proteins, potentially resulting in chemical fragmentation alongside increased vulnerability to proteases (Davies, 1987, Stadtman). Finally, Zn^{2+} accumulation in lysosomes has been suggested to encourage autophagic neuronal death via permeabilization of the lysosomal membrane (Hwang et al., 2008).

3.1.4 Zn^{2+} and NPC

Several findings initially suggested disrupted metal ion homeostasis within NPC tissues. This included several gene expression profiling studies whereby increased expression of a wide range of transporters

and solute carriers, including the Zn^{2+} transporter SLC392A, was observed within NPC1 human fibroblasts and mice (Reddy et al., 2006, Vazquez et al., 2011).

Hung et al. 2014 (Hung et al., 2014) then performed further comprehensive examination looking at transition metal levels within cerebrospinal fluid, plasma, and tissue samples obtained from both human NPC1 patients and $Npc1^{-/-}$ mice. He demonstrated a clear, significant increase in Zn^{2+} in both human and mouse NPC1 samples when compared with wild-type, including an increase within the cerebrum. Furthermore, most patients also show reduced Zn^{2+} within their plasma and cerebral spinal fluid.

As previously discussed, within healthy cells, Zn^{2+} homeostasis is tightly regulated by a variety of ion transporters (e.g. ZnTs and ZIPS) and buffering proteins (e.g. MTs) (Liuzzi and Cousins, 2004, Vallee, 1995, Maret and Vallee, 1998). Work within the Lloyd-Evans lab however has visualized Zn^{2+} redistribution and accumulation within the lysosomes of NPC1 cells and tissues, representing a novel disease phenotype. Furthermore, said Zn^{2+} is present in the Purkinje neurons of the cerebellum, which die in NPC, but not in the Purkinje neurons of lobe 10 which are known to survive. These observations are shown in Figure 3.1 (Waller-Evans and Lloyd-Evans, unpublished).
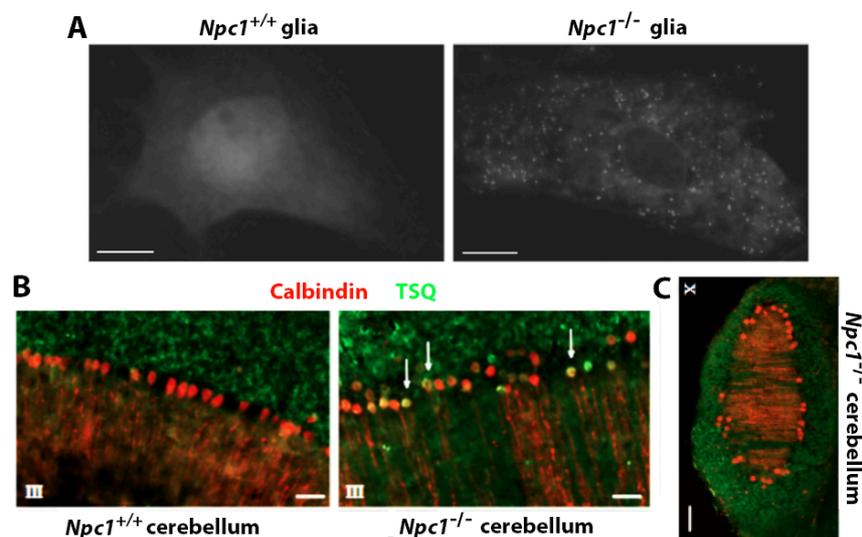
Figure 3.1. Zn^{2+} accumulation in $Npc1^{-/-}$ cells and the brain. A) Staining astrocytes with the zinquin probe for Zn^{2+} shows a disperse cytosolic distribution of this ion in wild-type (WT, $Npc1^{+/+}$) compared with increased punctate Zn^{2+} and decreased cytosolic in NPC1 cells ($Npc1^{-/-}$). B) $Npc1^{+/+}$ mouse Purkinje neurons of lobes I-IX (lobe III shown) shows low levels of Zn^{2+} (staining for Zn^{2+} with TSQ shown at 495nm) within the granule cell layer (staining for Purkinje neuron marker calbindin at 550nm). However, within $Npc1^{-/-}$ mice, Purkinje cells of lobe III show marked Zn^{2+} accumulation as early as 2 weeks. C) Purkinje cells of lobe X taken from $Npc^{-/-}$ mice show no Zn^{2+} accumulation even at 10 weeks (death occurs at 10-11 weeks). This indicates a correlation between lysosomal Zn^{2+} accumulation and Purkinje cell death. N>3. Figure by Waller-Evans and Lloyd-Evans, unpublished.

Other studies also suggest lysosomal Zn^{2+} accumulation as an upstream phenotype within the NPC1 pathogenic cascade. For example, Kobayashi et al. 1999 (Kobayashi et al., 1999) demonstrated that overexpression of ZnT2 (transports Zn^{2+} into lysosomes (Mocchegiani et al., 2010)) generates increased lysosomal Zn^{2+} resulting in increased inactive BMP and cholesterol alongside cellular trafficking defects. This potentially represents an NPC phenotype and raises an interesting possibility that Zn^{2+} accumulation may be responsible in part for the NPC pathogenic cascade. Finally, a study by Watari et al. 2000 showed how the intraluminal cysteine rich loop of NPC1 is in fact able to bind Zn^{2+}, with this region displaying a crucial role regarding function (Watari et al., 2000).

Following collective evidence, one aim of this PhD is to investigate NPC1 as a Zn^{2+} transporting RND permease. RND permeases have previously been shown to transport Zn^{2+} (Hantke, 2001, Pak et al., 2013), and whilst transporters are currently known to transport Zn^{2+} into lysosomes (Mocchegiani et al., 2010), so far none are known which can transport Zn^{2+} out (Chapel et al., 2013), with NPC1 acting as a potential candidate.

3.1.5 NPC1 as an RND permease

As previously discussed, following sequence alignments against the RND permease AcrB, found in *E. coli*, NPC1 has recently been proposed as the only known mammalian RND permease (Scott and Ioannou, 2004, Tseng et al., 1999). Further evidence for an RND permease function of NPC1 arose when the protein demonstrated the ability to transport acriflavine, a known RND permease substrate (Davies et al., 2000). Acting as an RND permease, it was suggested that NPC1 could act to regulate lysosomal content of numerous substances including endogenous amines (Kaufmann and Krise, 2008), for example the sphingoid base sphingosine, and metal ions such as Zn^{2+}.

3.1.6 Zn^{2+} chelators for the treatment of NPC

Zn^{2+} chelators have previously been investigated regarding the treatment of several neurodegenerative disorders such as Alzheimer's (Huang et al., 1997) and Parkinson's (Sheline et al., 2013).

Following observation of an NPC Zn^{2+} phenotype, Clark and Lloyd-Evans (unpublished) performed a comprehensive screen of Zn^{2+} chelators to see which, if any, were capable of correcting NPC lysosomal expansion (measured using lysotracker) and cholesterol storage (measured using

filipin) phenotypes within *Npc1*$^{-/-}$ mouse glial cells. Chelators tested included CaEDTA, Captopril, Clioquinol, Deferoxamine, DMPS, D-penicillamine, Phytic acid, SAHA and TPEN.

This screen identified phytic acid, a natural product found in nuts and cereals, as a best hit, following its ability to correct cholesterol storage within *Npc1*$^{-/-}$ cells (Figure 3.2). This molecule is able to bind most metal ions with high affinity, leading to the generation of strong, insoluble, complexes (Iyengar et al., 2010). Furthermore, this chelator has been shown to function at low pH (Cheryan, 1980), explaining how it could potentially act to chelate lysosomal Zn^{2+}.

Following previous evidence of Zn^{2+} storage in NPC and observed conservation of NPC1 with multi-substrate RND permeases, some of which are known to transport Zn^{2+}(Pak et al., 2013), as well as observations suggesting Zn^{2+} storage may act as an early, important event in the pathogenesis of NPC, we decided to investigate this phenotype further by characterizing a novel function for NPC1 as a lysosomal Zn^{2+} transporter.
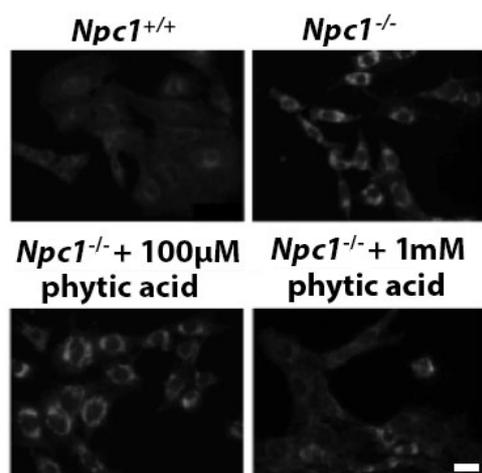
Figure 3.2. Treatment of cells with phytic acid appears to be able to correct *Npc1*$^{-/-}$ cholesterol storage phenotypes. *Npc1*$^{+/+}$ (wild-type) and *Npc1*$^{-/-}$ (NPC1) astrocytes were either left untreated of treated with either 100µM or 1mM phytic acid prior to staining with filipin for cholesterol. *Npc1*$^{+/+}$ cells show a disperse distribution of this lipid when compared with punctate staining in *Npc1*$^{-/-}$ cells representative of lysosomal storage. Treatment with 1mM, but not 100µM, phytic acid, appears able to partially revert the cholesterol storage phenotype of *Npc1*$^{-/-}$ null cells back to wild-type. Unpublished data Clark & Lloyd-Evans. Scale = 10µM.

3.2 Materials & Methods

Unless otherwise stated, all reagents were from Sigma-Aldrich. Any methods used in this chapter and not described here can be found in the general materials and methods section (Chapter 2).

3.2.1 Cell culture

Chinese hamster ovary (CHO) cells were obtained from Dr. D. Ory (Millard et al., 2000) and included wild-type CHO H1s, CHO 1-1s which overexpress NPC1 15 times as much as H1s and CHO M12s which are *Npc1*-null. Baby hamster kidney (BHK) cells were obtained from Dr J. Gruenberg (Kobayashi et al.,

1999) and included wild-type BHK-21 and those overexpressing the lysosomal Zn^{2+} import channel ZnT2 (ZnT2-BHK). Wild-type, NPC1 ($NPC1^{-/-}$ (P237S/I1061T)), NPC2 ($NPC2^{-/-}$), mucolipidosis type IV (MLIV, TRPML1 null), Niemann-Pick type A (NPA, ASM null), Tay-Sachs (hexosaminidase A null), CLN3 (CLN3 null, lysosomal transmembrane protein of unknown function) Gaucher (glucocerebrosidase null), mucopolysaccharidosis type II (MPS II, iduronate II sulfatase null) and farber (ceramidase null) human fibroblasts (HFs) were obtained from the coriell cell bank. MNNPC (I061T/I061T), BSNPC (G46V/P691L), KWNPC (I061T/P1007A) and MONPC (I0161T/D948N) HFs were obtained from Dr. C. Wassif, NIH.

All cells were cultured as monolayers in a humidified incubator at $37^{o}C$ and 5% CO_2. HFs and BHKs were grown in complete Dulbecco's modified Eagle's medium (DMEM) while CHOs were grown in complete DMEM Ham's F-12 medium. Flasks were used for maintenance and chamber slides (ibidi) or 24 well plates for most treatments and assays. With BHK cells, 10µl gelatin was applied to chamber slides and coverslips prior to seeding to promote adhesion.

3.2.2 Visualizing Zn^{2+} - FluoZin-3, AM, RhodZin and Newport green staining protocol

In order to compare Zn^{2+} levels both across cell lines and between cellular stores, cells grown in ibidi chamber slides were washed once in complete HBSS prior to incubation in HBSS with 0.025% pluoronic F127 and 5µM Zn^{2+} probe for 30 minutes at $37^{o}C$. Cells were then washed once more in complete HBSS and imaged live.

3.2.2.1 Zinquin ethyl ester staining for vesicular Zn^{2+}

Zinquin ethyl ester (Enzo) is a Zn^{2+} responsive fluorophore, which is highly specific for Zn^{2+} over other divalent cations. The ethyl ester improves cell loading, and this probe is has been shown very useful for determining vesicular Zn^{2+} (Snitsarev et al., 2001). Cells grown in ibidi chamber slides were washed once in complete HBSS prior to incubation with 25µM Zinquin ethyl ester for 30 minutes at $37^{o}C$. Cells were then washed once more in complete HBSS and imaged live. Excitation/Emission = 368/490.

3.2.2.2 FluoZin-3, AM staining for cytosolic and acidic compartment Zn^{2+}

FluoZin-3, AM (Invitrogen) is a cell-permeant, Zn^{2+} selective indicator that exhibits a >50-fold increase in fluorescence in response to saturating levels of Zn^{2+}. This high affinity probe (K_d = 15nM) is able to

detect changes in both cytosolic and acidic compartment Zn^{2+} (Gee et al., 2002). Excitation/Emission = 494/516nm.

3.2.2.3 RhodZin staining for mitochondrial Zn^{2+}

Replacing the fluorophore of FluoZin-3 with rhodamine led to the development of RhodZin (Invitrogen, K_d=65nM), a fluorescent probe specific for Zn^{2+} that concentrates in mitochondria due to the mitochondrial membrane potential (Sensi et al., 2003). Excitation/Emission = 555/575nm.

3.2.2.4 Newport green staining for ER Zn^{2+}

Newport green (Invitrogen) acts as a low affinity Zn^{2+} probe (K_d>30μM), likely to bind Zn^{2+} only when present at high concentrations (e.g. endoplasmic reticulum (ER) Zn^{2+})(Gee et al., 2002). Excitation/Emission = 505/535nm.

3.2.3 Mitotracker green staining for mitochondria

Mitotracker green (Invitrogen) is a fluorescent probe that appears to localize to mitochondria regardless of mitochondrial membrane potential. In order to compare mitochondrial levels between wild-type and NPC1, cells grown in ibidi chamber slides were washed once in complete HBSS prior to incubation in HBSS with 200nM Mitotracker green for 20 minutes at room temperature. Cells were then washed once more in complete HBSS and imaged live. Excitation/Emission = 490/516.

3.2.4 Exocytosis assay to measure NPC1 Zn^{2+} transport

In order to prove a function for NPC1 as a Zn^{2+} transporter, a novel assay was designed which exploits exocytosis in order to determine protein function. Each stage of this assay is described below with a summary diagram shown in Figure 3.3.
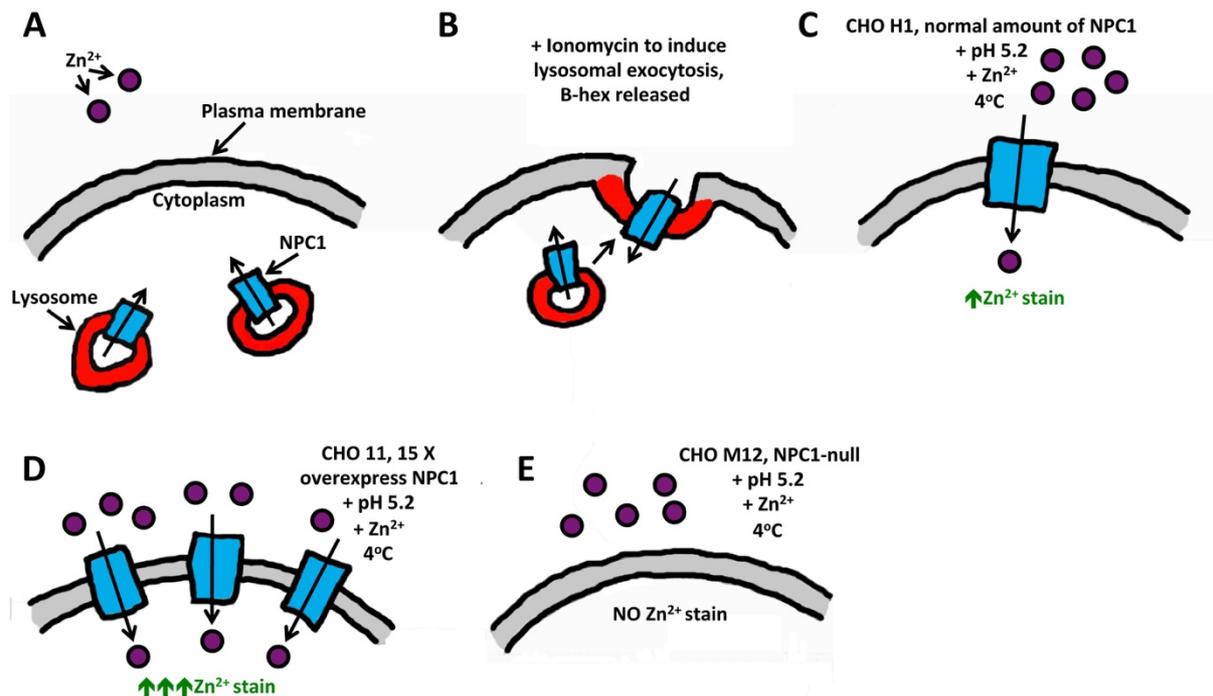
Figure 3.3. Exocytosis assay to measure NPC1 Zn^{2+} transport. A) NPC1 resides on lysosomes of wild-type CHO H1 cells. B) Addition of ionomycin induces lysosomal exocytosis and fusion with the plasma membrane. This results in release of the lysosomal enzyme β-hexosaminidase (β-hex, percent released can be measured as described below) alongside insertion of NPC1 into the plasma membrane, with the N and C termini that normally present into the lysosomal lumen now facing the extracellular milieu. C, D & E) In order to prevent re-endocytosis of NPC1, cells were kept on ice (4°C) throughout the experiment. Next, we added Zn^{2+} and pH 5.2 buffer to the medium in order to mimic the acidic lysosomal lumen environment. NPC1 is reliant on a proton motive force and therefore requires low pH to function. Cells were stained with the fluorescent Zn^{2+} probe FluoZin-3, AM, and in wild-type CHO H1's (C) we could visualize increased cytosolic FluoZin-3, AM staining overtime, indicative of Zn^{2+} transport. This increase was faster in the CHO 1-1s which overexpress NPC1 15X more than wild-types (D), and did not occur in CHO M12's which are *Npc1*-null.

3.2.4.1 Ionomycin treatment

Ionomycin (Calbiochem) treatment has been shown to induce lysosomal exocytosis (Xu et al., 2012a). CHO cells were grown in either 24 well plates with no coverslips (for β-hexosaminidase assay) or in ibidi chamber slides (prior to staining with FluoZin-3, AM and treatment with pH5.2 buffer/Zn^{2+}). 10μM ionomycin (Calbiochem) was added to cells for 10 minutes at 37°C, prior to removal of medium either for β-hexosaminidase assays to confirm exocytosis or FluoZin-3, AM staining to determine NPC1 protein function.

3.2.4.2 β-hexosaminidase (β-hex) assay to determine percentage β-hex released from CHO cells

Following lysosomal exocytosis, the lysosomal enzyme β-hex is released into the medium surrounding cells (Xu et al., 2012a). We can therefore measure β-hex activity in the medium surrounding cells, and compare this with total β-hex (both within cells and within medium) to find percentage released. Comparison between untreated CHO lines and ionomycin treated allows visualization of increased release following ionomycin treatment, representing increased exocytosis.

Following ionomycin treatment, medium was removed from both untreated and treated wells and transferred to eppendorfs (sample A). In order permeabilize the cells left on the plate and release β-hex, 0.1% triton X-100 detergent was then added to each well, and the plate was left on a gentle shaker for 2 minutes at room temperature. Cells were then homogenized further by freeze thawing (5 minutes in a $^-$80 freezer followed by 37°C for 10 minutes), and again put on a gentle shaker for another 2 minutes. Triton X-100 detergent, now containing homogenized cells, was transferred to new eppendorfs (sample B).

A β-hex assay was next performed on both samples A and B in order to find out exocytosed and total β-hex activity. This assay was performed as described in Jeyakumar *et al.* 2009 (Jeyakumar et al., 2009).

Percentage β-hex released is determined by using (sample A/(sample A + sample B))*100

3.2.4.3 Live FluoZin-3, AM staining for Zn^{2+}

The Zn^{2+} responsive fluorophore FluoZin-3, AM was used to measure cytosolic levels of this ion. CHO cells in ibidi chamber slides, either untreated or treated with ionomycin to induce exocytosis, were washed once with HBSS prior to incubation with 2μM FluoZin-3, AM for one hour at 4°C, low temperature was used to prevent endocytosis. Cells were then washed once more in HBSS and imaged live as described below. Excitation/Emission = ~494/516nm, K_d = ~ 15nM.

3.2.4.4 Treatment of cells with pH5.2 buffer and Zn^{2+}

In order to perform a novel assay aiming to establish NPC1 as a Zn^{2+} transporter, we dissolved 50μM ZnCl$_2$ in 100mM NaAcetate pH5.2 buffer (in HBSS). Following ionomycin treatment and FluoZin-3, AM staining (see above), cells in ibidi chamber slides were washed once in HBSS, imaged at time zero, and buffer was added prior to live imaging at 10, 40, 70 and 100 minutes.

3.2.5 Sequence alignments

In order to determine similarities between human NPC1 (NP_000262), the yeast ortholog ncr1 (KZV07510) heavy metal transporting RND permeases ZneA (4K0J_A, Zn^{2+} transporter) and CusA (3NE5_A, Cu^{2+} transporter), and cholesterol regulators PATCHED (AAC50550) and HMG-CoA reductase (P04035), amino acid sequence alignments were conducted in T-Coffee. T-coffee produces an alignment by combining the output of several different alignment methods, which include pairwise structural methods and multiple sequence alignments. Output format was FASTA.

3.2.6 Cell treatments

3.2.6.1 Treatment with U18666A to inhibit NPC1

U18666A is known to induce an NPC-like phenotype in cells (Lu et al., 2015)(for more information see general methods section (Chapter 2)). *Npc1*$^{+/+}$ glia were either left untreated or treated for 1, 2, 4, 6, or 24 hours with 2μg/ml U18666A in complete DMEM prior to live or fixed staining and imaging to examine the order that materials are stored within the lysosome following inhibition of the Npc1 protein.

3.2.6.2 Treatment with 1NMP to inhibit NPC1

1-(1-naphthylmethyl)-piperazine (1NMP) is known to induce an NPC-like phenotype in cells Lloyd-Evans *et al.,* unpublished observation)(for more information see general methods section (Chapter 2)). Wild-type glia were either left untreated or treated for 1, 2, or 24 hours with 50μM 1NMP in complete DMEM prior to live or fixed staining and imaging to examine the order that materials are stored within the lysosome following inhibition of the Npc1 protein.

3.2.6.3 Treatment with 50μM ZnCl$_2$ to increase lysosomal Zn^{2+}

To increase lysosomal Zn^{2+}, wild-type (BHK-21) or ZnT2 (lysosomal Zn^{2+} import channel) overexpressing BHK cells were treated (24, 48 or 72 hours) with 50μM ZnCl$_2$ in complete DMEM prior to live or fixed staining and imaging. Treatment with ZnCl$_2$ can be seen to induce NPC1 phenotypes in ZnT2 overexpressing BHK cells.

3.2.6.4 Treatment with the Zn²⁺ chelator phytic acid

Phytic acid, acting as a Zn^{2+} chelator (Iyengar et al., 2010), can be seen to correct lysosomal Zn^{2+} storage alongside downstream cholesterol storage phenotypes within *Npc1*⁺/⁺ glia (Clark and Lloyd-Evans unpublished observation). *Npc1*⁺/⁺ and *Npc1*⁻/⁻ glia were either left untreated or treated for 96 hours with 1mM phytic acid in complete DMEM prior to live or fixed staining and imaging to examine its effects on *Npc1*⁻/⁻ storage phenotypes.

3.2.6.5 Treatment with the sphingolipid biosynthesis inhibitor ISP1

ISP1, acting as an inhibitor of serine palmitoyltransferase (the first step in sphingolipid biosynthesis) (Miyake et al., 1995), can be seen to correct all NPC phenotypes. This therapy however is unable to correct suspected upstream lysosomal Zn^{2+} storage. *Npc1*⁺/⁺ and *Npc1*⁻/⁻ glia were either left untreated or treated for 96 hours with 150nM ISP1 in complete DMEM prior to live or fixed staining or imaging to examine its effects on *Npc1*⁻/⁻ storage phenotypes.

3.2.6.6 Treatment with the proposed NPC1 therapy HPβCD

Treatment of glia with the membrane-impermeant cyclic oligosaccharide HPβCD, which acts through a currently unknown mechanism of action, can be seen to correct all NPC phenotypes (Davidson et al., 2009), except for suspected upstream Zn^{2+} storage. *Npc1*⁺/⁺ and *Npc1*⁻/⁻ glia were either left untreated or treated for 24 hours with 0.4mg/ml HPβCD in complete DMEM prior to live or fixed staining or imaging to examine its effects on *Npc1*⁻/⁻ storage phenotypes.

3.3 Results

3.3.1 Specificity of the *Npc1*⁻/⁻ lysosomal Zn²⁺ storage phenotype

We began further investigation into the specificity of lysosomal Zn^{2+} storage in NPC1 by staining cells live with various probes specific for acidic compartment, ER or mitochondrial Zn^{2+} (Figure 3.4). Staining with Zinquin (Figure 3.4 A & B, acidic compartment) or FluoZin-3, AM (Figure 3.4 A & C, acidic compartment) confirms that *Npc1*⁺/⁺ cells show low levels of cytoplasmic Zn^{2+} (disperse staining throughout the cell) while *Npc1*⁻/⁻ cells have increased lysosomal Zn^{2+} (~90% increase in large punctate

stained structures indicative of Zn^{2+} storage in lysosomes, more easily seen in zoom image for FluoZin-3, AM). Newport green (Figure 3.4 A & D, ER Zn^{2+}) showed no difference between *Npc1$^{+/+}$* and *Npc1$^{-/-}$*. RhodZin showed reduced mitochondrial Zn^{2+} in *Npc1$^{-/-}$* cells compared with wild-type (~23% reduction in bright cells), however this could be at least partly due to reduced mitochondria observed using Mitotracker. Together, these results demonstrate how Zn^{2+} dyshomeostasis in NPC1 cells primarily involves lysosomal accumulation of this ion.
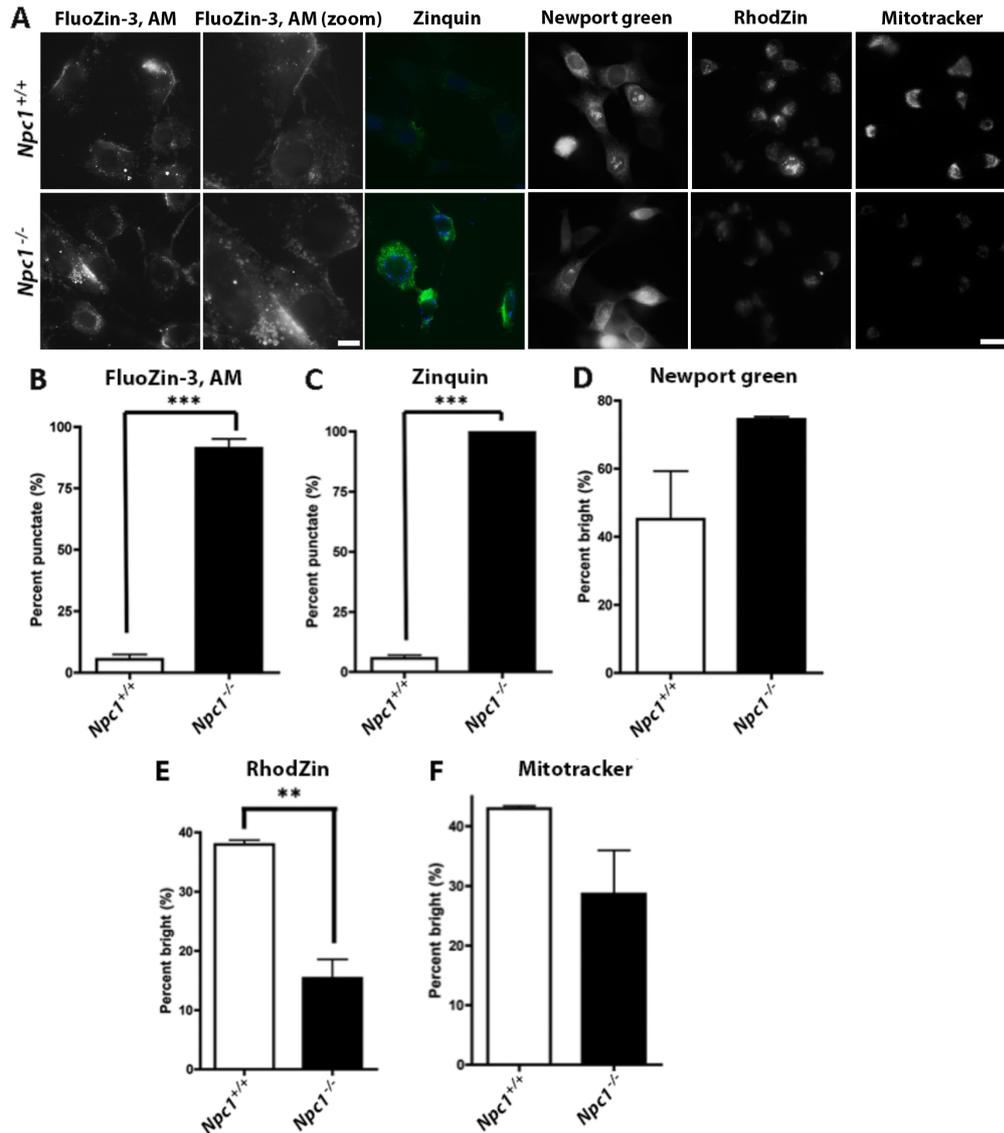
Figure 3.4. Zn^{2+} accumulates in *Npc1$^{-/-}$* lysosomes (organelle specific Zn^{2+}). *Npc1$^{+/+}$* (wild-type) and *Npc1$^{-/-}$* (NPC1) mouse astrocytes were stained and imaged live with either Zinquin or FluoZin-3, AM (acidic compartment Zn^{2+} - shown as both original image and zoom), Newport green (ER Zn^{2+}), Rhodzin (mitochondrial Zn^{2+}) or Mitotracker (mitochondria) (A). Pictures were quantified by either thresholding (Newport green (D), RhodZin (E), mitotracker (F)) or distribution (Zinquin (B), FluoZin-3, AM (C)) to generate graphs shown. N=3. Data contributed by Maguire, Clark, Lloyd-Evans. Analysed & compiled by Maguire.

N=3. Scale bar shown in bottom right of image = 10μM and shows scale for all images except FluoZin-3, AM (zoom), scale bar for FluoZin-3, AM (zoom) images = 5μM. ***=p<0.001, **=p<0.01. >50 cells analyzed per condition per N.

Having determined that Zn^{2+} accumulation in NPC1 was lysosome specific, we next wanted to investigate whether this accumulation was an NPC1 specific, rather than an LSD general phenotype. To do this, human LSD fibroblasts with deficiencies in a wide range of lysosomal proteins were stained with FluoZin-3, AM, imaged live and analyzed for Zn^{2+} storage (Figure 3.5 A & B). The only fibroblasts that showed significant Zn^{2+} accumulation when compared with wild-type was *NPC1* (~50% increase in bright cells), suggesting specificity of this phenotype.
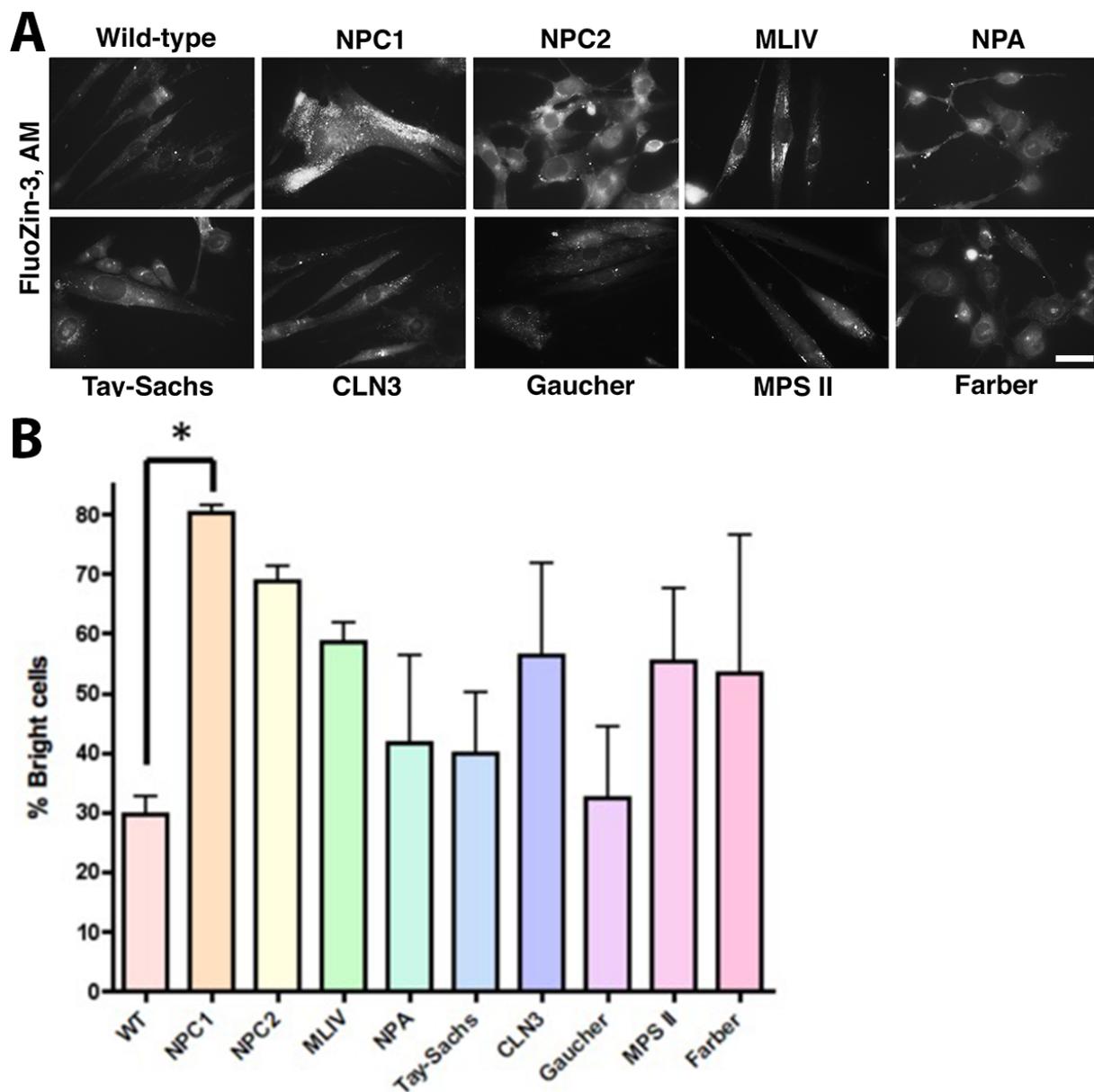
Figure 3.5. Specificity of the *NPC1* lysosomal Zn^{2+} storage phenotype. A) Wild-type (WT), NPC1, NPC2, mucolipidosis IV (MLIV), Niemann-pick type A (NPA), Tay-Sachs, CLN3, Gaucher, Mucopolysaccharidosis type II (MPS II) and Farber human

fibroblasts were stained and imaged live with FluoZin-3, AM to compare levels of acidic compartment Zn^{2+}. Pictures were quantified by thresholding to generate graphs shown (B). N=3. Scale bar = 10μM. *=p<0.05. >50 cells analyzed per condition per N.

3.3.2 Exploring lysosomal Zn^{2+} storage in $Npc1^{-/-}$ astrocytes

Having seen that lysosomal storage of Zn^{2+} occurred specifically in $NPC1$ cells, we next wanted to investigate where this phenotype occurred in the previously proposed pathogenic cascade.

Typical NPC1 phenotypes are demonstrated in Figure 3.6. These phenotypes have all been previously demonstrated and are well characterized within NPC cells and tissues. Indeed, filipin staining is currently used as a diagnostic assay for confirming NPC disease in patients (Vanier et al., 1991) and lysotracker is currently in use as a screening assay for monitoring patient response to therapy (Xu et al., 2014).

Following staining with the acidic pH activated lysosomal marker Lysotracker DND28 we see dim punctate staining, indicative of lysosomes, in $Npc1^{+/+}$ compared with much brighter punctate staining throughout the $Npc1^{-/-}$ cells (Figure 3.6 A & C). FITC-CtxB staining for ganglioside GM1 (Figure 3.6 A & F), filipin staining for cholesterol (Figure 3.6 A & D) and anti-BMP staining for BMP (Figure 3.6 A & E) all demonstrate a diffuse distribution in wild-type. This is indicative of previously described plasma membrane and early endosomal distribution of sphingomyelin, plasma membrane and endocytic compartment distribution for cholesterol and a punctate late endosomal and lysosomal distribution of BMP and GM1 within healthy cells. This can be compared with punctate lysosomal staining in $Npc1^{-/-}$ cells, note the increase in staining intensity with all probes in the $Npc1^{-/-}$ cells indicating accumulation of these lipids in lysosomes. As described in Figure 3.4, $Npc1^{-/-}$ cells also show lysosomal Zn^{2+} storage and redistribution when compared with $Npc1^{+/+}$ (Zinquin, FluoZin-3, AM).

Figure 3.6 also demonstrates how following treatment with the RND permease inhibitor 1NMP (Schumacher et al., 2006), the aforementioned NPC1 phenotypes begin to emerge in a specific order. This suggests an RND permease function of NPC1. Furthermore, knowledge of the specific order of events in the NPC pathogenic cascade will provide further clues as to the nature of the NPC1 protein. Additionally, therapeutically targeting early events in the pathway is likely to provide greater benefits than targeting later ones.

Zn^{2+} storage (FluoZin-3, AM) emerges first following treatment for 1 hour (Figure 3.6 A & B, ~95% increase), suggesting increased lysosomal Zn^{2+} as an early, possibly primary, phenotype in the NPC1 pathogenic cascade. This is followed by progressive accumulation of cholesterol (filipin) and GM1 (FITC-CtxB) from 2-4 hours (Figure 3.6 A, D & F). Lysosomal storage of BMP (anti-BMP) and lysosomal expansion (Lysotracker) phenotypes emerge last following 24-hour treatment (Figure 3.6 A, E & C).

In order to confirm Zn^{2+} storage as an early event, we next performed a slightly reduced version of the above time-course using another known inhibitor of the NPC1 protein, U18666A (Figure 3.7)(Lu et al., 2015). These results confirm observations of 1NMP: whilst NPC1-like lysosomal Zn^{2+} storage (FluoZin-3, AM) can be seen from 1 hour treatment (Figure 3.7 A & B, ~85% increase); cholesterol storage (filipin) is only observed at 24 hours (Figure 3.7 A & C, ~100% increase).
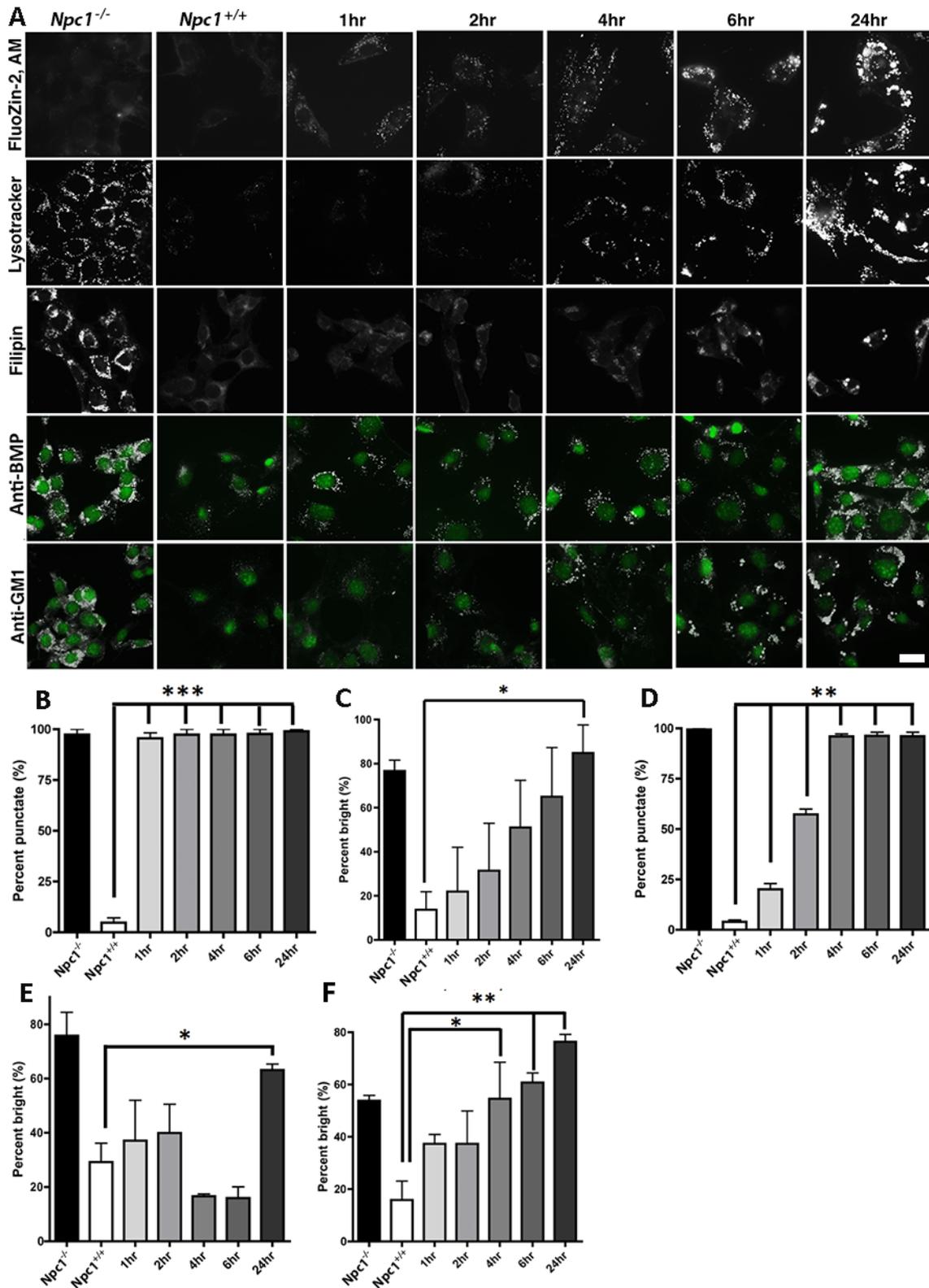
Figure 3.6. Inhibition of Npc1 with 1NMP induces early Zn²⁺ accumulation. Time course experiment showing emergence of Niemann-pick type C (NPC) phenotypes in *Npc1⁺/⁺* (wild-type) glia following inhibition of the NPC1 protein using the resistance-nodulation-cell division (RND) permease inhibitor 1-(1-naphthylmethyl)-piperazine (1NMP) (Lloyd-Evans *et al.* unpublished observation) (Schumacher et al., 2006) at 50µM. A) *Npc1⁺/⁺* cells where either untreated or treated for either 1 hour (hr), 2hr, 4hr, 6hr or 24hr with 1NMP prior to staining with the indicated probe (live or fixed) as described in materials

and methods. Untreated $Npc1^{-/-}$ (NPC1) cells were also grown as a positive control. Pictures were quantified by either thresholding (Lysotracker (C), Anti-BMP (E), FITC-CtxB (F)) or distribution (FluoZin-3, AM (B), Filipin (D)) to generate graphs shown. N=3. Scale = 10μM. *=p<0.05, **=p<0.01, ***=p<0.001. >50 cells analyzed per condition per N.
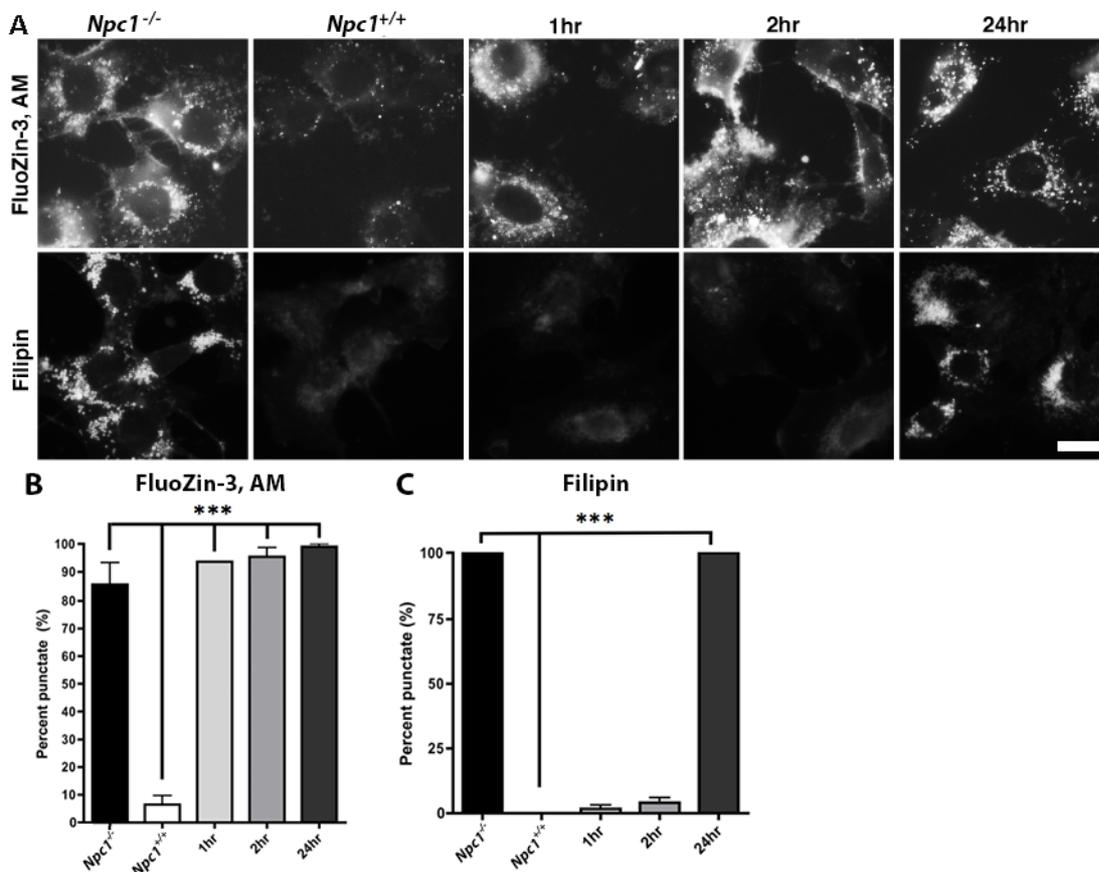
Figure 3.7. Inhibition of Npc1 with U18666A induces early Zn²⁺ accumulation, similarly to 1NMP. A) Time course experiment showing emergence of Niemann-pick type C (NPC) phenotypes in $Npc1^{+/+}$ (wild-type) astrocytes following inhibition of the NPC1 protein using U18666A (Lu et al., 2015) at 2μg/ml. $Npc1^{+/+}$ cells where either untreated or treated for either 1 hour (hr), 2hr or 24hr with U18666A prior to staining with the indicated probe (live or fixed) as described in materials and methods. Untreated $Npc1^{-/-}$(NPC1) cells were also grown as a positive control. Pictures were quantified by either thresholding (Filipin (C)) or distribution (FluoZin-3, AM (B)) to generate graphs shown. N=3. Scale = 10μM. ***=p<0.001. >50 cells analyzed per condition per N.

Having confirmed lysosomal Zn²⁺ storage as an early event in the pathogenesis of NPC1 disease, we next wanted to further investigate whether this phenotype was important regarding downstream lipid storage. We did this using BHK cells overexpressing ZnT2, a channel known to pump Zn²⁺ into lysosomes (Mocchegiani et al., 2010). Following 24, 48 or 72-hour treatment with extracellular ZnCl₂, these cells developed NPC1 phenotypes (Figure 3.8).

Lysosomal Zn²⁺ storage (Zinquin) occurred first, from 24-hour treatment (Figure 3.8 A & B, ~80% increase). Followed by cholesterol (filipin) at 24-48 hours (Figure 3.8 A & C, ~50% increase at 24

hours followed by a further 15% increase at 48 hours), and finally lysosomal expansion (lysotracker) from 48-72 hours (Figure 3.8 A & D, ~30% increase at 48 hours followed by ~30% increase at 72 hours). This data suggests that Zn^{2+} storage initiates downstream lipid storage.
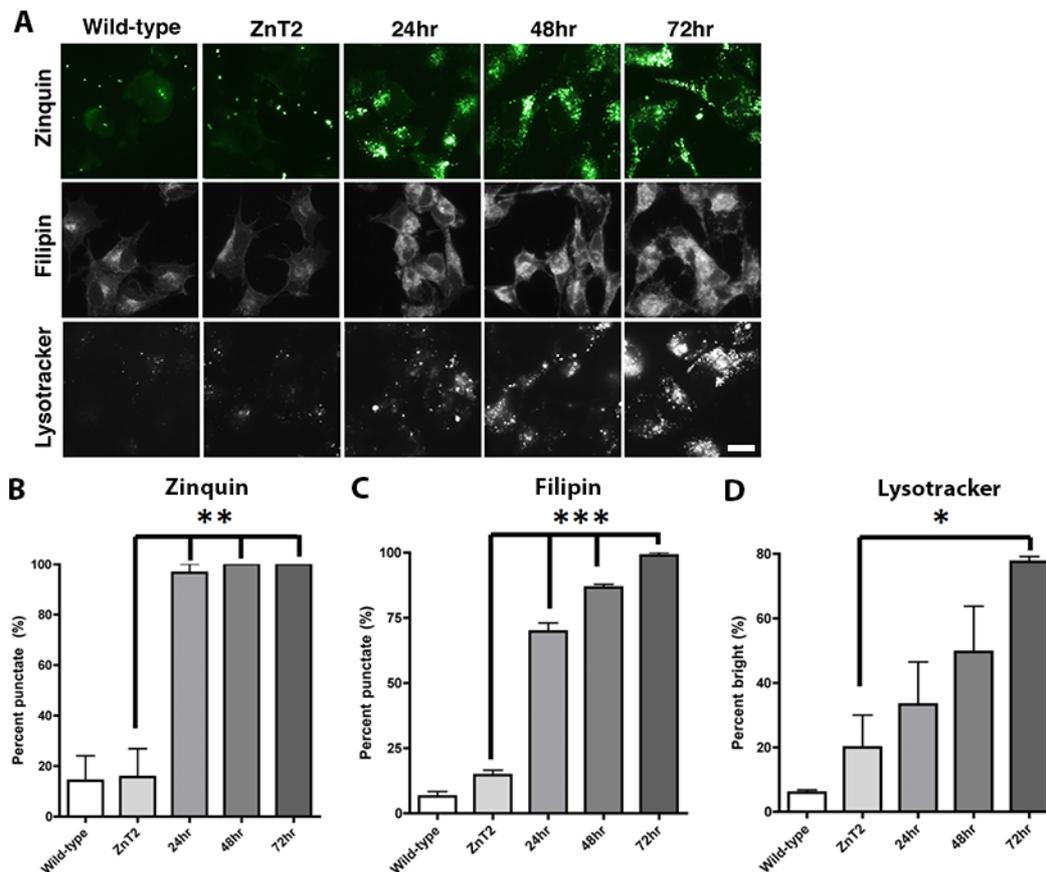
Figure 3.8. ZnT2 overexpressing cells show NPC1 phenotypes following treatment with Zn^{2+}. Treating baby hamster kidney (BHK) cells overexpressing ZnT2 (transports Zn^{2+} into lysosomes (Mocchegiani et al., 2010)) with 50µM ZnCl incudes lysosomal Zn^{2+} storage followed by NPC lipid phenotypes. A) ZnT2 overexpresing BHK cells (ZnT2) where either untreated or treated for 24 hours (hr), 48hr or 72hr with 50µM ZnCl prior to staining with the indicated probe (live or fixed) as described in materials and methods. Pictures where quantified either by thresholding (Lysotracker (D)) or distribution (FluoZin (B), Filipin (C)) to generate graphs shown. N=3. Scale = 10µM. *=p<0.05, **=p<0.01, ***=p<0.001. >50 cells analyzed per condition per N.

Having demonstrated lysosomal Zn^{2+} storage in NPC1 as an early event in the pathogenic cascade (Figure 3.6, 3.7 & 3.8), we next compared lysosomal cholesterol, Zn^{2+} storage, and localization of NPC1 within *NPC1$^{+/+}$* (wild-type) fibroblasts and 5 different NPC1 patient fibroblasts with a variety of pathogenic mutations.

Variant NPC cells are unusual as they show no cholesterol storage (Sun et al., 2001). In Figure 3.9 A & B, cholesterol storage (filipin) can be seen in all NPC1 fibroblasts (with at least a ~50% increase

in bright cells compared with wild-type) except in KW cells (1061T/P1007A), which are seen to have a variant cholesterol phenotype (Sun et al., 2001). Despite this, punctate Zn^{2+} storage (Zinquin) is observed in all *NPC1* fibroblasts (Figure 3.9 A & C, at least at ~30% increase in punctate staining when compared with wild-type). This demonstrates the importance of lysosomal Zn^{2+} storage over cholesterol accumulation regarding NPC1 pathogenesis, whilst highlighting Zn^{2+} and cholesterol storage as independent events. Figure 3.9 A & D demonstrates how within NPC1 (P237S/I1061T) and MN (I061T/I061T) NPC fibroblasts, NPC1 (anti-NPC1) does not localize to lysosomes, and this could therefore account for storage of both cholesterol (Figure 3.9 A & B) and Zn^{2+} (Figure 3.9 A & C). Within KW cells however, NPC1, whilst able to reach lysosomes (Figure 3.9 A & D), appears unable to transport Zn^{2+} (Figure 3.9 A & C), whilst transport of cholesterol appears intact (Figure 3.9 A & D). This presumably occurs due to KW cells having a mutation in a domain required for transport of Zn^{2+}, but not for other substrates. Mutations affecting BS (G46V/P691L) and MO (I061T/D948N) cells appear to affect transport of both cholesterol and Zn^{2+}, as while localization of NPC1 within these fibroblasts remains lysosomal (Figure 3.9 A & D), storage of both Zn^{2+} (Figure 3.9 A & C) and cholesterol (Figure 3.9 A & B) occur.
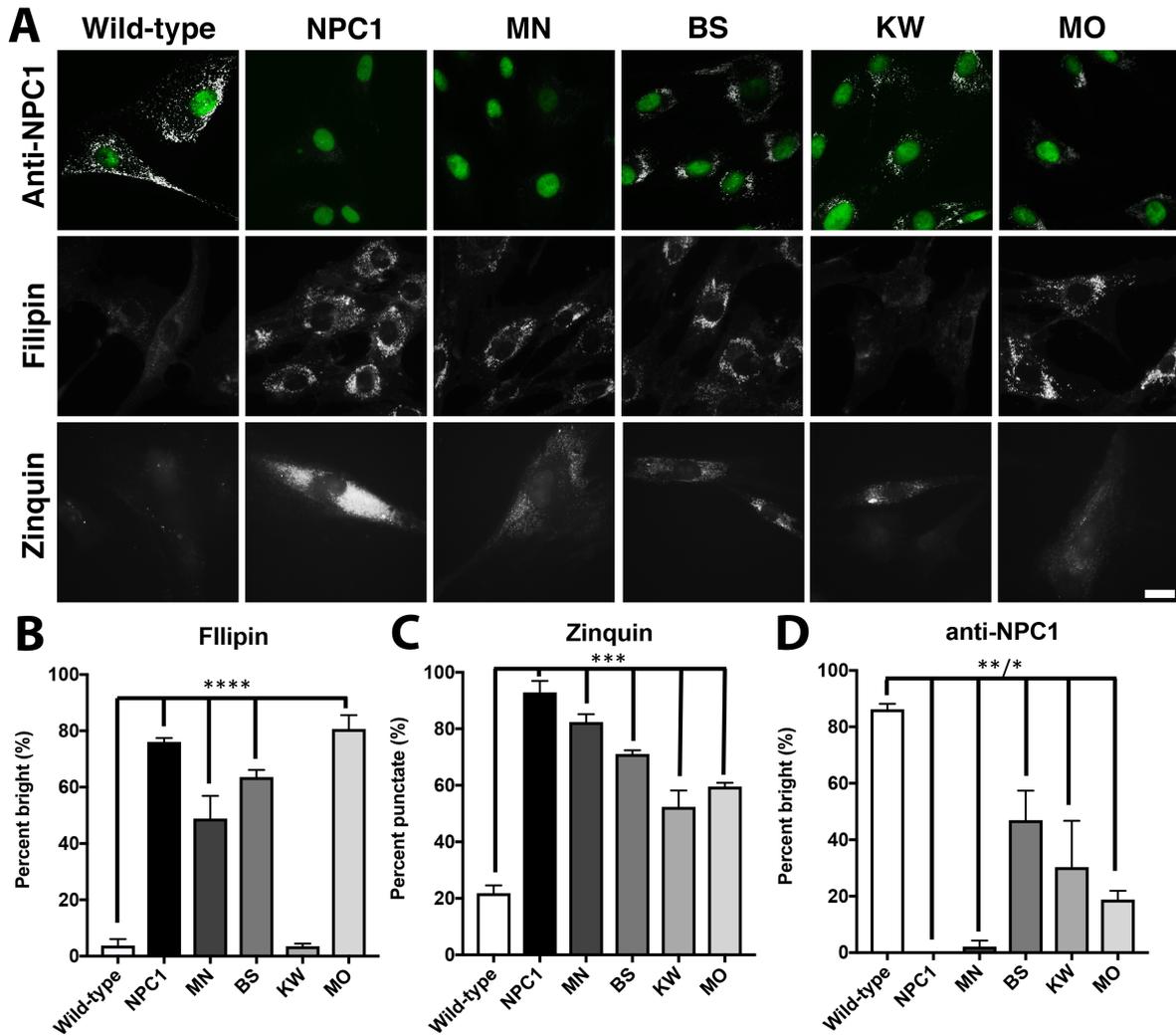
Figure 3.9. Zn²⁺ accumulates in variant *NPC1⁻/⁻* cells. In order to characterize cholesterol and Zn^{2+} storage as well as localization/presence of NPC1 within various NPC mutants, wild-type (*NPC1⁺/⁺*), NPC1 (P237S/I1061T), MNNPC (I061T/I061T), BSNPC (G46V/P691L), KWNPC (I061T/P1007A) and MONPC (I0161T/D948N) human fibroblasts were stained with the indicated probe (live or fixed) as described in materials and methods (A). Pictures were quantified either by thresholding (Filipin (B) and anti-NPC1 (D)) or distribution (Zinquin (C)) to generate graphs shown. N=3. Scale = 10µM. ****=p<0.0001, ***=p<0.001, **=p<0.01, *=p<0.05. >50 cells analyzed per condition per N.

Having shown the importance of the NPC1 lysosomal Zn^{2+} storage phenotype in the absence of cholesterol, we next looked to see whether treatment with either an inhibitor of sphingolipid synthesis (ISP1) or a cholesterol chelator (HPβCD) could reverse NPC1 Zn^{2+} accumulation (Figure 3.10).

We found that whilst both of these treatments were able to correct cholesterol (filipin) storage within *Npc1⁻/⁻* astrocytes, neither had any effect on the NPC1 Zn^{2+} phenotype (FluoZin-3, AM). This again suggests Zn^{2+} storage as an early NPC1 phenotype, occurring prior to lipid accumulation.
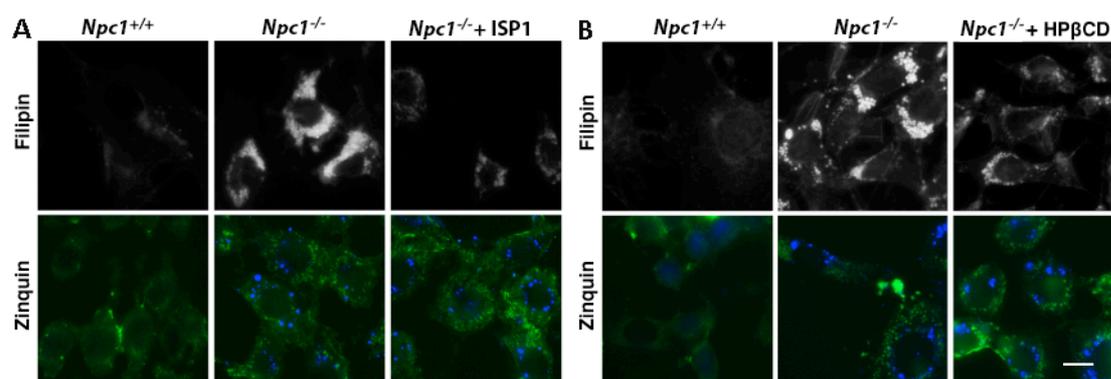
Figure 3.10. ISP1 and HPβCD do not correct lysosomal Zn²⁺ storage in *Npc1⁻ᐟ⁻* cells. *Npc1⁺ᐟ⁺* (wild-type) and *Npc1⁻ᐟ⁻* (NPC1) glia were either untreated or treated with A) ISP1 (250nM, inhibitor of sphingolipid synthesis) or B) (2-Hydroxypropyl)-β-cyclodextrin (HPβCD) (0.4mg/ml, cholesterol chelator) for 96 hours prior to staining with the indicated probe (live or fixed) as described in materials and methods. N=3. Scale = 10µM. >50 cells analyzed per condition per N.

3.3.3 NPC1 as a lysosomal Zn²⁺ transporter

As previously discussed, NPC1 acts as the only known mammalian RND permease (Scott and Ioannou, 2004). Having identified lysosomal Zn²⁺ storage as an early event in the NPC1 pathogenic cascade (Figure 3.6, 3.7 & 3.8), and knowing that several RND permeases transport metal ions, we decided to investigate a new function for NPC1 as a lysosomal Zn²⁺ transporter, acting to remove Zn²⁺ from lysosomes. This would explain early storage of Zn²⁺ following loss of NPC1 function.

T-Coffee software was used to compare sequences of NPC1 with ZneA: a recently discovered proton driven Zn²⁺ transporting RND permease found within the heavy-metal resistant bacteria *Cupriavidus metallidurans* CH34 (Pak et al., 2013)(for sequence alignment see Appendix 1). This demonstrated 20% sequence identity between the 2 proteins and suggested that NPC1 and ZneA may share a conserved Zn²⁺ transporting function (Figure 3.11 C). This identity is much higher than that observed when comparing NPC1 with cholesterol regulators HMG-CoA reductase and PATCHED (Figure 3.11 D).

Key residues involved in the binding and efllux of Zn²⁺ within ZneA can be seen in Figure 3.11 B. Looking closer at BLAST sequences showed how the majority (6/10) of said residues are conserved in the NPC1 protein sequence, further suggesting a key role of these moieties regarding function. A further observation following sequence comparison was that 14 NPC causing mutations occur within conserved residues between NPC1 and ZneA, including the most common NPC mutation (I1061T). Two NPC causing mutations are also found in corresponding ZneA Zn²⁺ binding domains, as seen in Figure 3.11 B. These sites are D654 in ZneA corresponding to D944N in NPC1, and D658 in ZneA corresponding to D948N in NPC1.

Another insight into the function of the NPC1 protein gained using sequence comparison to ZneA followed observations that 5 out of the 14 conserved residues found mutated in NPC generate a variant disease phenotype that lacks lipid storage (Sun et al., 2001). As an RND permease, NPC1 could be capable of transporting numerous substances. Variant patients are potentially unable to transport Zn^{2+}, whilst still retaining other transport functions (such as the ability to transport sphingosine).

Finally, in an effort to determine whether NPC1 showed homology to general metal ion transporting RND permeases, rather than only Zn^{2+} specific RND permeases, BLAST comparisons were performed with NPC1 and the Cu^{2+} transporting RND permease CusA (Delmar et al., 2013). This comparison revealed only 13% sequence identity between the 2 proteins (Figure 3.11 C).

A

Key residue in ZneA	D658	D654	D602	E610	E136	D172	H268	T180	R596	E72
Conserved in human?	✓ (D948)	✓ (D944)	✓ (D878)	✓ (D895)	✗	✓ (D445)	✓ (H512)	✗	✗	✗

C

	NPC1	ZneA	CusA
NPC1	X	20%	13%
ncr1	32%	18%	X

D

	HMG-CoA reductase	NPC1	PATCHED
HMG-CoA reductase	X	10.7%	9.2%
NPC1	10.7%	X	16.4%
PATCHED	9.2%	16.4%	X
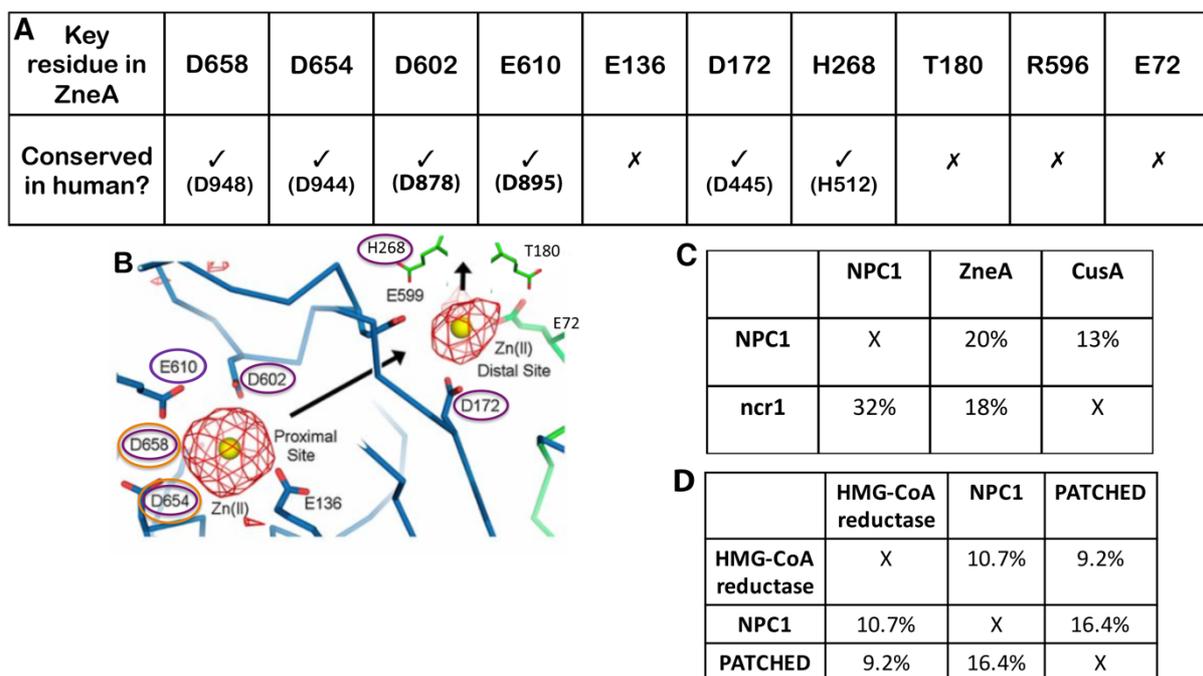
Figure 3.11. NPC1 shares functional features with ZneA. A) Table showing conservation between key Zn^{2+} binding (blue) and efflux (green) residues. B) Diagram showing how residues act to bind and transport Zn^{2+} in ZneA. Carbon atoms are colored to represent binding (blue) or efflux (green). Zn^{2+} ions are depicted as spheres in yellow. Electron density is shown in red. Purple circles highlight conservation, while orange highlight those affected in common NPC causing mutations. Image adapted from Pak *et al.* 2013 (Pak et al., 2013). C) Table showing sequence identity when comparing NPC1 with the yeast version of NPC1, the NPC1 yeast ortholog ncr1, ZneA, and the Cu^{2+} transporting RND permease CusA (Delmar et al., 2013). D) Table showing sequence identity when comparing NPC1 with cholesterol homeostasis proteins HMG-CoA reductase and PATCHED. Work performed in collaboration with Dr Kim Wager and Dr Emyr Lloyd-Evans.

As bioinformatics suggested a possible connection between NPC1 and the Zn^{2+} transporting RND permease ZneA, and as NPC1 has been shown to bind Zn^{2+} (Watari et al., 2000), we next designed a novel assay, which exploits lysosomal exocytosis in order to establish whether NPC1 functions as a Zn^{2+} transporter.

Lysosomal exocytosis is a process whereby lysosomes fuse with the plasma membrane following damage, thereby ensuring the membrane is once more intact and extruding their contents in the process (Xu et al., 2012a). Exocytosis leads to the emergence of lysosomal proteins on the plasma membrane, which under normal conditions will eventually be re-endocytosed to lysosomes. In order to prevent re-endocytosis of plasma membrane NPC1, cells were kept on ice throughout the experiment. Ionomycin treatment has previously been shown to induce lysosomal exocytosis via a combination of generating small fissures in the plasma membrane coupled to a large elevation in cytosolic Ca^{2+}, triggered by the ability of ionomycin to primarily act as a Ca^{2+} ionophore in all membranes apart from lysosomes (Xu et al., 2012a). This would transport NPC1 to the plasma membrane, with the N and C termini that normally present into the lysosomal lumen now facing the extracellular milieu, as well as releasing the lysosomal enzyme β-hex into surrounding medium. By adding Zn^{2+} and pH5.2 buffer to the medium, it was hoped that we could mimic the acidic lysosomal lumen environment observed in cells and that NPC1, which is reliant on a proton motive force, would become functional, and therefore transport extracellular Zn^{2+} into cells. Bearing this in mind, it was expected that this increase could be visualized over time using FluoZin-3, AM. This increase should be greater in Npc1 overexpressing cells (CHO 1-1's), and low to non-existent in Npc1-null cells (CHO M12's), depending on activity of residual plasma membrane Zn^{2+} transporters at acidic pH. Each stage of this assay is described diagrammatically in Figure 3.3

Figure 3.12 A shows how in all CHO lines tested (H1, 1-1, M12) treatment with ionomycin induces a much greater β-hex release into cellular medium when compared with untreated controls (~10-20% increase). This confirms previous observations that ionomycin treatment is able to induce lysosomal exocytosis (Xu et al., 2012a). As discussed, CHO cells treated with ionomycin to induce lysosomal exocytosis were then incubated on ice with the fluorescent Zn^{2+} probe FluoZin-3, AM, and we imaged cells at time zero before adding pH 5.2, 50μM $ZnCl_2$ buffer. Cells were then incubated on ice and imaged 10, 40, 70 and 100 minutes following treatment. Images of CHO's at 0 and 70 mins are shown in Figure 3.12 B, although time zero images have been brightened to a greater degree than 70 mins due to extremely dim images prior to the addition of $ZnCl_2$ containing buffer. At time zero, ionomycin treated cells show a punctate probe distribution. Percentage of cells showing cytoplasmic (rather than punctate) Zn^{2+} distribution over time in all CHO lines can be seen in Figure 3.12 C. Following treatment, all CHO's (at time 10 mins) appear brighter and begin to assume a more cytoplasmic probe distribution, suggesting transport of Zn^{2+} into cells. We see the highest increase in cytoplasmic Zn^{2+} when looking at CHO 1-1's at 10 mins, with an increase of ~80%. The next highest initial increase in seen in CHO H1's, with a ~60% increase at 10 mins. Finally, CHO M12's display the smallest increase at 10 mins with only ~43% of the cells showing cytoplasmic staining. Overtime, these values remain high in the 1-1s, with a slight fluctuation in the H1's, and consistently low amounts of

cytoplasmic staining in CHO M12's. This data suggests that amount of cytoplasmic staining, representative of Zn^{2+} influx into cells, is correlated with the amount of NPC1 present in the CHO cell lines.
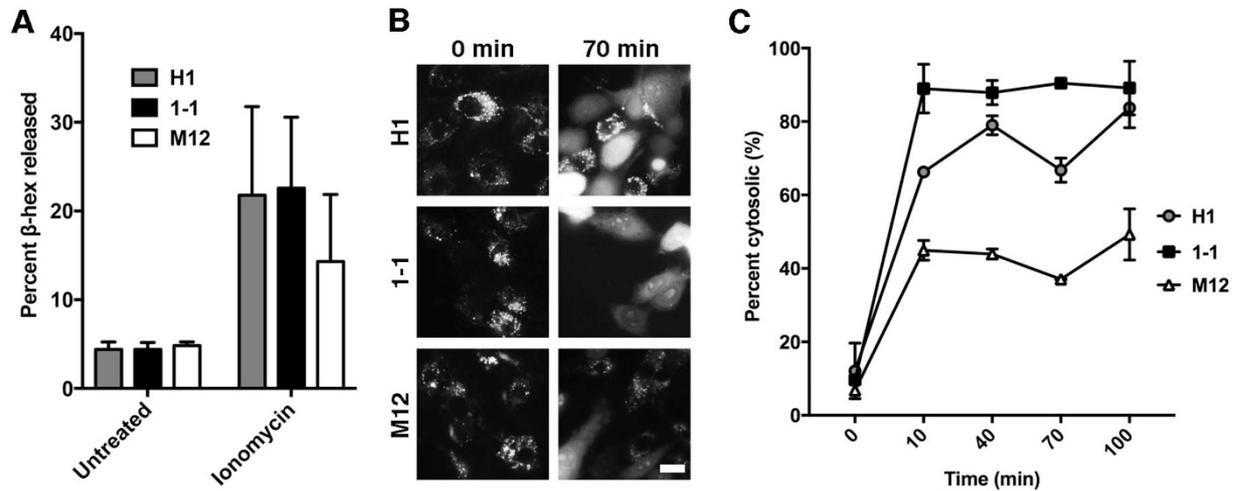
Figure 3.12. Preliminary results of a novel assay exploiting lysosomal exocytosis to confirm Npc1 function as a lysosomal Zn^{2+} transporter. A) CHO cells (H1, 1-1 and M12) were either untreated or treated with 10µM ionomycin for 10 minutes at 37°C to induce lysosomal exocytosis. A β-hexosaminidase assay was then performed on both cellular medium and the cells themselves, and percentage β-hexosaminidase (β-hex) released was calculated. B) Representative images of CHO H1, 1-1 and M12's at either 0 minutes (min) or 70 min following treatment with pH 5.2, 50µM $ZnCl_2$ buffer and incubation on ice. C) Graph showing percent of cells showing cytosolic (rather than punctate) staining in CHO H1, 1-1 and M12's at 0, 10, 40, 70 and 100 mins following treatment with $ZnCl_2$ buffer and incubation on ice. For A N = 3, B & C N = 2. Scale bar = 10µM. >50 cells analyzed per condition per N.

3.3.4 Treating NPC1 lysosomal Zn^{2+} storage: phytic acid

Having provided evidence for a new function for NPC1 as the first identified lysosomal Zn^{2+} transporter, and determined how loss of function leads to progressive Zn^{2+} storage in lysosomes, we next examined this phenotype as a potential therapeutic intervention point. As we know increased lysosomal Zn^{2+} in NPC1 contributes to lipid accumulation, by correcting this phenotype using chelators we can potentially reverse downstream lipid storage as well.

Figure 3.13 demonstrates how treatment with the heavy metal chelator phytic acid reverses lysosomal storage of Zn^{2+} (zinquin, ~60% reduction), cholesterol (filipin, ~20% reduction), BMP (anti-BMP, ~50% reduction) and sphingomyelin (anti-lysenin, ~60% reduction) in $Npc1^{-/-}$ astrocytes. However, treatment with this chelator was unable to correct NPC1 ganglioside GM1 (FITC-CtxB) storage or lysosomal expansion (lysotracker). This result suggests that whilst lysosomal Zn^{2+} storage

may be responsible for some downstream phenotypes in the NPC1 pathogenic cascade, other factors may also play a role.
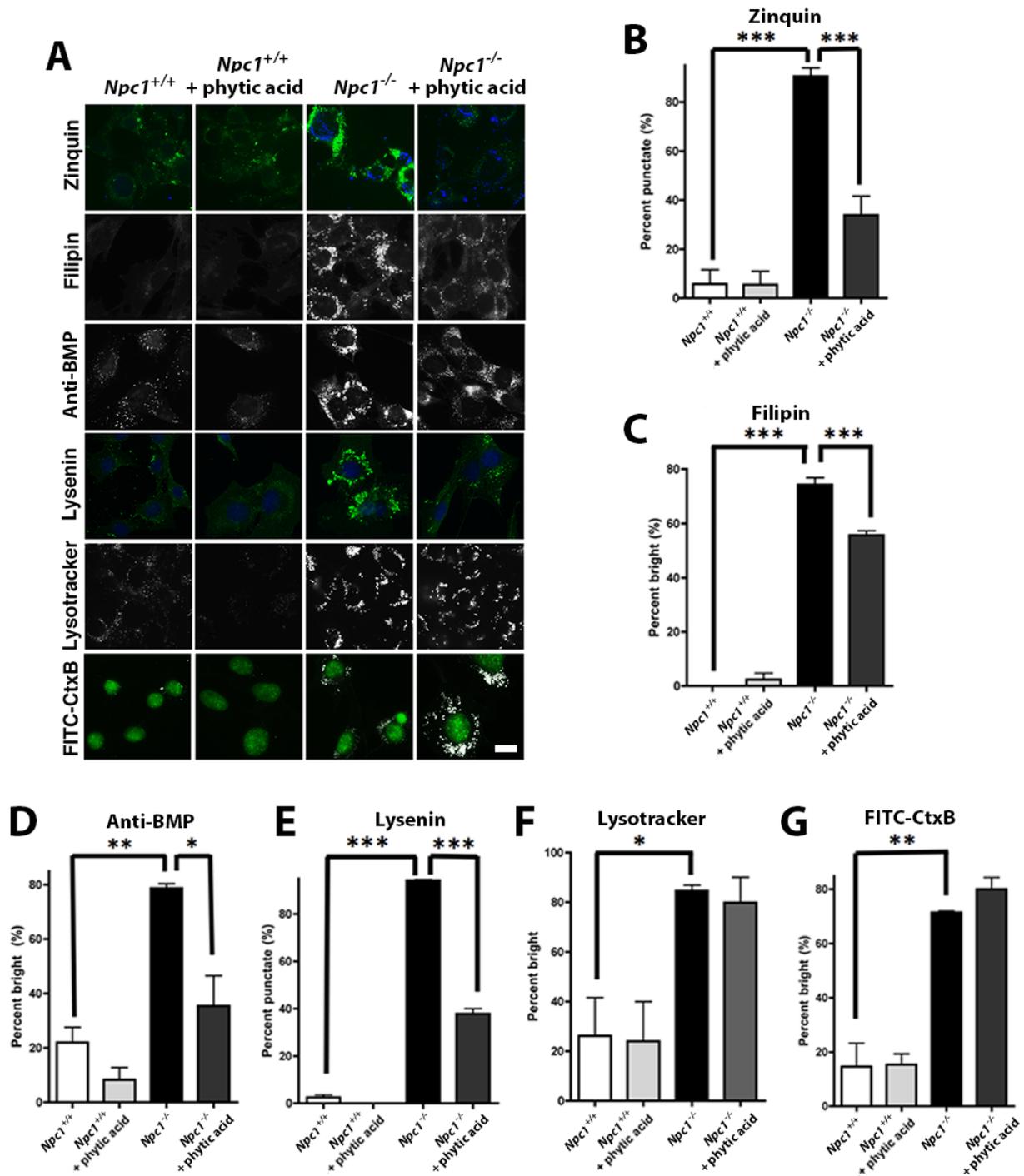
Figure 3.13. Treating *Npc1$^{-/-}$* lysosomal Zn^{2+} storage with the chelator phytic acid corrects some downstream phenotypes. A) *Npc1$^{+/+}$* (wild-type) and *Npc1$^{-/-}$* (NPC1) glia were either untreated or treated with 1mM phytic acid for 96 hours prior to staining with the indicated probe (live or fixed) as described in materials and methods. Pictures were quantified by either

thresholding (Filipin (C), anti-BMP (D), Lysotracker (F), FITC-CtxB (B), anti-Lysenin (E)) to generate graphs shown N=3. Scale = 10µM. *=p<0.05, **=p<0.01, ***=p<0.001. >50 cells analyzed per condition per N.

3.4 Discussion

Previous work within the Lloyd-Evans lab demonstrated accumulation of Zn^{2+} within NPC1 lysosomes (Clark, Waller-Evans, Lloyd-Evans, unpublished). This observation, in combination with previous research highlighting roles of Zn^{2+} in regulating the NPC1 phenotype (Reddy et al., 2006, Vazquez et al., 2011, Hung et al., 2014, Kobayashi et al., 1999, Watari et al., 2000), led to the development of this project to investigate the Zn^{2+} phenotype further.

3.4.1 Lysosomal Zn^{2+} storage appears specific to NPC1

In order to determine the importance of lysosomal Zn^{2+} accumulation in the NPC1 disease cascade, we first looked to see whether Zn^{2+} homeostasis was disturbed in other organelles (Figure 3.4). When staining $Npc1^{+/+}$ and $Npc1^{-/-}$ astrocytes with fluorescent probes for acidic compartment (FluoZin-3, AM, Zinquin), ER (Newport green) and mitochondrial Zn^{2+} (RhodZin) we confirmed mislocalization of Zn^{2+} to lysosomes in $Npc1^{-/-}$ cells whilst demonstrating no difference in ER Zn^{2+} when compared with controls. A significant reduction in mitochondrial Zn^{2+} was observed in $Npc1^{-/-}$ cells when compared to $Npc1^{+/+}$, however this can at least in part be explained by a reduction in mitochondria in $Npc1^{-/-}$ cells (mitotracker green). These results demonstrate how the NPC1 Zn^{2+} phenotype constitutes specific Zn^{2+} accumulation in lysosomes, as oppose to cellular Zn^{2+} redistribution.

Furthermore, as common cellular phenotypes are often observed amongst LSDs, we next sought to investigate the specificity of lysosomal Zn^{2+} storage to NPC1. We did this by comparing FluoZin-3, AM staining for acidic compartment Zn^{2+} in HFs from 9 different LSDs alongside wild-type. Results shown in Figure 3.5 demonstrate how only NPC1 HFs show a significant increase in acidic compartment Zn^{2+} when compared with wild-type. This suggests that Zn^{2+} storage occurs as a direct result of NPC1 dysfunction, occurring independently of more widespread LSD phenotypes (e.g. endocytosis defects, lipid storage).

Having determined the specificity of lysosomal Zn^{2+} storage, we next wanted to investigate this phenotype, as well as its position in the NPC1 pathogenic cascade, further.

3.4.2 Lysosomal Zn^{2+} storage initiates downstream lipid storage in *Npc1$^{-/-}$* astrocytes

Collectively, the results presented in chapter 3 clearly demonstrate the importance of the lysosomal Zn^{2+} storage phenotype regarding NPC1 lipid storage and lysosomal expansion.

For one, Figures 3.6 and 3.7 demonstrate how inhibition of NPC1 with either 1NMP or U18666A induces lysosomal Zn^{2+} storage first (1hr), followed by downstream storage of NPC1 lipids (cholesterol (filipin), BMP (anti-BMP), GM1 (FITC-CtxB – 4-6 hrs) and lysosomal expansion (Lysotracker, 24hr). Furthermore, when you add extracellular Zn^{2+} to ZnT2 overexpressing BHK cells, excess Zn^{2+} is pumped into lysosomes where it initiates downstream lipid storage and NPC1 phenotypes, which emerge in the same order as when initiated using U18666A or 1NMP. Lysosomal Zn^{2+} accumulation can be seen from 24hr treatment with ZnCl$_2$, followed by cholesterol storage (24-48hr) and finally lysosomal expansion (72hr)(Figure 3.8).

As discussed in my general introduction (Chapter 1), it has previously been proposed that NPC1 functions as a cholesterol transporter (Pentchev et al., 1985), with mutations preventing cholesterol efflux from lysosomes and initiating downstream phenotypes. Despite this claim, variant NPC1 cells exist which do not store cholesterol (Sun et al., 2001). Figure 3.9 reiterates the importance of Zn^{2+} storage regarding pathogenesis in these variant cells: despite the absence of cholesterol, lysosomal Zn^{2+} accumulation occurs in these cells. Another argument that Zn^{2+} storage may lie upstream of lipid accumulation in NPC1 can be seen in Figure 3.10, where *Npc1$^{-/-}$* astrocytes where treated with either a cholesterol chelator (HPβCD) or an inhibitor of sphingolipid synthesis (ISP1). These treatments, whilst able to partially correct NPC1 cholesterol, appear to have no effect on lysosomal Zn^{2+}.

Together, the above evidence suggests lysosomal Zn^{2+} storage in NPC1 as an early phenotype in the pathogenic cascade. Next, given high conservation between NPC1 and RND permease transporters, many of which are known to transport metal ions such as Zn^{2+}, we decided to investigate a new function for NPC1 as a Zn^{2+} transporting RND permease.

3.4.3 NPC1 is a Zn^{2+} transporting RND permease

In order to investigate protein function, we performed sequence alignments between NPC1 and heavy metal transporting RND permeases CusA (Cu^{2+} transporter) and ZneA (Zn^{2+}). We also performed alignments between NPC1 and cholesterol homeostasis proteins HMG CoA reductase and PATCHED. Original evidence that suggested NPC1 to be a cholesterol transporter followed alignments with these proteins (Carstea et al., 1997). As you can see in Figure 3.11, despite some similarity with cholesterol regulators, much greater conservation can be seen when comparing NPC1 with RND permeases, in

particular the Zn^{2+} transporter ZneA (20% identical). This suggests some conserved function between these 2 proteins.

As the structure of ZneA had recently been published (Pak et al., 2013), we next performed more detailed sequence alignments between key residues known to be important for binding and transport of Zn^{2+} in ZneA (Figure 3.11). We found that 6 out of these 10 residues were conserved in NPC1. This is higher than the 20% identity observed overall, suggesting that this area is particularly important regarding NPC1 protein function. Following this observation, we next looked to see if any of these residues were mutated in NPC1 disease patients, and found 2 NPC1 mutations occurred in these conserved Zn^{2+} binding residues. Strong conservation in this area of the protein suggests a shared Zn^{2+} transport function between ZneA and NPC1, whilst mutation analysis suggests the importance of this function regarding NPC disease.

We next performed further mutation analysis and found that 14 NPC1 mutations occur in conserved residues between ZneA and NPC1, including the most common NPC disease causing mutation, I0161T (Figure 3.11). This again suggests Zn^{2+} transport as an important function of the NPC1 protein. Furthermore, 5 out of these 14 conserved mutations are reported to cause a variant NPC phenotype (little or no cholesterol storage)(Sun et al., 2001). We have seen however (Figure 3.9) that variant cells still accumulate lysosomal Zn^{2+}. This suggests that NPC1 may function as a multi-substrate transporter, with variant cells specifically losing the ability to transport Zn^{2+} whilst still being capable of transporting other substrates.

As bioinformatics suggested a Zn^{2+} transport function of NPC1, we decided to utilize a novel assay to investigate this further (Figure 3.12). CHO cells where treated with ionomycin to induce exocytosis of NPC1 to the plasma membrane, where function can be assessed. Cells were then incubated on ice (to prevent internalization of exocytosed NPC1) with the Zn^{2+} probe FluoZin-3, AM. Following this, NaAcetate buffer (pH 5.2) provided the proton motive force required for function whilst addition of ZnCl$_2$ provided a substrate to transport. Transport of Zn^{2+} into cells (measured by increased FluoZin-3, AM fluorescence) was demonstrated to occur fastest in CHO 1-1's (which overexpress *Npc1* x15), second fastest in wild-type CHO H1's and slowest is M12s (*Npc1* null). This result demonstrates how Zn^{2+} transport into cells can be directly correlated with amount of NPC1 on the plasma membrane following lysosomal exocytosis, therefore proving a Zn^{2+} transport function for NPC1. Some transport would still be expected to occur in M12's due to the presence of other plasma membrane Zn^{2+} transporters, some of which may function at low pH.

When targeting a disease therapeutically, it is often better to focus on upstream events in the pathogenic cascade, as preventing these changes have the potential to correct all downstream phenotypes. Given our discovery of a Zn^{2+} transport function of NPC1, as well as our understanding of

the importance of lysosomal Zn^{2+} accumulation regarding downstream NPC1 phenotypes, we decided to investigate novel chelators to treat this phenotype.

3.4.4 Chelating lysosomal Zn^{2+} using phytic acid corrects certain *Npc1*^{-/-} phenotypes

Lloyd-Evans and Clark (unpublished) performed a screen of 9 heavy metal chelators to examine effects on *Npc1*^{-/-} cholesterol accumulation, and identified the natural product phytic acid as a best hit. Following observations that phytic acid was capable of correcting cholesterol storage in *Npc1*^{-/-} astrocytes, I investigated its effects on numerous other disease phenotypes.

Phytic acid treatment (1mM, 96hr) was able to significantly reduce Zn^{2+}, cholesterol, BMP and sphingomyelin storage within *Npc1*^{-/-} astrocytes. However, treatment was unable to reverse *Npc1*^{-/-} GM1 storage or lysosomal expansion. As an RND permease, NPC1 could be capable of transporting multiple substrates. If all NPC1 phenotypes developed as a result of loss of Zn^{2+} transport function, we would assume that chelating the Zn^{2+} using phytic acid would be able to revert all NPC1 phenotypes back to wild-type. Observations in Figure 3.13 therefore suggest that lysosomal Zn^{2+} transport is not the only function of NPC1, with loss of other transport functions responsible for other disease phenotypes.

3.5 Conclusions

To conclude this chapter, numerous lines of evidence highlight a novel and direct function for NPC1 as a Zn^{2+} transporting RND permease. Loss of transport function appears to result in downstream *Npc1*^{-/-} lipid storage, and chelating excess lysosomal Zn^{2+} using phytic acid appears to correct some, but not all, downstream NPC phenotypes. Future work would involve staining for Zn^{2+} within NPC1 zebrafish (Chapter 5) to see if we see the same lysosomal Zn^{2+} accumulation as *in vitro*, investigating a wider variety of Zn^{2+} chelators for their effects on NPC, and assessing the effects of Zn^{2+} chelators on the development of the NPC phenotype *in vivo*.

Chapter 4: Exploring effects of Ca^{2+} modulators on the NPC1 lysosomal Ca^{2+} defect and NPC disease cellular phenotypes

4.1 Introduction

4.1.1 The importance of Ca^{2+} as a ubiquitous messenger

Ca^{2+} acts as a highly important second messenger within the cytosol of eukaryotic cells, regulating numerous cellular processes including proliferation, differentiation, secretion, contraction, metabolism, trafficking, gene transcription and apoptosis (Mekahli et al., 2011).

Cellular Ca^{2+} is tightly controlled, as can be clearly seen when looking at the difference in extracellular (1.2-2.5mM) and cytosolic (50-100nM) Ca^{2+} levels (Bronner, 2001). This allows cells to utilize its binding energy for signal transduction following rapid, local increases in this ion. The importance of Ca^{2+} signaling can be seen when considering the hundreds of cellular proteins known to bind this ion at over a million-fold range of affinities (nM to mM) (Clapham, 2007).

4.1.2 Regulation of Ca^{2+} exchange at the plasma membrane

Ca^{2+} homeostasis at the plasma membrane is maintained mainly by selective, high affinity plasma membrane Ca^{2+} ATPases (PMCAs). PMCAs pump Ca^{2+} out of cells in order to maintain low global resting-state intracellular [Ca^{2+}] levels (Strehler, 2015). Other ion pumps such as Na$^+$/Ca^{2+} (NCX) and Na^{2+}/Ca^{2+}-K$^+$ (NCKX) also serve to maintain low intracellular levels by exploiting the concentration gradient of other ions to extrude Ca^{2+} (Karlstad et al., 2012)

Extracellular Ca^{2+} enters the cell via voltage and ligand-gated ion channels. Voltage-gated Ca^{2+} selective channels (CaV) utilize the electrochemical gradient created by the separation of charges between the intracellular and extracellular space in order to elicit rapid increases in cytosolic Ca^{2+}. Numerous ligand gated plasma membrane Ca^{2+} channels exist, and these include AMPAR (alpha-amino-3-hydroxy-5-methyl-4-propionic acid receptor). AMPARs display low-permeability to Ca^{2+}, with AMPAR mediated synaptic depolarization often initiating further Ca^{2+} entry via CaVs (Hartmann and Konnerth, 2005).

4.1.3 The extracellular Ca^{2+}-sensing receptor (CasR)

Changes in extracellular Ca^{2+} modulate cellular function via the plasma membrane GPCR CasR, which is activated by increasing concentrations of Ca^{2+}. CasR functions as a dimer, stabilized by extracellular disulfide bonds and hydrophobic interactions. Ca^{2+} and amino acid binding sites can be found within a large, amino terminal venus flytrap domain (VFTD). Following Ca^{2+} binding to the VFTD, several heterotrimeric G-protein mediated signaling pathways can be activated, depending on cell type and state, and these pathways activate phospholipase C, attenuate adenylyl cyclase and/or activate MAPK kinase pathways to induce changes in intracellular Ca^{2+} (Breitwieser, 2012).

CasR is expressed to varying degrees in numerous tissues known to be involved in Ca^{2+} homeostasis, including bone, kidney and intestine (Breitwieser, 2012). Within bone, CasR expression modulates cell proliferation and helps to maintain the balance between resporption and deposition (Theman and Collins, 2009), whilst in the intestine activation regulates production of acid and hormones (Feng et al., 2010, Geibel and Hebert, 2009). Furthermore, increased extracellular Ca^{2+}, sensed by CasR, has been shown to influence cellular differentiation, as evidenced by the roles of extracellular Ca^{2+} in the differentiation of induced pluripotent stem cells into neurons (Rushton et al., 2013).

A hypothetical transmembrane domain within CasR contains binding sites for positive and negative allosteric regulators (calcimimetrics & calcilytics, respectively), where they act to stabilize either active or inactive forms of this protein (Breitwieser, 2012). These regulators are now approved for the treatment of several conditions characterized by dysfunctional CasR signaling, including several disorders of the parathyroid. Parathyroid hormone release is controlled by CasR expression, and calcimimetrics can be used to treat many diseases in which parathyroid hormone levels are altered (Alon, 2007).

4.1.4 Intracellular Ca^{2+} stores: ER, mitochondria and the Golgi

The major Ca^{2+} stores in eukaryotic cells consist of the ER, mitochondria, Golgi, and the endolysosomal system.

The ER is the most well studied Ca^{2+} store within eukaryotic cells, with a resting Ca^{2+} concentration of between 620-860μM (Suzuki et al., 2014). Ca^{2+} uptake occurs via sarco-/endoplasmic reticulum Ca^{2+}-ATPase (SERCA) pumps, and release predominately through either the inositol 1,4,5-trisphosphate (IP_3) receptor (IP_3R) or the ryanodine receptor (RyR) (Berridge et al., 2000). Basal Ca^{2+} release also occurs via leak channels such as presenilin 1 (Tu et al., 2006) and Bax inhibitor 1 (Kim et al., 2008). The function of chaperone proteins in the ER often requires Ca^{2+} binding, with reduced ER

Ca^{2+} leading to inappropriate secretion, aggregation and degradation of misfolded proteins (Berridge et al., 2000).

Ca^{2+} exchange occurs between IP$_3$R, RyR and mitochondria, another cellular Ca^{2+} store. Within mitochondria, Ca^{2+} has numerous important roles, with increased mitochondrial Ca^{2+} activating mitochondrial dehydrogenases (e.g. pyruvate dehydrogenase (Denton et al., 1972)) and leading to increased ATP production (Jouaville et al., 1999). Prolonged accumulation of Ca^{2+} within mitochondria however may result in mitochondrial permeability transition and cell death (Danese et al., 2017). Uptake occurs mainly via the mitochondrial calcium uniporter (MCU), whilst release occurs via either Na^{2+}/Ca^{2+} or H^{+}/Ca^{2+} exchangers (Rizzuto et al., 2012).

The Golgi acts as another cellular Ca^{2+} store, with Ca^{2+} acting as cofactors for enzymes as well as having roles in retrograde trafficking from the golgi to the ER, and allowing aggregation of proteins. This organelle utilizes IP$_3$R, SERCA, RyR and the secretory pathway Ca^{2+} ATPase (SPCA1) to initiate rapid, local, cytosolic Ca^{2+} signals (Pizzo et al., 2011).

Furthermore, in recent years, the endolysosomal system has become increasingly recognized as an important acidic Ca^{2+} store (Morgan et al., 2015a, Patel and Cai, 2015).

4.1.5 Ca^{2+} movement through the endocytic system: Lysosomal Ca^{2+}

Rich in both H^{+} and Ca^{2+}, acidic stores include lysosomes, lysosome-related organelles, secretory vesicles, vacuoles and acidocalcisomes (Patel and Docampo, 2010). Within mammals, lysosomes act as the major acidic Ca^{2+} store, with ~500µM luminal Ca^{2+} (comparable to ER Ca^{2+}) (Lloyd-Evans et al., 2008, Christensen et al., 2002).

Ca^{2+} loading into these acidic organelles appears dependent on the H^{+} gradient, potentially via a currently unknown mammalian Ca^{2+}/H^{+} (CAX) exchanger (Christensen et al., 2002, Gerasimenko et al., 1998). CAX channels have been identified within acidic lysosomes/vacuoles of plants, protists, fungi and metazoa where they utilize proton gradients across membranes to transport Ca^{2+} into the lumen (Patel and Cai, 2015). Deletion of *Arabidopsis* CAX channels disrupts Ca^{2+} homeostasis, gas exchange, growth and fitness (Cheng et al., 2005, Conn et al., 2011) whilst deletion of yeast CAX impairs stress responses (Denis and Cyert, 2002). Within metazoa, CAX channels demonstrate key roles in migration of neural crest cells during development (Patel and Cai, 2015).

Ca^{2+} handling in the lysosome involves numerous ion channels, including members of the transient receptor potential (TRP) ion channel family, two-pore channels (TPCs) and ATP-gated ionotropic receptors. By both releasing and responding to Ca^{2+}, lysosomal Ca^{2+} signaling enables lysosomal exocytosis and fusion with the plasma membrane (important in numerous processes e.g. wound healing)(Cheng et al., 2015), endolysosomal fusion and trafficking (Pryor et al., 2000), and

autophagy (Medina and Ballabio, 2015). In addition to these local events, lysosomal Ca^{2+} signaling can regulate plasma membrane excitability, cell differentiation, and can trigger global Ca^{2+} signaling events by inducing Ca^{2+} release from the ER (Kilpatrick et al., 2013).

4.1.6 TRPML1 & MLSA1

The TRP channel superfamily includes a sub group of three isoforms of TRP channels called mucolipins (TRPML 1-3), these are voltage and ligand-gated ion channels that localize predominantly to endolysosomes (Kiselyov et al., 2005, Manzoni et al., 2004, Venkatachalam et al., 2006). Loss of function of the ubiquitously expressed TRPML1 results in the lysosomal storage disease mucolipidosis type IV (MLIV) (Puertollano and Kiselyov, 2009).

TRPML1 possesses non-selective cation conductance with permeability to Ca^{2+} at low pH, and is activated by either the endolysosomal phosphoinositide phosphatidylinositol 3,5-bisphosphate $(PI(3,5)P_2)$ (Dong et al., 2010) or the synthetic agonist ML-SA1 (Shen et al., 2012). Conversely, TRPML1 activity can be inhibited using phosphatidylinositol 4,5-bisphosphate $(PI(4,5)P_2)$, the main plasma membrane PIP species (Dong et al., 2010).

Following activation, Ca^{2+} release from TRPML1 enables vesicular trafficking and fusion (Chen et al., 1998) alongside activation of TFEB and regulation of autophagy (Medina and Ballabio, 2015). TRPML1 null cells (MLIV) display lysosomal storage of autofluorescent lipofuscin (Goldin et al., 1995), gangliosides, mucopolysacharides and phospholipid alongside a trafficking defect (Bach, 2001).

4.1.7 TPCs & NAADP (& Ned19)

TPC's represent another important family of lysosomal Ca^{2+} release channels. These voltage-gated ion channels appear to release Ca^{2+} in response to the most potent intracellular Ca^{2+} releasing second messenger, NAADP (nicotinic acid adenine dinucleotide phosphate) (Churchill et al., 2002). As NAADP is membrane-impermeant, a cell-permeant acetyoxymethyl ester derivative of NAADP (NAADP-AM) can be used when investigating NAADP-mediated Ca^{2+} release (Galione et al., 2014). Furthermore, in 2009, Naylor *et al.,* utilized virtual screening to identify a chemical probe for NAADP, known as Ned-19, capable of blocking NAADP signaling at nanomolar concentrations.

Numerous lines of evidence suggest that NAADP induces Ca^{2+} release from acidic stores via TPCs (Brailoiu et al., 2009a, Calcraft et al., 2009, Zong et al., 2009), most likely facilitated by a currently unknown accessory protein (Marchant and Patel, 2013, Pitt et al., 2016). TPC1 has been demonstrated to primarily transport H^+, K^+, Na^{2+} as well as some Ca^{2+}(Pitt et al., 2016), whilst TPC2 appears to predominately transport Ca^{2+}(Pitt et al., 2010, Schieder et al., 2010).

For more information on TPCs, NAADP and Ned-19, see Chapter 5.

4.1.8 NPC1 cells display a lysosomal Ca^{2+} defect

In 2008, Lloyd-Evans *et al.,* 2008 discovered a 60-70% reduction in lysosomal Ca^{2+} within NPC1 cells when compared with wild-type following treatment with either the cathepsin C substrate Gly-Phe β–Naphthylamide (GPN), which induces osmotic lysis of lysosomes, or bafilomycin A1, which induces lysosomal Ca^{2+} release via inhibition of the vATPase. This defect was seen to result in altered acidic compartment Ca^{2+} signaling via NAADP. No difference in ER or mitochondrial Ca^{2+} was found between wild-type and NPC1 cells.

In order to prevent interference of Ca^{2+}-induced Ca^{2+}-release (CICR) when measuring lysosomal Ca^{2+}, cells were pretreated with either thapsigargin or ionomycin, which release non-acidic compartment Ca^{2+} (Liu and Hermann, 1978), prior to incubation with GPN or bafilomycin A1. A defect in lysosomal Ca^{2+} was further confirmed using the low-affinity Rhod-dextran Ca^{2+} probe in combination with pH and Ca^{2+} insensitive Alexa Fluor 488-dextran (lysosomal probe) to directly measure the lysosomal luminal Ca^{2+} concentration *in situ*.

This paper also demonstrated how treating RAW macrophage cells with the NPC1 inhibitor U18666A (Lu et al., 2015) leads to a 60% reduction in lysosomal Ca^{2+} when compared with wild-type. Following treatment with U18666A, the NPC1 lysosomal Ca^{2+} defect appears to emerge prior to cholesterol and GSL storage. Moreover, chelating lysosomal Ca^{2+} from wild-type cells using a high affinity (strong Ca^{2+} buffering) Rhod-dextran resulted in endocytic trafficking defects alongside lipid storage; phenotypes comparable to those observed in NPC disease. Together, this evidence suggests that a reduction in lysosomal Ca^{2+} in NPC1 acts as an early event in disease pathogenesis, with reduced lysosomal Ca^{2+} affecting previously discussed lysosomal Ca^{2+} signaling, endocytosis, and autophagy, resulting in cellular lipid storage.

Reduced lysosomal Ca^{2+} is hypothesized to emerge following sphingosine storage within NPC1 cells (Lloyd-Evans et al., 2008); sphingosine has previously been observed to inhibit plasma membrane Ca^{2+} channels (Colina et al., 2002), and could therefore be acting in a similar way to inhibit lysosomal uptake of this ion via currently unknown channels. Indeed, sphingosine is the only lipid that when added exogenously is capable of reducing lysosomal Ca^{2+} levels (Roff et al., 1991) and reduction of sphingosine storage using ISP1 normalized lysosomal Ca^{2+} in NPC cells (Lloyd-Evans et al., 2008).

In contrast to the above hypothesis, Hölinger *et al.,* (2015) suggested that reduced lysosomal Ca^{2+} in NPC arises following sphingosine triggered Ca^{2+} release via TPC1 (Hoglinger et al., 2015). Despite this suggestion, as increased Ca^{2+} release from lysosomes should result in vesicular fusion (Pryor et al., 2000), this does not explain the endocytic trafficking defect observed in NPC (Lloyd-Evans et al., 2008,

Ko et al., 2001, Mayran et al., 2003). Furthermore, as discussed earlier, TPC1 primarily transports monovalent ions over Ca^{2+} (Pitt et al., 2014, Pitt et al., 2016). Finally, if sphingosine mediated Ca^{2+} release via TPCs acted as the primary defect, NPC phenotypes should be corrected following treatment with the TPC inhibitor Ned-19 (Naylor et al., 2009). Ned-19 can in fact be seen to induce lysosomal storage within cells (Xu et al., 2016).

Since the discovery of the NPC1 lysosomal Ca^{2+} defect, this phenotype has been confirmed by several groups (Visentin et al., 2013, Ferrante et al., 2016, Xu et al., 2012b, Hoglinger et al., 2015), and has also been implemented in a screening program by the NIH to discover new therapies for NPC disease (Xu et al., 2012).

4.1.9 Ca^{2+} modulation in NPC

Following observations that sphingosine storage in NPC1 cells leads to reduced lysosomal Ca^{2+}, Lloyd-Evans *et al.,* 2008 presented evidence for Ca^{2+} modulation therapies as potential treatments for NPC disease. Inhibiting sphingosine storage directly using the sphingolipid synthesis inhibitor ISP1, whilst able to normalize lysosomal Ca^{2+} levels in *Npc1$^{-/-}$* astrocytes (Lloyd-Evans et al., 2008), is not a viable therapy for NPC due to toxic effects of this molecule (Hanada et al., 2000). Via inhibition of SERCA, thapsigargin induces ER Ca^{2+} release (via Ca^{2+} leak from the ER) and subsequent cytosolic Ca^{2+} increase. This appears to compensate for reduced lysosomal Ca^{2+} signaling in *Npc1$^{-/-}$* astrocytes, therefore correcting endocytic trafficking defects and lipid storage within disease cells. Analogous effects were seen when using the less toxic, weaker SERCA agonist, curcumin, which will be further discussed in chapter 4. Beneficial effects can be prevented by co-treating *Npc1$^{-/-}$* cells with the intracellular Ca^{2+} chelator BAPTA-AM, confirming a Ca^{2+}-dependent mechanism of action.

Prior to this discovery, Yamamoto *et al.,* 1994, had in fact previously investigated the effects of Ca^{2+} modulation on cholesterol esterification defects in NPC1, and observed attenuated cytoplasmic Ca^{2+} elevation in NPC1 fibroblasts following uptake of LDL. Treatment with plasma membrane Ca^{2+} channel agonist YC-170 was able to increase cytosolic Ca^{2+} and cholesterol esterification in NPC1 cells, whilst treatment with Ca^{2+} channel antagonists (e.g. Nifedipine, Diltiazem, Verapamil) further attenuated cholesterol esterification (Yamamoto et al., 1994). This provides further support that modulation of intracellular Ca^{2+} is a therapeutic target for NPC and since the findings of Lloyd-Evans *et al.,* 2008, other Ca^{2+} modulators have also been investigated regarding treatment of NPC disease. These therapies include adenosine A_{2A} receptor agonists (Visentin et al., 2013, Ferrante et al., 2016) and δ-tocopherol (activated vitamin E) (Xu et al., 2012b).

Adenosine A_{2A} receptors are G-coupled receptors with a diverse range of physiological effects often linked to lysosomal trafficking, pH, and Ca^{2+} concentration (Klinger et al., 2002, Carini et al., 2004,

Liu et al., 2008, Christensen et al., 2002). With this in mind, Visentin *et al.,* 2013 decided to investigate potential beneficial effects of the A_{2A} receptor agonist CGS21680 on NPC1 fibroblasts (Visentin et al., 2013) and neurons (Ferrante et al., 2016). Treatment with 100nM CGS21680 was able to restore intralysosomal Ca^{2+} in NPC1 cells to levels comparable with wild-type, whilst correcting mitochondrial defects and reducing cholesterol storage. Co-treating with either the A_{2A} receptor antagonist ZM241384, or BAPTA-AM, prevented beneficial effects. As the main transduction mechanism of A_{2A} receptors is via activation of the cAMP/PKA pathway, the authors co-treated with the PKA inhibitor KT57TA. Co-treatment prevented correction of lysosomal cholesterol storage in NPC1 neurons, suggesting that activation the cAMP/PKA pathway following CGS21680 treatment plays a key role in the correction of the NPC1 lysosomal Ca^{2+} defect and downstream lipid storage.

Xu et al., 2012 further demonstrated potential benefits of Ca^{2+} modulators when treating NPC1 fibroblasts with 40μM δ-tocopherol, where it appeared able to increase both cytosolic and lysosomal Ca^{2+}. This in turn appears to partially correct trafficking defects whilst reducing lysosomal expansion and cholesterol accumulation towards wild-type levels (Xu et al., 2012b), although the signaling mechanisms involved remain unknown.

4.1.10 TRPML1 function in NPC1, MLSA1 as a therapy

In 2012, Shen *et al.,* 2012 suggested that TRPML1 function is inhibited by sphingomyelin, with sphingomyelin build-up in both NPA and NPC disease leading to inhibition of TRPML1 and subsequent endocytic trafficking defects. Despite aforementioned evidence of decreased lysosomal Ca^{2+} in NPC1 cells (Lloyd-Evans et al., 2008, Visentin et al., 2013, Ferrante et al., 2016, Xu et al., 2012b, Hoglinger et al., 2015), this group suggested that this is not the case, and instead hypothesized that decreased lysosomal Ca^{2+} release from TRPML1 results in the observed block in trafficking and lipid storage. This followed observations of reduced Ca^{2+} release in NPC1 cells compared with wild-type following addition of MLSA1. Based on above hypotheses, Shen *et al.,* 2012 proposed the synthetic TRPML1 agonist MLSA1 as a potential therapy for NPC.

In spite of claims by Shen *et al.,* 2012, a lysosomal Ca^{2+} defect in NPC1 rather than a defect in Ca^{2+} release from TRPML1 appears likely following confirmation of this phenotype by several groups as previously discussed (Visentin et al., 2013, Ferrante et al., 2016, Xu et al., 2012b, Hoglinger et al., 2015). Moreover, when measuring lysosomal Ca^{2+}, it is necessary to first empty other cellular Ca^{2+} stores using ionomycin in order to prevent CICR interfering with the lysosomal measurement (Liu and Hermann, 1978), this does not appear to have been done in Shen *et al.,* 2012. Furthermore, in Shen *et al.,* 2012 their use of recombinant TRPM1-GCaMP to measure the reduced lysosomal Ca^{2+} release in NPC1 cells is at odds with their own data from the paper showing that over-expression of TRPML1 can

rescue the Ca^{2+} signaling defects. If TRPML1 overexpression rescues the NPC1 Ca^{2+} defect then how are they able to measure any defect via overexpression of TRPML1 coupled to a GCaMP sensor? Indeed, recent work from our laboratory has shown that reduction in sphingomyelin storage has no impact on either lysosomal Ca^{2+} levels or TRPML1 mediated Ca^{2+} release in NPC disease cells (Waller-Evans and Lloyd-Evans, unpublished observations).

Bearing above observations in mind, we hypothesize that utilizing MLSA1 to induce lysosomal Ca^{2+} release in NPC1 cells could potentially worsen the lysosomal Ca^{2+} phenotype whilst exacerbating trafficking and lipid storage phenotypes.

4.1.11 Acetyl-DL-leucine (tanganil)

A recent case series investigated the effect of the acetylated amino acid tanganil on 12 NPC patients. Using a dose of 3g/day for 1 week followed by 5g/day for a further 3 weeks led to a significant improvement in cerebellar symptoms and quality of life within patients (Bremova et al., 2015). This trial arose following a previous study demonstrating beneficial effects of tanganil against other cerebellar ataxias of various etiologies (Strupp et al., 2013).

Tanganil, or acetyl-DL-leucine, has been widely prescribed since 1957 for the treatment of acute vertigo, and therefore possesses an extensive safety record. Whilst its mechanism of action against vertigo remains elusive, it appears to alter the membrane potential of abnormally hyperpolarized and depolarized vestibular neurons, most likely through an effect on ion channels, perhaps Ca^{2+} channels, within the plasma membrane (Vibert and Vidal, 2001). It has previously been proposed that beneficial effects occur primarily via the L isomer (Gunther et al., 2015).

4.1.12 Aims

Given the observed benefits of Ca^{2+} modulation in NPC1, we decided to investigate several of these modulators further. In particular, we aimed to explore any benefits and potential pitfalls of the TRPML1 agonist MLSA, proposed as a potential therapy for NPC disease. Moreover, we proceeded to investigate whether observed benefits of the acetylated amino acid tanganil occurred via Ca^{2+} modulation.

4.2 Materials & Methods

Unless otherwise stated, all reagents were from Sigma-Aldrich. Any methods used in this chapter and not described here can be found in the general materials and methods section (Chapter 2).

4.2.1 Cell culture

For more detailed cell culture methods, please see general methods section. Wild-type post-natal day 4 mouse cerebellar neurons were obtained from Prof Susan Cotman (Fossale et al., 2004), and human embryonic kidney cells stably transfected with human CaSR (HEK-CaSR) were obtained from Prof Riccardi (Ward et al., 2013). Both lines were grown in complete DMEM as monolayers in a humidified incubator (37°C, 5% CO_2).

4.2.2 Cell treatments

4.2.2.1 Treatment with the TRPML1 agonist, MLSA1 (Mucolipin Synthetic Agonist 1)

MLSA1 acts as a synthetic agonist for the voltage-gated endolysosomal ion channel TRPML1 (Grimm et al., 2010), and has been proposed to correct cholesterol storage within NPC1 cells (Shen et al., 2012). $Npc1^{+/+}$ and $Npc1^{-/-}$ glia where either left untreated or treated overnight (~15 hours) with 30μM MLSA1, made up from a 10mM stock in DMSO, in complete DMEM prior to live or fixed staining and imaging. For details on performing direct addition Ca^{2+}-signaling experiments, see general materials and methods (Chapter 2).

4.2.2.2 Treatment with δ-tocopherol (activated vitamin E)

$Npc1^{+/+}$ and $Npc1^{-/-}$ glia were treated overnight (~15 hours) with 10μM δ-tocopherol (a Ca^{2+} modulator proposed to correct NPC1 cholesterol storage (Xu et al., 2012b)), made up from a 10mM stock in dimethyl sulfoxide (DMSO), in complete DMEM prior to live or fixed staining and imaging in order to confirm previously reported effects. For details on performing direct addition Ca^{2+}-signaling experiments, see general materials and methods (Chapter 2).

4.2.2.3 Treatment with the adenosine A_{2A} receptor agonist CGS21680

$Npc1^{+/+}$ and $Npc1^{-/-}$ glia were treated overnight (~15 hours) with 10nM CGS21680 (Tocris, an adenosine A_{2A} receptor agonist previously proposed to correct NPC1 cholesterol storage via modulation of lysosomal Ca^{2+} (Visentin et al., 2013, Ferrante et al., 2016)), made up from a 10μM stock in DMSO, in complete DMEM prior to live or fixed staining and imaging in order to confirm previously reported effects. For details on performing direct addition Ca^{2+}-signaling experiments, see general materials and methods (Chapter 2).

4.2.2.4 Treatment with acetyl-X-leucine

The acetylated amino acid acetyl-X-leucine (TCI chemicals) can be composed of D, L or a mixture of D and L isomers. Acetyl-DL-leucine is licensed as Tanganil, a drug prescribed for over 50 years to treat acute vertigo (Vibert and Vidal, 2001), and recently shown to provide benefit regarding ataxic phenotypes in a case series involving 12 NPC patients (Bremova et al., 2015). $Npc1^{+/+}$ and $Npc1^{-/-}$ glia were treated overnight (~15 hours) with either 1, 10, 30 or 100µM acetyl-DL-leucine, made up from 1 and 30mM stocks in DMSO, in complete DMEM prior to live or fixed staining and imaging in order to determine effects of treatment on cellular Ca^{2+} and characteristic NPC storage phenotypes. For details on performing direct addition Ca^{2+}-signaling experiments (using D, L and DL isomers of acetyl-X-leucine), see general materials and methods (Chapter 2). For direct addition Ca^{2+} experiments, cells were imaged in HBSS in either the presence (1mM $CaCl_2$) or absence of extracellular Ca^{2+} in order to determine whether Ca^{2+} elevation following addition of acetyl-DL-leucine was due to extracellular uptake or intracellular release from stores.

4.2.2.5 Treatment with the low-affinity Ca^{2+} chelator BAPTA-AM

In order to determine whether tanganil's ability to correct NPC phenotypes occurs via Ca^{2+} modulation, we treated $Npc1^{+/+}$ and $Npc1^{-/-}$ glia overnight (~15 hours, complete DMEM) with the low-affinity Ca^{2+} chelator BAPTA-AM (molecular probes, stock concentration 10mM in DMSO, used at 10µM in complete DMEM)(Wang et al., 1997), either alone or in combination with acetyl-DL-leucine, prior to live or fixed staining and imaging. AM demonstrates modification of BAPTA with an AM ester, which allows this chelator to permeate cell membranes. Once inside the membrane, the AM group is hydrolyzed by intracellular esterases (Galione et al., 2014), leaving BAPTA to accumulate within the cell and chelate Ca^{2+}.

4.2.3 Lysosomal Ca^{2+} measurements

Effects of overnight treatment with MLSA1 (30µM), δ-tocopherol (30µM), CGS21680 (10nM) and tanganil (10µM) on lysosomal Ca^{2+} levels in $Npc1^{+/+}$ and $Npc1^{-/-}$ glia was determined by staining with cell-permeable cytosolic Ca^{2+} probe Fura-2AM (ThermoFisher Scientfic, see general methods, chapter 2) prior to addition of acid free ionomycin (Merck Millipore, 2mM stock in DMSO, 5µM working solution in complete HBSS) to release Ca^{2+} from all stores except lysosomes (Liu and Hermann, 1978). Nigericin was then added to depolarize lysosomes (Tapper and Sundler, 1990), releasing lysosomal Ca^{2+} into the cytoplasm were we recorded any change in cytoplasmic Ca^{2+} levels (340/380).

4.2.4 TRPML1 overexpression

Following claims by Shen *et al.,* 2012 suggesting that TRPML1 overexpression rescues NPC1 cellular phenotypes we decided to investigate further.

TRPML1-YFP (yellow fluorescent protein) in a pcDNA3.1+ vector was purchased from Addgene as bacteria in an agar stab. To amplify the plasmid cDNA, bacteria was streaked from the agar onto Luria Bertani agar plates supplemented with 50µg/ml ampicillin and grown overnight at 37°C with agitation. The plasmid was then prepared for transfection using a PureLink HiPure plasmid purification kit (ThermoFisher) according to manufacturers instructions, resuspended in Tris-EDTA buffer and stored at -20°C until needed. Transfection was carried out with 2 different concentrations of TRPML1-YFP: 1103ng (low concentration, determined via nanodrop) and 3309ng/well (high). To prepare the low and high concentrations of TRPML1-YFP, 1 and 3µl of stock solution was combined with 49 and 47µl of 150mM RNase free NaCl (Polyplus transfection, SA) respectively before being briefly vortexed. Separately, for both concentrations, 2µl of jetPei DNA transfection reagent (Polyplus transfection, SA) was added to 48µl RNase free NaCl and briefly vortexed. 50µl of this JetPei solution was then combined with 50µl of either the high or low concentration TRPML1-YFP solution and was briefly vortexed prior to a 30-minute incubation at room temperature. Following this incubation, 100µl of the appropriate solution was added to *Npc1$^{+/+}$* and *Npc1$^{-/-}$* glia grown in complete DMEM as monolayers in a 24-well plate (see general methods), and incubation occurred for 72-hours at 37°C.

Following this incubation, cells were fixed and stained overnight with anti-GFP (green fluorescent protein, 2µl/ml, Abcam, ab6556) prior to staining with an anti-rabbit secondary (Abcam). Anti-GFP stains YFP as the only difference between the two proteins is a point mutation that does not affect antibody binding (Wachter et al., 1998). Cells were next stained with the fluorescent cholesterol binding probe filipin prior to imaging (see general materials and methods).

Controls included non-transfected *Npc1$^{+/+}$* and *Npc1$^{-/-}$* glia, JetPei only (no TRPML1-YFP) treated *Npc1$^{-/-}$* glia to determine any effects of transfection vector alone and primary (anti-GFP) and secondary only controls to identify non-specific staining.

4.2.5 Measurements of Ca^{2+} in different populations of cells using a fluorescence plate reader

In order to investigate the effects of acetyl-L-leucine on cellular Ca^{2+} levels at increasing extracellular Ca^{2+} concentration we performed a Ca^{2+} plate reader assay in collaboration with Prof. Riccardi's lab.

HEK-293 cells that stably express CasR (HEK-CasR, ~30,000 cells per well) were seeded into 96 well plates, either left untreated or treated with acetyl-L-leucine (10µM), and grown to confluence before being loaded with 2µM Fluo-4 (Fisher) for 30 minutes. Using a Fluoroskan Ascent plate reader,

an initial baseline reading of 10 measurements was taken to determine the 0 second value. A Ca^{2+} solution that increased in Ca^{2+} concentration (0.2-10mM) was dispensed into a single well after 5 seconds. Emission at 538nm for each well (excitation = 485) was then followed for a further 25 seconds (1 reading every 5 seconds). Dose response curves were generated from the peak fluorescence upon the addition of the Ca^{2+} solution and corrected for the initial baseline measurement. Peak fluorescence was then normalized to the 10mM Ca^{2+} and 2µM ionomycin response to enable comparison between different plates. PRISM was used to perform non-linear regression and generate R^2 values shown.

4.2.6 Sphingosine assay

A modified version of the BCA assay (see general methods) was used to measure levels of the NPC1 lipid sphingosine in blood plasma of patient's pre-and post-tanganil treatment. The BCA assay is conventionally used to detect the amount of protein in a sample. Copper (II) Sulphate ($Cu(II)SO_4$) is added to a solution, where the peptide bonds in any proteins present reduce the Cu^{2+} ions to Cu^+. Next, the BCA solution is added, and two molecules of the acid chelate with each of the Cu^+ ions to form an intense purple-colored product, with the intensity of the purple color being indicative of the amount of protein in the solution. In the absence of protein, sphingosine contains a free amine group capable of reducing Cu^{2+} ions and producing a purple product. Therefore, following removal of protein from plasma, levels of sphingosine pre-and post-tanganil treatment can be determined (Gribben and Lloyd-Evans, unpublished).

Solvent extraction was used to precipitate and remove protein from patient blood samples by combining 30µl of each sample with 120µl of Chloroform:Methanol (1:1) and leaving overnight on a roller at 4°C. The next day, samples were vortexed prior to being spun at 1000rpm for 5 minutes, and lipid-containing solvent was removed from the protein pellet and transferred to a new tube.
30µl chloroform and 30µl PBS were added to the solvent mix, and samples were vortexed and spun at 1000rpm for 5 minutes, initiating a phase separation. The top layer of this mixture was discarded (aqueous phase), whilst 30µl chloroform and 30µl PBS was added to the lower lipid containing layer, and the previous step was repeated twice more to remove salts.

Following these three wash steps, samples were dried down under nitrogen and resuspended in 20µl acetonitrile (CH_3CN) prior to sonication for 30 minutes to disperse lipid aggregates.

Solutions were then transferred to 96 well plates prior to addition of 180µl complete BCA solution (BCA + $Cu(II)SO_4$) and sphingosine levels were determined based on degree of color change compared with a standard curve of known concentrations of C18 D-erythro sphingosine dissolved in acetonitrile plus complete BCA.

4.3 Results

4.3.1 Examining the effects of previously investigated Ca^{2+} modulators on the *Npc1$^{-/-}$* phenotype

In order to determine the effects of direct addition of previously investigated Ca^{2+} modulators on intracellular Ca^{2+} release, *Npc1$^{+/+}$* and *Npc1$^{-/-}$* glia were loaded with the Ca^{2+} probe Fura-2AM prior to treatment with either CGS21680 (10nM), δ-tocopherol (30μM) or MLSA1 (30μM), and changes in cytoplasmic Ca^{2+} levels were recorded. Effects of modulators on lysosomal Ca^{2+} was investigated by treating cells overnight with either CGS21680 (10nM), δ-tocopherol (30μM) or MLSA1 (30μM) before staining cells with Fura-2AM and adding ionomycin to release Ca^{2+} from all stores except lysosomes (Liu and Hermann, 1978), and then nigericin to depolarize lysosomes and release their Ca^{2+} content (Tapper and Sundler, 1990).

As can be seen in figures 4.1 A and B, all compounds were capable of increasing cytosolic Ca^{2+} in *Npc1$^{+/+}$* cells, with MLSA1 having the greatest effect followed by δ-tocopherol and finally CGS21680. We next confirmed that the A2A receptor agonist, CGS21680, is able to increase lysosomal Ca^{2+} in *Npc1$^{-/-}$* glia to levels comparable to *Npc1$^{+/+}$* (figure 4.1 B & C), despite having minimal effect on cytosolic Ca^{2+} (figure 4.1 A & B)(Visentin et al., 2013, Ferrante et al., 2016). Furthermore, δ-tocopherol was able to increase both cytosolic (figure 4.1 A & B) and lysosomal Ca^{2+} (figure 4.1 C & D) in *Npc1$^{-/-}$* glia (Xu et al., 2012b). A greater ~35% increase in cytosolic Ca^{2+} was seen in *Npc1$^{-/-}$* over *Npc1$^{+/+}$* glia following addition (figure 4.1 A & B). TRPML1 agonist MLSA1, despite causing a significant increase in cytosolic Ca^{2+} (figure 4.1 A & B), appeared to have no effect on lysosomal levels (Figure 4.1 C & D) in *Npc1$^{-/-}$*. MLSA1 addition did however cause significantly higher (~28%) cytosolic Ca^{2+} elevation in *Npc1$^{+/+}$* when compared to *Npc1$^{-/-}$*, confirming results by Shen *et al.,* 2012 (figure 4.1 A & B).

To determine the effects of these Ca^{2+} modulators on characteristic *Npc1$^{-/-}$* cholesterol storage, we analyzed *Npc1$^{-/-}$* glial cells treated overnight with either CGS21680 (10nM), δ-tocopherol (30μM) or MLSA1 (30μM) prior to fixation and staining with the fluorescent cholesterol binding probe filipin. Treatment with either CGS21680 or δ-tocopherol was able to reverse cholesterol storage in *Npc1$^{-/-}$* glia to levels comparable to *Npc1$^{+/+}$* (figure 4.1 E), mimicking previous observations (Visentin et al., 2013, Ferrante et al., 2016, Xu et al., 2012b) and confirming potential benefits of these Ca^{2+} modulators in NPC. However, despite confirming the ability of MLSA1 to increase cytosolic Ca^{2+} (figure 4.1 A & B), we were unable to reproduce results of Shen *et al.,* 2012 suggesting that MLSA1 reduced cholesterol storage in NPC1 (figure 4.1 E). These results demonstrate how whilst Ca^{2+} modulation can correct *Npc1$^{-/-}$* storage, not all molecules capable of elevating cytosolic Ca^{2+} will have a beneficial effect on the NPC phenotype.
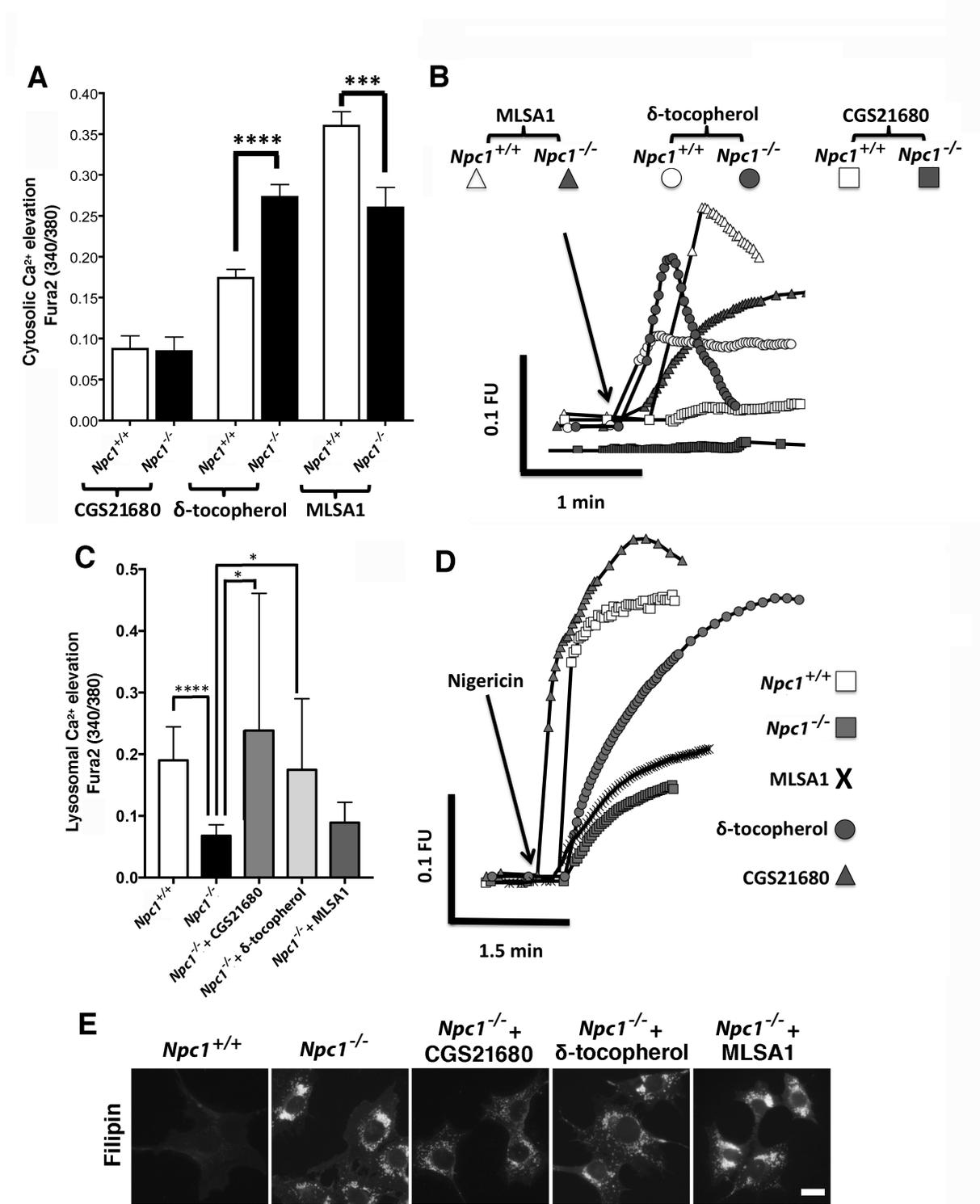
Figure 4.1. CGS21680, δ-tocopherol and MLSA1 all modulate cellular Ca²⁺ (either cytoplasmic, lysosomal, or both) but only CGS21680 and δ-tocopherol are able to reverse *Npc1⁻/⁻* lipid storage. *Npc1⁺/⁺* (wild-type) and *Npc1⁻/⁻* (NPC1) mouse astrocytes were stained and imaged live with the cytoplasmic Ca²⁺ probe Fura-2AM prior to direct addition of CGS21680 (10nM), δ-tocopherol (30μM) or MLSA1 (30μM). Following treatment, we proceeded to measure changes in intracellular Ca²⁺ levels (ratiometric measurement at 340nm and 380nm, expressed as 340/380). Graphs summarizing Ca²⁺ release (A) and representative Ca²⁺ traces (B, FU = fluorescence units) are shown (MLSA1 = Δ, δ-tocopherol = O, CGS21680 = □, wild-type (*Npc1⁺/⁺*) = white, NPC1 (*Npc1⁻/⁻*) = grey). Following overnight treatment (~15 hours) with the above drugs (same

concentrations used in A & B), we investigated effects of treatment on either lysosomal Ca^{2+} (following staining with Fura-2AM, addition of ionomycin to release Ca^{2+} from all stores except lysosomes (data not shown), nigericin to release Ca^{2+} from lysosomes, and measurement of changes in intracellular Ca^{2+}, graphs C, traces D ($Npc1^{+/+}$ = □, $Npc1^{-/-}$ = ■, $Npc1^{-/-}$ + MLSA1 = X, $Npc1^{-/-}$ + δ-tocopherol = O, $Npc1^{-/-}$ + CGS21680 = Δ) or effects on lysosomal cholesterol storage by fixing cells and staining with filipin (E). It should be stated that $Npc1^{+/+}$ cells often have very dim staining with filipin because of high levels in $Npc1^{-/-}$, which would be saturated if $Npc1^{+/+}$ cells were taken at higher comparable exposures. N=2, scale bar = 10μm. Work completed in collaboration with CUROP student Adam Whitall. >50 cells analyzed per condition per N.

As we were unable to reproduce data by Shen *et al.,* 2012 suggesting that MLSA1 treatment can reduce lipid storage in NPC1 cells, and given that MLSA1 has previously been suggested as a potential therapy for NPC1 patients (Shen et al., 2012), we next decided to investigate the effects of this TRPML1 agonist further.

4.3.2 MLSA1 treatment induces a lysosomal Ca^{2+} defect in $Npc1^{+/+}$ glia whilst further reducing lysosomal Ca^{2+} in $Npc1^{-/-}$ cells

We began by staining $Npc1^{+/+}$ and $Npc1^{-/-}$ glia with the Ca^{2+} probe Fura-2AM and investigating the effects of MLSA1 on lysosomal Ca^{2+} levels.

As previously discussed, when measuring lysosomal Ca^{2+}, cells must first be treated with ionomycin to release Ca^{2+} from all other (non-acidic) cellular stores (Liu and Hermann, 1978) and prevent interference of CICR.

Following addition of ionomycin, nigericin was added to release acidic-store (lysosomal) Ca^{2+} (Tapper and Sundler, 1990). As seen in the traces and graphs (figure 4.2 A & B), lysosomal Ca^{2+} was indeed reduced in $Npc1^{-/-}$ cells when compared with $Npc1^{+/+}$ (~80%), confirming previous observations (Lloyd-Evans et al., 2008, Visentin et al., 2013, Ferrante et al., 2016, Xu et al., 2012b, Hoglinger et al., 2015). MLSA1 pretreatment of either $Npc1^{+/+}$ or $Npc1^{-/-}$ cells appeared to reduce lysosomal Ca^{2+} levels below that seen in untreated control lines (treatment reduced lysosomal Ca^{2+} by ~57% in $Npc1^{+/+}$, ~55% in $Npc1^{-/-}$), with acidic store Ca^{2+} in the treated $Npc1^{+/+}$ resembling levels observed in $Npc1^{-/-}$ (figure 4.2 A & B). As reduced lysosomal Ca^{2+} in NPC1 appears to account for observed lipid storage, we next decided to investigate whether or not the MLSA1-induced lysosomal Ca^{2+} defect was inducing NPC-like phenotypes in $Npc1^{+/+}$ glia.
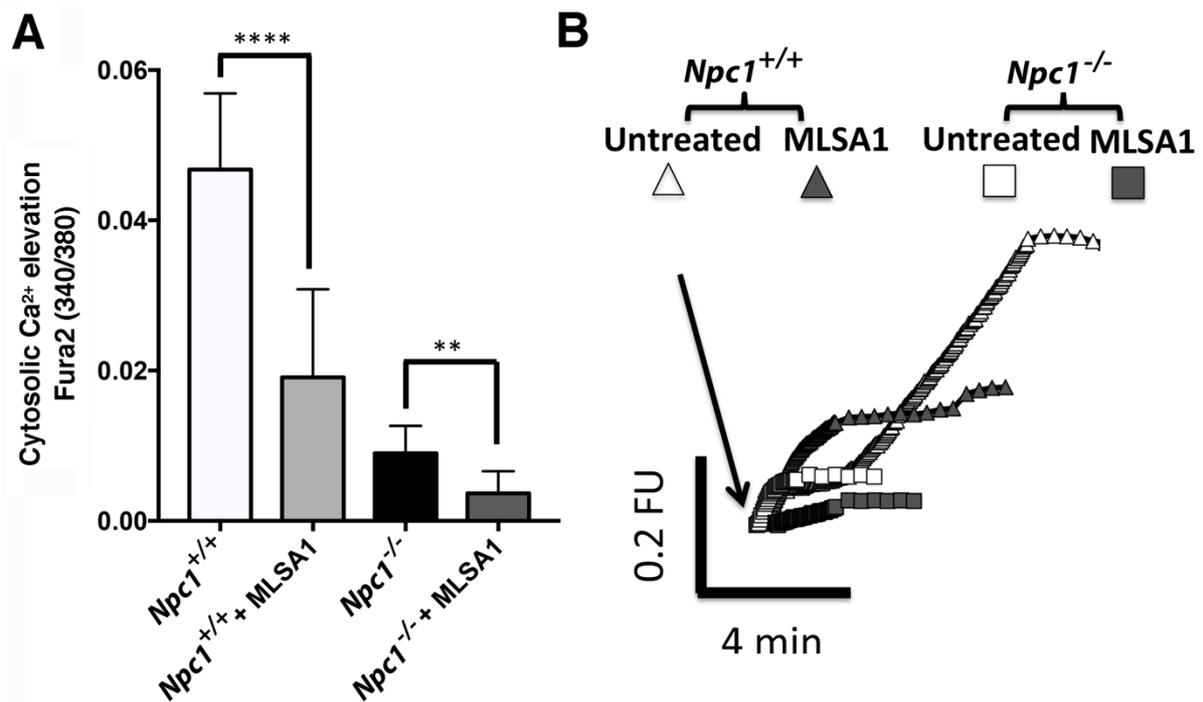
Figure 4.2. *Npc1*$^{+/+}$ **and** *Npc1*$^{-/-}$ **glia treated overnight with the TRPML1 agonist MLSA1 have reduced lysosomal Ca²⁺.** *Npc1*$^{+/+}$ (wild-type) and *Npc1*$^{-/-}$ (NPC1) mouse astrocytes were either untreated or treated overnight with 10 or 30μM MLSA1 prior to staining and live imaging with the ratiometric cytoplasmic Ca²⁺ probe Fura-2AM (340/380). 5μM ionomycin was added to release Ca²⁺ from non-acidic stores prior to addition of 10μM nigericin to induce Ca²⁺ release from lysosomes and measuring the increase in cytosolic Ca²⁺. Graphs summarizing lysosomal Ca²⁺ release (A) and representative Ca²⁺ traces (B, FU = fluorescence units) are shown (*Npc1*$^{+/+}$ = Δ, *Npc1*$^{-/-}$ = □, untreated = white, MLSA1 = grey). N=2. Work completed in collaboration with final year project student Lucy Walker. >50 cells analyzed per condition per N.

4.3.3 Reduced lysosomal Ca²⁺ in *Npc1*$^{+/+}$ glia treated with MLSA1 induces NPC lipid storage phenotypes

In order to determine the effect of reduced lysosomal Ca²⁺ in MLSA1 treated *Npc1*$^{+/+}$ cells we first stained *Npc1*$^{+/+}$ and *Npc1*$^{-/-}$ glia, either untreated or treated with MLSA1 overnight, with the cholesterol probe filipin (Representative images Figure 4.3 A & B, quantified by thresholding 4.3 C & D). We observed that whilst DMSO vehicle control had no effect, treatment of either cell line with 10 or 30μM MLSA1 appeared to slightly increase cholesterol levels, worsening the disease phenotype in *Npc1*$^{-/-}$ cells compared with controls (~15% increase, $P<0.05$) and potentially, although non-significantly, inducing partial storage in the *Npc1*$^{+/+}$ astrocytes.

This finding is supported by preliminary experimental analysis by TLC (figure 4.4 A, quantified 4.4 D), where cholesterol, GSLs, BMP, phospholipids, sphingomyelin and gangliosides appear to increase in *Npc1*$^{+/+}$ and *Npc1*$^{-/-}$ glia following treatment.

Whilst this data is discouraging for the use of MLSA1 as a potential therapy for NPC1, our findings clarify the importance of the lysosomal Ca^{2+} defect in NPC1 with regards to downstream lipid storage.
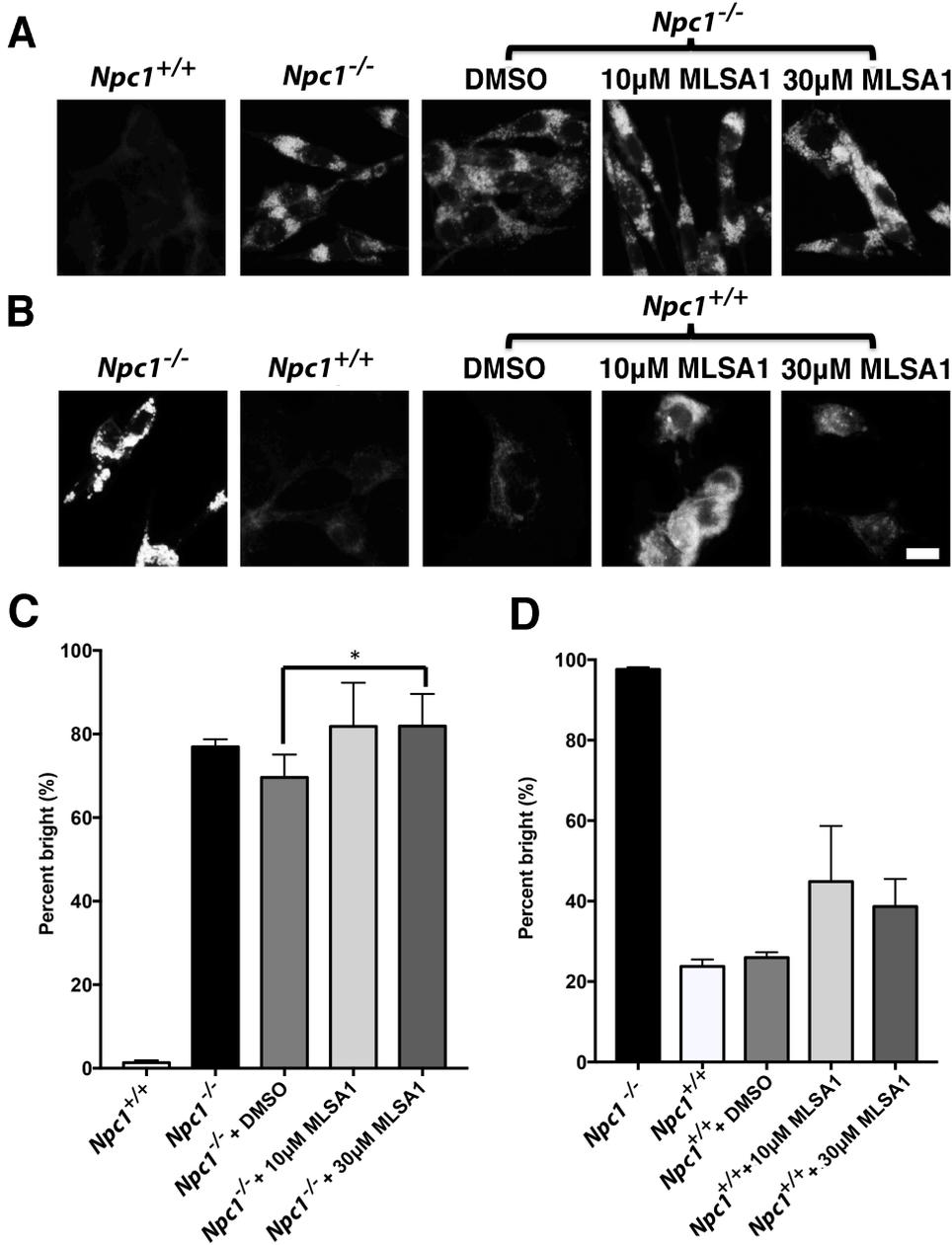
Figure 4.3. *Npc1+/+* and *Npc1-/-* glia treated overnight with the TRPML1 agonist MLSA1 show increased lysosomal cholesterol storage following staining with filipin. Following overnight treatment with 10 or 30µM MLSA1, *Npc1+/+* (wild-type) (B) and *Npc1-/-* (NPC1) (A) cells were fixed and stained with the cholesterol probe filipin. Representative cells can be seen in A & B and images were quantified by thresholding to generate graphs C & D. N=3 for *Npc1-/-* cells, N=2 for *Npc1+/+*, scale bar = 10µm. Work completed in collaboration with CUROP student Adam Whitall and final year project student Lucy Walker. >50 cells analyzed per condition per N.
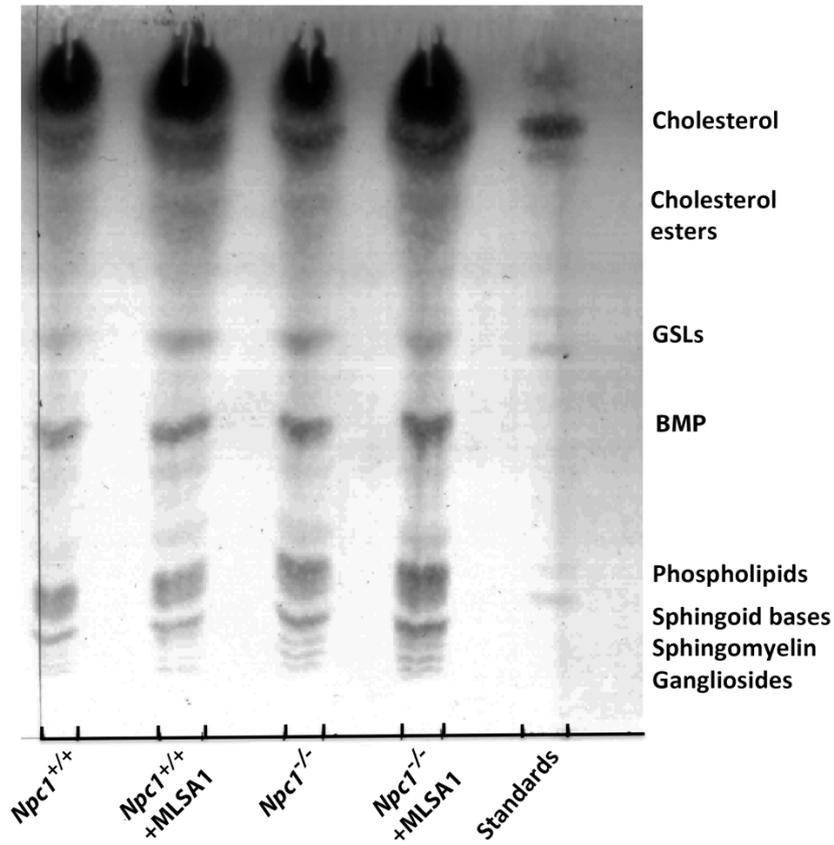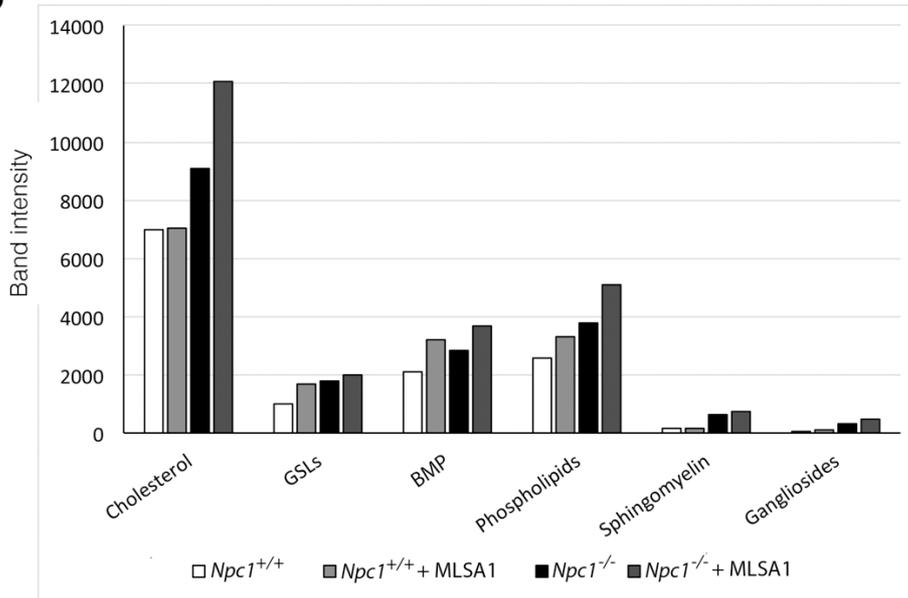
Figure 4.4. *Npc1*^{+/+} and *Npc1*^{-/-} glia treated overnight with the TRPML1 agonist MLSA1 show increased storage of a variety of lipids following solvent extraction and TLC analysis. *Npc1*^{+/+} (wild-type) and *Npc1*^{-/-} (NPC1) glia were either untreated or treated overnight with the TRPML1 agonist MLSA1 prior to lipid extraction and TLC analysis (A). Standard lipid formulations were run alongside samples, GSLs = glycosphingolipids, BMP = bis(monoacylglycero)phosphate. Band intensity of the different lipids across the samples was quantified using ImageJ (B). N=1, work completed in collaboration with final year project student Lucy Walker.

4.3.4 Overexpression of TRPML1 is unable to correct *Npc1^-/-* cellular phenotypes

Shen *et al.,* 2012 demonstrated how overexpression of TRPML1 in NPC1 cells reversed cholesterol storage. As we were unable to reproduce other results from this publication (e.g. the finding that treatment with TRPML1 agonist MLSA1 could reduce NPC1 cholesterol storage), and in fact found that MLSA1 treatment exacerbated the lysosomal Ca^{2+} defect and lipid storage in *Npc1^-/-* glia whilst inducing a phenotype in wild-types (Figures 4.2, 4.3 & 4.4), we decided to investigate this claim by repeating the experiment and overexpressing a TRPML1-YFP construct in *Npc1^+/+* and *Npc1^-/-* glia. Two concentrations of TRPML1-YFP were used, 1103 (Figure 4.5 B) and 3309ng/ml (Figure 4.5 C). Following transfection, cells were fixed and stained with an anti-GFP followed by a fluorescent secondary (488nm). As expected, treatment with the higher concentration of TRPML1-YFP led to ~20% more cells expressing GFP when compared with the lower concentration (Figure 4.5 E). Cells expressing GFP can be considered to have incorporated and expressed the TRPML1-YFP vector, and therefore should be overexpressing TRPML1. Primary and secondary only antibody controls had no effect on fluorescence (data not shown).

We used filipin (380nm) to examine the distribution of the characteristic NPC lipid cholesterol. Our first finding was that *Npc1^-/-* cells treated with the JetPei transfection vector alone showed a small increase in filipin staining (~19%), representative of increased cholesterol storage in lysosomes, when compared to untreated *Npc1^-/-* glia (Figure 4.5 A).

We next compared cholesterol storage (via filipin staining, 380nm) within *Npc1^-/-* cells grown on the same coverslip, treated with low (Figure 4.5 B) or high (Figure 4.5 C) concentrations of TRPML1-YFP. We found that following treatment with either plasmid concentration, *Npc1^-/-* cells expressing the TRPML1-YFP construct (488nm, GFP positive) showed increased cholesterol storage when compared with GFP negative *Npc1^-/-* cells in the same well or JetPei controls (Figure 4.5 B, C & D). This suggests that contrary to claims by Shen *et al.,* 2012, overexpression of TRPML1 in NPC1 is unable to rescue cellular phenotypes, and may in fact worsen lipid storage.
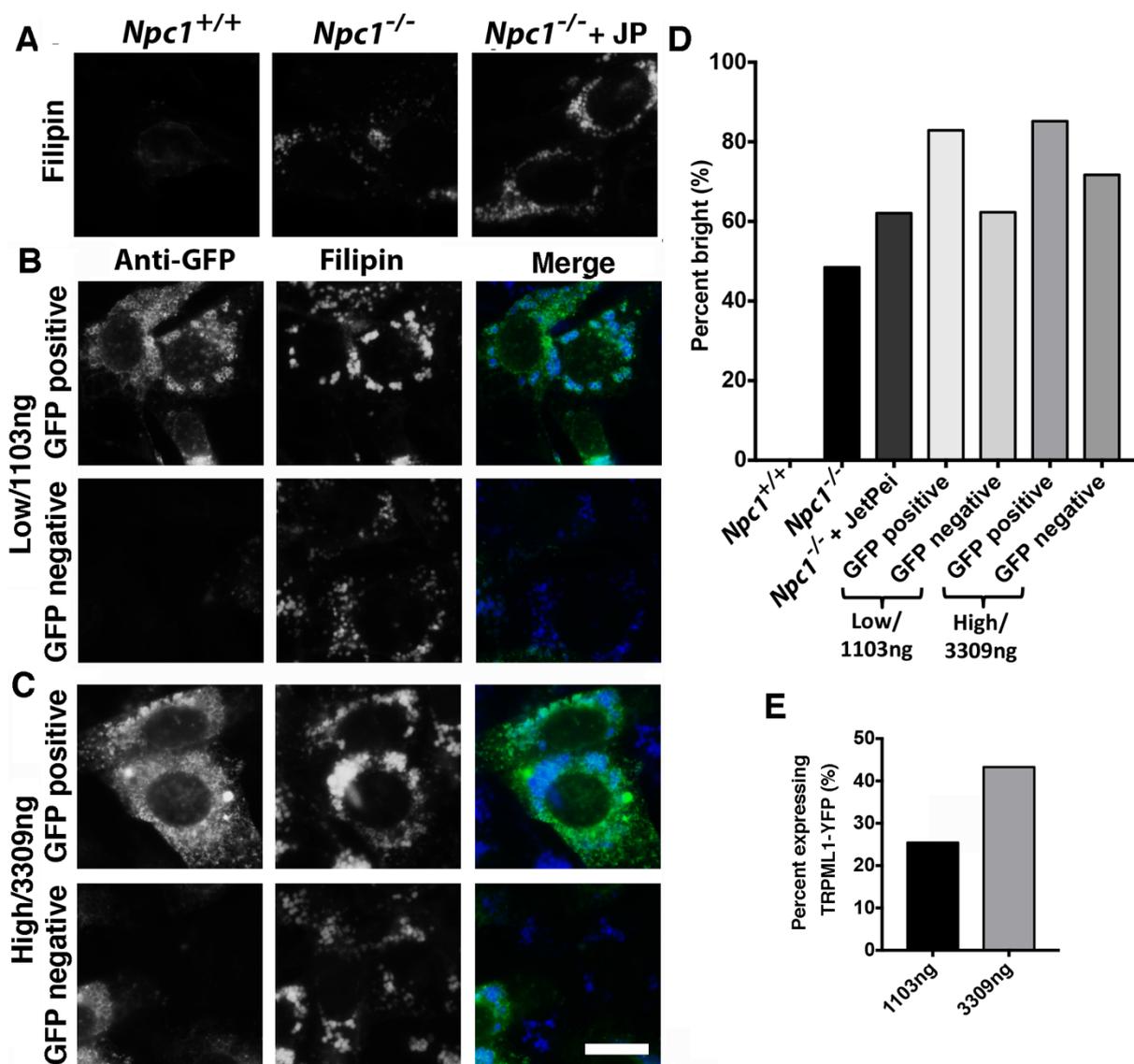
Figure 4.5. Npc1-/- glia over-expressing TRPML1 show increased cholesterol storage when compared with non-GFP tagged controls. Panel A shows control images: non-transfected $Npc1^{+/+}$ (wild-type) and $Npc1^{-/-}$ (NPC1) glia and $Npc1^{-/-}$ glia treated with JetPei transfection vector alone prior to staining with filipin. It should be stated that $Npc1^{+/+}$ cells often have very dim staining with filipin because of high levels of cholesterol in $Npc1^{-/-}$, which would result in probe saturation within $Npc1^{-/-}$ cells if wild-type's were taken at comparable exposures. Dr Helen Waller-Evans prepared TRPML1-YFP for transfection as described in materials and methods. Following this, $Npc1^{-/-}$ glia were transfected using JetPei DNA transfection reagent (JP) combined with either a low (1103ng, B) or high (3309ng, C) concentration of TRPML1-YFP and incubated for 72-hours prior to fixation and staining with both anti-GFP (binds YFP, followed by anti-rabbit secondary, 488nm) and the cholesterol binding probe filipin (380nm). Filipin staining in GFP positive and negative $Npc1^{-/-}$ cells following treatment with either low or high gene concentrations can be seen in B & C respectively, and staining intensity was quantified via thresholding to generate graph D. Following transfection, percent of $Npc1^{-/-}$ cells anti-GFP positive (therefore expressing TRPML-YFP) for low and high gene concentrations can be seen in graph E. N=2. Preliminary data, more repeats needed. Scale bar = 10µm. >50 cells analyzed per condition per N.

4.3.5 Tanganil interacts with plasma membrane ion channels leading to changes in intracellular Ca^{2+} levels

In a recent case study involving 12 NPC patients, the acetylated amino acid Tanganil was demonstrated to provide benefits both in terms of ataxic phenotypes and quality of life (Bremova et al., 2015). Whilst its mechanism of action against NPC is currently unknown, research suggests that effects against vertigo may involve interaction with neuronal Ca^{2+} channels (Vibert and Vidal, 2001). Following these observations, we set out to determine whether Tanganil was capable of acting as a Ca^{2+} modulator within *Npc1$^{-/-}$* cells. To do this, we measured Ca^{2+} release following addition of various concentrations of this drug. *Npc1$^{+/+}$* and *Npc1$^{-/-}$* glia were loaded with the Ca^{2+} probe Fura-2 AM prior to treatment with either 1, 10, 30 or 100μM Tanganil, in both the presence (Figure 4.6 A & C) or absence (Figure 4.6 B & D) of extracellular Ca^{2+}.

As can be seen in Figure 4.6 A & C, when imaged in HBSS plus Ca^{2+}, treatment of *Npc1$^{+/+}$* glia with all tested concentrations of Tanganil resulted in increased cytosolic Ca^{2+}. In comparison, only 10, 30 and 100μM Tanganil treatments led to a release in *Npc1$^{-/-}$*. Significantly reduced Ca^{2+} release can be seen within *Npc1$^{+/+}$* cells at 100μM when compared with that observed at 30μM (~29%), although this is not seen within *Npc1$^{-/-}$* cells. Overall, release in *Npc1$^{+/+}$* glia at comparable concentrations of Tanganil was significantly higher than in *Npc1$^{-/-}$* (e.g. ~57% increase at 10μM, ~40% at 30μM). These results are the first to demonstrate an ability of Tanganil to modulate Ca^{2+} levels within glia.

When imaged in HBSS without Ca^{2+}, significantly increased cytosolic Ca^{2+} was observed in *Npc1$^{+/+}$* glia only when treated with 30μM Tanganil. This can be compared with *Npc1$^{-/-}$* glia where no concentrations were able to invoke a significant Ca^{2+} release. Responses in HBSS without Ca^{2+}, as can be seen by comparing the scale bars of graphs A & B and the Ca^{2+} traces, are much reduced when compared with comparable concentrations in HBSS plus Ca^{2+} (e.g. *Npc1$^{+/+}$* cells plus 10μM Tanganil experience a 7-fold increase in Ca^{2+} release in the presence, compared to the absence, of extracellular Ca^{2+}). As removing extracellular Ca^{2+} prevents or reduces responses to Tanganil, we can conclude that this drug acts mainly via plasma membrane receptors to modulate cellular Ca^{2+} levels in glia.
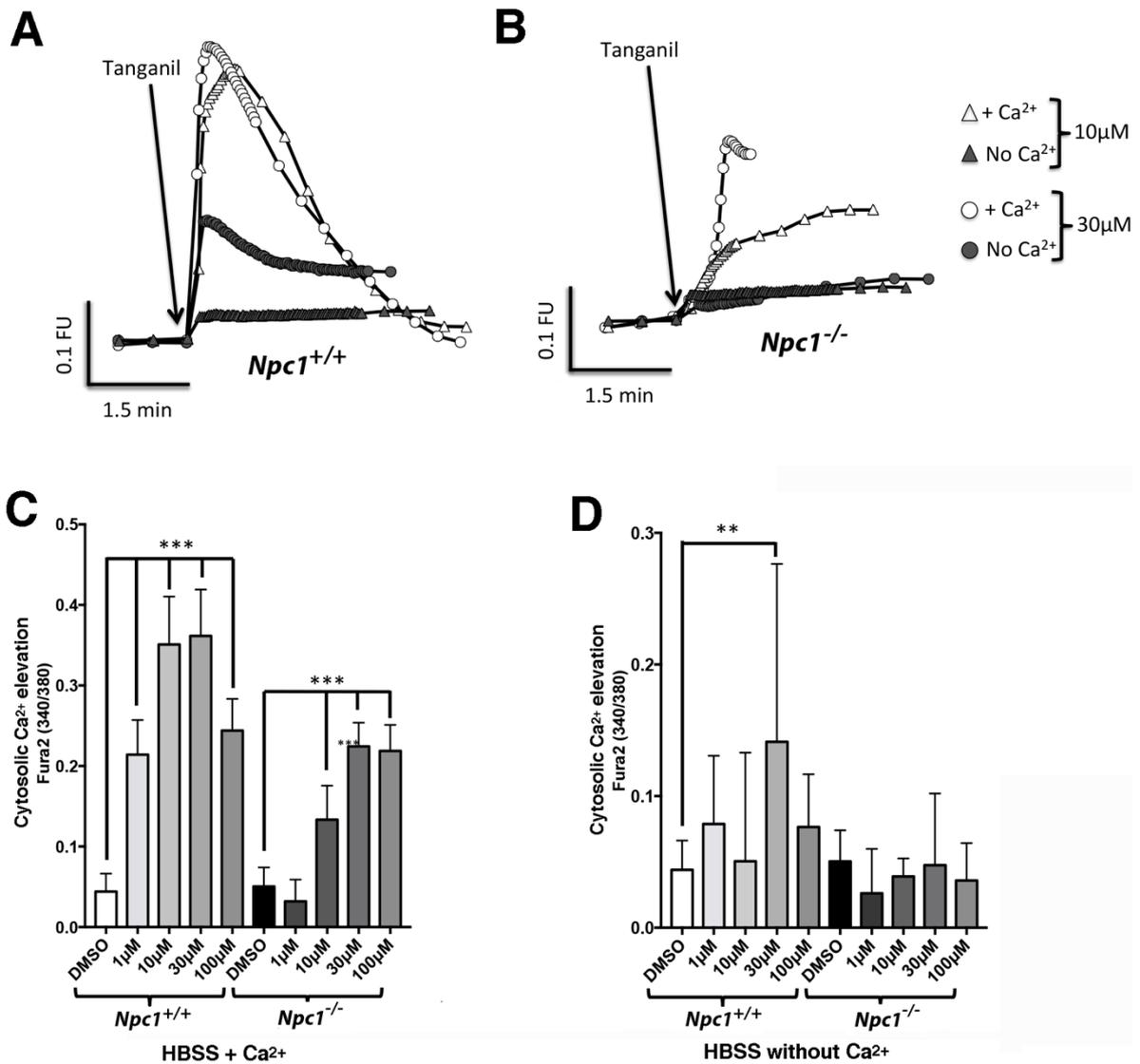
Figure 4.6. Tanganil interacts with plasma membrane ion channels leading to Ca²⁺ release. *Npc1⁺/⁺* (wild-type) and *Npc1⁻/⁻* (NPC1) glia were stained with the Ca²⁺ probe Fura-2AM (340/380) prior to treatment with either DMSO or 1, 10, 30 or 100µM tanganil in either the presence or absence of extracellular Ca²⁺. Following treatment, we proceeded to measure changes in intracellullar Ca²⁺ levels. Representative Ca²⁺ traces are shown for *Npc1⁺/⁺* (A) and *Npc1⁻/⁻* (B) glia treated with either 10 (Δ) or 30µM (O) Tanganil in the presence (white shapes) or absence (grey shapes) of extracellular Ca²⁺. Traces were quantified to make graphs showing average release in presence (C) and absence (D) of extracellular Ca²⁺. N=3. ***=p<0.001, **=p<0.01. >50 cells analyzed per condition per N.

4.3.6 Acetyl-L-leucine appears responsible for the Ca²⁺ increase observed in *Npc1⁺/⁺* glia following treatment with Tanganil, whilst in *Npc1⁻/⁻* glia L and D isoforms appear to have synergistic effects

Tanganil, or acetyl-DL-leucine, contains both D and L isomers. As it has previously been suggested that the L isomer is responsible for beneficial effects of tanganil observed in vertigo (Gunther et al., 2015), we decided to investigate whether the same was true in NPC1.

$Npc1^{+/+}$ and $Npc1^{-/-}$ glia were loaded with the Ca²⁺ probe Fura-2 AM prior to treatment with 10µM of either acetyl-D-leucine, acetyl-L-leucine, or acetyl-DL-leucine (Tanganil, Figure 4.7). $Npc1^{+/+}$ glia release more Ca²⁺ following addition of acetyl-D, L, and DL-leucine when compared with NPC1, confirming results obtained in figure 4.6.

In $Npc1^{+/+}$ glia, application of L and DL isoforms was able to induce significant Ca²⁺ release when compared with DMSO controls (P<0.0001, ~90%), whilst D was not, replicating findings in vertigo (Gunther et al., 2015)(Figure 4.7 A & C) and suggesting that Ca²⁺ release is dependent on the L isomer. In contrast, $Npc1^{-/-}$ cells released Ca²⁺ in response to L (P<0.01, ~80%) DL (P<0.01, ~93%) and D (P<0.0001, ~60%) isoforms when compared with DMSO controls, with D and L isoforms showing a synergistic effect and acetyl-DL-leucine treatment inducing significantly more Ca²⁺ release when compared with L alone (P<0.01, ~29% increase).
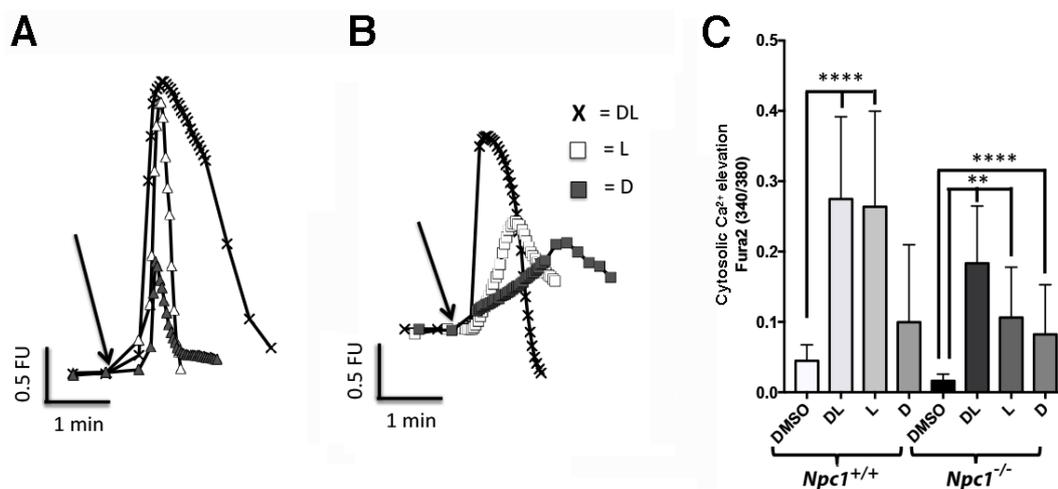
Figure 4.7. Acetyl-L-leucine appears responsible for the Ca²⁺ increase observed in *Npc1⁺/⁺* glia following treatment with tanganil, whilst in *Npc1⁻/⁻* glia L and D isoforms appear to have synergistic effects. *Npc1⁺/⁺* (wild-type) and *Npc1⁻/⁻* (NPC1) glia were stained with the Ca²⁺ probe Fura-2AM (340/380) prior to treatment with 10µM of either acetyl-D-leucine, acetyl-L-leucine, or acetyl-DL-leucine (Tanganil). Following treatment, we proceeded to measure changes in intracellular Ca²⁺ levels. Representative Ca²⁺ traces are shown for *Npc1⁺/⁺* (A) and *Npc1⁻/⁻* (B) glia treated with either acetyl-D-leucine (■), acetyl-L-leucine (□), or acetyl-DL-leucine (X). FU = fluorescence units. Traces were quantified to make graphs showing average release (C). N=3. ****=p<0.0001, **=p<0.01. >50 cells analyzed per condition per N.

4.3.7 Tanganil treatment partially reduces lysosomal Ca^{2+} in *Npc1*$^{-/-}$ glia

Following observations that some Ca^{2+} modulators exert their beneficial effects of *Npc1*$^{-/-}$ glia via modulation of lysosomal Ca^{2+} levels (Figure 4.1), and given that MLSA1 appears to increase cytosolic Ca^{2+} whilst decreasing lysosomal levels (Figures 4.1 & 4.2), potentially resulting in lysosomal storage within glia (Figures 4.3 & 4.4), we next decided to investigate the effects of Tanganil on lysosomal Ca^{2+} levels within cells. *Npc1*$^{-/-}$ glia were either untreated or treated overnight with 10μM Tanganil and lysosomal Ca^{2+} levels were compared with *Npc1*$^{+/+}$ cells. This was done by staining with Fura-2AM and adding ionomycin (to prevent interference from CICR) prior to nigericin (releases lysosomal Ca^{2+}), and measuring the change in cytosolic Ca^{2+} levels. As expected, reduced lysosomal Ca^{2+} was seen in *Npc1*$^{-/-}$ cells when compared with *Npc1*$^{+/+}$ (Lloyd-Evans et al., 2008).

We found that Tanganil treatment partially reduced lysosomal Ca^{2+} in *Npc1*$^{-/-}$ cells (P<0.05, ~10%). As this is also seen with MLSA1 (Figure 4.2), albeit to much greater levels, where the reduced Ca^{2+} appears to generate lipid storage in treated cells, we next decided to further examine the effects of tanganil treatment on lipid storage in *Npc1*$^{-/-}$ glia.
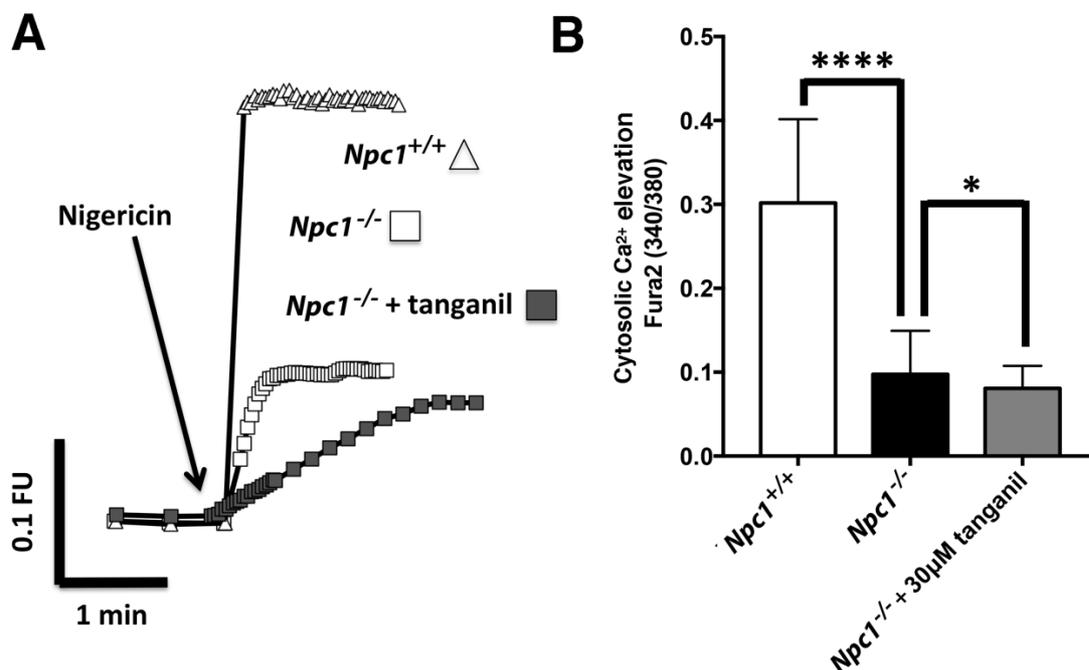
Figure 4.8. Tanganil treatment partially reduces lysosomal Ca^{2+} in *Npc1*$^{-/-}$ glia. *Npc1*$^{+/+}$ (wild-type) cells were left untreated whilst *Npc1*$^{-/-}$ (NPC1) mouse astrocytes were either untreated or treated with 10μM Tanganil overnight prior to staining and live imaging with the ratiometric cytoplasmic Ca^{2+} probe Fura-2AM (340/380). 5μM ionomycin was added to release Ca^{2+} from non-acidic stores prior to addition of 10μM nigericin to induce Ca^{2+} release from lysosomes and measuring the increase in cytosolic Ca^{2+}. Representative Ca^{2+} traces (A, FU = fluorescence units) and graphs summarizing Ca^{2+} release (B) are shown. N=3. Work completed in collaboration with CUROP student Adam Whitall. ****=p<0.0001, *=p<0.05. >50 cells analyzed per condition per N.

4.3.8 Tanganil corrects *Npc1*$^{-/-}$ cellular phenotypes

To determine whether Tanganil was capable of correcting NPC1 cellular phenotypes, we analyzed *Npc1*$^{-/-}$ glial cells treated with various concentrations of this drug for characteristic lipid storage. *Npc1*$^{+/+}$ and *Npc1*$^{-/-}$ glial cells were treated with either DMSO (vehicle control, 10μl/ml) or 1, 10, 30 or 100μM Tanganil for 24 hours prior to fixed or live imaging.

We used Lysotracker Green to compare size and number of lysosomes within cells (Figure 4.9 A & B). *Npc1*$^{+/+}$ cells show dim punctate staining in a perinuclear location, indicative of functional lysosomes, whilst a much brighter and expanded punctate staining pattern can be observed throughout *Npc1*$^{-/-}$ cells (~95% increase). Whilst no significant difference is seen with this probe when comparing untreated *Npc1*$^{-/-}$ cells and those treated with either DMSO vehicle control or 1μM Tanganil, a significant decrease in lysotracker intensity and distribution can be seen following treatment with either 10 or 30μM Tanganil ($P < 0.05$, ~24% & ~50%). Treatment with 100μM Tanganil however is unable to correct *Npc1*$^{-/-}$ lysotracker phenotypes, presumably as this concentration induces less cytosolic Ca^{2+} elevation (Figure 4.6).

We used filipin to examine the distribution of the characteristic NPC1 storage lipid cholesterol, and found expected staining patterns for untreated *Npc1*$^{-/-}$ and *Npc1*$^{+/+}$ glia (Figure 4.9 A & C). *Npc1*$^{-/-}$ cholesterol storage appears significantly reduced following treatment with 30μM Tanganil ($P < 0.05$, ~42%), and appears to be approaching significance with 10μM treatment (more repeats needed), although no correction is seen at 1 and 100μM.

Given above observations, we can conclude that alongside Tanganil's ability to evoke Ca^{2+} release within *Npc1*$^{-/-}$ cells, it is also capable of correcting multiple NPC1 cellular phenotypes. Despite a reduction in lysosomal Ca^{2+} seen in *Npc1*$^{-/-}$ cells following overnight treatment with Tanganil (figure 4.8), we do not see increased storage in *Npc1*$^{-/-}$ cells as observed with MLSA1 (figure 4.3). Furthermore, we do not see increased cholesterol storage or lysosomal expansion in *Npc1*$^{+/+}$ cells treated overnight with 30μM Tanganil (data not shown), which suggests that the lysosomal Ca^{2+} is not reduced to the same extent as it is with MLSA1.
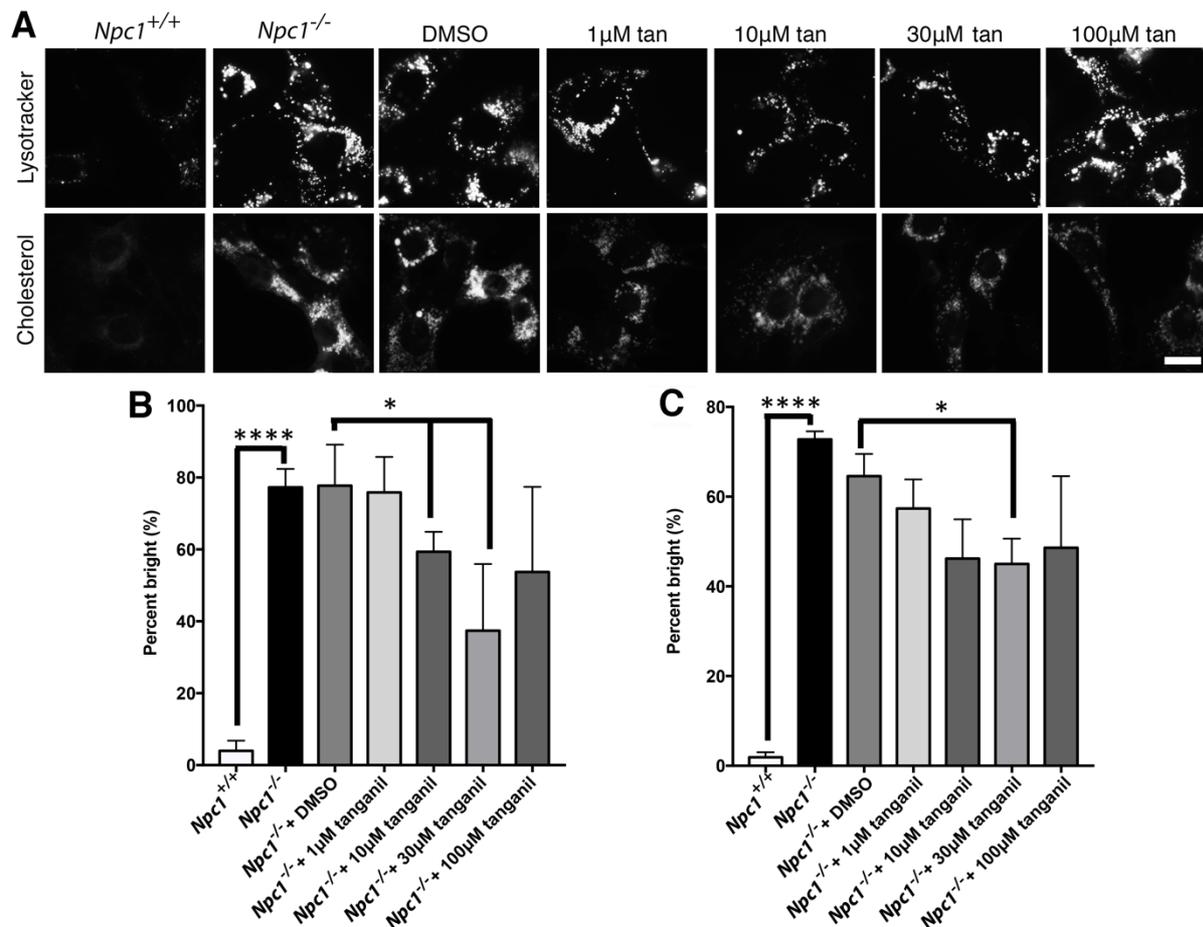
Figure 4.9. Tanganil corrects *Npc1*^{-/-} cellular phenotypes. Following treatment with either DMSO vehicle control (10μl/ml) or 1, 10, 30 or 100μM Tanganil (tan) (DMSO concentration at 100μM Tanganil is comparable to vehicle control), *Npc1*^{-/-} (NPC1) glia were either fixed or imaged live and stained with lysotracker green for lysosomes or filipin for cholesterol (A). Untreated *Npc1*^{+/+} cells were also stained for comparison. It should be stated that *Npc1*^{+/+} cells often have very dim staining with filipin and lysotracker because of the very high levels in *Npc1*^{-/-}, which would be saturated if wild-type's were taken at comparable exposures. Quantification of lysotracker and cholesterol fluorescence microscopy experiments (via thresholding) is shown in graphs B & C respectively. Scale bar = 10μm. N=3 for lysotracker and *Npc1*^{-/-} + 30μM Tanganil filipin experiments, N=2 for all others. ****=p<0.0001, *=P<0.05. >50 cells analyzed per condition per N.

4.3.9 Correction of *Npc1*^{-/-} phenotypes by tanganil is prevented when co-treated with the Ca²⁺ chelator BAPTA-AM

We next sought to examine whether mechanism of correction of NPC1 lipid storage relied on the ability of Tanganil to modulate Ca²⁺. We did this using co-treatment with Tanganil and the intracellular Ca²⁺ chelator, BAPTA-AM. *Npc1*^{+/+} and *Npc1*^{-/-} glial cells were either left untreated or treated with DMSO (vehicle control, 4μl/ml), 30μM Tanganil, 30μM Tanganil & 10μM BAPTA-AM or 10μM BAPTA-AM for 24 hours prior to fixed or live imaging (Figure 4.10). Data for *Npc1*^{+/+} cells treated with tanganil with or without BAPTA-AM is not shown, although no difference in either lysotracker or filipin staining was observed following treatment.

Npc1$^{+/+}$ and *Npc1*$^{-/-}$ cells showed characteristic staining patterns for both lysotracker and cholesterol (Figure 4.9, 4.10) when either untreated, treated with DMSO or treated with 30μM Tanganil for 24 hours. Co-treatment of Tanganil with BAPTA-AM however prevented any benefit achieved with acetyl-DL-leucine alone, and no difference was observed here in comparison with untreated or DMSO control *Npc1*$^{-/-}$ cells. Treating *Npc1*$^{+/+}$ and *Npc1*$^{-/-}$ cells with BAPTA-AM alone does not appear to influence either cholesterol or lysotracker phenotypes (Figure 4.10).

As the beneficial effect of Tanganil on *Npc1*$^{-/-}$ cells is prevented following removal of intracellular Ca^{2+}, we can conclude that reversal of phenotypes following drug treatment occurs via Ca^{2+} modulation.
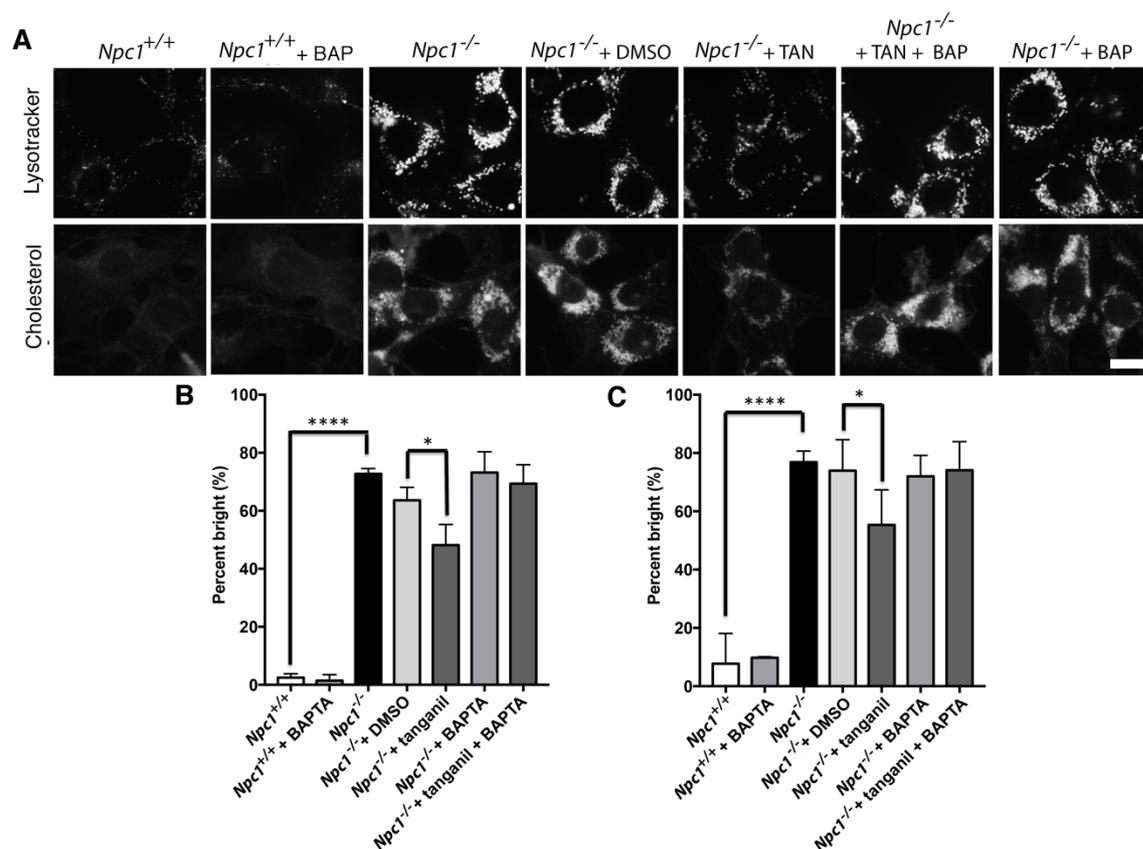
Figure 4.10. Correction of *Npc1*$^{-/-}$ phenotypes by tanganil is prevented when co-treated with the Ca^{2+} chelator BAPTA-AM. Following treatment with either DMSO vehicle control (4μl/ml), 30μM Tanganil (TAN), 30μM Tanganil & 10μM BAPTA-AM (TAN + BAP) or 10μM BAPTA-AM (BAP), *Npc1*$^{+/+}$ (wild-type) and *Npc1*$^{-/-}$ (NPC1) cells were either fixed or imaged live and stained with lysotracker green for lysosomes or filipin for cholesterol (A). It should be stated that *Npc1*$^{+/+}$ cells often have very dim staining with filipin and lysotracker because of the very high levels in *Npc1*$^{-/-}$, which would be saturated if wild-type's were taken at comparable exposures. Quantification of lysotracker and cholesterol fluorescence microscopy experiments (via thresholding) is shown in graphs B & C respectively. Scale bar = 10μm. N=3. ****=p<0.0001, *=P<0.05. >50 cells analyzed per condition per N.

4.3.10 Tanganil releases more Ca²⁺ in *Npc1⁺/⁺* cerebellar neurons than in *Npc1⁺/⁺* glia

Acetyl-DL-leucine has been suggested to work specifically against the ataxic phenotypes in NPC patients (Bremova et al., 2015). As the degeneration of cerebellar neurons in NPC appears responsible for these ataxic phenotypes (Higashi et al., 1993), we next looked to see the effects of tanganil on cerebellar neurons in comparison to glia.

Npc1⁺/⁺ glia and cerebellar neurons were loaded with the Ca²⁺ probe Fura-2 AM prior to treatment with 10μM acetyl-DL-leucine (Figure 4.11). We observed significantly more Ca²⁺ release in *Npc1⁺/⁺* cerebellar neurons when compared with *Npc1⁺/⁺* glia (P<0.05, ~60%), suggesting that tanganil acts on a specific receptor, or subset of receptors, with variable expression across the brain. Furthermore, this observation explains how tanganil may be acting to specifically improve ataxic phenotypes in patients.
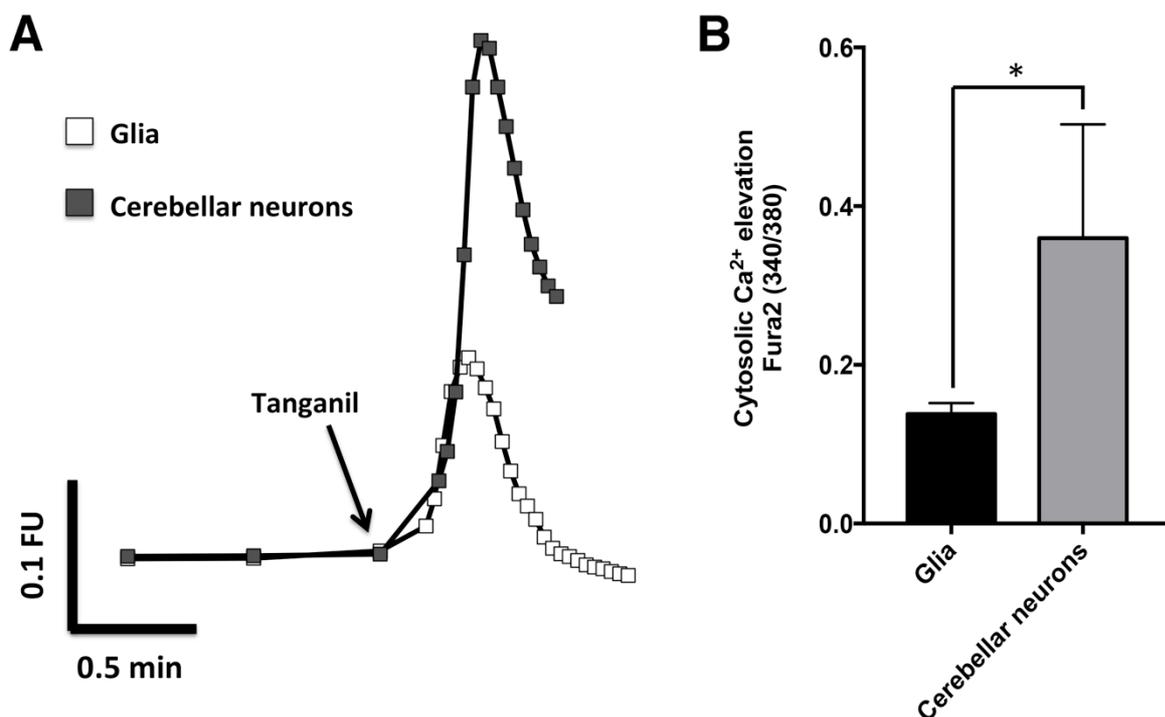
Figure 4.11. Tanganil releases more Ca²⁺ in *Npc1⁺/⁺* cerebellar neurons than in *Npc1⁺/⁺* glia, potentially due to differential expression of its receptor. *Npc1⁺/⁺* glia and immortalized cerebellar granule neurons (cerebellar neurons) were stained with the Ca²⁺ probe Fura-2AM (340/380) prior to treatment with 10μM acetyl-DL-leucine (tanganil). Following treatment, we proceeded to measure changes in intracellullar Ca²⁺ levels. Representative Ca²⁺ traces are shown for wild-type glia (□) and cerebellar neurons (■) (A, FU = fluorescence units). Traces were quantified to make graphs showing average release (B). N=3. *=p<0.05. >50 cells analyzed per condition per N.

4.3.11 Acetyl-L-leucine increases activation of CaSR at increasing Ca^{2+} concentrations

As tanganil contains acetyl-L-leucine, and as L amino acids are known to activate CaSR (Busque et al., 2005), a plasma membrane GPCR known to alter intracellular Ca^{2+} levels (Breitwieser, 2012) and which is variably expressed across the brain (Yano et al., 2004), we decided to investigate whether tanganil was acting via CaSR to increase cytosolic Ca^{2+}. We initially utilized CaSR overexpressing HEK cells in a 96 well plate assay to determine Ca^{2+} elevation induced by acetyl-L-leucine at increasing Ca^{2+} concentrations. Increasing Ca^{2+} concentration activates CaSR. What we found is that cells treated with 10µM acetyl-L-leucine potentiated activation of CaSR, shown by increased intracellular Ca^{2+} elevation, when compared to untreated controls with increasing extracellular Ca^{2+} concentration, particularly in the physiologically relevant range of 1.8-2.5mM Ca^{2+} (Figure 4.12).
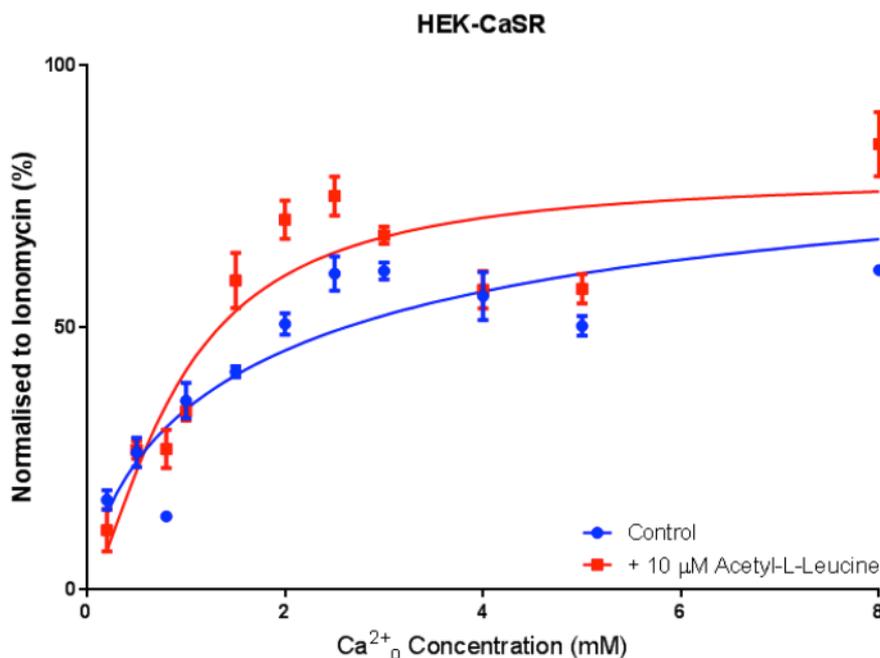
Figure 4.12. Acetyl-L-leucine increases intracellular Ca^{2+} elevation (when compared with untreated controls) via activation of CaSR at increasing extracellular Ca^{2+} concentrations. Human embryonic kidney (HEK) cells overexpressing CaSR (HEK-CaSR, (Ward et al., 2013)) were seeded into 96 well plates, either left untreated or treated with acetyl-L-leucine (10µM), and grown to confluence before being loaded with 2µM Fluo-4 for 30 minutes. Using a Fluoroskan Ascent plate reader, an initial baseline reading of 10 measurements was taken to determine the 0 second value. A Ca^{2+} solution that increased in Ca^{2+} concentration (0.2-10mM) was dispensed into a single well after 5 seconds. Emission at 538nm for each well was then followed for a further 25 seconds (1 reading every 5 seconds). Dose response curves were generated from the peak fluorescence upon the addition of the Ca^{2+} solution and corrected for the initial baseline measurement. Peak fluorescence was then normalized to the 10mM Ca^{2+} and 2µM ionomycin response to enable comparison between different plates. N=2. Experiments performed by the lab of Prof Riccardi. For control $R^2 = 0.7398$, for 10µM Acetyl-L-Leucine $R^2 = 0.7347$.

4.3.12 In a preliminary study, plasma sphingosine levels appear reduced post-tanganil treatment in NPC1 patient blood samples

Following the 2015 NPC1/Tanganil case study (Bremova et al., 2015), we received patient blood plasma pre- and post-Tanganil treatment, with the aim of performing lipidology for characteristic NPC lipids, and ELISAs for Ca^{2+}-modulators and other NPC biomarkers. It can be assumed that changes in Ca^{2+} within patients following treatment with acetyl-DL-leucine will be reflected by changes in lipids and Ca^{2+} binding proteins in the blood. Whilst more work is needed, we performed a preliminary experiment to measure levels of the NPC lipid sphingosine before and after treatment. This assay utilizes a modified version of the BCA assay, and Figure 4.13 indicates a reduction in patient plasma sphingosine levels following 4-week treatment with Tanganil. Whilst more experiments will need to be performed, this data, in combination with observations of benefits in cells (Figure 4.9 & 4.10), further highlights the potential benefit of Ca^{2+} modulation therapies for NPC.
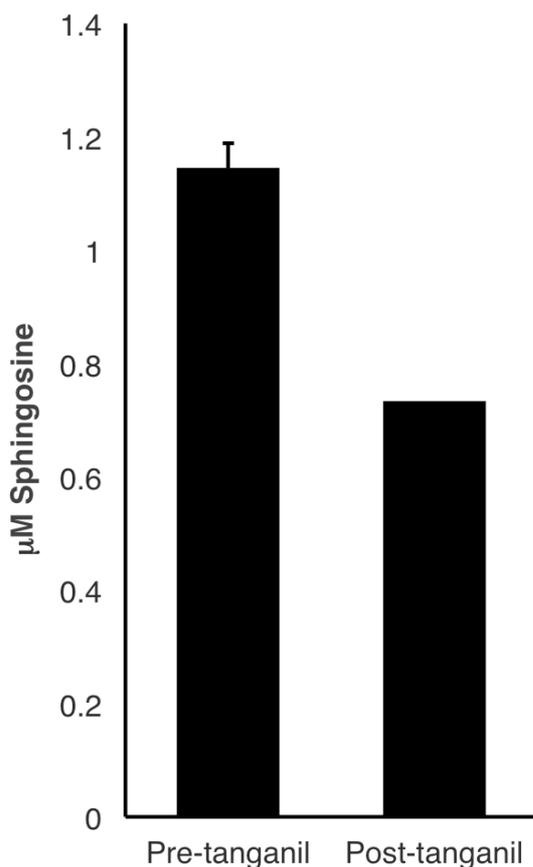
Figure 4.13. In a preliminary study, plasma sphingosine levels appear reduced post-tanganil treatment in NPC1 patient blood samples. Blood samples taken pre/post (4 weeks) Tanganil treatment during the 2015 NPC/Tanganil case study (Bremova et al., 2015) were analyzed for sphingosine levels (μM) using a modified version of the BCA assay, see materials and methods. N=2 for pre-Tanganil, 1=post-Tanganil.

Figure 4.14. Sagittal mouse brain sections taken from the Allen Brain Atlas shows high levels of CaSR RNA in the cerebellum. *Npc1*$^{+/+}$ (wild-type) mouse brain sections following in situ hybridization with an antisense probe for CaSR RNA (purple). A) Entire mouse brain, arrow points to the cerebellum, scale bar = 839µm. B) Zoomed in image of cerebellum showing staining within individual cells, scale bar = 200µm. Images obtained from Allen Brain Atlas (Casr – RP_050331_03_A12).

4.4 Discussion

4.4.1 Ca^{2+} modulators have varied effects on the *Npc1*$^{-/-}$ cellular phenotype

When investigating various Ca^{2+} modulators (CGS21680, δ-tocopherol, MLSA1 and Tanganil) for their effects on cytoplasmic and lysosomal Ca^{2+} levels as well as lipid storage within *Npc1*$^{-/-}$ glia, we discovered that depending on their mechanism of action, although all modulators elevate cytosolic Ca^{2+}, they have a diverse effect on NPC disease phenotypes.

Tanganil and MLSA1 both act by elevating cytosolic, rather than lysosomal Ca^{2+} directly (Figures 4.1, 4.2, 4.6 & 4.8). MLSA1 however, despite the increase in cytoplasmic Ca^{2+} seen, appears to increase storage of lipids within *Npc1*$^{+/+}$ and *Npc1*$^{-/-}$ glia (Figures 4.3 & 4.4). This can be explained because treatment with MLSA1 appears to reduce lysosomal Ca^{2+} in both *Npc1*$^{+/+}$ and *Npc1*$^{-/-}$ cells (Figure 4.2), and this likely worsens trafficking defects and explains increased lipid storage. Tanganil treatment however, whilst also causing a very slight reduction in lysosomal Ca^{2+} (Figure 4.8), is able to correct trafficking defects and partially reverse storage within *Npc1*$^{-/-}$ cells via elevation of cytosolic

Ca^{2+} (Figures 4.9 & 4.10). A potential reason why reduced lysosomal Ca^{2+} results in lipid storage in cells treated overnight with MLSA1 but not with Tanganil could be that with Tanganil, cytoplasmic Ca^{2+} elevation following CaSR activation results in CICR from intracellular stores such as lysosomes, which readily re-fill allowing signaling events. Treatment with MLSA1 however will lead to constant activation of the lysosomal Ca^{2+} channel TRPML1, leading to long-term lysosomal Ca^{2+} reduction, signaling problems and trafficking defects. This is confirmed by the presence of lipid storage in control cells treated with MLSA1 but not Tanganil (Figures 4.3 & 4.9). We confirmed the results of Shen *et al.,* 2012 that MLSA1 induces more Ca^{2+} release in *Npc1*$^{+/+}$ cells when compared to *Npc1*$^{-/-}$. However, unlike Shen et al., we believe this to be the result of the reduced lysosomal Ca^{2+} levels in NPC (Lloyd-Evans et al., 2008), which limits Ca^{2+} release following addition of MLSA1. Future work would involve looking at the effects of Tanganil on lysosomal Ca^{2+} in *Npc1*$^{+/+}$ cells, although, as no lipid storage is seen in *Npc1*$^{+/+}$ cells following treatment (data not shown), it is unlikely that tanganil induces a Ca^{2+} defect in *Npc1*$^{+/+}$ similar to that seen following treatment with MLSA1.

Interestingly, and as previously reported, CGS21680 appears to correct *Npc1*$^{-/-}$ cholesterol storage by increasing lysosomal Ca^{2+}, whilst having minimal effect on cytosolic levels, and δ-tocopherol appears to correct *Npc1*$^{-/-}$ cells by elevating both lysosomal and cytosolic Ca^{2+} (Figure 4.1). These findings confirm previous work (Lloyd-Evans et al., 2008, Visentin et al., 2013, Ferrante et al., 2016, Xu et al., 2012b) and demonstrate beneficial effects of Ca^{2+} modulators on cellular models of NPC.

The fact that different modulators, despite having similar effects on Ca^{2+} levels, can have very different effects within cells, suggests that more work must be done to further characterize Ca^{2+} dyshomeostasis within NPC1 and that multiple therapies must be investigated before deciding the best therapeutic option for NPC patients.

4.4.2 Despite claims by Shen *et al.,* treatment with MLSA1 appears to induce an NPC phenotype in *Npc1*$^{+/+}$ cells whilst exacerbating storage in *Npc1*$^{-/-}$ cells. Overexpression of TRPML1 in *Npc1*$^{-/-}$ glia also appears to increase storage.

Following overnight treatment with MLSA1 (10 or 30μM), we observe a reduction in lysosomal Ca^{2+} in both *Npc1*$^{+/+}$ and *Npc1*$^{-/-}$ glia (Figure 4.2). This most likely occurs following sustained lysosomal Ca^{2+} release from TRPML1 after treatment with its agonist, and following evidence that reduced lysosomal Ca^{2+} in *Npc1*$^{-/-}$ results in trafficking defects and lipid storage (Lloyd-Evans et al., 2008), this reduction could have negative effects on storage. Indeed, reduced lysosomal Ca^{2+} results in lipid storage in both cell lines as demonstrated by filipin staining for cholesterol (Figure 4.3) and TLC (Figure 4.4). We also investigated claims by Shen *et al.,* 2012 suggesting that overexpression of TRPML1 in *Npc1*$^{-/-}$ glia could reverse NPC cholesterol storage. Our results however suggest that overexpression in fact exacerbates

cholesterol storage (Figure 4.5). Above evidence combined, despite recommendations by Shen *et al.,* 2012 suggest MLSA1 is not a viable therapeutic option for NPC; if lysosomal Ca^{2+} is already reduced in NPC then clearly activating lysosomal Ca^{2+} release channels is not a viable treatment strategy as it reduces lysosomal Ca^{2+} even further.

4.4.3 Acetyl-DL-leucine (Tanganil) corrects *Npc1*$^{-/-}$ cellular phenotypes via elevation of cytosolic Ca^{2+}

During this study, we demonstrated how Tanganil is able to elevate cytosolic Ca^{2+} and reverse lysosomal storage within *Npc1*$^{-/-}$ cells via interaction with the GPCR CaSR.

When applied to *Npc1*$^{+/+}$ and *Npc1*$^{-/-}$ glia at various concentrations (1, 10, 30 and 100µM), Tanganil is able to elevate cytosolic Ca^{2+}, with 30µM releasing the most Ca^{2+}, followed by 10µM and finally 1µM (for *Npc1*$^{+/+}$ only, no elevation in *Npc1*$^{-/-}$ with 1µM). Treatment with 100µM, while resulting in cytoplasmic Ca^{2+} elevation, occurs to a lesser degree than at 30µM in both cell lines (Figure 4.6). This may occur following competitive inhibition for binding to receptors at higher concentrations, or potentially due to toxic effects of this drug at higher concentrations. Ca^{2+} elevation is significantly reduced when cells were imaged in Ca^{2+}-free HBSS when compared with Ca^{2+}-containing (Figure 4.6), suggesting to us that Tanganil acts via a mechanism that activates plasma membrane channels to elevate cytosolic Ca^{2+}, as oppose to inducing release from intracellular stores, as is seen with other Ca^{2+} modulators like curcumin (Lloyd-Evans et al., 2008). More Ca^{2+} release is observed in *Npc1*$^{+/+}$ cells when compared to *Npc1*$^{-/-}$ at comparable Tanganil concentrations (Figure 4.6). Tanganil likely invokes CICR from intracellular stores following initial elevation, and lower lysosomal Ca^{2+} in *Npc1*$^{-/-}$ could therefore explain the reduced response.

Having determined that Tanganil is able to induce Ca^{2+} influx within *Npc1*$^{+/+}$ and *Npc1*$^{-/-}$ glia, we wanted to find out how. Figure 4.12 demonstrates how Tanganil elevates cytoplasmic Ca^{2+} via interaction with the GPCR CaSR. As CaSR is known to be activated by extracellular Ca^{2+}, we utilized CaSR overexpressing HEK cells in a plate assay that looks at intracellular Ca^{2+} elevation at increasing extracellular Ca^{2+} concentration. We found that cells treated with 10µM acetyl-L-leucine show greater Ca^{2+} elevation when compared to untreated controls with increasing Ca^{2+} concentration (Figure 4.12). CaSR is a plasma membrane receptor reliant on extracellular Ca^{2+} to function, so if acetyl-L-leucine is acting via CaSR, this explains why Tanganil was unable to increase cytosolic Ca^{2+} in HBSS without Ca^{2+} (Figure 4.6).

As Tanganil consists of a mixture of D and L isomers, we next investigated whether the D or L forms were individually capable of elevating Ca^{2+} following treatment, and if so how this compared with elevation following addition of the mixed isomer (Figure 4.7). Within *Npc1*$^{+/+}$, the L isomer (acetyl-L-leucine) appeared wholly responsible for Ca^{2+} increase following addition of Tanganil, with acetyl-D-

leucine alone resulting in minimal, non-significant, Ca^{2+} elevation. This fits with previous evidence from studies into vertigo that L isomers work as the active isomer in Tanganil (Gunther et al., 2015). Within $Npc1^{-/-}$ cells however, both D and L isomers are capable of significantly elevating cytoplasmic Ca^{2+}, and the mixed isomer formulation (Tanganil) appears to have a synergistic effect regarding Ca^{2+} elevation. Differential effects of D, L and DL isomers in $Npc1^{-/-}$ when compared with $Npc1^{+/+}$ could be due to different membrane properties in NPC1 (Miersch et al., 2008), which could potentially have effects on channel gating or ligand binding to CaSR. Alternatively, differential expression of CaSR in $Npc1^{+/+}$ compared to $Npc1^{-/-}$ could affect Ca^{2+} elevation following addition of Tanganil, and future work could involve western blots of CaSR in $Npc1^{+/+}$ and $Npc1^{-/-}$ glia to investigate this. Whilst it's clear that further questions remain regarding interactions of the different isomers in the glial cell lines, as the mixed isomer formulation (acetyl-DL-leucine) appears induce the most Ca^{2+} release in $Npc1^{-/-}$ glia, this suggests current treatment with Tanganil would be more effective than treating with L or D isomers individually.

Figure 4.9 demonstrates how treatment with Tanganil is able to partially reverse lysosomal expansion (at 10 or 30μM) and cholesterol storage (at 30μM) phenotypes in $Npc1^{-/-}$ glia, although no correction is seen with 1 or 100μM. Co-treating $Npc1^{-/-}$ cells with 30μM Tanganil and the cytosolic Ca^{2+} chelator BAPTA-AM (10μM) however prevents any reduction in storage (Figure 4.10), demonstrating how correction occurs via Ca^{2+} modulating abilities (Figure 4.6). No phenotype is observed when treating $Npc1^{+/+}$ or $Npc1^{-/-}$ cells with BAPTA-AM alone (Figure 4.10), demonstrating how lack of correction when co-treating follows inhibition of correction by Tanganil rather than induction of storage by BAPTA-AM alone. Following this observation, lack of correction at 1μM likely occurs following a lack of Ca^{2+} elevation (Figure 4.6C), and 100μM Tanganil may be unable to correct storage following either toxic effects or competitive inhibition when using this compound at higher concentrations.

Alongside our *in vitro* studies investigating the mechanism of action of Tanganil on NPC, patient blood samples obtained pre- and post-Tanganil treatment during the 2015 case study by Bremova *et al.,* (2015) were analyzed for changes in the NPC storage lipid sphingosine (Figure 4.13); we observed reduced sphingosine in blood plasma following treatment. Although very preliminary (N=1), this data suggests that acetyl-DL-leucine is able to reduce lipid storage in NPC patients, presumably via modulation of Ca^{2+}. Future work will involve repeating this experiment on additional samples, as well as performing more lipidology, ELISAs for Ca^{2+} binding/modulating proteins (e.g. calbindin, calmodulin) and other known NPC biomarkers.

Finally, as acetyl-DL-leucine has been suggested to work specifically against the ataxic phenotypes present in NPC, and as ataxic phenotypes in this disorder occur following degeneration of cerebellar neurons, we compared Ca^{2+} elevation in $Npc1^{+/+}$ glia and an immortalized cerebellar granule

neuron cell line following addition of acetyl-DL-leucine (10μM) (Figure 4.11). We observed significantly more Ca^{2+} release in the cerebellar neuron cell line when compared with glia, suggesting that tanganil acts on a specific receptor with variable expression across the brain. Based on the Allen Brain Atlas, CaSR appears more highly expressed in the cerebellum when compared to other brain areas like the cortex (Figure 4.14). As cytosolic Ca^{2+} elevation following tanganil addition appears to correlate with CaSR expression levels, this strengthens our hypothesis that tanganil is acting via CaSR to elevate Ca^{2+} and reverse storage in NPC.

As the action of acetyl-DL-leucine on NPC may be limited by the expression pattern of CaSR, future work will involve investigating other Ca^{2+} modulators able to work on a greater number of cell types.

4.4.4 Limitations and future work

Having demonstrated beneficial effects of Ca^{2+} modulators on the NPC phenotype both *in vitro* and *in vivo* within human patients, this work highlights the need to investigate a plethora of Ca^{2+} modulators as treatments for NPC. Whilst exploring this new area of therapeutics, a variety of phenotypes, alongside cell-type specificity, must be considered when assessing benefit. Future investigations will involve looking at *in vitro* effects of previously investigated and novel drugs on known NPC storage molecules such as cholesterol, gangliosides BMP and Sphingomyelin alongside lysosomal expansion and trafficking phenotypes, to help us further our understanding of how these molecules work. TLC and electron microscopy can also be used to assess effects of Ca^{2+} modulators on storage. *In vivo* studies into the effectiveness of these drugs will also be undertaken in our zebrafish models of NPC1, which will be discussed in Chapter 5.

When investigating Ca^{2+} modulators, potential negative effects of Ca^{2+} overload must be examined. For example, elevated cytosolic Ca^{2+}, exceeding physiological levels, is known to promote neuronal cell death, and also appears to accelerate the generation and aggregation of β-amyloid in Alzheimer's (Qi and Shuai, 2016). As amyloid plaques are also seen in NPC (Yamazaki et al., 2001), this should be taken into account when investigating new therapies. Furthermore, excess Ca^{2+} signaling in the heart can effect function and potentially lead to cardiac failure (Vassalle and Lin, 2004).

Future work will involve further investigating the effects of tanganil on CaSR. Treating with agonists (calcilytics) and antagonists (calcimimetrics) of CaSR signaling (Breitwieser, 2012), both alone and in combination with tanganil, will allow us to fully characterize the interaction. Moreover, staining brain sections with anti-CaSR and looking at its expression pattern in glia compared with will allow us to determine the effectiveness of tanganil in the NPC brain. As discussed, future investigations into

tanganil will involve more thorough testing of patient blood samples for NPC biomarkers pre- and post-treatment.

4.5 Conclusions

Whilst further investigation is needed, Ca^{2+} modulating therapies show great promise as therapeutics for NPC disease. Despite this, not all molecules capable of elevating cytosolic Ca^{2+} act as effective treatments for NPC, and some may in fact worsen storage phenotypes (e.g. MLSA1). Furthermore, tanganil, whilst able to reduce lipid storage both *in vitro* and *in vivo* within human patients, may have only limited clinical benefit due to the variable expression pattern of its receptor, CaSR. Nevertheless, as tanganil appears to correct ataxic phenotypes within NPC patients via modulation of intracellular Ca^{2+} levels, Ca^{2+} modulation can be seen as a key therapeutic intervention point in NPC pathogenesis and further research in this area is vital to develop future NPC small molecule therapies.

Chapter 5: Generation of a NPC zebrafish colony for the purposes of phenotyping and future drug screening

5.1 Introduction

5.1.1 Animal models of NPC disease (excluding zebrafish)

Murine, feline, nematode worm, fly and yeast models of NPC disease have all been developed (Table 5.1). Species differences, in comparison to human patients, lead to different disease manifestation across models (Hemsley and Hopwood, 2010). Despite this, use of animal models has been shown to be vital regarding study of LSDs. For example, testing of HPβCD in both mouse (Griffin et al., 2004) and cat (Vite et al., 2015) models has highlighted its efficiency as a potential therapy for NPC disease, as well as potential side effects (Crumling et al., 2012, Vite et al., 2015, Ward et al., 2010). Positives and negatives of the existing NPC1 disease models can be seen in table 5.2.

Organism	Gene	Amino acid identity to human NPC1 (%)	Null mutant phenotype
Mus musculus (mouse) (Walkley and Suzuki, 2004, Stein et al., 2012)	*Npc1*	86	- Gastrointestinal, liver and respiratory dysfunction - Disease onset 4-5 weeks, death 10-12 weeks - Accumulation of gangliosides, neutral glycolipids and sphingosine in the brain - Accumulation of cholesterol, phospholipid (e.g. sphingomyelin) and glycolipids in the liver - Neurodegeneration (although without neurofibrillary tangles) - Small brain (less complex)
Felis catus (cat) (Walkley and Suzuki, 2004)	*Npc1*	91	- Neurological, gastrointestinal and liver dysfunction - Disease onset 8-12 weeks, death before 11 months - Ganglioside, neutral glycolipid and sphingosine accumulation in the brain - LacCer, GlcCer, phospholipid and cholesterol accumulation in the liver

Drosophila melanogaster (fly) (Huang et al., 2005, Fluegel et al., 2006)	dnpc1a	44	• Survive until first larval stage where they are unable to molt (live to adulthood with 20-hydroxyecdysone, cholesterol and 7-dehydroxycholesterol supplementation) • Experience accumulation of sterols in a punctate pattern throughout their bodies • Male infertility • No neurodegeneration
Caenohabditis elegans (nematode) (Sym et al., 2000)	ncr1	27	• Hypersensitive to cholesterol/progesterone deprivation • Slow late-stage embryogenesis • Arrested development at the dauer larvae stage
Saccharomyces cerevisae (yeast) (Walkley and Suzuki, 2004, Malathi et al., 2004)	ncr1	33	• No impact on viability • Missense allele in sterol-sensing domain confers accumulation of sphingolipids

Table 5.1 Model organisms used to study NPC. This table states gene name corresponding to human *NPC1* within each organism, amino acid sequence identity when compared with human *NPC1* and null mutant phenotypes. Adapted from Munkacsi *et al.,* 2007 (Munkacsi et al., 2007).

Organism	Advantages	Disadvantages
Mus musculus (mouse) (Hemsley and Hopwood, 2010)	• Mammal • Cheaper housing & easier breeding when compared with cats • Relatively easy to genetically manipulate	• Highly expensive to maintain when compared with non-mammalian models • Use of multiple $Npc1^{-/-}$ mouse strains displaying different genetic backgrounds across studies creates problems (different symptoms/times of occurrence) • Acute phenotype and short life-span
Felis catus (cat) (Hemsley and Hopwood, 2010)	• Mammal	• Large size limits where colonies can be established and makes them expensive to maintain

	• Large complex brain which, out of all the NPC models, appears most similar to humans • Greater longevity and genetic diversity allows for both study of later disease events as well as how genetic variation effects phenotype	• Low levels of breeding (het/het mating) results in restricted numbers of litters, and very long gestation time results in very few kittens • Heterogeneity provides problems when characterizing the model • Considerable ethical issues
Drosophila melanogaster (fly) (Pandey and Nichols, 2011)	• 75% of human disease-causing genes are believed to have a functional homolog in the fly (Reiter et al., 2001, Lloyd and Taylor, 2010) • Basic biological pathways conserved • Low maintenance costs • Suitable for high-throughput drug screening & toxicity testing • Numerous genetic manipulation techniques availaible • Rapid life cycle – single genetic mating can produce hundreds of genetically identical offspring within 10-12 days • Simple behavioral testing • Conserved neurotransmitter pathways	• Not a mammal • BBB permeability differences (Stork et al., 2008) • The most high-throughput mechanism of drug-delivery is within food – and this may cause problems regarding drug action, absorption, variability of dosage • Considerable differences between human and fly brain, eye, immune system, heart
Caenohabditis elegans (nematode) (Pandey and Nichols, 2011)	• Rapid life cycle (~4 days) • Prolific • Highly amendable to genetic manipulation • Transparent throughout its lifecycle	• Not a mammal • Fewer gene homologs in mammals when compared with other models (except yeast), and some families display no homologs at all (Rikke et al., 2000)

	• Suitable for high-throughput drug screening	• No sophisticated immune system/heart/reproductive system/centralized brain • Only very simple behavioral tests can be performed
Saccharomyces cerevisae (yeast) (Stork et al., 2008, Botstein and Fink, 2011)	• Eukaryote • Cost effectiveness • Availability • Reproducibility • Ease and safety of handling • Ease of genetic manipulation • Yeast *NPC1* analog ncr1 rescues function in mammalian *Npc1*$^{-/-}$ null cells (Malathi et al., 2004)	• No nervous system • No lysosomes • Unicellular

Table 5.2 Advantages and disadvantages of model organisms used in the study of NPC. BBB = blood brain barrier.

5.1.2 Zebrafish as a model organism

Zebrafish are becoming increasingly employed throughout the fields of embryogenesis and disease modeling (Wager and Russell, 2013). This follows from several useful properties of this model organism. For one, zebrafish can produce ~300 eggs per breeding, with embryos developing externally to the mother and remaining optically transparent. The ease at which zebrafish can be bred to produce large amounts of embryos greatly reduces cost and increases speed when comparing with mammalian systems, whilst transparency allows for ease when imaging fluorescent probes or GFP expression following genetic manipulation. Rapid development is also observed, with neurogenesis commencing ~10 hours post fertilization (hpf) (Kabashi et al., 2011), synaptogenesis at ~16hpf (Kabashi et al., 2011), advanced brain development seen at 24hpf (Kimmel, 1993), and complete morphogenesis by 3dpf (Kimmel et al., 1995). Rapid, external development seen with this organism means that disease phenotypes tend to manifest in the larval stages, often by 4-5 days post fertilization (dpf), allowing data to be collected quickly.

Widespread use of this model organism prompted whole genome sequencing, with this information now being easily accessible on bioinformatics databases. Sequencing demonstrated how most zebrafish genes share 50-80% sequence identity with their human counterparts (Kabashi et al., 2011), and consequently further validated the use of zebrafish as a model for human diseases. High

amino acid conservation can also be seen across these species, especially within functional domains of proteins (Kabashi et al., 2011) .

High throughput drug screening is also highly amenable to the zebrafish system following the ease of mass maturing embryos in separate wells of a 96 well plate. Pharmacological modulators can be added to the fish water in order to efficiently develop and screen candidate drugs, as well as to perform toxicity tests, *in vivo*. Furthermore, zebrafish are capable of complex behaviors, relevant to humans, which can be used to both characterize disease models and test response to therapy. These behaviors include spontaneous tail coiling, which begins at 17hpf; touch response, which begins at 21hpf and finally the first swimming behavior at 27hpf (Brustein et al., 2003).

Considering above points, zebrafish appear highly favorable regarding study off and development of therapies for genetic diseases.

5.1.3 What molecular tools are available to manipulate the zebrafish genome?

Another reason justifying the use of *Danio rerio* when studying genetic disease is the wide variety of molecular tools available to manipulate their genomes. These techniques include transient knockdown technology using morpholino oligonucleotides (MOs), forward genetic screens invoking N-ethyl-N-nitrosourea (ENU), reverse genetic screens based on Targeting Induced Local Lesions IN Genomes (TILLING), and finally reverse genetic techniques that induce specific and permanent genetic knockdown using zinc finger nucleases (ZFN), transcription activator-like effector nucleases (TALEN) and finally the clustered regularly interspaced short palindromic repeats (CRISPR)/Cas system (Wager and Russell, 2013).

5.1.3.1 Morpholino oligonucleotides (MOs)

A commonly used method of knockdown explored in zebrafish utilizes MOs. These antisense oligonucleotide analogs bind to complementary RNA sequences in order to block translation of a target gene (Morcos et al., 2008). MOs are injected at the 1- to 4-cell embryos and become evenly distributed throughout the embryo as it develops, producing a morphant (Morcos et al., 2008). Two types of MOs are used. Ones designed to target the ATG start codon and therefore prevent progression of the initiation complex (Bill et al., 2009), and ones that target intron/exon boundaries therefore resulting in either splice variants lacking specific domains within proteins of interest or else introduce a frame-shift, thereby producing an in-frame stop codon (Draper et al., 2001). Those targeting intron/exon boundaries do not affect the maternal transcript, thereby providing an advantage when examining a target gene that presents with a maternal function (Bennett et al., 2007).

Whilst transient knockdown using MOs acts as a powerful technique, one disadvantage lies in the fact that MOs become more and more dilute as the embryo grows, and therefore they can only act for a few days (up to ~5dpf)(Wager and Russell, 2013).

5.1.3.2 Controls for MO specificity

MO specificity can be assessed using a BLAST search of the target genome. This method helps ensure that no single-nucleotide polymorphisms or sequence errors in the reference sequence are present (Wager and Russell, 2013). Following knockdown, consequent reduction in protein expression must be validated. When using start-codon directed MOs several mechanisms can be employed, although most display difficulties (Eisen and Smith, 2008). Whole-mount immunohistochemistry can be used when an antibody is available which both binds to the protein of interest and is reactive against zebrafish *in vivo* (Wager and Russell, 2013). Western blotting is another common method used to confirm knockdown, although large amounts of material may be required (Wager and Russell, 2013). A final way of confirming successful start codon blocking MO action utilizes co-injection of GFP-tagged mRNA for the transcript of interest (Yang et al., 2001). Less fluorescence tends to suggest successful knockdown, although an assumption is made regarding accessibility of the endogenous mRNA to the MO (Wager and Russell, 2013). On the other hand, when using splice-blocking MOs, missplicing can be easily confirmed using RT PCR and sequencing of the spliced product (Wager and Russell, 2013).

Various controls can be performed to ensure that phenotypes observed in the morphant are not due to off-target effects. These controls include injection of nonsense oligos, injection of a sense version of the experimental oligo and injection of a mismatched oligo. None of these pseudo MOs will bind the target sequence, and therefore any effect observed can be considered non-specific. Furthermore, observing identical effects when using a variety of morpholino types against the same target gene (i.e. translation and splice blocking oligos) indicates specificity. Looking for off-target effects may also involve rescue experiments whereby a wild-type mRNA off your protein of interest is co-injected alongside your MO. Problems with this method however include knockdown of the mRNA by the MO, incorrect translation of the mRNA and ectopic expression of the mRNA. Potential solutions include engineering mRNA transcripts that include mismatches to prevent binding to the MO, or alternatively, splice site directed MOs might be used, which do not recognized spliced mRNA (Wager and Russell, 2013).

Testing for specificity is highly important as non-specific effects often include neurodegeneration, widespread cell death, and epibolic failure. All of the above can greatly hinder accurate identification of specific knockdown phenotypes. As these non-specific events usually occur

following inactivation of p53, co-injection of an anti-p53 MO alongside MO of interest allows us to control for these events (Bedell et al., 2011).

5.1.3.3 Other techniques utilized to manipulate the zebrafish genome

Forward genetic screens using ENU can also be used to manipulate the zebrafish genome. This chemical induces numerous point mutations within the germ line of male fish. Following one generation of out crossing and two generations of in crossing to produce homozygotes for each mutation, transparent zebrafish embryos can then be screened for phenotypes of interest (Lieschke and Currie, 2007). In addition to forward screens, reverse genetic screens are utilized which make use of TILLING. This technique invokes random mutagenesis within numerous zebrafish embryos, prior to sequencing for mutations in a specific gene within individual fish (Vettori et al., 2011, Moens et al., 2008). This allows detection of mutations that may only produce subtle phenotypes, and mutations are then isolated by out-crossing the single fish.

Reverse genetic techniques, such as ZFN and TALEN, are able to produce permanent genetic knockdown within a gene of interest. ZFNs consist of multiple Cys_2His_2 zinc finger proteins, bound to a type IIS Fok1 endonuclease. Each zinc finger can specifically recognize a 4 base pair DNA sequence via an α-helical domain, and joining of several of these proteins allows for site-specific recognition. Following binding to the sequence of interest, cleavage is initiated by the linked endonuclease, creating a double strand break. Finally, eukaryotic repair mechanisms often initiate non-homologous end joining (NHEJ), resulting in either loss or gain of a small amount of sequence, and often a frameshift allele (Urnov et al., 2005). ZFNs do present with some specificity issues however, and not all sequences can be targeted (Wager and Russell, 2013).

Considering the above disadvantages, TALEN represents a more predictable and specific approach when compared with ZFNs (Boch and Bonas, 2010). These molecules consist of a transcription activator-like effector, which can be engineered to specifically bind any sequence, attached to a FokI endonuclease. Whilst the Fok1 endonuclease can be used to introduce knockout similarly to ZFNs (Sander et al., 2011), TALENs can also be used to knockin specific sequences at the predefined locus. This is achieved via exogenously added DNA, which is then used as a template for NHEJ (Bedell et al., 2012).

The CRISPR/Cas system was developed from an adaptive immune response found in bacteria and viruses. Here, this system acts to protect the organism's genome from invading viruses and plasmids. CRISPR/Cas induced knockout relies on the injection of multiple guide RNAs that bind to complementary sequences at a target site. Next, co-injection of guide RNAs linked to a Cas nuclease

results in a combination of targeted deletions, inversions and translocations. Knockins can also be introduced using this system, similarly to with TALEN (Ota et al., 2014).

5.1.4 Zebrafish models of neurodegenerative disease

Several observations have prompted the use of zebrafish for the study of neurological disease. For one, the zebrafish brain possesses many similarities when compared with humans. A telencephalon, diencephalon, mesencephalon, metencephalon, and myelencephalon (Kimmel, 1993) can all be observed alongside cell types such as astrocytes (Grupp et al., 2010), oligodendrocytes (Yoshida and Macklin, 2005), and microglia (Svahn et al., 2013, Cuoghi and Mola, 2007). Neurons also display a similar structure across the species, with soma, dendrites, and an axon, which can be either myelinated or unmyelinated. Zebrafish also develop a BBB at 3dpf with similar properties to the human equivalent (Jeong et al., 2008), allowing studies into delivery of drugs to the brain. The zebrafish CNS also displays many structural similarities to mammalian systems, further justifying the use of this model. Conserved structures include the cerebellum, optic tracts and tectum, medulla, hypothalamus and cranial nerves (Sager et al., 2010). Finally, the main neurotransmitter systems involving acetylcholine, dopamine, gama-aminobutyric acid, glycine, glutamate, noradrenaline, and serotonin are all present within zebrafish (Best and Alderton, 2008). Following above advantages, zebrafish have previously been used to model numerous neurological diseases including Parkinson's, Huntington's, Alzheimer's (Xi et al., 2011) and NPC (Schwend et al., 2011, Louwette et al., 2013).

5.1.5 Zebrafish models of NPC1

Previously, two groups have made use of morpholinos to generate models of NPC1 disease. The first study, published by Schwend *et al.,* 2011, aimed to decipher the function of *npc1* during development. Firstly, they found that Zebrafish *npc1* (60% identity and 66% sequence similarity to humans) is widely expressed during early embryonic development, with knockdown leading to expected cholesterol mislocalization, an abnormal actin cytoskeleton, and delayed epiboly phenotypes. Epiboly presents as one of the earliest morphogenic movements of gastrulation, enabling development of the embryos complex body plan (Hsu et al., 2002). Cholesterol has a key role promoting cell migration at this stage, and therefore low bioavailability of this lipid following *npc1* knockdown may underlie the observed epiboly defect. Finally, this study demonstrated how the *npc1* zebrafish morphant can be rescued by injection of mouse *Npc1* mRNA at either the one cell stage or into the yolk of a 1000 cell stage embryo,

indicating the specificity of this morpholino. In addition, this rescue experiment further indicates cross species conservation of the NPC1 protein.

A second study performed by Louwette *et al.,* 2013 aimed mainly to investigate hematopoietic NPC phenotypes within MO treated zebrafish embryos. Within human patients, coagulation and platelet changes, thrombocytopenia, anemia and petechial rash have been described (Del Principe et al., 1971, Spiegel et al., 2009). Complications such as red blood cell abnormalities, abundant ghost erythrocytes in addition to aberrations in white blood cells such as cytoplasmic granulation and neutrophil hyper-segmentation, that included lymphopenia and atypias, can also be observed within the *Npc1*$^{-/-}$ mouse (Parra et al., 2011). By creating *npc1* transient knockdown zebrafish using MOs and performing flow cytometry and real-time quantitative polymerase chain reaction (QPCR) experiments, hematopoietic phenotypes such as thrombocytopenia and mild anemia were also confirmed within zebrafish, further justifying this model as an accurate representation of human NPC disease. This study also confirmed accumulation of free cholesterol within the morphants via filipin staining, whilst determining high levels of NPC1 expression within the developing brain, eyes, and yolk syncytial layer (YSL) of the embryos. The MO generated knockdowns in this study displayed malformed heads and dysmorphic brain and eyes, accompanied by increased apoptosis in these regions.

These studies demonstrated characteristic *npc1* knockdown phenotypes within zebrafish, as well as potentially providing us with predesigned MOs, able to induce NPC disease with no reported off-target effects. However, neither study fully characterized the NPC1 morphant: no behavioral testing was performed and only cholesterol accumulation was reported.

5.1.6 Zebrafish lipidology

Numerous aspects of lipid biology in zebrafish are conserved in humans. This includes both a similar lipid profile and homologous genes involved in lipid metabolism (Fraher et al., 2016).Fraher *et al.,* 2016 demonstrated how 0 hpf zebrafish contain all the major lipids known to be important in human development including cholesterol and cholesterol esters, phospholipids and lysophospholipids, sphingolipids including sphingomyelin and ceramide, and ganglioside GM3. Many of these lipids are known to be stored within NPC (Lloyd-Evans et al., 2008, te Vruchte et al., 2004), and their presence is therefore important when looking to develop a zebrafish model for this disease.

Alongside these lipid species, expression of numerous genes known to be important in lipid signaling and metabolism in humans can be seen in the developing zebrafish (Fraher et al., 2016). These genes include those required to produce the sphingosine-1-phosphate receptor (Kupperman et al., 2000). Disrupted sphingosine signaling is an important NPC cellular phenotype (Lloyd-Evans et al.,

2008), and the presence of its receptor suggests that signaling pathways associated with sphingosine are present in the zebrafish, further demonstrating the benefits of this organism as a model for NPC. Furthermore, cholesterol synthesis enzymes such as HMG CoA reductase have also been identified within the zebrafish (Li et al., 2001), suggesting conserved lipid biosynthesis pathways.

Finally, work by Schwend *et al.,* 2011 and Louwette *et al.,* 2013 demonstrated how filipin staining for cholesterol resulted in a punctate distribution in *npc1*-morphant fish, compared with a disperse staining pattern in wild-types, suggesting that NPC disease zebrafish display lysosomal cholesterol storage, similarly to NPC patients and mice (Lloyd-Evans et al., 2008, te Vruchte et al., 2004). It is of considerable interest, bearing in mind the usefulness of zebrafish as a drug-screening tool, to determine whether *npc1*-morphant zebrafish phenocopy human NPC disease with respect to the accumulation of other lipids and behavioral abnormalities, which would provide an amenable animal model for high-throughput drug screening in this disease.

5.1.7 Drug screening strategies

As previously discussed, zebrafish are highly amenable to high throughput drug screening. Chemical suppression screens can be implemented following characterization of disease phenotypes within morphants. Screening protocols involve arraying embryos within individual wells of a 96-well plate prior to addition of a multitude of promising therapeutics. Following treatment, severity of morphant phenotype can be assessed, and any drugs that appear to provide benefit can then undergo further validation using dose and toxicity assessments (Lieschke and Currie, 2007). With these high throughput screens, no presumptions are made regarding specific molecular mechanisms. This means that previously unsuspected proteins or pathways can potentially be identified as drug targets (Lieschke and Currie, 2007). Given the currently unknown and controversial function of the NPC1 protein, this characteristic provides key benefits when studying NPC disease.

5.1.8 Inhibiting lysosomal Ca^{2+} release via TPCs using an inhibitor of NAADP signaling: Ned-19

As previously discussed, NPC cells display a lysosomal Ca^{2+} defect, resulting in endocytosis defects and lipid storage (Lloyd-Evans et al., 2008). Under normal circumstances, voltage-gated TPCs release Ca^{2+} from lysosomes in response to the second messenger NAADP (Morgan et al., 2015b). The resulting cytosolic Ca^{2+} elevation drives numerous physiological events including cellular differentiation, muscle contraction, endothelial cell activation, membrane trafficking, autophagy, nutrient sensing, exocytosis, angiogenesis, fertilization & embryogenesis and cytokinesis (Morgan et al., 2015b).

In 2009, Naylor *et al.,* utilized virtual screening to identify a chemical probe for NAADP, known as Ned-19, able to block NAADP signaling at nanomolar concentrations. The screen was performed using the ZINC database searching for compounds with similar 3-dimensional shapes and electrostatics to NAADP. Ned-19 is also auto-fluorescent, allowing fluorescent imaging of the NAADP receptor (Naylor et al., 2009). Less Ca^{2+} release is observed in NPC cells compared with wild-type following addition of Ned-19 (Lloyd-Evans *et al.,* unpublished observation), presumably due to reduced acidic compartment Ca^{2+} levels in NPC (Lloyd-Evans et al., 2008). Furthermore, by treating with this compound, it is possible to block lysosomal Ca^{2+} release, therefore inducing an NPC-like phenotype and lipid storage within wild-type cells (Lloyd-Evans *et al.,* unpublished observation). NPC1 phenotypes can also be induced using U18666A (Lu et al., 2015) and 1NMP (Schumacher et al., 2006, Lomovskaya et al., 2001, Renau et al., 1999) (see Chapter 1).

5.1.9 Aims

This chapter sought to generate, characterize (both behaviorally and biochemically) and compare drug-induced zebrafish models of NPC1 and *npc1*-morphants generated following morpholino microinjection, with the aim of testing previously investigated and novel NPC therapies. Furthermore, by treating fish with the inhibitor of NAADP signaling, Ned-19, we aimed to characterize the importance of the NPC lysosomal Ca^{2+} defect *in vivo* using imaging methods not possible with mouse models.

5.2 Materials & Methods

Unless otherwise stated, all reagents were from Sigma-Aldrich. Any methods used in this chapter and not described here can be found in the general materials and methods section (Chapter 2).

5.2.1 Establishment and maintenance of the zebrafish colony

Zebrafish (Tubingen) were purchased from UCL and were reared at 28.5 ± 0.5°C on a 14 hour light, 10 hours dark cycle to mimic the natural zebrafish environment. Following adult breeding, the embryos produced were incubated in the dark at either 28°C or 31°C, depending on the desired speed of development, in 'embryo water' containing 0.06mg/ml Instant Ocean Salts (Amazon) in distilled water and methylene blue (anti-fungal, 0.0002%). Where required developmental staging was carried out according to Kimmel *et al.* (Kimmel et al., 1995). All procedures were performed in accordance with the UK Home Office Animals Scientific Procedures Act (1986).

5.2.2 Inducing NPC in zebrafish embryos using either U18666A, 1NMP or Ned-19

U18666A, 1NMP and Ned-19 are all known to induce an NPC-like phenotype in cells (for more information on U18666A and 1NMP, see general methods section (Chapter 2)). Ned-19 acts as an inhibitor of NAADP signaling (Naylor et al., 2009). 6hpf zebrafish were arranged at 25 embryos per well in a 24-well plate prior to treatment with 1µg/ml U18666A, 300µM 1NMP or 100µM Ned-19 in embryo water. DMSO controls were also performed. Drug treated and untreated embryo water was refreshed daily.

5.2.3 Light microscopy imaging of zebrafish

For live imaging of morphology, larvae were anesthetized with MS222 (0.016% w/v). For both live and fixed imaging, embryos were visualized using a SZMN light microscope with a Watec camera and Debut software.

5.2.4 Behavioral testing in zebrafish: spontaneous coiling and touch response

Spontaneous coiling and touch response represent two complex behaviors of the zebrafish that can be analyzed to assess both disease phenotypes and response to treatment. These motor behaviors demonstrate the development of locomotor networks in the zebrafish brain and spinal cord (Brustein et al., 2003).

Spontaneous coiling in zebrafish consists of spontaneous alternating side-to-side contractions of the trunk generated by their limited electrically coupled spinal network (Brustein et al., 2003). These movements begin at 17hpf, peak in frequency by 19hpf and then progressively decline over the course of 6-7 hours (Brustein et al., 2003). At either 24 or 48hpf, 3 minute videos were taken of control, drug-treated, or morpholino injected embryos (~15-30 embryos per video) using light microscopy (see 5.2.3) and number of coils per embryo was recorded.

Touch response behavior begins at 21hpf, with embryos responding to touch with vigorous coiling (Brustein et al., 2003). This behavior is dependent on interactions between the developing zebrafish hindbrain and spinal cord, and by 27hpf, it extends to the embryos swimming off at speed following contact (Brustein et al., 2003). Videos of 4 embryos per condition (either control, drug-treated, morpholino) were taken at both 48hpf and 72hpf. Time taken (frames per second, FPS) for the embryo to leave the screen following contact was recorded.

5.2.5 Fixation of zebrafish

5dpf zebrafish were transferred to labeled eppendorfs prior to addition of the anesthetic MS222. The MS222 was then removed and embryos were washed twice in 1ml PBS. 1ml of 4% PFA was then added to each tube before leaving embryos overnight. The next day, 3 washes in 1ml PBS was performed and embryos were stored at -4°C ready for either fixed staining and imaging or biochemistry.

5.2.6 Homogenization of zebrafish

Excess PBS was removed from the fixed zebrafish embryos (or whole zebrafish brain, removed using a scalpel and forceps) and the eppendorfs were dropped into liquid N_2 for 1 minute. Embryos were then fished out using pliers and transferred from the eppendorf into a pestle and mortar, where they were crushed into a powder. 250µl dH_2O was then added to the pestle, and the entire mixture was transferred to a dounce homogenizer where it was further homogenized using 15 strokes. Samples were then transferred to new eppendorfs and stored at -80°C ready for biochemistry.

5.2.7 Alkaline hydrolysis TLC to analyze lipid content of drug treated embryos

Protein content of the homogenized embryos was determined using the BCA assay (see general methods, chapter 2) prior to lipid extraction (Chapter 2) in conjunction with alkaline hydrolysis to remove phospholipids (Brockerhoff, 1963). Alkaline hydrolysis is required when performing TLC on zebrafish embryos as high levels of phospholipid within the samples form multi-vesicular bodies that proceed to disrupt the running of the sample up the silica plate. Unfortunately, this process also reduces levels of other lipids within the sample (e.g. sphingomyelin), therefore hindering our ability to accurately measure all NPC storage lipids. Alkaline hydrolysis was performed by adding 0.2M KOH to the standard lipid extraction mixture (see general methods) and incubating for 2 hours at 65°C (Weber et al., 2002). Following lipid extraction and hydrolysis, TLC was performed as described in general materials and methods (65:25:4 mobile phase). The TLC was then analyzed using ImageJ software and quantified using known amounts of each lipid present within the standard lane to determine concentrations (mg/ml) of a variety of lipids within the embryos.

5.2.8 Biochemical assays for sphingomyelin and acid sphingomyelinase activity on 5dpf zebrafish embryos

Sphingomyelin and acid sphingomyelinase assays were performed using an amplex red sphingomyelinase assay kit (Invitrogen), as per manufacturers instructions, on homogenized 5dpf zebrafish embryos. When measuring levels of sphingomyelin in samples, bacterial sphingomyelinase

was added, along with a pH7 buffer, however no endogenous sphingomyelin was added. When measuring acid sphingomyelinase activity, 5mM endogenous sphingomyelin was added alongside a pH5 buffer with no bacterial sphingomyelinase.

5.2.9 Cryosectioning of 5dpf zebrafish embryos

Fixed embryos were cryoprotected in 30% (w/v) sucrose in PBS at 4°C overnight or until sunk. All samples were embedded in TissueTek (Bayer) and lowered slowly into isopentane cooled with dry ice. Embryos were then stored at -80°C prior to sectioning. 12µm sections were taken using a Bright 5000 cryostat onto X-tra adhesive slides (Surgipath), which were air-dried and stored at -80°C until stained.

5.2.10 Staining cryosections with fluorescent lipid probes filipin and FITC-CtxB

For more information on filipin staining for cholesterol and FITC-CtxB staining for ganglioside GM1, please see general methods section (Chapter 2). Sections were removed from the -80°C freezer and left to defrost for 30 minutes prior to use. Next, a 1mm Edge hydrophobic barrier PAP pen (Vector labs) was used to draw around individual sections prior to 3 x 5 minutes washes with PBS-T (PBS + 0.1% triton).

For imaging cholesterol, we then applied a 187.5µg/ml solution of filipin (stock was made up in PBS-T with 5% FBS and 1% BSA) to each section for 45 minutes at room temperature in the dark.

For imaging ganglioside GM1, following the 3 initial PBS-T washes, a blocking solution (1% BSA in PBS-T) was applied for 30 minutes at room temperature prior to overnight incubation with 2.5µg/ml FITC-CtxB.

Sections were then washed 3 x 5 minutes to PBS-T before being mounted onto a coverslip using mowiol (Calbiochem), and left to dry and store at room temperature in the dark until visualized using a Leica DM2500 microscope.

5.2.11 Morpholino oligonucleotide (MO) knockdown

An ATG (start codon blocking) MO (5'-TGTGGTTTCTCCCCAGCAGAAGCAT-3'), already known from previous studies to successfully knock-down *npc1* in zebrafish (Louwette et al., 2013, Schwend et al., 2011), was ordered from GeneTools, LLC and dissolved in 300µl ddH$_2$O to generate a 1mM stock solution.

Glass needles were pulled from borosilicate glass capillary tubes, 1.0mm O.D. x 0.58mm I.D. (Harvard Apparatus) using a flaming/brown micropipette puller (Sutter Instrument Co)(Heat 546, Pull 85, Velocity 85, Time 200).

Morpholino working solutions were made in 1X Danieau's solution (see table 5.1) plus 1% phenol red (to allow visualization of injected solution), whilst injected control solutions contained Danieau's plus 1% phenol red only.

Needle tips were clipped using forceps under a light microscope (SZMN) prior to backloading with 4µl of either MO or control solution and insertion into a three-axis micromanipulator (UM-1PF, UM-3C, Narishige). To improve reproducibility, needle calibration was performed prior to MO injection. To calibrate the amount of MO solution injected, a drop of mineral oil was placed on a microscope graticule and MO injected into the oil. The pulse duration was adjusted such that each injection delivered a sphere of the desired diameter. Since the concentration of the MO is known, the amount delivered per volume can be calculated.

Approximately 40 embryos were arrayed for injection by lining them up against a microscope slide placed in a petri dish. This prevents the embryos from rolling and rotating during injections and maintains them in enough embryo water to prevent dehydration. Embryos were injected into the yolk cytoplasmic stream of 1-2 cell stage embryos using a pico-liter injector (PLI-10, Warner instruments) and then maintained at 28°C prior to examination.

Reagent	Amount per 1 litre	Concentration
NaCl	101.7g	1740mM
KCl	1.56g	21mM
$MgSO_4 \cdot 7H_2O$	2.96g	12mM
$Ca(NO_3)_2$	4.25g	18mM
HEPES buffer	35.75g	150mM

Table 5.3. Composition of 30X Danieau's microinjection solution.

5.2.12 Lightsheet microscopy

Imaging of fluorescent probes on whole live or fixed 5dpf zebrafish embryos utilized a ZEISS Lightsheet Z.1 microscope as per manufacturer's instructions. Prior to lightsheet microscopy, whole live embryos were washed twice in PBS prior to staining with either lysotracker green for lysosomes (10µM, see general methods) or Rhod-2AM (Excitation/emission = 552/581nm) for Ca^{2+} imaging, followed by a further 2 PBS washes and live imaging. For Rhod-2AM, a small volume of 1mM probe was microinjected into zebrafish brains as previously described (Brustein et al., 2003).

The Lightsheet Z.1 allows high temporal resolution imaging of optical sections within large samples, and results in virtually no phototoxicity or bleaching. Light sheet fluorescence microscopy works by splitting fluorescence excitation and detection into two separate light paths, with the axis of illumination perpendicular to the detection axis. This allows illumination of only a thin section of your sample at any time, therefore generating an inherent optical section by exciting only fluorescence

from the in-focus plane. Light from the in-focus plane is then collected on the pixels of a camera, rather than pixel by pixel (e.g. with confocal or other laser scanning microscopy). Parallelization of the image collection on a camera-based detector increases the speed of image acquisition and reduces the amount of excitation light required when compared with many other microscopy techniques (Lim et al., 2014).

5.3 Results

5.3.1 TLC reveals a similar lipid profile in wild-type zebrafish compared with humans, whilst demonstrating increased NPC lipids in 1NMP and U18666A treated embryos

In order to determine whether or not adult wild-type zebrafish brains produced the lipids known to be stored in NPC patients, an adult zebrafish was sacrificed, its brain removed and homogenized and lipids were extracted for TLC analysis. As can be seen in Figure 5.1 A, with increasing amount of protein in the zebrafish sample, we get increased lipid as expected. Comparison with lipid standards shows the presence of NPC lipids cholesterol, ceramide, GM3, phospholipids, neutral lipids, GM1 and sphingomyelin within the wild-type zebrafish brain. However, GlcCer, GalCer (galactosylceramide), LacCer and BMP were not detected. If these lipids are not present within zebrafish brains, this is unfortunate as these lipids are stored in NPC humans and measuring changes in levels in response to drug treatment of zebrafish embryos would be useful for future studies. Alternatively, very low levels of these lipids within the zebrafish brain may prevent detection via TLC: as is demonstrated in Figure 5.1 B where small amounts of GlcCer and LacCer were detected within wild-type embryos, although this could also be due to different expression of lipid metabolic and catabolic enzymes during zebrafish development.

Having observed that wild-type zebrafish appear to have a similar lipid distribution to humans, we next sacrificed, homogenized and extracted lipids from zebrafish embryos that had either been left untreated or treated with 1NMP to induce an NPC phenotype. In order to prevent interference from high levels of phospholipid (which alters separation of lipids as they run up the silica plate) an alkaline hydrolysis TLC was performed on the samples. A graph summarizing levels of key lipids is shown in figure 5.1 B. As expected, treating zebrafish embryos with 1NMP induced storage of lipids also known to accumulate in NPC humans and mice. Within wild-type embryos, cholesterol represents the most prevalent lipid, and 1NMP treatment slightly increases levels by ~1mg/ml. GlcCer, sphingosine and GM3 all show very low levels within untreated wild-type embryos (see figure 5.2 A), with at least a 4-fold increase following treatment with 1NMP. Sphingosine in fact demonstrates the

greatest fold elevation when compared with all lipids examined. GM1 can be seen at ~2mg/ml within wild-type fish, and increases 4-fold following inhibition of NPC1. Other lipids appear to decrease following treatment of zebrafish embryos with 1NMP: namely ceramide (~50% decrease) and LacCer (~20% decrease).
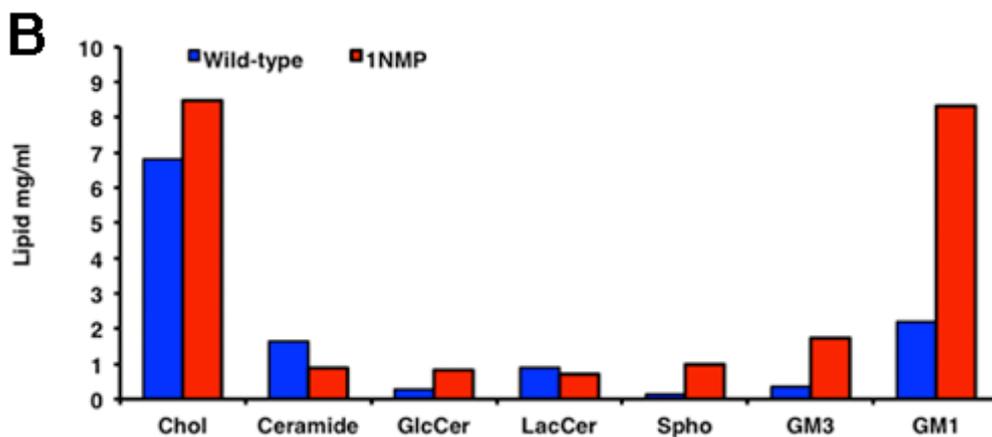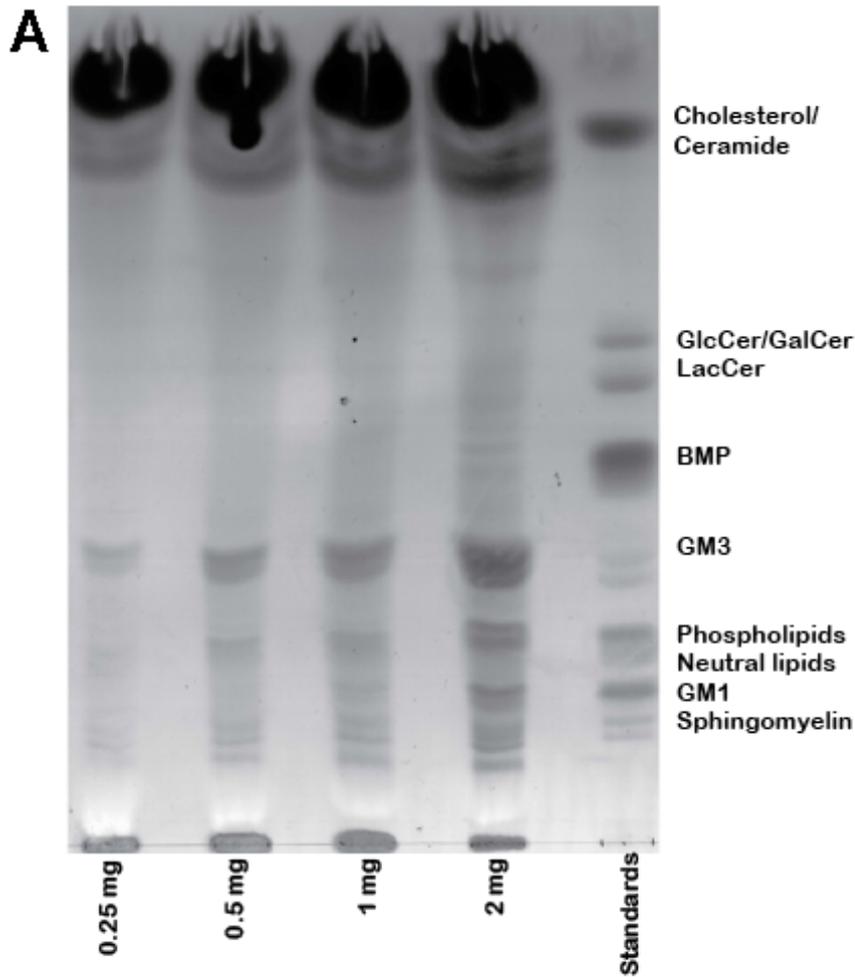
Figure 5.1. Zebrafish contain comparable lipids to humans, and lipids stored in NPC humans increase following treatment of zebrafish embryos with the npc1 inhibitor 1NMP. Thin layer chromatography (TLC) was used to analyze lipid content either within the adult zebrafish brain (A – TLC plate shown) or within 5dpf zebrafish embryos treated with 300μM 1NMP (1-naphthyl-methylpiperazine) (B – graph comparing lipid levels (mg/ml) in untreated wild-type (blue) and 1NMP treated (red) embryos). Chol = cholesterol, GlcCer = glucosylceramide, LacCer = lactosylceramide, spho = sphingosine. N=1, preliminary data.

5.3.2 Increased sphingomyelin and decreased acid sphingomyelinase activity is observed in 5dpf U18666A and 1NMP treated zebrafish embryos

NPC patients and the *Npc1*^{-/-} mouse model show storage of sphingomyelin (Lloyd-Evans et al., 2008) alongside reduced activity (Elleder and Smid, 1985) and mislocalization (Tamura et al., 2006) of its degradative enzyme, acid sphingomyelinase. In order to validate these biochemical characteristics in our zebrafish model of NPC, we performed assays for both levels of sphingomyelin (Figure 5.2 A) and acid sphingomyelinase activity (Figure 5.2 B) on 5dpf zebrafish either untreated (wild-type), treated with DMSO vehicle control or treated with npc1 inhibitors U18666A and 1NMP. As alkaline hydrolysis prevented the detection of sphingomyelin when performing TLC analysis on npc1-inhibited embryos (Figure 5.1 B), these assays allow us to analyze the effects of treatment on this lipid. Increased sphingomyelin was observed in 5dpf zebrafish embryos treated with either 1NMP or U18666A (~20 & 30% increase compared with wild-type), suggesting inhibition of acid sphingomyelinase. However, only 1NMP treated embryos, which show greater storage of sphingomyelin when compared with U18666A, showed a decline in acid sphingomyelinase activity when compared with wild-type and DMSO treated controls (~40% decrease). No difference was seen in acid sphingomyelinase activity when comparing wild-type and DMSO treated controls.
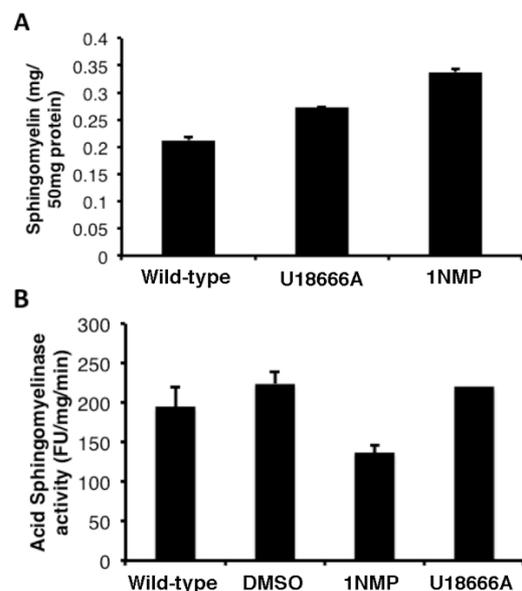
Figure 5.2. Increased sphingomyelin and decreased acid sphingomyelinase activity is observed in 5dpf U18666A and 1NMP treated zebrafish embryos. Enzyme assays were used to analyze the effects of *npc1*-inhibitors 1NMP (300µM) and U18666A (1µg/ml) on sphingomyelin storage (A) and sphingomyelinase activity (B) in 5dpf zebrafish embryos. Embryos were treated with DMSO as a vehicle control. FU = fluorescence units. N=1. Preliminary data.

5.3.3 Treating zebrafish embryos with either U18666A or 1NMP induces storage of both cholesterol and ganglioside GM1

NPC1 patients, mice and cells show storage of both cholesterol and ganglioside GM1 (te Vruchte et al., 2004). In order to determine whether our zebrafish models show storage of these lipids following treatment with npc1-inhibitors, we imaged fixed 5dpf zebrafish either untreated (control) or treated with either U18666A or 1NMP following staining with either filipin for cholesterol or FITC-CtxB for ganglioside GM1. We observed increased cholesterol and ganglioside GM1 within embryos treated with either U18666A and 1NMP when compared with wild-type (Figure 5.3). These results mimic data from NPC1 patients and other animal models (te Vruchte et al., 2004) and suggest that our model accurately recapitulates human disease phenotypes. A greater increase in cholesterol can be seen following treatment with U18666A when compared with 1NMP, and a greater increase in ganglioside GM1 can be seen in 1NMP treated embryos when compared with U18666A.
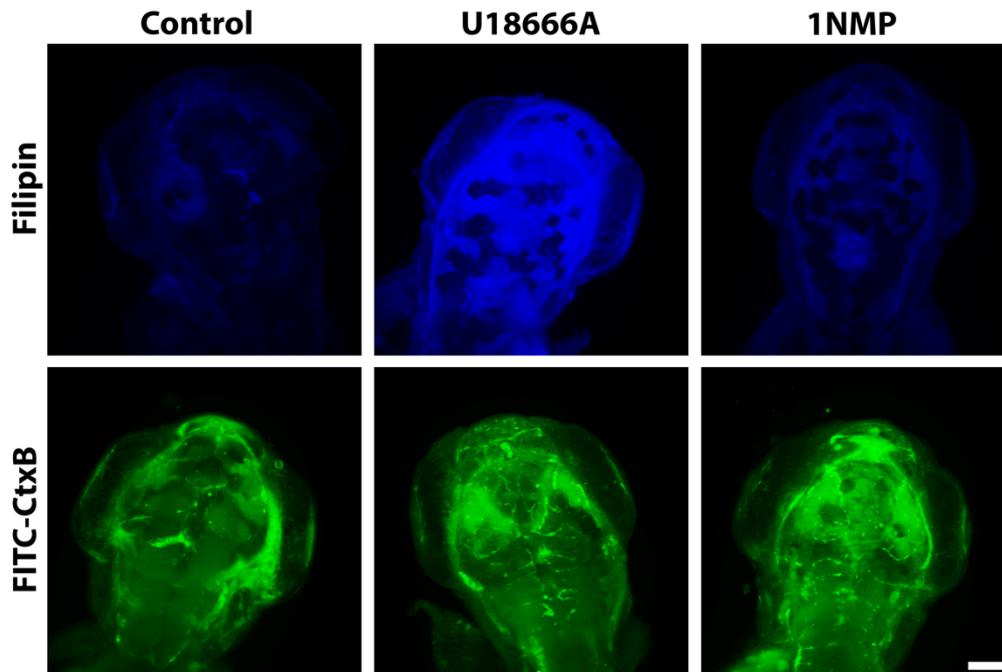
Figure 5.3. Inhibition of npc1 induces storage of both cholesterol and ganglioside GM1 in 5dpf U18666A and 1NMP treated zebrafish embryos. Zebrafish embryos were either left untreated or treated with *npc1*-inhibitors U18666A (1µg/ml) or 1NMP (300µM). At 5dpf, embryos were fixed and stained with filipin for cholesterol or FITC-CtxB for ganglioside GM1 prior to imaging using a Zeiss Lightsheet Z.1. N=2, scale bar = 50µm.

5.3.4 Treating zebrafish embryos with either U18666A or 1NMP induces movement abnormalities

NPC1 patients and mice present with progressive ataxia (Sevin et al., 2007). As zebrafish are capable of performing complex behaviors (Brustein et al., 2003), we investigated whether our U18666A and 1NMP treated zebrafish exhibited any movement defects.

First, we analyzed spontaneous coiling behavior in 24 and 48hpf embryos. Representative images of embryos within their chorions at 24 and 48hpf are shown in figures 5.4 A and C respectively. As can be seen in figure 5.4 B, at 24hpf, there is a significant decrease in the number of coils observed following treatment with either 1NMP (~20% decrease) or U18666A (~30% decrease) when compared with control embryos. Again, at 48hpf, we see a significant decrease in coils in 1NMP embryos when compared with controls. No decrease is seen at 48hpf with U18666A however, although this may become significant with further experimental repeats.

Next, we analyzed response to touch in 48hpf embryos. Representative images of control and *npc1*-inhibited embryos at both 0ms and 180ms after touch can be seen (Figure 5.4), alongside a graph showing the percent of embryos responding to the touch and swimming away within 180ms (Figure 5.4). There is a significant decrease in embryos responding to touch following treatment with 1NMP (~80% decrease), and a non-significant reduction (~30% decrease) following treatment with U18666A. Collectively, these results demonstrate ataxia-like movement defects within npc1-inhibited zebrafish embryos.
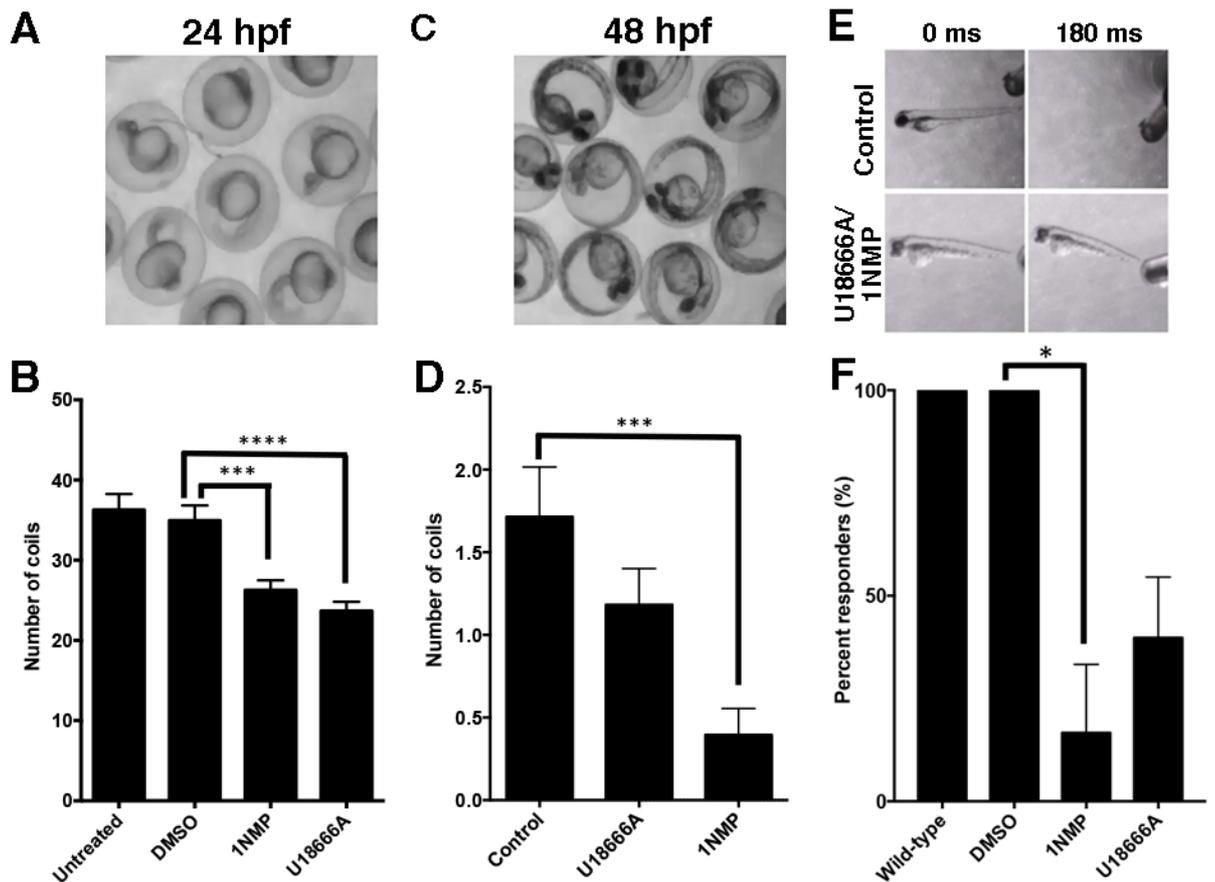
Figure 5.4. Inhibition of *npc1* induces movement abnormalities in U18666A and 1NMP treated zebrafish embryos. Zebrafish embryos were either left untreated, treated with DMSO vehicle control, or treated with *npc1* inhibitors U18666A (1µg/ml) or 1NMP (300µM). At 24hpf (A & B) or 48hpf (C & D) embryos were filmed, and the amount of coils per embryo was recorded over 3 minutes. For spontaneous coiling we examined at least 50 embryos per condition for each experiment. Also at 48hpf, we performed the touch response test on treated and untreated embryos. Representative images of embryos at 0 and 180ms following touch (E) and the percent of embryos responding to touch within 180ms (F) is shown. For touch response experiments, we examined at least 10 embryos per condition for each experiment, N=2. *=$p<0.05$, ***=$p<0.001$, ****=$p<0.0001$.

5.3.5 Treating zebrafish embryos with U18666A induces lysosomal expansion and movement defects, which are reversed by co-treating with miglustat

Having seen that treatment with either U18666A or 1NMP induces NPC-like lipid storage (Figure 5.3) and behavioral defects (Figure 5.4) in 5dpf zebrafish embryos, we next wanted to investigate whether the only currently approved NPC therapy, miglustat (Lachmann et al., 2004), has any efficacy in reversing these defects. As shown in figure 5.5, we stained and imaged live 5dpf zebrafish either untreated, treated with U18666A to induce NPC or treated with both U18666A and miglustat, with the lysosomal probe lysotracker green prior to imaging on a ZEISS Lightsheet Z.1 microscope. As can be seen in figure 5.5 A, embryos show increased lysotracker staining, indicative of lysosomal

expansion, following treatment with U18666A. Furthermore, co-treating these cells with miglustat reduces lysotracker staining towards wild-type levels. As previously demonstrated (Figure 5.4) spontaneous coiling behavior can be seen to decrease in embryos treated with U18666A at 24hpf (~50% decrease). In preliminary studies, this phenotype also appears to be corrected towards wild-type levels following co-treatment with miglustat (Figure 5.5 B), although this will need to be replicated and significance testing performed before firm conclusions can be drawn from this data. These results confirm previously demonstrated benefits of miglustat in NPC (Zervas et al., 2001, Lachmann et al., 2004).
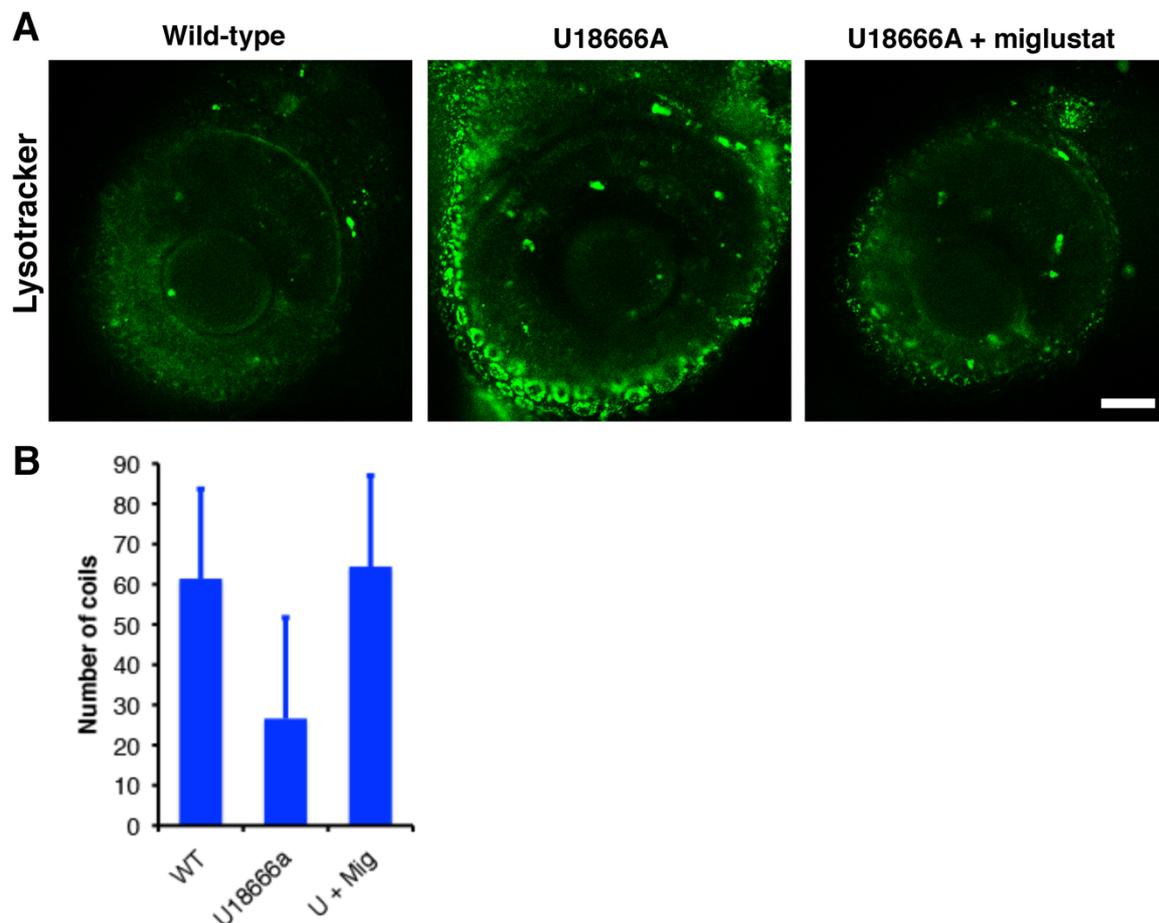
Figure 5.5. Treating zebrafish embryos with U18666A induces lysosomal expansion and movement defects, which appear reversed following co-treatment with miglustat. Zebrafish embryos were either left untreated or treated with the *npc1* inhibitor U18666A (1µg/ml) either with or without miglustat (500µM). Spontaneous coiling behavior of the embryos was recorded at 24hpf (B). At 5dpf, embryos were stained and imaged live with the lysosomal probe lysotracker green prior to imaging on a ZEISS Lightsheet Z.1 microscope (A). N=3 for A, 1 for B. For B, at least 50 embryos were examined per condition: 1 experiment, preliminary data. Scale bar = 10µm. Work done in collaboration with Dr Luke Haslett (A) and Sophie Cook (B).

5.3.6 Treating zebrafish embryos with Ned-19, an inhibitor of NAADP signaling, induces NPC-like phenotypes

As reduced lysosomal Ca^{2+} has been shown to be an early NPC phenotype (Lloyd-Evans et al., 2008), and having previously investigated Ca^{2+} modulators as treatments for NPC (see chapter 4), we investigated the effects of inducing a lysosomal Ca^{2+} signaling defect *in vivo* using the NAADP signaling inhibitor Ned-19 (Naylor et al., 2009). This is particularly pertinent as NAADP signaling is reduced in NPC disease cells, presumably due to reduced lysosomal Ca^{2+} (Lloyd-Evans et al., 2008), and by using Ned-19 we might be able to confirm which phenotypes in NPC are a direct result of this defect. Firstly, we fixed Ned-19 treated 5dpf zebrafish embryos prior to staining with either filipin for cholesterol or FITC-CtxB for ganglioside GM1. We observed increased levels of these lipids within Ned-19 treated embryos when compared with wild-type (Figure 5.6 A), similarly to treatment with U18666A, 1NMP or following MO injection (Figures 5.3 & 5.8). Live 5dpf embryos, either untreated or treated with Ned-19, where also imaged with the lysosomal probe lysotracker green (Figure 5.6 A), demonstrating increased lysosomes, highly characteristic of NPC disease, within Ned-19 treated zebrafish.

Next, we investigated how Ca^{2+} signaling was affected within the Ned-19 treated 5dpf zebrafish directly by staining live embryos with the Ca^{2+} probe Rhod2-AM. We observed much reduced Ca^{2+} levels within Ned-19 treated embryos (Figure 5.6 A). We next picked a region of interest within the live zebrafish forebrain and measured changing Ca^{2+} levels over 30 seconds. As can be seen in the Ca^{2+} traces (Figure 5.6 B) and graphs (Figure 5.6 C & D) shown, Ned-19 treated zebrafish show a slightly reduced number of spontaneous Ca^{2+} events coupled with a large reduction in the amplitude of each individual spontaneous event (4-fold reduction).

Together, these data demonstrate how inducing a lysosomal Ca^{2+} signaling defect using Ned-19 can induce NPC lipid storage and lysosomal expansion phenotypes *in vivo*, therefore confirming the importance of this phenotype in the disease cascade, and highlighting the importance of developing Ca^{2+} modulating therapies for NPC (see Chapter 4). Moreover, the ability to perform live Ca^{2+} imaging *in vivo* indicates the benefits of using transparent zebrafish models to study diseases displaying disrupted Ca^{2+} homeostasis.
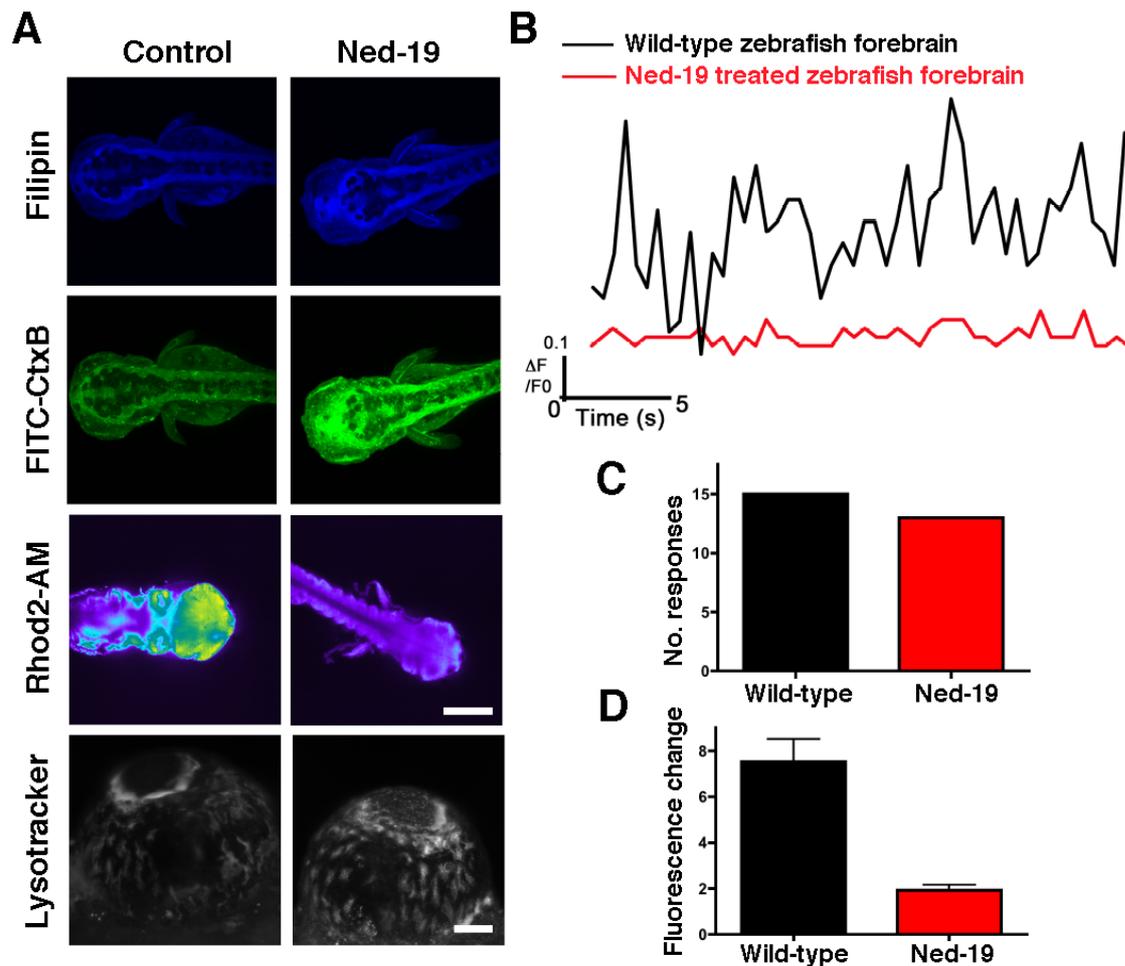
Figure 5.6. Treating zebrafish embryos with Ned-19, an inhibitor of NAADP signaling, induces NPC-like phenotypes. Zebrafish embryos were either left untreated or treated with the NAADP signaling inhibitor Ned-19 (100µM). A) At 5dpf, embryos were either fixed and stained with filipin for cholesterol or FITC-CtxB for ganglioside GM1, or imaged live with the Ca^{2+} probe Rhod2-AM (images are pseudocoloured to represent Ca^{2+} levels, high Ca^{2+} = yellow, low Ca^{2+} = purple) or the lysosomal probe lysotracker green. All embryos were imaged using a Zeiss Lightsheet Z.1. Following staining with the Ca^{2+} probe Rhod2-AM, regions of interest where picked in the live zebrafish forebrain and changing Ca^{2+} levels were measured over 30 seconds and represented as Ca^{2+} traces (B). Graphs show C) number of Ca^{2+} responses and D) fluorescence change obtained from B. N=3. Top scale bar = 50µm for filipin, FITC-CtxB and Rhod2-AM, bottom scale bar = 10µm for lysotracker images. Work done with help from Dr Luke Haslett and Dr Emyr Lloyd-Evans.

5.3.7 Inhibition of zebrafish *npc1* using an ATG-targeting morpholino induces movement abnormalities and storage of NPC1 lipids cholesterol and ganglioside GM1

NPC1 patients and mice show storage of cholesterol and ganglioside GM1 within their lysosomes alongside progressive ataxia (te Vruchte et al., 2004). Having seen that zebrafish treated with either U18666A, 1NMP or Ned-19 show storage of cholesterol and ganglioside GM1 (Figures 5.3 & 5.6), and that embryos treated with U18666A or 1NMP show reduced spontaneous coiling and response to touch (Figure 5.4), we next investigated whether this was also true within *npc1*-morphant zebrafish.

First, we analyzed spontaneous coiling behavior within our *npc1*-morphant zebrafish (Figure 5.7 A). As can be seen in figure 5.7 A, at 24hpf there is a significant decrease (~50%) in the number of coils observed following microinjection with an ATG-targeting morpholino against *npc1* when compared with injected control zebrafish. This mimics what was seen previously following treatment of embryos with pharmacological inducers of the NPC phenotype (Figure 5.4).

Next, we analyzed response to touch in 48hpf embryos (Figure 5.7 B & C). Figure 5.7 B demonstrates how *npc1*-morphant zebrafish display a non-significant increase in response time following touch, although a higher N could potentially allow significance. No decrease is seen in number of embryos responding altogether (Figure 5.7 C).

Injected control and *npc1*-morphant 5dpf embryos were next stained with either filipin for cholesterol of FITC-CtxB for ganglioside GM1. We observed increased cholesterol and ganglioside GM1 within *npc1*-morphant embryos when compared with controls (Figure 5.7 D). These results mimic those in Figure 5.3 where embryos were treated with pharmacological inhibitors of NPC1, as well as data from patients and other disease models, confirming the specificity of the phenotype.
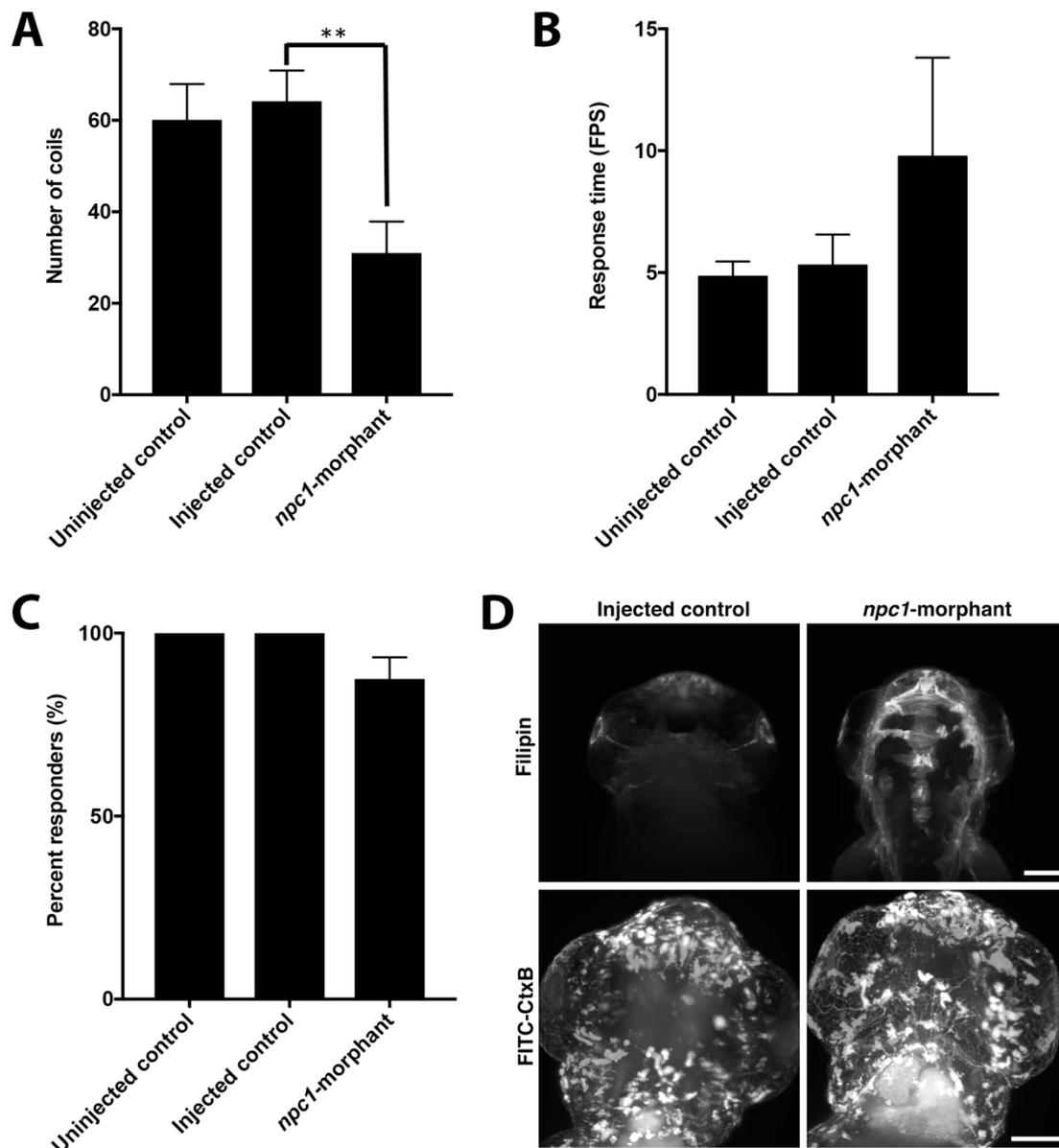
Figure 5.7. Inhibition of zebrafish *npc1* using an ATG-targeting morpholino induces movement abnormalities and storage of NPC1 lipids cholesterol and ganglioside GM1. Zebrafish embryos were either left untreated (uninjected control), injected with Danieau's microinjection solution with 1% phenol red only (injected control), or injected with an ATG (start codon blocking) *npc1*-morpholino (in Danieau's microinjection solution with 1% phenol red). At 24hpf embryos were filmed, and the amount of coils per embryo was recorded over 3 minutes (A). For spontaneous coiling we examined at least 50 embryos per condition for each experiment. At 48hpf, we performed the touch response test on embryos. Time taken for embryos to respond to touch in frames per second (FPS, B) and percent of embryos not responding to touch within 180ms (C) is shown. For touch response experiments, we examined at least 10 embryos per condition for each experiment. D) A) At 5dpf, embryos were either fixed and stained with filipin for cholesterol or FITC-CtxB for ganglioside GM1 prior to imaging using a Zeiss Lightsheet Z.1. For behavioural testing (A, B & C) N=2, for fluorescent staining (D) N=3. Scale bar = 50µm. ** =P<0.01

5.4 Discussion

There is currently only one approved therapy for NPC, miglustat, and whilst able to slow disease progression it is far from a cure (Zervas et al., 2001), meaning more therapies are required to treat patients with this devastating disorder. Zebrafish act as an emerging animal model for the study of and development of therapies for neurodegenerative diseases. Baring this in mind, and given that previous studies exist demonstrating successful knock-down of *npc1* in zebrafish using MOs, we decided to generate our own *npc1*-morphant zebrafish and to characterize this model further, with the eventual aim of testing novel NPC disease modifying therapies in this organism. Furthermore, we developed and characterized pharmacological models of NPC in zebrafish embryos using known *npc1*-inhibitors U18666A and 1NMP, as well as Ned-19, known to induce an NPC-like phenotype in cells.

In order to determine whether our NPC zebrafish show phenotypes present in the human disease, therefore verifying the importance of this model, we examined lipid storage and lysosomal expansion within embryos. Zebrafish treated with either U18666A, 1NMP, Ned-19 or microinjected with *npc1*-MO show storage of both cholesterol and ganglioside GM1, with the presence of these lipids and other species known to be stored in NPC being confirmed using TLC for 1NMP treated embryos (Figure 5.1, 5.3, 5.6 & 5.8). Furthermore, lysosomal expansion, indicative of lipid storage and characteristic of NPC disease, is seen following treatment with either U18666A or Ned-19 (Figures 5.5 & 5.6). In addition to this, preliminary studies suggest both sphingomyelin storage and inhibition of its degradative enzyme acid sphingomyelinase (Figure 5.2) within U18666A and 1NMP treated zebrafish, again, both of which are observed within humans and mice (Lloyd-Evans et al., 2008, Elleder and Smid, 1985, Tamura et al., 2006). These data suggest that a similar lipid storage profile exists within both NPC humans and zebrafish, and therefore the effects of any lipid-lowering treatments (e.g. miglustat, see figure 5.5), could be examined.

As ataxic phenotypes are prevalent within both NPC patients and mice, we also performed behavioral tests, notably spontaneous coiling and touch response tests, on NPC embryos. We found reduced coiling behavior alongside reduced response to touch in drug-induced models (treated with either U18666A or 1NMP) and MO injected embryos (Figures 5.4 & 5.8, although response to touch is non-significant for *npc1*-morphants, more repeats needed), suggesting that movement defects within NPC patients are replicated within our zebrafish models. This will allow us to assess the effects of therapies, for example the approved NPC therapy miglustat (Figure 5.5), on behavioral defects in NPC. Many drugs and MOs have off-target effects at certain concentrations, and therefore treatment can occasionally generate phenotypes unrelated to inhibition of NPC function. As identical lipid storage and behavioral defects are observed in all forms of NPC zebrafish generated however, this suggests

that either direct or indirect inhibition of the NPC pathway is responsible for the phenotypes generated. Furthermore, preliminary results suggest beneficial effects of the only currently approved NPC therapy miglustat (Figure 5.5), which if replicable suggest this therapy is working via the same pathway to improve NPC phenotypes in both humans and zebrafish.

Ned-19, an inhibitor of NAADP mediated lysosomal Ca^{2+} signaling (Naylor et al., 2009), induces NPC-like phenotypes in wild-type cells (Lloyd-Evans, unpublished observation). It has been previously suggested that reduced lysosomal Ca^{2+}, which in turn leads to reduced lysosomal Ca^{2+} signaling, acts as an early phenotype in the NPC1 disease cascade (Lloyd-Evans et al., 2008). Treating zebrafish with Ned-19 appears to induce reduced Ca^{2+} signaling within 5dpf zebrafish embryos alongside lipid storage (Figure 5.6). This suggests that initiating the Ca^{2+} signaling defect within NPC zebrafish is responsible for much of the lipid storage observed, therefore highlighting the benefits of Ca^{2+} modulating therapies for the treatment of NPC (see Chapters 4 and 6). These results also demonstrate benefits of using zebrafish as a model organism: small, transparent zebrafish allow us to perform live Ca^{2+} imaging not possible within other animal models such as mice. This benefit is likely to be highly useful when studying any disease associated with Ca^{2+} dyshomeostasis, particularly the lysosomal storage disorders where to date no one has confirmed the presence of Ca^{2+} signaling abnormalities *in situ* in the brain, despite significant evidence of Ca^{2+} signaling disruption within these disorders. Future work could examine whether specifically inducing a lysosomal Ca^{2+} signaling defect within zebrafish using Ned-19 is responsible for the movement defects and neuronal loss observed within other NPC animal models, or whether another disease pathway (e.g. lysosomal Zn^{2+} storage, see Chapter 3), has a greater effect regarding ataxic phenotypes.

To conclude, our zebrafish models, which all show identical lipid storage and movement defects, appear to actively recapitulate several known NPC phenotypes, therefore justifying its use to study NPC disease mechanisms and the effects of novel therapeutics and demonstrating no obvious off-target effects. Furthermore, the ease by which zebrafish models can be characterized behaviorally, biochemically and even using *in vivo* live Ca^{2+} imaging suggests it acts as a highly useful model organism when studying NPC. Future work would involve further characterizing the diseased embryos and testing emerging therapies including the Ca^{2+} modulator tanganil (see Chapter 4) and the Zn^{2+} chelator phytic acid (see Chapter 3) to see if any beneficial effects can be seen within the NPC zebrafish.

Chapter 6: Effects of curcumin nanoformulations on *Npc1^{-/-}* cellular function

6.1 Introduction

6.1.1 Curcumin

The widely used spice, coloring, flavoring and herbal medicine known as turmeric is a product of the rhizome of *Curcuma longa L.* The key active ingredient of turmeric is curcumin [E,E)-1,7-bis(4-hydroxy-3-methoxyphenyl)-1,6-heptadiene-3,5-dione] (Figure 6.1) which bestows anti-inflammatory, anti-cancer, anti-oxidant, anti-athlerosclerotic, anti-microbial and wound healing effects onto this yellow root extract (Bilmen et al., 2001). Demethoxycurcumin (17%) and bisdemethoxycurcumin (3%) are also present within turmeric extract (Figure 6.1).
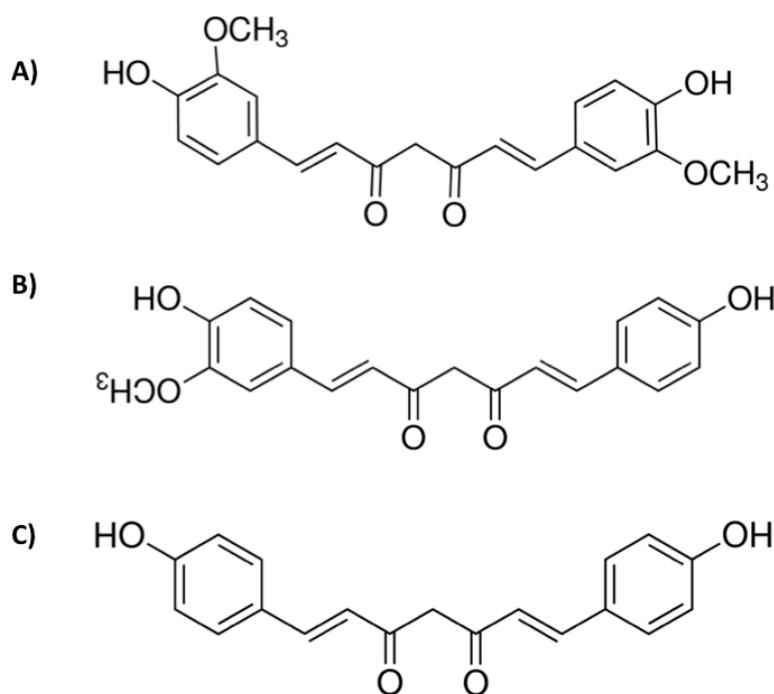
Figure 6.1. Chemical structures of the 3 curcuminoids present with turmeric extract. (A) Curcumin [(E,E)-1,7-bis(4-Hydroxy-3-methoxyphenyl)-1,6-heptadiene-3,5-dione] makes up 77% of turmeric (B) demethoxycurcumin [(*E,E*)-1-(4-Hydroxy-3-methoxyphenyl)-7-(4-hydroxyphenyl)-1,6-heptadiene-3,5-dione] (17%) and (C) bisdemethoxycurcumin [(1E,6E)-1,7-bis(4-hydroxyphenyl)hepta-1,6-diene-3,5-dione] (3%).

Approximately 7600 publications on this compound demonstrate curcumins ability to improve symptoms of patients with diverse disorders, including cancer (Shanmugam et al., 2015) and cystic fibrosis (Egan et al., 2004) as well as providing benefit following radiological exposure (Kma, 2014) and

cobra bites (Shabbir et al., 2014). Recently, treatment with this extract has also been shown to improve neurological symptoms in patients with Alzheimer's disease (Monroy et al., 2013) and *Npc1*^{-/-} mice (Lloyd-Evans et al., 2008). Widespread use of this 'edible' drug to treat various ailments without side effect has led to the belief of low health risks associated with this molecule.

6.1.2 Curcumin in neurodegenerative disease

Treatment with curcumin has recently been suggested to provide benefit against various non-LSD neurological conditions including Alzheimer's, Parkinson's and Huntington's disease. These 3 disorders are all characterized by abnormal aggregation of aberrant forms of specific proteins (β-amyloid in Alzheimer's, α-synuclein in Parkinson's and huntingtin in Huntington's) that likely contribute to disease onset and/or progression (Monroy et al., 2013). This characteristic can also be seen in NPC where abnormal β-amyloid accumulates in the brain (Burns et al., 2003), suggesting treatment may provide similar benefit in NPC patients. Curcumin is able to cross the blood-brain barrier (BBB)(Tsai et al., 2011) where it likely acts against neurological disease via a combination of anti-plaque, anti-oxidative anti-inflammatory mechanisms (Monroy et al., 2013).

6.1.3 Curcumin as a therapy for NPC disease

Benefit within NPC cells and tissues occurs following one distinctive property of curcumin: its ability to inhibit all 3 isoforms of the sarco/endoplasmic reticulum Ca^{2+} ATPase (SERCA). It does this by inducing a conformational change which blocks ATP from binding (Bilmen et al., 2001). Within cells, SERCA acts to transport Ca^{2+} from the cytosol into the sarcoplasmic or endoplasmic reticulum. Following inhibition of this process with curcumin, Ca^{2+} continues to be released from the ER via leak channels, resulting in further Ca^{2+} release from the ER and transiently elevated cytosolic Ca^{2+} levels. Increased cytosolic Ca^{2+} levels are predicted to benefit NPC by overcoming the lysosomal Ca^{2+} defect, which likely results in defective Ca^{2+}-dependent endocytic trafficking and fusion events within diseased cells, which in turn results in lipid storage (Lloyd-Evans et al., 2008).

Beneficial effects of curcumin on NPC symptoms were first realized by Lloyd-Evans *et al.,* (2008) who demonstrated how treatment of mouse *Npc1*^{-/-}-mutant glial cells with 30μM curcumin restored sphingolipid trafficking. Co-treatment in these same cells with curcumin and the membrane permeant Ca^{2+} chelator BAPTA-AM prevented benefit, demonstrating that the correction occurred via curcumin-induced changes in cytosolic Ca^{2+}. Following this observation, Lloyd-Evans *et al.,* 2008 then proceeded to test the therapeutic effects of oral curcumin (150 mg/kg per day from 1 day post-weaning) in the *Npc1*^{-/-} mouse. Curcumin-treated mice displayed improved coat condition, increased weight gain, increased activity and reduced tremor when compared with untreated. This was

accompanied by reduction in total brain GSL and sphingosine-1-phosphate, although elevated sphingosine levels were not significantly changed after treatment. In another study, *Npc1*^{-/-} mice treated with curcumin experienced a ~16% increase in lifespan (Borbon et al., 2012b)(not dissimilar to the 25% observed with miglustat). Despite demonstrating an increase in lifespan following treatment with pure curcumin, Borbon *et al.,* 2012 declared no beneficial effects of curcumin on *Npc1*^{-/-} mice. This surprising statement may be due in part to their findings that lipidated curcumin formulations, proposed to cross the blood-gut and BBB more easily, showed no improvement at all in *Npc1*^{-/-} mice. Since these initial findings, several groups have confirmed the beneficial effects of curcumin on NPC both *in vivo* and *in vitro* (Williams et al., 2014, Fineran et al., 2016, Efthymiou et al., 2015).

6.1.4 The need for vectors to increase the bioavailability of curcumin

A pharmacologically approved curcumin formulation would most likely require a vector to increase its bioavailability due to this molecule's poor absorption and fast metabolism (Anand et al., 2007). When ingested, only 1% of curcumin enters blood plasma and much of this is then rapidly conjugated to form inactive products. Several ways to circumvent this bioavailability problem include formation of curcumin-liposomes (as tested in Borbon *et al.,* 2012), use of adjuvants (e.g. piperine), curcumin phospholipid complexes, combining curcumin with turmeric oils, and nano-sized compounds (Anand et al., 2007).

Adjuvants such as piperine act by blocking curcumin metabolism; thereby increasing its half-life in the body, with co-administration leading to a 2000% increase in bioavailability (Shoba et al., 1998). Curcumin-containing liposomes can also be generated. Liposomes are able to solubilize hydrophobic compounds, altering their pharmacokinetic properties and increasing rate of absorption. Higher plasma levels, lower clearance and improved gastrointestinal absorption (~1.5 increase in half-life in rats) can be achieved by combining curcumin with micelles and phospholipids (Liu et al., 2006). Furthermore, curcumin can be combined with turmeric oil to increase absorption into the blood and increase retention time (700% more activity and 7-8 times more bioavailability in humans)(Anand et al., 2007). Despite the above observations of increased retention of curcumin formulations when combined with lipid, there is a possibility that the lipid vector itself may accumulate in NPC cells, which show defects in the efflux of phosphatidyl choline to apolipoprotein A1 (Choi et al., 2003), therefore potentially worsening storage phenotypes. This could explain the reduced efficiency of curcumin in *Npc1*^{-/-} mice published by Borbon *et al.,* 2012 when a lipid carrier was used to increase bioavailability.

Studies indicate that nanoformulations of curcumin increase bioavailability, with injection of 5mg/kg nanocurcumin in mice resulting in 0.5% entering the brain within 1 hour and a serum concentration of ~10μM (Chiu et al., 2011): a concentration known to inhibit SERCA activity and elevate

cytosolic Ca^{2+} (Bilmen et al., 2001). Tissue penetrance of nanosuspensions appears to be dependent on particle size, with intravenous injection of nano-curcumin resulting in 3mM plasma concentrations resulting in high concentrations of curcumin in the liver (200nM, 10 min post injection) and the brain (70nM, 20-30 min post injection) (Bi et al., 2017).

6.1.5 Curcumin aggravates inhibition of cytochrome P450 enzymes in NPC

One of the symptoms observed in NPC is reduced liver function following substantial storage of lipids such as cholesterol. This often manifests in the neonatal period as cholestatic jaundice, progressing in ~10% of patients to liver failure and premature death (Patterson et al., 2012). These symptoms, combined with observations that therapeutic drugs (including curcumin, Lloyd-Evans personal communication) require lower dosing in $Npc1^{-/-}$ mice when compared with $Npc1^{+/+}$, suggested a potential drug metabolism defect in NPC that has since been confirmed (Nicoli et al., 2016). A normal dose of curcumin would consist of 300-1250mg/kg/day, whilst in the $Npc1^{-/-}$ mouse this dose must be adjusted to 150mg/kg/day to prevent toxicity (Nicoli et al., 2016, Lloyd-Evans et al., 2008). Nicoli *et al.,* 2016 discovered a defect in the cytochrome P450 (CYP) system, involved in hepatic metabolism, within NPC1 mice, cats and human liver explants. Poor metabolism means breakdown products build-up to toxic levels. Impairment of the CYP system within NPC most likely occurs following storage of cholesterol within late endosomes and lysosomes, resulting in altered regulation and synthesis of oxysterols and bile acids (Alvelius et al., 2001, Maekawa et al., 2013, Maekawa et al., 2015, Porter et al., 2010), both of which are known to regulate transcription of CYP-related genes (Diczfalusy, 2013, Hafner et al., 2011, Eloranta and Kullak-Ublick, 2005). Nicoli *et al.,* (2016) demonstrated how bile acid therapy using ursodeoxycholic acid (UDCA) could increase CYP enzyme activities, whilst reducing tremor and improving motor function with $Npc1^{-/-}$ mice.

Alongside reduced CYP enzyme activity in NPC, curcumin itself is also known to inhibit a substantial number of the major human CYP enzymes (Volak et al., 2008). However, despite inhibition by curcumin of CYP enzymes, Lloyd-Evans *et al.,* 2008 still demonstrated improvement when treating the $Npc1^{-/-}$ mouse, suggesting that the positive effects of this molecule outweigh drug toxicity effects at certain doses. As previously discussed, curcumin is often modified to increase bioavailability (Anand et al., 2007). These modifications could potentially effect degree of inhibition of CYP enzymes, therefore preventing benefits in NPC, and this could potentially explain lack of benefit in Borbon *et al.,* 2012.

6.1.6 Crohn's disease and inflammatory bowel disease in NPC1: implications when administering curcumin formulations

A percentage of NPC patients develop early-onset Crohn's disease (CD) or inflammatory bowel disease (IBD) like symptoms including intestinal inflammation with granuloma (Jolliffe and Sarkany, 1983, Schwerd et al., 2016, Steven and Driver, 2005), and this likely arises following defects in autophagosomal maturation (Sarkar et al., 2013). These defects prevent antibacterial autophagy by the NOD2-RIPK2-XIAP pathway, and hinder degradation of bacteria known to be responsible for CD (e.g. *Salmonella enterica serovar typhimurium* (*S. typimurium*) (Grassl et al., 2008) and CD-associated adherent-invasive *Escherichia coli* (Darfeuille-Michaud et al., 2004, Lapaquette et al., 2012, Darfeuille-Michaud et al., 1998)) (Schwerd et al., 2016).

As the NPC gastrointestinal tract is already dysfunctional following lipid build-up and inhibition of autophagosomal maturation, and as curcumin is absorbed via the gut, oral administration of curcumin formulations solubilized in lipid to increase bioavailability could potentially worsen CD and IBD symptoms in patients.

6.1.7 Combination treatment as a strategy for NPC disease

Ultimately, as a variety of dysfunctions in NPC cells culminate in symptoms within patients, targeting several aspects of the pathogenic cascade at the same time using different drugs will most likely act as the most effective treatment. Previous attempts of combination therapy in $Npc1^{-/-}$ mice by Williams *et al.,* 2014 used miglustat to reduce sphingolipid synthesis and storage, curcumin to elevate cytosolic Ca^{2+} and overcome the lysosomal Ca^{2+} defect, and ibruprofen to reduce neuroinflammation. Mice treated with combination therapies show greater improvement when compared to those treated with mono-therapies, with improved body weight and motor function alongside reduced Purkinje cell loss (Williams et al., 2014). Co-treating NPC patients with curcumin alongside UDCA to prevent CYP-enzyme inhibition (Nicoli et al., 2016) would perhaps act as a viable therapeutic approach in the future.

6.1.8 Potential risks associated with the use of curcumin nutraceuticals for the treatment of NPC

Following the publication of Lloyd-Evans *et al.,* (2008) which highlighted benefits of curcumin within $Npc1^{-/-}$ mice, many NPC patients began taking curcumin nutraceuticals (Vockley, 2009). Considering the differences observed between Lloyd-Evans *et al.,* 2008 and Borbon *et al.,* 2012, where unformulated curcumin was beneficial in both but lipidated curcumin was unable to provide benefit in Borbon *et al.,* 2012, we decided to investigate the effects of lipidated curcumin on $Npc1^{-/-}$ cells. This is especially important as NPC patients are taking lipidated curcumin, and considering the potential for

accumulation of phospholipid in NPC cells (Choi et al., 2003), these particular formulations may therefore be damaging instead of beneficial.

In addition to these concerns, an inadequate system for monitoring their safety means that over the counter supplements are often associated with toxicity. Unlike prescription medication, supplements do not require premarketing approval and are often inaccurately labeled. For example, in 2008, a poorly manufactured multivitamin proved responsible for over 200 cases of selenium poisoning (Cohen, 2014). Risks associated with taking uncontrolled nutraceuticals suggest a need for a clinically approved bioavailable formulation of curcumin, which would provide benefits against NPC phenotypes without toxicity.

6.1.9 Aims

Given that NPC patients are currently taking lipidated curcumin supplements (Vockley, 2009), and considering that lipidation appears to negate the benefits observed with curcumin alone (Lloyd-Evans et al., 2008, Borbon et al., 2012b), we instigated a study into a number of lipidated curcumin formulations taken by NPC patients in order to determine what impact they may have at the cellular level on NPC1 disease phenotypes.

6.2 Materials & Methods

Unless otherwise stated, all reagents were from Sigma-Aldrich. Any methods used in this chapter and not described here can be found in the general materials and methods section (Chapter 2).

6.2.1 Preparation and solubilisation of curcumin nutraceuticals

Curcumin supplements (Table 6.1) were purchased in multiple batches from commercial retailers. Three different tablets from each batch were opened, weighed and solubilized in DMSO (VWR, UK). We estimated the curcumin content from the manufacturers stated ratios of curcumin to lipid carrier and bulking agent (see Table 6.1) and generated a 10mM stock solution in each case. Each curcumin supplement was used at a final concentration of 30μM ensuring that the DMSO content always remained below 0.3% v/v. Appropriate DMSO and, where possible, lipid or bulking agent controls were also used. Analytical standard curcumin (>98%) was made up in the same way to a final concentration of 30μM in DMSO.

Referred to in this study as	Formulation	Producer	Reported lipid content	% Curcuminoid
TRE	N/A (total root extract)	Solgar	No added lipids	93%
CGM	Curcumagalacto-mannoside	Akay/Swanson	Fenugreek galactomannans	>35%
BCM95$_g$	BCM-95	Dolcas Biotech/Genceutic Naturals	Turmeric essential oil, lecithin, triglycerides, beeswax, sunflower oil	95%
BCM95$_s$	BCM-95	Dolcas Biotech/LifeExtension	Turmeric essential oil	95%
SLN$_A$	MicroActive (Solid lipid curcumin particle)	Maypro Industries/Dr. Mercola	Medium chain triglycerides, polyglycerol oleate, sodium alginate	25%
SLN$_L$	Longvida (Solid lipid curcumin particle)	Verdure Sciences/AOR, Nutravene	Soy lecithin, palmitate, stearic acid	23%
SLN$_M$	Meriva (Solid lipid curcumin particle)	Indena/Dr.'s Best, Inc	Phospholipid	37.2%

Table 6.1. Properties of the curcumin nanoformulations.

6.2.2 Treating cells with curcuminoids

$Npc1^{+/+}$ (wild-type) and $Npc1^{-/-}$ (NPC1 disease) glia were either left untreated or treated overnight (~16 hours) with 30µM of each curcumin formulation (prepared and solubilized as described above) in complete DMEM prior to live or fixed staining and imaging.

6.2.3 Nanoparticle size analysis of curcuminoids

Nanoparticle size analysis was performed in collaboration with Dr Joanne Welton (Cardiff Metropolitan University, Cardiff, UK) on a NanoSightTM LM10 system with a high sensitivity sCMOS camera system (OrcaFlash2.8, Hammamatsu C11440) and a syringe-pump system (Malvern Instruments). The analysis

was performed as described by Webber and Clayton (2014), with some modifications. Nanoparticles present in the curcumin formulations were diluted 1 in 50,000 in particle free water after solubilisation in DMSO to concentrations up to 2×10^9 particles/ml within the linear range of the instrument, and for each formulation 5 videos of 30 seconds were analyzed using the batch analysis tool of NTA 3.1 software (build 3.1.54) where minimum particle size, track length and blur were set as "automatic".

6.2.4 TLC's to seperate curcuminoids

One whole capsule of formulated curcumin was solvent extracted and separated by TLC, as described in general materials and methods. Solvent systems used were: Chloroform:methanol:H_2O 65:24:4 for better separation of curcuminoids (unstained) and phospholipids, and 80:10:1 for improved separation of cholesterol from ceramides.

6.2.5 Measuring curcumin release from the nanoformulations

The *in vitro* release properties of curcumin nanoformulations were studied using dialysis by a modified method of Nasra *et al.,* 2017 (Nasra et al., 2017). 1ml of each curcumin nanoformulation was placed into cellular dialysis bags with a 12,000 molecular weight cut off (Sigma). Bags were immersed in 10ml EtOH at room temperature and were placed on a shaker at 30rpm. At the indicated intervals 200µM of EtOH was collected and stored at 4°C until analysis using a Tecan Infinate F50 absorbance plate reader at 450nm.

6.2.6 Cell viability assays following treatment with curcuminoids

Cellular viability following either 16 or 48 hour treatment with the curcumin nanoformulations was determined on live cells by fluorescence microscopy using the early apoptotic marker Annexin A5. As a positive control, cells were also treated with nigericin (40µM, 2 hours): a Na^{2+}/K^+ ionophore that depolarizes mitochondria and lysosomes leading to apoptosis. Following curcumin or nigericin treatment, cells were incubated for 30 mins on ice with 5µg/ml FITC-Annexin A5 (eBioscience) in complete HBSS. Cells were then washed three times and imaged in the same buffer chilled to 4°C (to prevent internalization of the Annexin A5 during imaging). Independently, cellular viability was also determined using the CellTiter 96 MTS assay (Promega). Cells were grown in 96 well plates at a density of 20,000 cells per well, allowed to adhere and then incubated for 48 hours with the curcumin nanoformulations. Viability was determined by the addition of the tetrazolium MTS compound for 30-60 minutes, which undergoes a colour change in functional mitochondria that was measured at an absorbance of 490nm in a Tecan Infinite F50 microplate reader (LabTech).

6.2.7 Texas Red dextran staining to investigate the effects of curcuminoid treatment on endocytosis

Fluid phase endocytosis of Texas Red dextran was measured in live cells incubated for 4 hours with the curcumin nanoformulations in conjunction with 0.25mg/ml 10kDa Texas Red dextran in complete DMEM. Cells were then washed 3 x 5 min with complete DMEM supplemented with 1% BSA and 0.5mg/ml unlabeled 10kDa amino-dextran to remove non-internalized Texas Red dextran that was associated with the plasma membrane. Cells were then washed three times with PBS prior to live imaging. Excitation/emission = 595/615nm.

6.2.8 Analysis of phospholipidosis induced by curcuminoids using HCS LipidTOX Red

The accumulation of phospholipid in live cells was determined using HCS LipidTOX Red (Thermofisher) at a 1:1000 dilution in complete DMEM at 37°C. Cells were incubated with the LipidTOX Red reagent for 4 hours prior to three washes in PBS and live imaging. Excitation/emission = 595/615nm.

6.3 Results

6.3.1 Determining nanoparticle size, curcuminoid content, and curcumin release kinetics of the supplements

In order to determine whether the curcumin supplements were nanoformulations, and if so, how the particles compared across the samples, we examined the size distribution and concentration of all types of nanoparticles within the mixtures using a NanoSight LM10.

As can be seen in Figure 6.2 A, all curcumin supplements analyzed were nanoparticles. Three, including TRE, CGM, and SLN_M have mean sizes less than or equivalent to 100nm (Figure 6.2 B), a further three, SLN_L, SLN_A and $BCM95_g$ have mean sizes between 100 and 150nm and one, BCM95s, has a mean size of above 150nm. In addition, the modal peak sizes of these nanoparticles vary considerably. The three nanoformulations with the lowest mean size also have the lowest modal peak size (~75nm), two, SLN_A and $BCM95_g$, have a modal peak size of ~85-100nm, and a further two, SLN_L and BCM95s have a modal peak size of more than 120nm (Figure 6.2 C). A second broader peak ranging from 110-175nm also exists for SLN_L, SLN_M and $BCM95_s$, which may represent aggregation of these particles. A third peak at 220nm can also be seen for $BCM95_s$ indicating this formulation made from the essential oils of turmeric has the most diversity in terms of particle size (this diversity is presumably tempered by the addition of lecithin and beeswax in the case of $BCM95_g$).

In addition to confirming that these curcumin formulations are nanoparticles, we also confirmed the curcuminoid content in the nanoformulations via solvent extraction and separation by TLC. Using this method we were able to separate the three major curcuminoids, namely curcumin (largest band), desmethoxycurcumin and bis-desmethoxycurcumin in all of the nanoformulations (Figure 6.2 D). Our results are largely in keeping with the total curcumin content as reported by the manufacturers (Table 6.1), with TRE having the highest overall curcuminoid content followed by BCM95$_g$ and BCM95$_s$, whereas SLN$_L$, SLN$_A$ and SLN$_M$ have the lowest curcumin content.

We next investigated how quickly the curcumin formulations release their curcumin *in vitro* using a dialysis-based method (Figure 6.2 E). This demonstrated how all the formulations release their curcumin slowly, with absorbance saturation taking at least 1 hour for all the formulations. BCM95$_g$ and BCM95$_s$ appear to release curcumin the fastest (~1 hour to saturate), with the next fastest formulations (CGM & TRE) taking ~2 hours to achieve maximum release. The formulations that appear to release curcumin the slowest are SLN$_M$, SLN$_A$ (3-4 hours) and SLN$_L$. SLN$_L$ in fact never achieves the same degree of curcumin release as that seen with the other formulations.
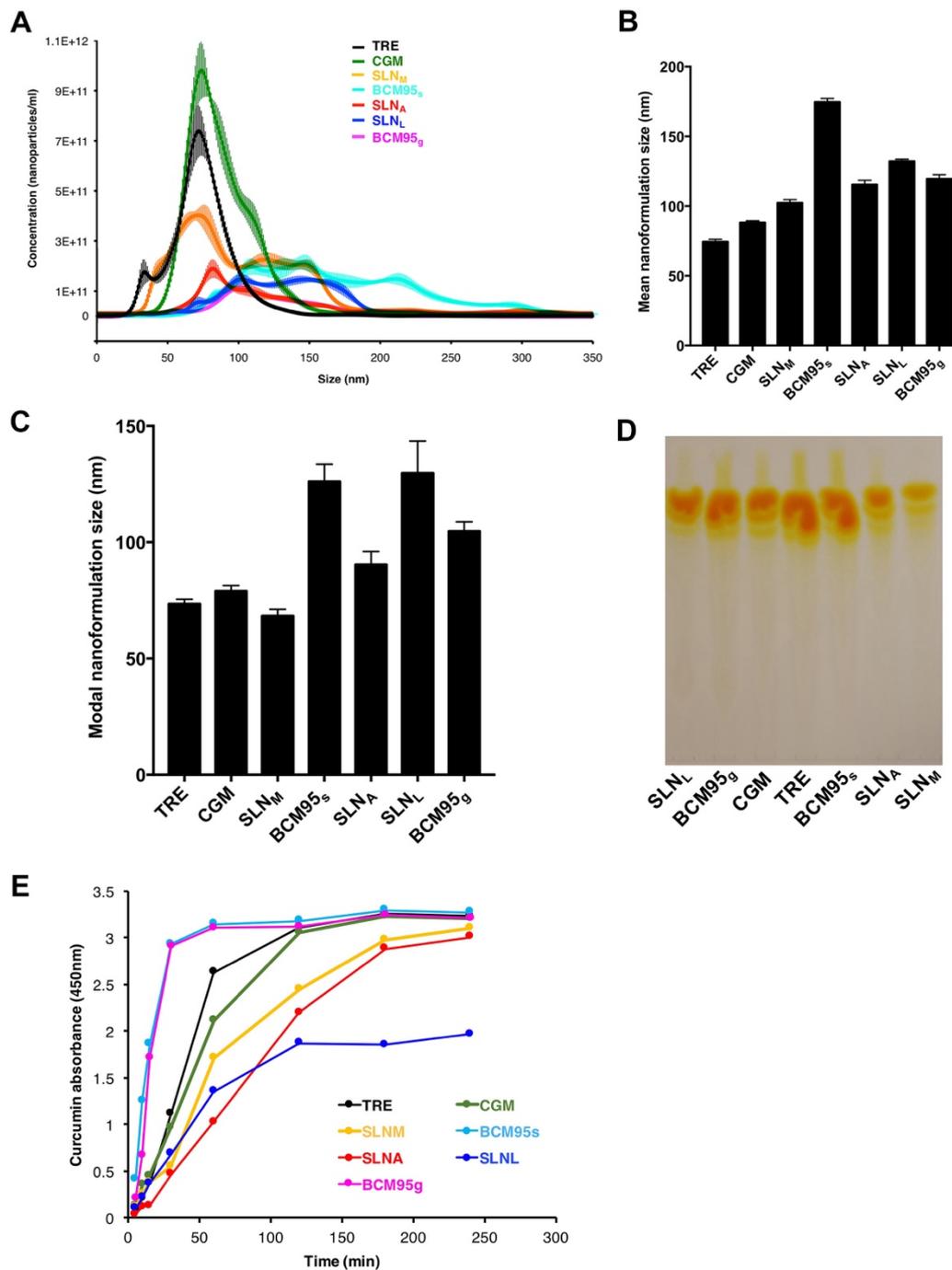
Figure 6.2. Different curcumin mixtures have different mean and mode nanoparticle size, curcumin content and curcumin release kinetics. Particle size (nm) of the nanoformulated curcumin was determined using a NanoSight™ L10 system (see chapter specific methods). Results are displayed graphically (A) and quantification the mean nanoparticle size can be seen in B, and the model nanoparticle size distribution in C. The mean ± standard deviation is shown for 5 separate measurements. These experiments were performed in collaboration with Dr Joanne L. Welton and Dr Richard Webb at Cardiff Metropolitan University. D) One whole capsule of each formulated curcumin was solvent extracted and separated by TLC to determine curcuminoid content (unstained, see chapter specific methods, C. Performed by Dr Luke Haslett). E) Curcumin release from nanoformulations over time (min) measured using dialysis (Performed by Dr Emyr Lloyd-Evans). N=3.

6.3.2 Whilst all curcumin formulations elevate cytosolic Ca²⁺, some cause higher, prolonged elevation in *Npc1⁻/⁻* when compared with *Npc1⁺/⁺* glia, suggesting possible toxicity

in order to determine whether the curcumin supplements were likely to have any beneficial effect on *Npc1⁻/⁻* cells we first determined whether they could induce an elevation in cytosolic Ca^{2+} levels. All of the supplements were able to induce rapid elevation in cytosolic Ca^{2+} in both *Npc1⁺/⁺* and *Npc1⁻/⁻* astrocytes at 30μM (Figure 6.3 A). Interestingly, whilst the TRE, BCM95ₛ and BCM95ₑ supplements all released similar levels of Ca^{2+} in *Npc1⁺/⁺* and *Npc1⁻/⁻* astrocytes, the CGM, SLN_L, SLN_M and SLN_A supplements all induced greater release in the *Npc1⁻/⁻* disease cells compared to controls (Figure 6.3 B). The SLN_A formulation elevated intracellular Ca^{2+} by 2-2.5 times more in the *Npc1⁻/⁻* cells compared to the controls. This could occur following altered NPC1 disease plasma membrane fluidity (Miersch et al., 2008) leading to greater release of curcumin within the cell. Following addition of analytical standard curcumin (Figure 6.3 A), the subsequent increase in cytosolic Ca^{2+} can be seen to return to baseline ~3 minutes after treatment. This is not seen following treatment with the curcumin nanoformulations, presumably due to the slow curcumin release seen with these formulations when compared with analytical standard curcumin (Figure 6.2 E).
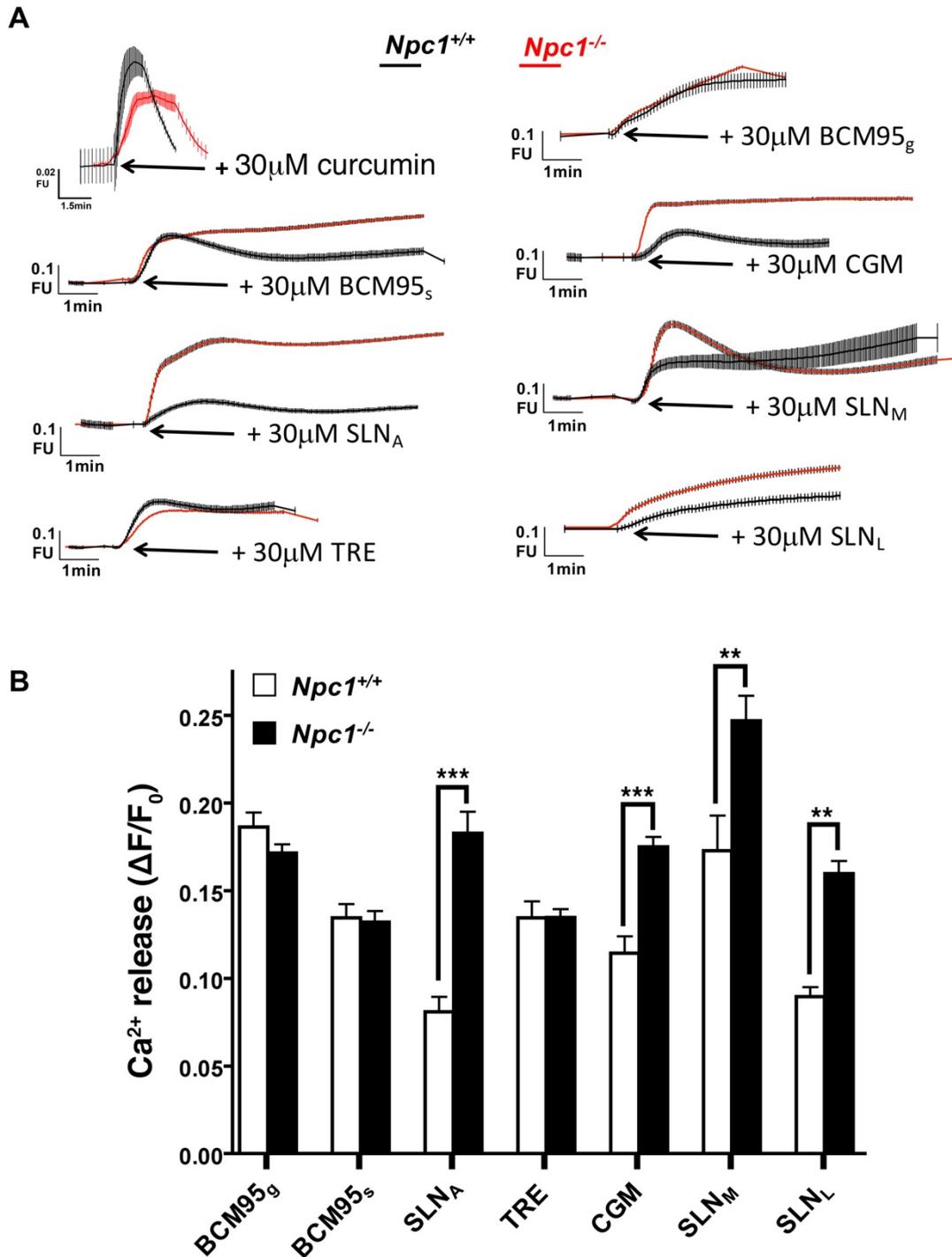
Figure 6.3. Whilst all curcumin formulations elevate cytosolic Ca²⁺, some cause higher elevation in *Npc1⁻/⁻* when compared with *Npc1⁺/⁺* glia, suggesting possible toxicity. $Npc1^{+/+}$ (wild-type) and $Npc1^{-/-}$ (NPC1) mouse astrocytes were stained and imaged live with the cytoplasmic Ca²⁺ probe Fura2 prior to direct addition of either analytical standard curcumin (>98% curcumin), TRE, CGM, BCM95$_g$, BCM95$_s$, SLN$_A$, SLN$_L$ or SLN$_M$ (30µM). Following treatment, we proceeded to measure changes in intracellular Ca²⁺ levels (ratiometric measurement at 340nm and 380nm, expressed as $\Delta F/F_0$). Ca²⁺ traces (A) and graphs summarizing Ca²⁺ release from the ER into the cytoplasm following inhibition of SERCA by curcumin (B) are shown. N=4. **=$p<0.01$, ***=$p<0.001$.

6.3.3 Whilst several curcumin formulations reduce $Npc1^{-/-}$ lysosomal storage, others appear to exacerbate phenotypes

Having confirmed that all the curcumin formulations were capable of elevating intracellular Ca^{2+} levels we next determined whether this could induce a reduction in $Npc1^{-/-}$ lysosomal lipid storage, as previously reported with pure unformulated curcumin (Lloyd-Evans et al., 2008). Surprisingly, although SLN_M had the greatest effect on elevating cytosolic Ca^{2+} in $Npc1^{-/-}$ disease astrocytes it had no beneficial effect on lysosomal storage. Indeed, we observed an increase in lysosomal accumulation of cholesterol (Figure 6.4 A), a smaller but significant increase in ganglioside GM1 (Figure 6.4 B), and a further expansion of the lysosomal system (Figure 6.4 C) in $Npc1^{-/-}$ cells treated with SLN_M. Despite their ability to elevate cytosolic Ca^{2+} to a greater degree in the $Npc1^{-/-}$ astrocytes, CGM had no effect on lipid storage (Figure 6.4 A & B) or lysosomal expansion (Figure 6.4 C), whereas SLN_L, in a manner similar to SLN_M, consistently led to an increase in lipid storage of cholesterol (Figure 6.4 A), gangliosides (Figure 6.4 B) and an expansion of lysosomes (Figure 6.4 C). In contrast to the two other SLN nanoformulations, SLN_A had no effect on cholesterol storage (Figure 6.4 A), ganglioside storage (Figure 6.4 B) or lysosomal expansion (Figure 6.4 C). Two curcumin supplements consistently emerged as having the greatest impact on lowering lysosomal lipid storage in the $Npc1^{-/-}$ cells, namely $BCM95_S$ and TRE, with reductions in cholesterol (Figure 6.4 A), ganglioside GM1 (Figure 6.4 B) and lysosomal expansion (Figure 6.4 C) observed with $BCM95_S$, and reductions in cholesterol (Figure 6.4 A) and lysosomal expansion (Figure 6.4 C) with TRE. No detrimental effect of any of the supplements on inducing lysosomal storage of these lipids in $Npc1^{+/+}$ cells was observed (data not shown).
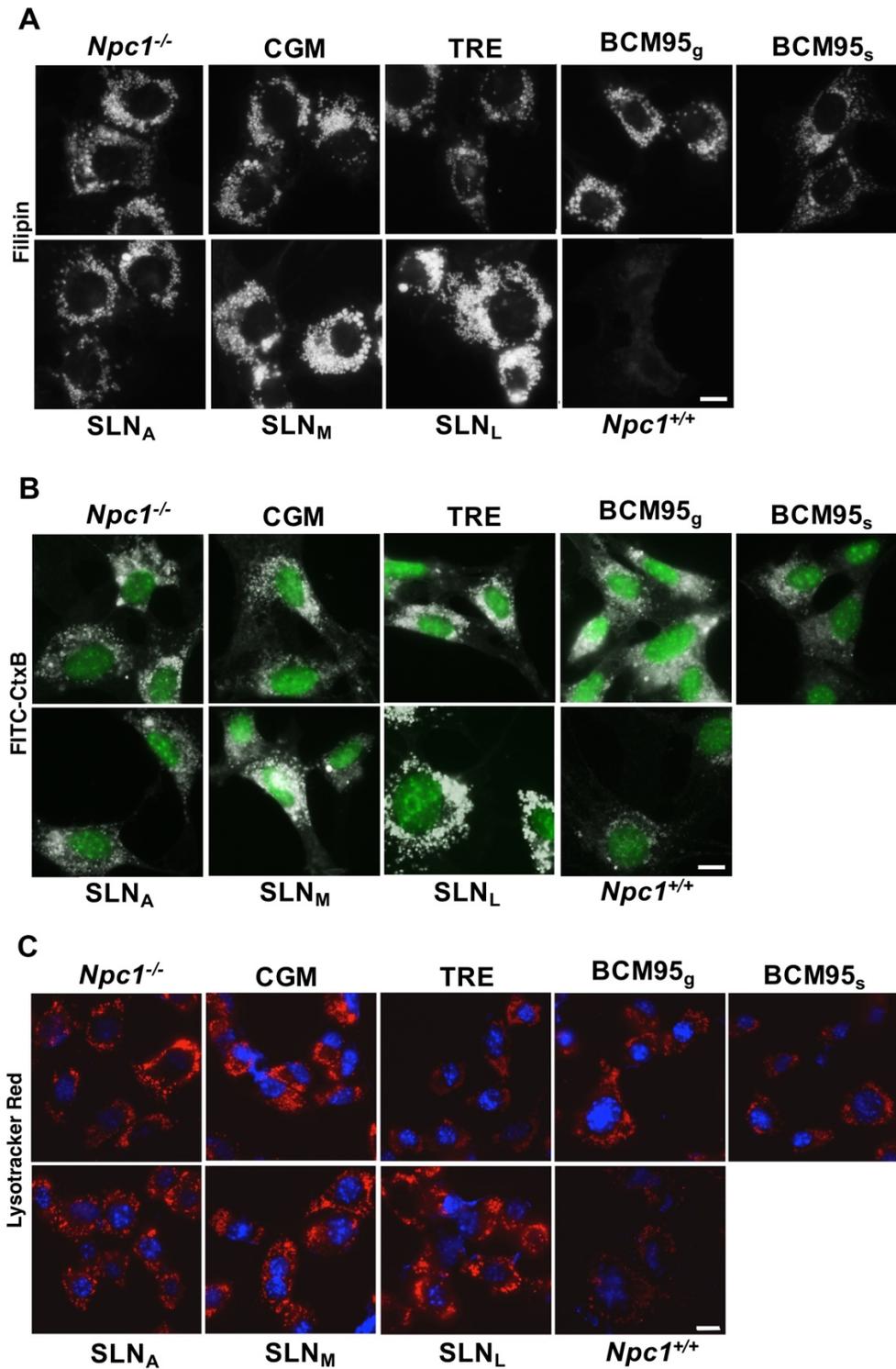
Figure 6.4. Whilst several curcumin formulations reduce *Npc1*^{-/-} lysosomal storage, others appear to exacerbate phenotypes. *Npc1*^{+/+} (wild-type) cells were left untreated whilst *Npc1*^{-/-} (NPC1) astrocytes were either untreated or treated with TRE, CGM, BCM95g, BCM95s, SLNA, SLNL or SLNM (30µM). Cells were then fixed or imaged live following staining with either filipin for cholesterol (A), FITC-CtxB for visualizing ganglioside GM1 (B) or lysotracker green for lysosomes (C) (in A & B, nuclei were counterstained using hoechst 33258). N=3, scale bar = 10µM.

6.3.4 Curcumin nanoformulations have varying effects on endocytosis in *Npc1^{-/-}* glia

To determine the cause of the elevated lipid storage levels in the *Npc1^{-/-}* cells treated with SLN$_L$ and SLN$_M$ we investigated whether incubation with these curcumin nanoformulations had any effect on endocytosis, which is known to be altered in NPC disease (te Vruchte et al., 2004) and is the main route for bulk lipid entry into the cell. Following a joint incubation of the cells with both the curcumin nanoformulations and 10kDa Texas Red Dextran for 4 hours, we observed some key differences between the formulations. In parallel with the reduced lipid storage observed in *Npc1^{-/-}* cells treated with TRE and BCM95s (Figure 6.4), and in keeping with previous data on curcumin (Lloyd-Evans et al., 2008) we also observed a partial correction in the endocytic transport defect (Figure 6.5) with these two curcumin formulations. *Npc1^{-/-}* disease cells have been shown to have a delay in transport between early and late endosomes (Lloyd-Evans et al., 2008, Lachmann et al., 2004, Mayran et al., 2003). Following 4 hour treatment with Texas Red Dextran, this probe can be seen to cluster around the nucleus in late endosomes and lysosomes in the *Npc1^{+/+}* cells (Figure 6.5 A), whereas in the *Npc1^{-/-}* cells it has a broader distribution (including staining close to the plasma membrane) predominantly representative of early endosomes and to a lesser degree some late endosomes. Both TRE and BCM95$_s$, as well as SLN$_A$, appear to have partially rescued this transport defect with Texas Red Dextran staining now clustered in a peri-nuclear region indicative of late endosomes and lysosomes, very little staining in proximity to the plasma membrane, indicative of early endosomes, can be seen. Interestingly, both SLN$_M$ and SLN$_L$ appear to have either reduced the entry of Texas Red Dextran into the *Npc1^{-/-}* astrocytes or enhanced it's recycling out of the cell as the total level of fluorescence is lower by ~65% and ~85% respectively compared to the untreated cells (Figure 6.5). This would appear to suggest a connection between the elevated lipid storage and a further defect in endocytosis in the *Npc1^{-/-}* cells, however, we also observed reduced fluorescence indicating reduced internalization of the Texas Red Dextran probe in the *Npc1^{-/-}* cells treated with BCM95$_g$ (~88%) and CGM (~65%). As no lipid storage was observed in these cells (Figure 6.4) it must be concluded that the defect in endocytosis of Texas Red Dextran is not the cause of the elevated lipid storage observed with SLN$_M$ and SLN$_L$. In an attempt to reconcile these data, we attempted to measure phospholipid accumulation in the curcumin formulation treated cells. Unfortunately, we mainly observed reduced staining of the phospholipidosis probe HCS LipidTOX red (Figure 6.6) correlating with the cells that had the greatest defect in endocytosis. This suggests that the probe, the identity of which has not been made public knowledge by Invitrogen, is more than likely an endocytosed phospholipid and as such is not a useful probe when cells have a considerable endocytosis defect.
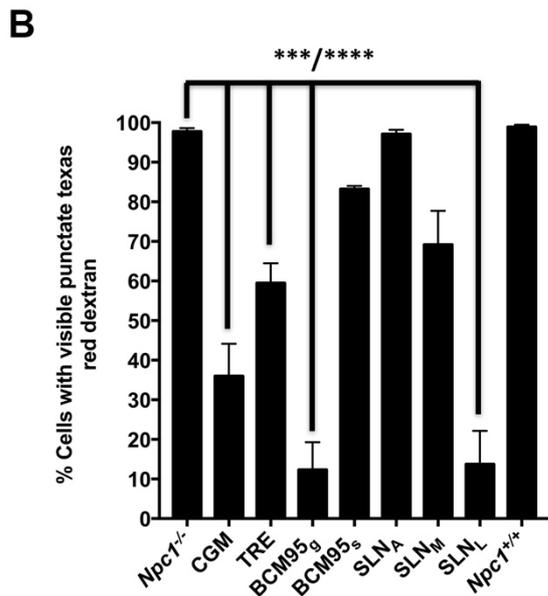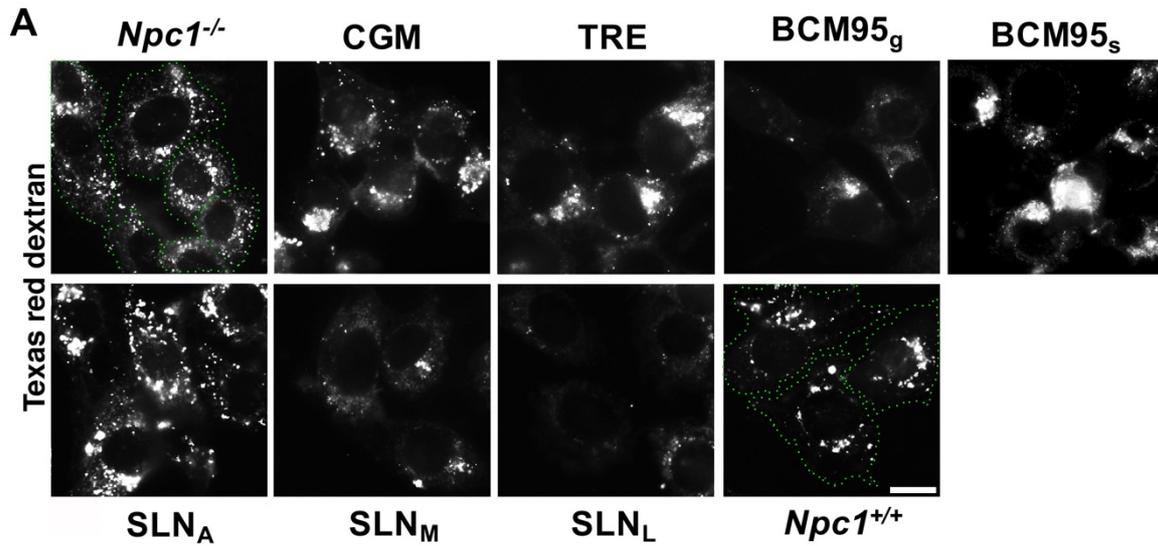
Figure 6.5. Curcumin nanoformulations have varying effects on endocytosis in *Npc1-/-* glia. *Npc1+/+* (wild-type) cells were left untreated whilst *Npc1-/-* (NPC1) astrocytes were either untreated or treated with TRE, CGM, BCM95$_g$, BCM95$_s$, SLN$_A$, SLN$_L$ or SLN$_M$ (30µM). Cells were then incubated for 4 hours with supplement plus 0.25mg/ml Texas Red Dextran, and imaged live. Representative images can be seen in A and images were quantified according to probe distribution to generate graph B. Dotted lines around *Npc1-/-* and *Npc1+/+* cells show the location of the plasma membrane. N=3, scale bar = 10µM. ***=P<0.001, ****=P<0.0001.
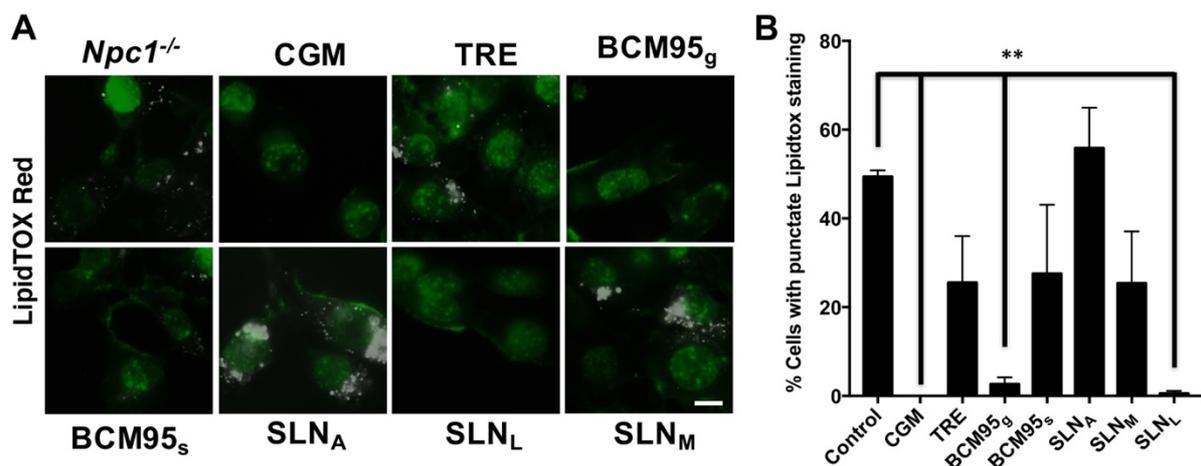
Figure 6.6. Phospholipidosis does not appear to occur following treatment with the curcumin nanoformulations. Following overnight treatment with TRE, CGM, BCM95$_g$, BCM95$_s$, SLN$_A$, SLN$_L$ or SLN$_M$ (30μM) $Npc1^{-/-}$ cells were incubated for 4 hours with supplement plus the phospholipidosis probe HCS LipidTOX Red (nuclei counterstained with hoechst 33258, pseudocolored green) prior to live imaging. Representative images can be seen in A and images were quantified depending on punctate probe distribution, indicative of phospholipidosis, (compared with no stain) to generate graph B. A complete absence of staining following treatment with several supplements suggests that this probe is endocytosed, and therefore is not particularly useful when measuring phospholipid levels in cells that have a considerable endocytosis defect (Figure 6.5). N=3, scale bar = 10μM. **=P<0.01.

6.3.5 Lipid content varies greatly across the curcumin nanoformulations

Having observed that some of the curcumin nanoformulations increased lipid storage in $Npc1^{-/-}$ disease cells, and that this did not completely correlate with defects in endocytosis induced by the curcumin formulations, we decided to determine the nature of the lipid species in each formulation by solvent extraction and separation by HPTLC. Perhaps unsurprisingly, TRE had the lowest lipid content with very few bands present which correlate with those observed at a higher level in BCM95$_s$ and BCM95$_g$ (Figure 6.7 A & B), both of which contain essential oils of curcumin that are presumably present in lower concentrations in TRE. CGM, which has few lipids, also contains one of these bands, the identity of which is currently unknown but could possibly be related to the galactomannan present in CGM or is a component of the curcumin used in manufacturing CGM. Interestingly, the three curcumin species are visible in all lanes (compare with Figure 6.2 D) between the glucosylceramide and cholesterol bands (Figure 6.7 A). As well as TRE and CGM, two other curcumin nanoformulations, BCM95$_s$ and SLN$_A$, contained very few lipids with only the reported triglycerides and fatty acids present for SLN$_A$ (the band above cholesterol). Otherwise, the remaining curcumin supplements (SLN$_L$, BCM95$_g$, and SLN$_M$) had significant levels of a variety of lipids. SLN$_M$ had the highest lipid content (Figure 6.7 A & B) and is reported as using phospholipid to solubilize curcumin, by similarity to the standard this could represent

lecithin (Table 6.1, Figure 6.7 C) as well as to BCM95$_g$ (Figure 6.7 A, B, & C) which incorporates lecithin (Table 6.1). SLN$_L$ is also reported to contain lecithin (Table 6.1), this appears to be the case although there are fewer bands when compared to the standard (Figure 6.7 C) with one or two fainter additional bands also present which are also seen in SLN$_M$ (Figure 6.7 C). For the purposes of this study, our TLC analysis largely confirms the stated lipid content of these formulations whilst also indicating the presence of a few other lipids. Perhaps of most importance is that none of the supplements contained lipids that are known to accumulate in NPC1 disease. To confirm this we ran the HPTLC plates in 2 solvent systems (Figure 6.7 A & B). First we used a solvent system comprising $CHCl_3:MeOH:H_2O$ 65:25:4 to separate BMP from sphingomyelin and which also allows visualization of neutral glycosphingolipids such as GlcCer (three lipids that are stored in NPC disease). We observed a small amount of BMP and sphingomyelin in SLN$_M$ but did not observe any of these lipids in the other formulations (Figure 6.7 A). In order to separate cholesterol and ceramide we used a solvent system comprising $CHCl_3:MeOH:H_2O$ 80:10:1. We did not observe any appreciable amount of cholesterol in any of the formulations (Figure 6.7 B). We can therefore rule out that the lipid formulations are themselves the source of the additional lipid storage that we observe in the *Npc1*^{−/−} astrocytes treated with SLN$_L$ and SLN$_M$. However, both SLN$_L$ and SLN$_M$ contain high amounts of phospholipid (Figure 6.7 A, B & C), so a change in NPC1 lysosomal metabolism as a result of phospholipid accumulation cannot be ruled out.
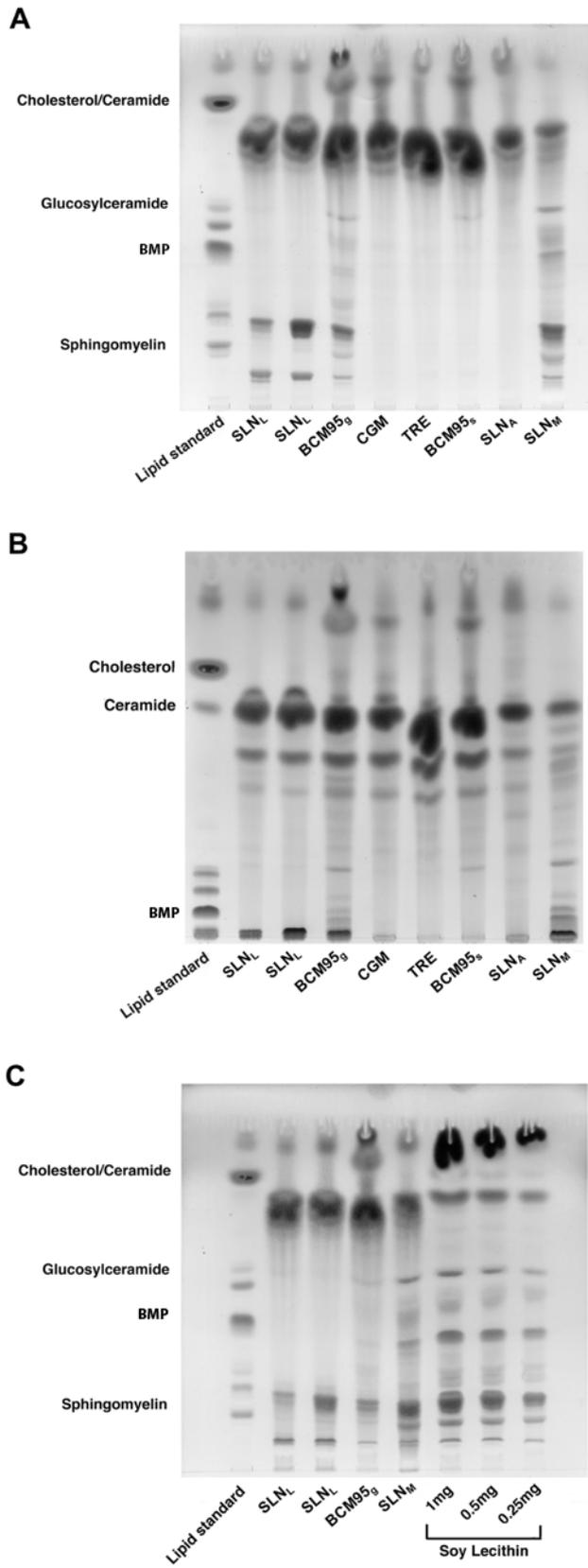
Figure 6.7. Lipid content varies greatly across the curcumin nanoformulations. TLC was used to analyze solvent extracted curcumin nanoformulations. Lipid content was visualized with p-anisaldehyde: in (A) phospholipids were seperated using a development solvent system of chloroform:methanol:H_2O 65:25:4, in (B) improved separation of cholesterol from ceramides

was achieved using a developing solvent system of chloroform:methanol:H_2O 80:10:1. C) shows a comparison of selected nanoformulations alongside lecithin standards, a common component of the nanoformulations. Lipid standards (15µg) corresponding to the unknown sample bands are indicated on the left hand side. BMP = bis(monoacylglycero)phosphate. N=2, experiments were performed by Dr Luke J Haslett, Post Doctoral researcher in the ELE lab.

6.3.6 Curcumin nanoformulations have varying effects on *Npc1*$^{-/-}$ disease cellular viability

Having shown that some of the supplements could alter Ca^{2+} levels differentially between the *Npc1*$^{+/+}$ and the *Npc1*$^{-/-}$ astrocytes, with greater release in *Npc1*$^{-/-}$ (Figure 6.3), that some caused an increase in lysosomal storage (Figure 6.4), and that some induced defects in endocytosis (Figure 6.5) potentially caused by membrane damage triggered by the nanoformulation itself (Panariti et al., 2012), we decided to test whether any of the curcumin formulations had any effect on cellular viability. First we utilized an early marker of apoptosis, extracellular live binding of FITC-Annexin A5 to plasma membrane phosphatidylserine (PS). PS is externalized to the outer leaflet of the plasma membrane as one of the first events in apoptosis. Following 16 hour treatment with the supplements, no staining of extracellular PS by FITC-Annexin A5 is detected in any of the conditions apart from the *Npc1*$^{-/-}$ cells treated with CGM and SLN$_L$ (Figure 6.8 A). As a positive control to confirm that staining is indicative of apoptosis we treated cells with nigericin, a molecular poison, and observed plasma membrane FITC-Annexin A5 staining (Figure 6.8 A). Interestingly, some intracellular staining of FITC-Annexin A5 indicative of endosomes in observed in the *Npc1*$^{-/-}$ disease cells treated with SLN$_L$ (Figure 6.8 A), suggesting either the possibility of necrosis or that the curcumin nanoformulation has disrupted the plasma membrane sufficiently to allow Annexin A5 to enter but not a 10kDa dextran (Figure 6.5). To confirm our viability findings with FITC-Annexin A5 we used a metabolic marker of cellular viability, namely mitochondrial activity measured using MTS. Of the curcumin formulations tested, all bar SLN$_A$ had some effect on *Npc1*$^{-/-}$ mitochondrial activity and cellular viability following a 30 hour incubation with the supplements (Figure 6.8 B). TRE, BCM95$_g$ and BCM95$_s$ had a minimal ~7-8% reduction in mitochondrial function whereas SLN$_M$, SLN$_L$ and CGM substantially, and significantly, reduced cellular viability by ~40-50% respectively. No detrimental effect on cell viability of any of these formulations was observed on *Npc1*$^{+/+}$ cells (not shown).
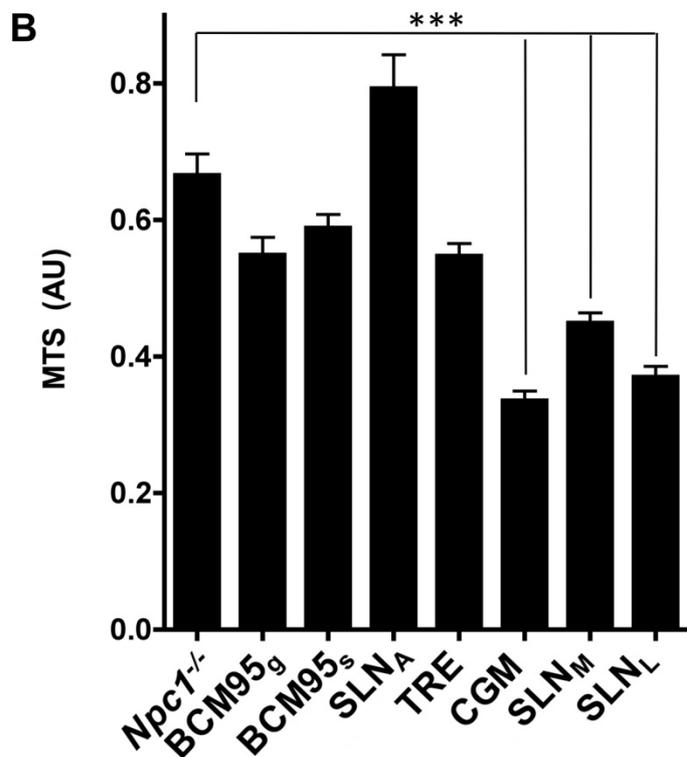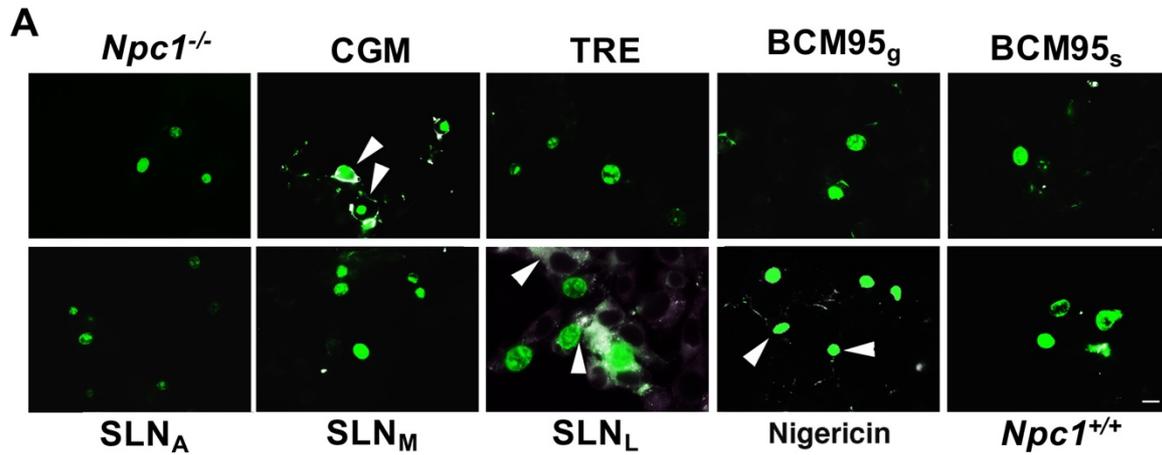
Figure 6.8. Curcumin nanoformulations have varying effects on *Npc1*−/− cellular viability. A) Following 16-hour treatment with TRE, CGM, BCM95$_g$, BCM95$_s$, SLN$_A$, SLN$_L$ or SLN$_M$ (30μM), *Npc1*−/− cells (plus untreated *Npc1*−/− and *Npc1*+/+ controls) were stained using the apoptotic marker Alexa Fluor 488-Annexin A5 (white, nuclei counterstained with hoechst 33258, pseudocoloured green) prior to live imaging. Nigericin (40μM, 2 hours) was used as a positive control. White arrows indicate examples of apoptotic cells with plasma membrane staining. B) Cells were treated with curcumin nanoformulations (as above) for 48 hours prior to measurement of mitochondrial activity via the MTS assay (AU = absorbance units). N=3, scale bar = 10μM, ***=P<0.001.

| CONTROL CELLS | Ca CALCIUM ION | NAADP INDUCED CA2+ RELEASE | UNFORMULATED CURCUMIN |
| NPC CELLS | ENDOCYTOSIS | CURCUMIN INDUCED CA2+ RELEASE | CURCUMIN NANOPARTICLE |
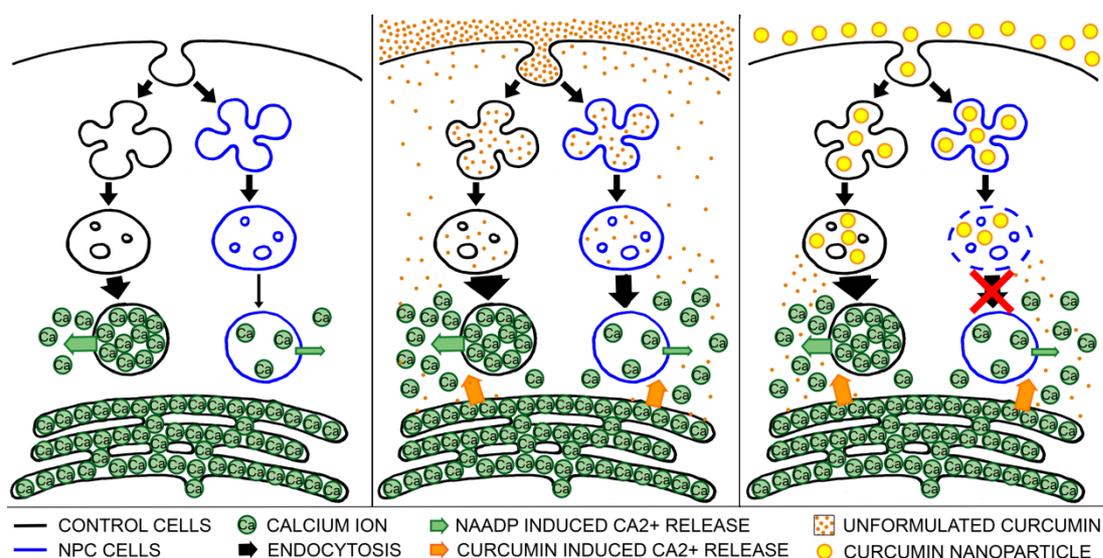
Figure 6.9. Proposed impact of curcumin nanoformulations on *Npc1*^{-/-} cells. A) In control cells (*Npc1*^{+/+}) endocytosis culminates in lysosomes where lysosomal Ca^{2+} release enables fusion of the different organelles involved. In NPC disease (*Npc1*^{-/-}), reduced lysosomal Ca^{2+}, and associated reduced lysosomal Ca^{2+} release leads to a reduction in endocytosis and endosomal fusion events. B) Unformulated curcumin releases Ca^{2+} from the ER via partial inhibiton of SERCA and subsequent uncovering of ER Ca^{2+} leak. This Ca^{2+} release around lysosomes stimulates endocytosis and can overcome the defect in endosomal fusion in NPC disease. C) Curcumin nanoformulations, which are endocytosed, interact with early endosomal membranes leading to potential membrane damage (as they are more fluid in NPC). This in turn further inhibits endocytosis and prevents the benefit mediated by ER Ca^{2+} release induced by the released curcumin. Slower curcumin release from these nanoformulations results in prolonged intracellular Ca^{2+} release and the triggering of apoptosis. Figure provided by Dr Helen Waller-Evans.

6.4 Discussion

Unformulated curcumin has been shown to be able to ameliorate NPC disease in five separate studies (Lloyd-Evans et al., 2008, Borbon et al., 2012b, Williams et al., 2014, Efthymiou et al., 2015, Fineran et al., 2016), whilst curcumin formulated into a lipid vector has been shown to have little to no benefit in the *Npc1*^{-/-} mouse (Borbon et al., 2012b). Despite this, reports of NPC patients taking formulated curcumin exist (Vockley, 2009). The aim of the present study was therefore to compare a number of commercially available lipidated curcumin formulations and determine whether they could mediate any benefit at the cellular level using *Npc1*^{-/-} disease cells. Our project focused on a range of lipidated curcumin nanoformulations, which are used for increasing the bioavailability of curcumin, which is otherwise poorly absorbed through the intestines (Prasad et al., 2014). Formulation of curcumin into a lipid vector allows for improved delivery across the blood-gut barrier, the achievement of higher concentrations of curcumin in the blood and tissues, and reduced renal clearance, all of which is essential for treating disease (Bi et al., 2017). Recent evidence has shown that formulation into

nanoparticles allows for even greater penetration into the blood and higher steady state levels, dependent on particle size (Bi et al., 2017). Our study is the first to demonstrate that all of these formulated lipidated curcumin particles are nanoparticles (and therefore are nanoformulations), ranging in size from 50-250nm (Figure 6.2 A, B & C).

With respect to the ability of these nanoformulations to modulate intracellular $Ca^{2+,}$ all were capable of inducing Ca^{2+} release from the ER and elevating cytosolic Ca^{2+} levels (Figure 6.3). It was interesting to note that four, CGM, SLN_A, SLN_M and SLN_L induced greater Ca^{2+} elevation in the $Npc1^{-/-}$ cells but this did not correspond with a reduction in lysosomal storage as would have been expected (Lloyd-Evans et al., 2008)(Figure 6.4). However, this enhanced intracellular Ca^{2+} release elicited by the majority of these nanoformulations (with the exception of SLN_A) did correspond with increased cellular toxicity, namely reduced mitochondrial activity and apoptosis (Figure 6.8). Results in Figures 6.3 A and 6.2 E demonstrate how the nanoformulations cause slow curcumin release, resulting in prolonged Ca^{2+} increase with $Npc1^{-/-}$ cells. This property could be useful when choosing an appropriate NPC therapy as cellular benefits may be observed over longed time periods that seen with unformulated curcumin.

A surprising result of our work is that although all of the nanoformulations of curcumin could modulate intracellular Ca^{2+} (Figure 6.3), very few actually had an impact on $Npc1^{-/-}$ disease lysosomal lipid storage (Figure 6.4). As unformulated curcumin has been shown in several studies to be effective (Lloyd-Evans et al., 2008, Williams et al., 2014, Efthymiou et al., 2015, Fineran et al., 2016), we hypothesized that this was due in some way to the properties of the lipid carrier. Although SLN_A appears to have a small benefit on some components of $Npc1^{-/-}$ lysosomal storage, no effect is seen with CGM, whilst treatment with SLN_M and SLN_L led to an elevation in lysosomal storage (Figure 6.4). This worsening of the $Npc1^{-/-}$ lysosomal storage phenotype was greatest with SLN_L, but the exact reasons underlying this unexpected phenotype are unclear. SLN_L and SLN_M both appeared to significantly reduce endocytosis of Texas Red Dextran (Figure 6.5), which might explain the elevated lysosomal storage (Figure 6.4). However, we also observed this endocytosis defect with CGM and $BCM95_g$ (Figure 6.5), neither of which had any effect on lysosomal storage (Figure 6.4), which rules this out as a possibility. Based on the similar properties of SLN_L and SLN_M particles one possibility is that their lipid content is related to the enhanced lysosomal storage we observed in the $Npc1^{-/-}$ cells treated with these nanoformulations (Figure 6.4). This is supported by the lack of effect of SLN_A, which has a similar formulation but is substantially different in that it contains sodium alginate, which can restrict the diffusion of phospholipids (Mackie et al., 2016) and may therefore ameliorate its effects on the $Npc1^{-/-}$ cell. However, we did not observe the presence of any NPC disease storage lipids in these nanoformulations, ruling this out as a possible cause of the elevated storage (Figure 6.7). One further potential cause of the elevated lipid storage is that the curcumin itself is trapping cholesterol within

the $Npc1^{-/-}$ disease lysosome. Curcumin has been suggested to be capable of interacting with cholesterol (Jourghanian et al., 2016) and as such, delivery of curcumin into the endocytic system as a nanoparticle could potentially result in further entrapment of cholesterol within these compartments that would reduce any benefit of the elevated intracellular Ca^{2+}. This mechanism could explain why only a small number of the curcumin nanoformulations led to any observable benefit. Another possibility underlying the increased lipid storage is that three of the four nanoformulations, CGM, SLN_M and SLN_L have elicited some toxicity in the cells (Figure 6.8). The associated cellular stress would lead to reduced turnover and a greater degree of lipid accumulation in the non-dividing cells, supported by the reduced mitochondrial activity (Figure 6.8 B). However this lipid accumulation occurs, it is clearly not beneficial for lysosomal lipid levels to be elevated in cells from a lysosomal storage disease. One additional outcome of our findings is that they argue against curcumin working to rescue NPC1 lysosomal storage by exocytosis, as has been suggested (Canfran-Duque et al., 2014), as the supplement that elevates cytosolic Ca^{2+} the most (and would therefore elicit the greatest degree of exocytosis), SLN_A, only has a minimal effect on reducing lysosomal storage levels. Of the curcumin formulations we have tested it is those least modified with lipids that overall have had the greatest beneficial effect on reducing lysosomal lipid storage in $Npc1^{-/-}$ disease cells (BCM95$_s$ and TRE, Figure 6.4). These nanoformulations were able to elevate cytosolic Ca^{2+} (Figure 6.3) without inducing toxicity (Figure 6.8) and were able to reduce lipid storage in $Npc1^{-/-}$ astrocytes (Figure 6.4) as previously reported with pure curcumin (Lloyd-Evans et al., 2008)(Figure 6.9). Our findings are in keeping with the published data from the $Npc1^{-/-}$ mouse model where unmodified curcumin had the greatest effect on survival and function (Lloyd-Evans et al., 2008) whereas lipidated curcumin (SLN_L) had no benefit on $Npc1^{-/-}$ mouse function (Borbon et al., 2012b).

Although this is an *in vitro* study it is important to note that the benefit of curcumin to NPC disease comes from modulation of Ca^{2+} at the ER and not as an anti-oxidant (Williams et al., 2014). It is therefore the effect of curcumin on the individual cells of the body that needs to be considered and as such our study provides useful insight into the potential effects of curcumin formulations on NPC disease cellular function. For example, as previously discussed, the function of the NPC1 intestine and liver is known to be abnormal (Patterson et al., 2012), and it is therefore these tissues that will be primarily affected by short-term treatment with these formulations. Some may transcytose, enter the blood stream and be carried to various other organs before releasing their cargo of curcumin and lipids (Kadam et al., 2012). What impact this may have on disease course is unknown and as the only lipidated nanoformulation of curcumin to be tested in NPC disease has been SLN_L, in the mouse model (Borbon et al., 2012b), which provided no benefit it is clear that more work is needed to determine the safety and efficacy of these nanoformulations on NPC disease prior to any use in human patients.

6.5 Conclusions

As NPC1 is a lipid storage disease the use of a lipidated vehicle may not be the best approach due to the possibility that the additional lipid load could alter metabolism or endocytosis and lead to further lipid storage as we have observed. Based on our evidence, from this report and others (Lloyd-Evans et al., 2008, Borbon et al., 2012b, Williams et al., 2014, Efthymiou et al., 2015, Fineran et al., 2016) it is perhaps the least modified forms of curcumin that appear to have the greatest benefit for NPC1 disease both *in vitro* and *in vivo*. Ultimately, the utilization of curcumin itself may not be ideal for treating NPC1 disease, owing to its low bioavailability (Prasad et al., 2014), and other more bioavailable Ca^{2+} modulators (Visentin et al., 2013, Xu et al., 2012b), see Chapter 3, may yet prove to be the most effective therapeutic approach for targeting the lysosomal Ca^{2+} dysfunction in NPC disease.

Chapter 7: General Discussion

7.1 Summary

Overall, this thesis aimed to investigate ion dyshomeostasis in NPC1 both *in vitro* and *in vivo*. Results in Chapter 3 illustrated a Zn^{2+} transport function for NPC1, and demonstrated partial reversal of the NPC phenotype i*n vitro* using the Zn^{2+} chelator phytic acid. Chapter 4 investigated various Ca^{2+} modulators for the treatment of NPC, including tanganil, previously found to provide benefit against ataxic phenotypes in NPC patients (Bremova et al., 2015). Chapter 5 investigated the effects of different formulations of curcumin, a Ca^{2+} modulator known to provide benefit in *Npc1*$^{-/-}$ mice. And finally, Chapter 6 details the development of zebrafish models of NPC, required to test any potential therapies *in vivo*, whilst demonstrating NPC-like phenotypes following treatment of zebrafish with an inhibitor of lysosomal Ca^{2+} signaling via NAADP, called Ned-19. Together, these results demonstrate the importance of both Ca^{2+} and Zn^{2+} dyshomeostasis within NPC and suggest ways to treat these defects.

7.2 NPC1 functions as a lysosomal Zn^{2+} transporter, with loss of function of NPC1 resulting in downstream lipid storage

Prior to this project, indirect observations of Zn^{2+} accumulation within NPC1 cells, brain (Waller-Evans and Lloyd-Evans, unpublished) and patient blood samples (Hung et al., 2014), as well as upregulation of a variety of Zn^{2+} transporters and solute carriers (Reddy et al., 2006, Vazquez et al., 2012), suggested dyshomeostasis of this ion within NPC. Although NPC1 is often referred to as a cholesterol transporter following observations by Pentchev *et al.* 1985, there exists no direct evidence that full length purified NPC1 transports cholesterol (Lloyd-Evans and Platt, 2010). The results presented in Chapter 3 however clearly demonstrate the first direct function for NPC1 as a lysosomal Zn^{2+} transporting RND permease, with loss of function initiating downstream lipid storage and lysosomal expansion.

Within this thesis, specificity of the NPC1 lysosomal Zn^{2+} storage phenotype was determined by showing that other cellular Zn^{2+} stores (ER, mitochondria) are not affected in NPC (Figure 3.4), and that Zn^{2+} storage is specific to NPC1 rather than being a general phenotype of lysosomal storage diseases (Figure 3.5). Indirect evidence for a Zn^{2+} transporting function for NPC1 included observations that Zn^{2+} storage occurs prior to lysosomal expansion and lipid storage phenotypes following either treatment with NPC1 inhibitors (U18666A (Figure 3.6), 1NMP (Figure 3.7)) or addition of Zn^{2+} to cells overexpressing the lysosomal Zn^{2+} import channel ZnT2 (Figure 3.8). Following characterization of

NPC1 as the only known mammalian RND permease (Scott and Ioannou, 2004, Tseng et al., 1999), evidence for a Zn^{2+} transporting function was supported by observations of sequence conservation, especially in residues known to be important for Zn^{2+} transport, between NPC1 and the Zn^{2+} transporting RND permease ZneA (Figure 3.11). Finally, direct proof for a Zn^{2+} transporting function of NPC1 can be seen when looking at the results of a novel assay which exploits lysosomal exocytosis in order to assess the function of lysosomal membrane proteins (Figure 3.12).

7.3 NAADP-mediated Ca^{2+} signaling is important within the brain, and reduced lysosomal Ca^{2+} in NPC1 is responsible for downstream lipid storage

The importance of lysosomal Ca^{2+} signaling can be seen in Chapter 5 when treatment with Ned-19, an inhibitor of lysosomal Ca^{2+} signaling via NAADP, resulted in a profound Ca^{2+} signaling defect in 5dpf zebrafish alongside storage of cholesterol and ganglioside GM1 (Figure 5.6). The substantial reduction in Ca^{2+} signaling within the zebrafish brain following treatment with Ned-19 is in line with numerous evidence suggesting the importance of lysosomal Ca^{2+} signaling via NAADP. Firstly, NAADP binding sites are observed throughout the brain (Patel et al., 2000) and exogenous stimulation with glutamate triggers both NAADP synthesis and lysosomal Ca^{2+} release (Pandey et al., 2009). In addition, lysosomal Ca^{2+} release via NAADP regulates the long-term structural plasticity of dendritic spines by triggering extracellular matrix remodeling (Padamsey et al., 2017). Moreover, addition of NAADP can be seen to elicit Ca^{2+} release in brain microsomes (Bak et al., 1999), promote neuronal differentiation (Brailoiu et al., 2006), augment neurite outgrowth (Brailoiu et al., 2005), drive membrane depolarization (Brailoiu et al., 2009b) and increase Ca^{2+} influx via N-type voltage gated Ca^{2+} channels (Hui et al., 2015).

Reduced lysosomal Ca^{2+} in NPC1 has been predicted to be due to inhibition of lysosomal Ca^{2+} uptake by the important cellular metabolite and signaling lipid, sphingosine (Lloyd-Evans et al., 2008, Lloyd-Evans and Platt, 2010). This lipid has previously been shown to inhibit plasma membrane Ca^{2+} channels (Colina et al., 2002), and following inhibition of the NPC1 protein with U18666A, sphingosine acts as the first lipid stored at 10 minutes – followed by reduced lysosomal Ca^{2+} from 30 minutes of treatment (Lloyd-Evans et al., 2008), suggesting it may inhibit lysosomal Ca^{2+} channels as well. Sphingosine storage was demonstrated to be directly responsible for the lysosomal Ca^{2+} defect in NPC following endogenous addition to cells; which resulted in a lysosomal Ca^{2+} defect and lipid storage mimicking that observed in patients, cells and mice (Roff et al., 1991, Lloyd-Evans et al., 2008).

Given the importance of lysosomal Ca^{2+} signaling, it is hardly surprising that reduced lysosomal Ca^{2+} in NPC, most likely caused by lysosomal storage of sphingosine, appears to have a big impact on disease phenotypes, with Ned-19 treatment reducing the amplitude of neuronal Ca^{2+} spikes and initiating downstream lipid storage *in vivo* (Figure 5.6). The importance of the lysosomal Ca^{2+} defect

in NPC is also highlighted by observations that tanganil (Figures 4.9 & 4.10), CGS1680 (Figure 4.1)(Visentin et al., 2013, Ferrante et al., 2016), δ-tocopherol (Chapter 4)(Xu et al., 2012b), and curcumin (Chapter 6)(Lloyd-Evans et al., 2008), are able to reverse NPC lipid storage via their Ca^{2+} modulating abilities. Also, further reducing lysosomal Ca^{2+} by treating with the TRPML1 agonist MLSA1 (Figure 4.2) appears to initiate lipid storage in wild-type cells whilst worsening storage in NPC (Figures 4.3 & 4.4), again demonstrating the importance of lysosomal Ca^{2+} regarding NPC pathogenesis.

7.4 Despite benefits observed, care must be taken when investigating Ca^{2+} modulators for the treatment of NPC

Whilst clear beneficial effects of Ca^{2+} modulators on NPC are demonstrated, work in Chapter's 4 and 6 demonstrate how care must be taken when selecting Ca^{2+} modulators to move to the clinic. This was first demonstrated when looking at effects of the proposed NPC1 therapy and TRPML1 activator MLSA1, which despite previous studies suggesting beneficial effects (Shen et al., 2012), was demonstrated to in fact induce lipid storage within NPC cells (Figures 4.3 & 4.4). Curcumin acts as another potential NPC therapy, however, the low bioavailability of this molecule limits its effects in patients (Anand et al., 2007) and although available over the counter, this natural product is often combined with other compounds to increase its absorption (Anand et al., 2007), and combination effects are rarely investigated. The addition of certain lipid vectors combined with a lack of regulation when developing supplements means that several curcumin nutraceuticals currently being taken by NPC patients may in fact exacerbate lipid storage within cells and induce cellular toxicity (Chapter 6). These results demonstrate how a small change to a formulation can result in big changes to therapeutic effectiveness at the cellular level, and this is also seen when comparing D, L and DL forms of tanganil, whereby mixed isomer (DL) formulations initiate greater Ca^{2+} release in $Npc1^{-/-}$ astrocytes when compared with single isomer (D or L) treatments (Figure 4.7). Finally, whilst results in Chapter 4, combined with the recent case study by Bremova *et al.,* 2015 demonstrate the benefits of Ca^{2+} modulation via tanganil within human patients, potential limited effects of tanganil on certain cell types due to variable expression of its receptor, CaSR, may mean alternative Ca^{2+} modulators would act as better therapies for NPC patients (Figures 3.11 & 3.14).

7.5 How do the Zn^{2+} and Ca^{2+} phenotypes fit together? Potential new pathogenic cascade for NPC1

Pentchev *et al.,* 1985 hypothesized a pathogenic cascade for NPC whereby a primary defect in cholesterol trafficking resulted in all downstream NPC phenotypes (Figure 7.1 A). This however now

appears unlikely following numerous observations (see Chapter 1.4). Having determined the importance of both Ca^{2+} and Zn^{2+} dyshomeostasis in NPC, I next asked how these two phenotypes fit together in order to generate a novel disease cascade (Figure 7.1 C).

Sphingosine, storage of which occurs early in the NPC disease cascade following 10-min treatment with the NPC1 inhibitor U18666A (Lloyd-Evans et al., 2008), is an amine known to require a transmembrane pump to transport it out of lysosomes due to its net positive charge (Lloyd-Evans and Platt, 2010). One study suggested a role of NPC1 in the transport of amines, which could include sphingosine, out of lysosomes (Kaufmann and Krise, 2008). In addition to evidence that sphingosine is able to initiate a lysosomal Ca^{2+} defect (Lloyd-Evans et al., 2008), several factors highlight the importance of this lipid in the development of the NPC phenotype. For one, within NPC patients, sphingosine is increased up to 12-fold in peripheral areas such as the liver and spleen, with a 4-fold increase in the brain (te Vruchte et al., 2004). Furthermore, the yeast ortholog of *NPC1*, *ncr1*, which is able to compensate for *NPC1* deficiency when expressed in mammalian cells (Malathi et al., 2004), appears to transport sphingolipids following observations that mutating its sterol sensing domain results in a primary sphingolipid trafficking defect (Malathi et al., 2004). As previously discussed, NPC1 acts as the only mammalian RND permease (Scott and Ioannou, 2004, Tseng et al., 1999), a class of multi-drug efflux pumps primarily found within gram-negative bacteria. As an RND permease, in combination with above observations, NPC1 may function to transport sphingosine out of lysosomes, resulting in the disease cascade described in Figure 7.1 B (Lloyd-Evans and Platt, 2010).

In addition to potential roles in sphingosine transport, NPC1 appears to act as a lysosomal Zn^{2+} transporter, permitting Zn^{2+} efflux from lysosomes (Chapter 3). Figure 7.1 C shows a newly proposed pathogenic cascade for NPC1: a 2-armed pathway where NPC1 is a multi-substrate RND permease capable of transporting both sphingolipids and Zn^{2+}. As previously discussed, storage of sphingosine, via a currently unknown mechanism, appears to initiate a lysosomal Ca^{2+} defect within NPC1 cells (Lloyd-Evans et al., 2008, Lloyd-Evans and Platt, 2010). As lysosomal Ca^{2+} release is important for endocytosis, this reduction in turn leads to trafficking defects and consequently lipid storage (e.g. cholesterol, sphingomyelin) (Lloyd-Evans et al., 2008). When NPC1 loses its ability to transport Zn^{2+}, Zn^{2+} accumulates in NPC1 lysosomes and is chelated by the head-groups of BMP and other phospholipids (Kobayashi et al., 1999). Zn^{2+} binding to BMP could potentially prevent this phospholipid interacting with ASM, a necessary interaction for the degradation of the sphingomyelin (Kolter and Sandhoff, 2005), in turn leading to lysosomal storage of this lipid. As sphingomyelin and cholesterol interact (Garcia-Arribas et al., 2016), storage of sphingomyelin may in turn lead to some cholesterol storage. It can be seen that from both sides of the cascade, lipid storage self-potentiates and worsens endocytosis defects.

Several observations suggest that the Zn^{2+} and Ca^{2+} storage phenotypes make up separate parts of the disease cascade, as represented in Figure 7.1 C. For one, treating $Npc1^{-/-}$ astrocytes with the Zn^{2+} chelator phytic acid appears to reduce lysosomal storage of Zn^{2+}, cholesterol, BMP, and sphingomyelin whilst unable to correct ganglioside GM1 storage and lysosomal expansion (Figure 3.13), suggesting that Zn^{2+} storage alone is not responsible for the development of all NPC cellular phenotypes. Moreover, treating cells with either ISP1, an inhibitor of sphingolipid synthesis, or HPβCD, a proposed NPC therapy that seems to work via modulation of cholesterol, was unable to correct lysosomal Zn^{2+} storage within $Npc1^{-/-}$ astrocytes, suggesting that storage of this ion is either upstream or independent of sphingosine and cholesterol storage. In addition, miglustat, the only approved NPC therapy (Lachmann et al., 2004) and an inhibitor of glycosphingolipid synthesis (Platt et al., 1994) is able to reduce storage of sphingosine (Stein et al., 2012)(Lloyd-Evans *et al.*, unpublished observation) but not Zn^{2+} (Hung et al., 2014). Another observation which suggests a 2-armed cascade is that variant NPC cells, showing minimal cholesterol storage, still accumulate lysosomal Zn^{2+}. The ability of an RND permease to transport one substrate can be affected by its ability to transport others (Kinana et al., 2013), which means loss of one transport function can potentially initiate either whole or half of the disease cascade. Variant cells may experience only half of the cascade (lysosomal Zn^{2+} accumulation), explaining the lack of substantial cholesterol storage.

Future work investigating the proposed NPC disease cascade (Figure 7.1 C) would include addition of both sphingosine and Zn^{2+} to cells (both astrocytes and cells overexpressing ZnT2 in the case of Zn^{2+}) to the determine effects on Zn^{2+} and sphingosine storage respectively. If the 2 phenotypes occupy different sides of a pathogenic cascade, we would expect addition of sphingosine to be unable to increase Zn^{2+}, and Zn^{2+} addition unable to increase sphingosine.
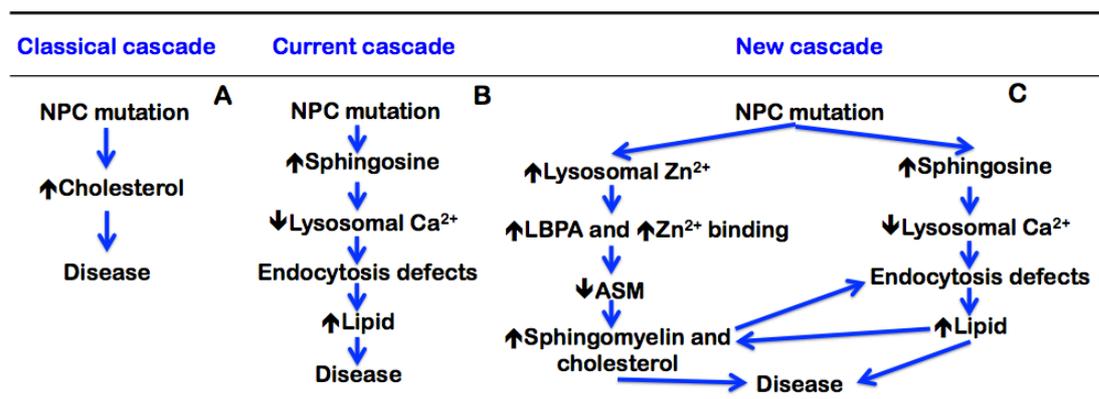
Figure 7.1. Potential NPC pathogenic cascades. A) The classical cascade whereby NPC1 acts as a cholesterol transporter: disruption leads directly to cholesterol storage within lysosomes and disease symptoms. B) Current cascade whereby NPC1 acts as a sphingosine transporter. Defects lead to initial sphingosine storage within lysosomes, Ca2+ signaling and

endocytosis defects, and finally lipid storage and disease. C) As an RND permease, NPC1 could have multiple substrates including Zn2+ and sphingosine, both of which are stored following loss of function. Zn2+ interacts with BMP, and blocks the interaction of BMP with acid sphingomyelinase (ASM); an interaction required for enzymatic function. This leads to storage of sphingomyelin, and consequently cholesterol. Within this proposed cascade, sphingosine storage itself results in a pathway resembling the current cascade (B). Lipid storage from both pathways results in endocytosis defects. Above events combine to cause NPC disease pathogenesis.

7.6 Plausible interactions between the Zn^{2+} and Ca^{2+} arms of the pathogenic cascade

Whilst we suspect that Zn^{2+} and Ca^{2+} dyshomeostasis lie on separate arms of the NPC pathogenic cascade (Figure 7.1 C), some interaction between the 2-pathways is likely. For one, lipid storage that emerges following lysosomal Zn^{2+} accumulation is likely to contribute to further lysosomal dysfunction and endocytosis defects. Furthermore, NPC cells showing lysosomal accumulation of Zn^{2+} are likely to show reduced Zn^{2+} in the cytosol. Low cytosolic Zn^{2+} has been previously hypothesized to prevent endocytosis and increase plasma membrane localization of the Zn^{2+} transporter ZIP4, most likely in order to increase Zn^{2+} import into cells (Kim et al., 2004). In addition to its potential role in regulating endocytosis, numerous studies also suggest Zn^{2+} as a positive regulator of autophagy, although the mechanisms behind this remain largely unknown (Liuzzi et al., 2014). Bearing this in mind, both Zn^{2+} and Ca^{2+} dyshomeostasis may contribute to endocytosis and autophagy defects characteristic of NPC (Lloyd-Evans et al., 2008, Ko et al., 2001, Mayran et al., 2003). In addition, both Ca^{2+} and Zn^{2+} have well established roles in CNS function and synaptic transition, with dyshomeostasis of both of these ions having been implicated in the pathology of numerous neurodegenerative diseases (Corona et al., 2011, Prakash et al., 2015, Pchitskaya et al., 2017). Within Alzheimer's, disrupted Ca^{2+} and Zn^{2+} appear to have a synergistic effect on Aβ and tau accumulation, oxidative stress and glutamate receptor over activation, ultimately promoting synaptic and neuronal loss (Corona et al., 2011). Baring this in mind, similar interactions may take place within NPC1 neurons.

7.7 Developing combination therapies to treat both sides of the NPC1 2-armed pathogenic cascade

Simultaneously treating *Npc1*$^{-/-}$ mice with miglustat to target glycosphingolipid storage, curcumin to overcome the lysosomal Ca^{2+} signaling defect and ibuprofen to reduce inflammation can be seen to have a greater neuroprotective benefit when compared with single or dual therapies (Williams et al., 2014), suggesting combinational therapy as an optimal route for NPC. If the 2-armed disease cascade shown in Figure 7.1 C is representative of what happens in NPC1 cells and patients, perhaps the best treatment option would involve co-treating with a Ca^{2+} modulator such as tanganil (Chapter 4) and a Zn^{2+} chelator like phytic acid (Chapter 3). Future work would involve testing these combinatorial

therapies both alone (in our NPC zebrafish, Chapter 5) and in combination (both *in vitro* and *in vivo*). Within zebrafish, effects of both individual and combination treatments on lipid storage (via fluorescent staining and thin layer chromatography) and behavioral defects (spontaneous coiling and touch response) would be assessed. This would both confirm which arms of the pathogenic cascade are responsible for which phenotypes (e.g. is the lysosomal Ca^{2+} defect and/or Zn^{2+} accumulation responsible for the behavioral defects observed in the NPC zebrafish?), as well as providing information about the best combination therapies to take to the clinic.

Gene therapy holds great promise for the treatment of NPC1, with AAV-NPC1 injection leading to increased expression of lysosomal NPC1 (Chandler et al., 2017), presumably allowing NPC1 to transport its substrates out of lysosomes (e.g. sphingosine, Zn^{2+}). This results in reduced cholesterol storage, reduced Purkinje cell death, improved behavior, and increased lifespan (Chandler et al., 2017). Despite benefits observed, AAV-NPC1 injected mice still present with shortened lifespan and neuronal death when compared with wild-type, most likely due to variable expression of the AAV vector in the brain (Chandler et al., 2017). As previously discussed, lysosomal Zn^{2+} accumulation in NPC most likely results in reduced cytosolic levels of this ion. Perhaps using gene therapy to increase lysosomal NPC1 levels would stimulate Zn^{2+} transport out of lysosomes, potentially overcoming the cytoplasmic Zn^{2+} deficiency, whilst in turn reducing toxic lysosomal levels. This may have some beneficial effects regarding endocytosis and autophagy, both of which are reliant on cytosolic Zn^{2+} (Kim et al., 2004, Liuzzi et al., 2014). On top of this, increasing NPC1 in the lysosomal membrane via gene therapy in combination with small-molecule therapies (e.g. tanganil, phytic acid, miglustat) may optimize benefits following AAV-NPC1 injection by increasing the number of cells receiving therapy and reducing lysosomal storage of lipids and Zn^{2+}, stimulating lysosomal Ca^{2+} signaling, and improving endocytosis defects from multiple directions.

7.8 Concluding remarks

To conclude this thesis, reduced lysosomal Ca^{2+} in NPC1 is instrumental in the development of the NPC phenotype. This phenotype emerges following lysosomal accumulation of sphingosine, which appears to inhibit lysosomal Ca^{2+} uptake channels. Moreover, having discovered a novel function for NPC1 as a lysosomal Zn^{2+} transporter, acting to transport Zn^{2+} out of lysosomes, lysosomal Zn^{2+} accumulation also appears crucial in the NPC disease cascade. These findings allowed elucidation of a potential new 2-armed pathogenic cascade for NPC, whereby NPC1 acts as an RND permease able to transport both Zn^{2+} and sphingosine, and inhibition of NPC1 transport function leads to the primary accumulation of both these substrates. Combination treatments utilizing Ca^{2+} and Zn^{2+}-modulating therapies, more of

which need to be investigated to optimize benefits in patients, perhaps alongside gene therapy approaches, may act as the best way to treat both arms of the pathogenic cascade. Future work will involve testing therapies both alone and in combination within our NPC zebrafish.

Appendices

Appendix 1: T-Coffee software was used to compare sequences of NPC1 with ZneA: a recently discovered proton driven Zn^{2+} transporting RND permease found within the heavy-metal resistant bacteria *Cupriavidus metallidurans* CH34 (Pak et al., 2013)

T-Coffee alignment result

MSA

The multiple sequence alignment result as produced by T-coffee.

```
T-COFFEE, Version_11.00.8cbe486 (2014-08-12 22:05:29 - Revision 8cbe486 - Build 477)
Cedric Notredame
SCORE=632
*
 BAD AVG GOOD
*
NPC1  :  53
ZneA  :  66
cons  :  63

NPC1   MTARGLALGLLLLLLCPAQVFSQSCVWYGECGIAYGDKRYNCEYSGPPKPLPKDGYDLVQELCPGFFFGNVSLCC
ZneA   MIERLVTLCFNRRG-IVALVFAM---------------------------------------------------

cons   *  *  *::* :       * **:

NPC1   DVRQLQTLKDNLQLPLQFLSRCPSCFYNLLNLFCELTCSPRQSQFLNVTATEDYVDPVTNQTKTNVKELQYYVGQ
ZneA   --VALYGWYAWKQLPLE-------------------------------AYPDIAD-TTSQVVTQVNGLA-----

cons        *       ****:                              *  *  .*  .*.*. *:*: *

NPC1   SFANAMYNACRDVEAPSSNDKALGLLCGKDADACNATNWIEYMFNKDNGQAPFTITPVFSDFPVHGMEPMNNATK
ZneA   --------------------------------------------------------------------------

cons

NPC1   GCDESVDEVTAPCSCQDCSIVCGPKPQPPPPPAPWTILGLDAMYVIMWITYMAFLLVFFGAFFAVWCYRKRYFVS
ZneA   --------------------AEEVEQQITIPLEREIMGVPGMHVMRSKSTFG----------------------

cons                       .    *  .  *    *:*: .*:*:   : :.

NPC1   EYTPIDSNIAFSVNASDKGEASCCDPVSAAFEGCLRRLFTRWGSFCVRNPGCVIFFSLVFITACSSGLVFVRVTT
ZneA   --------------------------------------------------------------LSLITVVFKD

cons                                                                 .*: *  ..

NPC1   NPVDLWSAPSSOARLEKEYFDOHFGPFFRTEQLIIRAPLTDKHIYQPYPSGADVPFGPPLDIOILHOVLDL----
ZneA   GAEDYWSRQRLQERINGVSLPYGAQPSL----DPLTSPI-----------------GEIYRYTLVSKTRDLRELS

cons   .. * **    * *::  :       * :      : :*:            *       :: :. **

NPC1   ------------OIA----------------IENITASYDNETVTLODICLAPLSPYNTNCTILSVLNYFONS--
ZneA   ELQFWKVIPRLKQVAGVVDVANFGGLTTQFMLEFDPVMLSKYNISLNQITQA-ISENNANAG-GSILNRGEQGLV

cons                *:*               :*  ..  .: .::*::*  * :* *:*.  *:** ::.

NPC1   --------------HSVLDHKKGDDFF-------VYADYHTHF-LYCVRAPASLNDTSLLHDPCLGTFGGPVFPW
ZneA   VRGVGLIRNLDDLGNIVVTQKNGVPVLVKDLGRVVLGNPQRHGILGMDRNPDT----------------------

cons                 : *: :*:* .:       * .: : *  *   * * :

NPC1   LVLGGYDDQNYNNATALVITFPVNNYYNDTEKLQRAQAWEKEFINFVKNYKNPNLTIS--FTAERSIEDELNR--
ZneA   ---------------IQGITLLLK------------------------NENPSVVMEGVHAAVRDLNDNILPKD

cons                  **: ::                        :**.:.:.  .:* *.::*::

NPC1   -----------ESDSDVFTVVISYAIMFLYISLAL----GHMKSCRRLLVDSKVSLGIAGILIVLSSVACSLGVF
ZneA   VKVVPYIDRSNLVDATVHTVGKTLMEGMFLVSLVLLLFLGSPRAAI-----------IVAVTIPLSL-LMAFILM

cons            *: *.**  :    :: :**.*    *  ::.         *..: * **    :: :.

NPC1   SYIGLPLTLIVIEVIPFLVLAVGVDNIFILVO-AYORDERLOGETLDOOLGRVLGEVAPSMFLSSFSETVAFFLG
ZneA   HHFKIPANLLSLGAIDFGIIVDGAI--VVMENILRRREEDAEKELHGRDIMQSVLQVARPIFFGMIVIITAY-LP

cons   :: :* .*: : .** ::. *.  .:: :  :*:* : *  .::: : :** .:*:. . .*: *

NPC1   ALSVMPAVHTFSLFAGLAVFIDFLLOITCFVSLL---GLDIKROEKNRLDIF---CCVRGAEDGTSVOASESCLF
ZneA   LFA-FQ-RIEYKLFSPMAFAVGFALFGALLVALLLIPGLAYWAYRKPRK-VFHNPALVWLA------PRYESVLN
```

```
cons     :: :      :.**: :*. :.* *  : :*:**  **     .* * :*  . * *        ** *

NPC1    RFFKNSYSPLLLKDWMRPIVIAIFVGVLSFSIAVLNKV-----------DIGLDQSLSMPDDSYMVDYFKSISQY
ZneA    RLVGSTRTA-------IGIAVATLVGVMILGATIGRDFLPYLDEGSIWLQVTLPPGISLEKAGQMADNLRAATME

cons    *:. .: :.          *.:* :***: :. :: ...         :: * .:*: . . *.* ::: :

NPC1    LHAGPPVYFVL------EEGHDYTS-SKGO------NMVCGGMGCNNDSLVOOIFNAAOLDNYTRIGFAPSSWID
ZneA    F---PEVEHVVTQVGRNDEGTDPFSPSHIETAVTLHPYSTWTSGRDKQQLIEAMATRFRDLPGTQVGFSQ-PMID

cons    :   * * .*:    :** * * *: :          * :::.*:: : . :   *::**: . **

NPC1    DYFDWVKPQSSCCRVDNITDQFCNASVVDPACVRCRPLTPEGKQ-----------------------RPQGGDF
ZneA    GVLDKLAGAHSDLVVKVYGNDFAETRQVATAITRLLKTVPGAQDVIIDQEPPLPQVRIDVDRAAAARLGINVADV

cons    . :* :   *  *.  ::*.:: * .* .*   .* .::              : .*.

NPC1    MRFLP---------MFLS--------------------DNPNPKCGKGGHAAYSSAVNILLGHGTRVGATYFM
ZneA    MALIQTGIGGSPVTQVFVEDRSYNVVARFIGSSRNDPEAIGNLTLTAANGAHVALAQVAHIRLAEGETTITREMN

cons    * ::            :*:.                  .* . ...:*.*.* :...:* *..*  .: :

NPC1    TYHTVLQT---SADFIDALKKARLIASNVTETMGINGSAYRVFPYSVFYV--FYEQYLTIIDDTIFNLGVSLGAI
ZneA    KRHLTVRLNLRGRDLSTFLEEARMRID-------------KEVPYDRTHIQVAWGGQFENQQRAQARLAVILPMV

cons    . * .::   . *: *::**: .         : .**. :: : :  : : .*.* * :

NPC1    FLVTMVLLGCELWS----AVIMCATIAMVLVNMFGVMWLWGISLNAVSLVNLVMSCGISVEFC-------SHITR
ZneA    LALMFVLLFGEFKNLRQPALILMA-VPLATLGGLVALHLRGMTLNVSSAVGFIALFGVAVLNAIIMIANLNRWRD

cons    : : :*** *: .   *:*: * :.:. :. : .: * *::**. * *.::   *::*   .       .:

NPC1    AFTVSMKGSRVERA------------------EEALAH-MGSSVFSGITLTKFGGIVVLAFAKSQIFQIFYFRM
ZneA    TSGVSLKEAVVRGAGERMRPVLMTATVAALGLIPAALAHGLGSDVQRPLATVVVGGLITA---------------

cons    :  **:* : *. *                 **** :**.*  :: . .**::.

NPC1    YLAMVLLGATHGLIFLPVLLSYIGPSVNKAKSCATEERYKGTERERLLNF
ZneA    --------TALTLVLLPALYYLIETRAAKQVREEPPVQFGPTSEGD---L

cons           :: *::**.*  * . .  *    . ::  *..     :
```

Citation

Please cite this result referring the papers at this link.

Result files

8 output files - download them all

Input(s)	Input sequences (2KB)
System	Command line (217 B) Log file (42KB)
Multiple Alignment	score_html file (39KB) clustalw_aln file (5KB) fasta_aln file (2KB) score_ascii file (4KB) phylip file (3KB)

[Copy to your Dropbox]

Send results

Forward this result to other online tools.

[Core/TCS]   Evaluates your Alignment indicating the local reliability

ProtoGene	Turning amino acid alignments into bona fide COS nucleotide alignments
MSA.hub	MyHits: a new interactive resource for protein annotation and domain identification
JalView	Open this alignment in the Jalview viewer
ESPript	ESPript server renders sequence similarities and secondary structure information from aligned sequences

Info

Some information about this alignment job

Mode: T-Coffee
Request ID: 27e78713
Created at: 26 Sep 2015, 13:09 (CEST)
Elapsed time: 17 sec
Expiration at: 06 Oct

Command Line

This is the command line used to execute your alignment. You can use it as reference to run this alignment on your desktop.

```
t_coffee -in=data_d83fc9f0.in -mode=regular -output=score_html clustalw_aln fasta_aln score_ascii phylip -maxnseq=150 -maxlen=10000 -case=
seqnos=off -outorder=input -run_name=result -multi_core=4 -quiet=stdout
```

Replay

Change some input parameters and resubmit this alignment clicking here.

Are you a T-Coffee guru? You may want to use the full featured T-Coffee command line options.

Feedback

Give us feedback about T-coffee web server

Are you satisfied with this result? Do you like this alignment server? If so recommend it using Google+1 or Facebook.

G+1 75   Recommend   325 people recommend this. Sign Up to see what your friends recommend.

For suggestions, questions or any problem send an email to tcoffee@googlegroups.com

T-Coffee Server is hosted by the **Centre for Genomic Regulation** (CRG) of Barcelona

Bibliography

ABI-MOSLEH, L., INFANTE, R. E., RADHAKRISHNAN, A., GOLDSTEIN, J. L. & BROWN, M. S. 2009. Cyclodextrin overcomes deficient lysosome-to-endoplasmic reticulum transport of cholesterol in Niemann-Pick type C cells. *Proc Natl Acad Sci U S A,* 106**,** 19316-21.

ALON, U. S. 2007. Diseases and clinical applications of the calcium sensing receptor. *Pediatr Endocrinol Rev,* 5**,** 482-8.

ALVELIUS, G., HJALMARSON, O., GRIFFITHS, W. J., BJORKHEM, I. & SJOVALL, J. 2001. Identification of unusual 7-oxygenated bile acid sulfates in a patient with Niemann-Pick disease, type C. *J Lipid Res,* 42**,** 1571-7.

ANAND, P., KUNNUMAKKARA, A. B., NEWMAN, R. A. & AGGARWAL, B. B. 2007. Bioavailability of curcumin: problems and promises. *Mol Pharm,* 4**,** 807-18.

AYDEMIR, T. B., LIUZZI, J. P., MCCLELLAN, S. & COUSINS, R. J. 2009. Zinc transporter ZIP8 (SLC39A8) and zinc influence IFN-gamma expression in activated human T cells. *J Leukoc Biol,* 86**,** 337-48.

AYE, I. L., SINGH, A. T. & KEELAN, J. A. 2009. Transport of lipids by ABC proteins: interactions and implications for cellular toxicity, viability and function. *Chem Biol Interact,* 180**,** 327-39.

BABALOLA, J. O., WENDELER, M., BREIDEN, B., ARENZ, C., SCHWARZMANN, G., LOCATELLI-HOOPS, S. & SANDHOFF, K. 2007. Development of an assay for the intermembrane transfer of cholesterol by Niemann-Pick C2 protein. *Biol Chem,* 388**,** 617-26.

BACH, G. 2001. Mucolipidosis type IV. *Mol Genet Metab,* 73**,** 197-203.

BAK, J., WHITE, P., TIMAR, G., MISSIAEN, L., GENAZZANI, A. A. & GALIONE, A. 1999. Nicotinic acid adenine dinucleotide phosphate triggers Ca2+ release from brain microsomes. *Curr Biol,* 9**,** 751-4.

BAUDRY, M., YAO, Y., SIMMONS, D., LIU, J. & BI, X. 2003. Postnatal development of inflammation in a murine model of Niemann-Pick type C disease: immunohistochemical observations of microglia and astroglia. *Exp Neurol,* 184**,** 887-903.

BEDELL, V. M., WANG, Y., CAMPBELL, J. M., POSHUSTA, T. L., STARKER, C. G., KRUG, R. G., 2ND, TAN, W., PENHEITER, S. G., MA, A. C., LEUNG, A. Y., FAHRENKRUG, S. C., CARLSON, D. F., VOYTAS, D. F., CLARK, K. J., ESSNER, J. J. & EKKER, S. C. 2012. In vivo genome editing using a high-efficiency TALEN system. *Nature,* 491**,** 114-8.

BEDELL, V. M., WESTCOT, S. E. & EKKER, S. C. 2011. Lessons from morpholino-based screening in zebrafish. *Brief Funct Genomics,* 10**,** 181-8.

BENNETT, J. T., STICKNEY, H. L., CHOI, W. Y., CIRUNA, B., TALBOT, W. S. & SCHIER, A. F. 2007. Maternal nodal and zebrafish embryogenesis. *Nature,* 450**,** E1-2; discussion E2-4.

BERRIDGE, M. J., LIPP, P. & BOOTMAN, M. D. 2000. The versatility and universality of calcium signalling. *Nat Rev Mol Cell Biol,* 1**,** 11-21.

BEST, J. D. & ALDERTON, W. K. 2008. Zebrafish: An in vivo model for the study of neurological diseases. *Neuropsychiatr Dis Treat,* 4**,** 567-76.

BETTO, R., TERESI, A., FACHECHI-CASSANO, G., SALVIATI, G. & SABBADINI, R. A. 1992. Sphingosine inhibits calcium release from sarcoplasmic reticulum membranes. *Adv Exp Med Biol,* 311**,** 403-4.

BI, C., MIAO, X. Q., CHOW, S. F., WU, W. J., YAN, R., LIAO, Y. H., CHOW, A. H. & ZHENG, Y. 2017. Particle size effect of curcumin nanosuspensions on cytotoxicity, cellular internalization, in vivo pharmacokinetics and biodistribution. *Nanomedicine,* 13**,** 943-953.

BILL, B. R., PETZOLD, A. M., CLARK, K. J., SCHIMMENTI, L. A. & EKKER, S. C. 2009. A primer for morpholino use in zebrafish. *Zebrafish,* 6**,** 69-77.

BILMEN, J. G., KHAN, S. Z., JAVED, M. H. & MICHELANGELI, F. 2001. Inhibition of the SERCA Ca2+ pumps by curcumin. Curcumin putatively stabilizes the interaction between the nucleotide-binding and phosphorylation domains in the absence of ATP. *Eur J Biochem,* 268**,** 6318-27.

BOCH, J. & BONAS, U. 2010. Xanthomonas AvrBs3 family-type III effectors: discovery and function. *Annu Rev Phytopathol,* 48**,** 419-36.

BORBON, I., TOTENHAGEN, J., FIORENZA, M. T., CANTERINI, S., KE, W., TROUARD, T. & ERICKSON, R. P. 2012a. Niemann-Pick C1 mice, a model of "juvenile Alzheimer's disease", with normal gene expression in neurons and fibrillary astrocytes show long term survival and delayed neurodegeneration. *J Alzheimers Dis,* 30**,** 875-87.

BORBON, I. A., HILLMAN, Z., DURAN, E., JR., KIELA, P. R., FRAUTSCHY, S. A. & ERICKSON, R. P. 2012b. Lack of efficacy of curcumin on neurodegeneration in the mouse model of Niemann-Pick C1. *Pharmacol Biochem Behav,* 101**,** 125-31.

BORNIG, H. & GEYER, G. 1974. Staining of cholesterol with the fluorescent antibiotic "filipin". *Acta Histochem,* 50**,** 110-5.

BOTSTEIN, D. & FINK, G. R. 2011. Yeast: an experimental organism for 21st Century biology. *Genetics,* 189**,** 695-704.

BOTTEGA, R., EPAND, R. M. & BALL, E. H. 1989. Inhibition of protein kinase C by sphingosine correlates with the presence of positive charge. *Biochem Biophys Res Commun,* 164**,** 102-7.

BRADY, R. O., KANFER, J. N., MOCK, M. B. & FREDRICKSON, D. S. 1966. The metabolism of sphingomyelin. II. Evidence of an enzymatic deficiency in Niemann-Pick diseae. *Proc Natl Acad Sci U S A,* 55**,** 366-9.

BRAET, K., PAEMELEIRE, K., D'HERDE, K., SANDERSON, M. J. & LEYBAERT, L. 2001. Astrocyte-endothelial cell calcium signals conveyed by two signalling pathways. *Eur J Neurosci,* 13**,** 79-91.

BRAILOIU, E., CHURAMANI, D., CAI, X., SCHRLAU, M. G., BRAILOIU, G. C., GAO, X., HOOPER, R., BOULWARE, M. J., DUN, N. J., MARCHANT, J. S. & PATEL, S. 2009a. Essential requirement for two-pore channel 1 in NAADP-mediated calcium signaling. *J Cell Biol,* 186**,** 201-9.

BRAILOIU, E., CHURAMANI, D., PANDEY, V., BRAILOIU, G. C., TULUC, F., PATEL, S. & DUN, N. J. 2006. Messenger-specific role for nicotinic acid adenine dinucleotide phosphate in neuronal differentiation. *J Biol Chem,* 281**,** 15923-8.

BRAILOIU, E., HOARD, J. L., FILIPEANU, C. M., BRAILOIU, G. C., DUN, S. L., PATEL, S. & DUN, N. J. 2005. Nicotinic acid adenine dinucleotide phosphate potentiates neurite outgrowth. *J Biol Chem,* 280**,** 5646-50.

BRAILOIU, G. C., BRAILOIU, E., PARKESH, R., GALIONE, A., CHURCHILL, G. C., PATEL, S. & DUN, N. J. 2009b. NAADP-mediated channel 'chatter' in neurons of the rat medulla oblongata. *Biochem J,* 419**,** 91-7, 2 p following 97.

BREITWIESER, G. E. 2012. Minireview: the intimate link between calcium sensing receptor trafficking and signaling: implications for disorders of calcium homeostasis. *Mol Endocrinol,* 26**,** 1482-95.

BREMOVA, T., MALINOVA, V., AMRAOUI, Y., MENGEL, E., REINKE, J., KOLNIKOVA, M. & STRUPP, M. 2015. Acetyl-dl-leucine in Niemann-Pick type C: A case series. *Neurology,* 85**,** 1368-75.

BROCKERHOFF, H. 1963. BREAKDOWN OF PHOSPHOLIPIDS IN MILD ALKALINE HYDROLYSIS. *J Lipid Res,* 4**,** 96-9.

BRONNER, F. 2001. Extracellular and intracellular regulation of calcium homeostasis. *ScientificWorldJournal,* 1**,** 919-25.

BRUCKDORFER, K. R. 1998. Lipid oxidation products and vascular function. *Free Radic Res,* 28**,** 573-81.

BRUSTEIN, E., SAINT-AMANT, L., BUSS, R. R., CHONG, M., MCDEARMID, J. R. & DRAPEAU, P. 2003. Steps during the development of the zebrafish locomotor network. *J Physiol Paris,* 97**,** 77-86.

BURGLIN, T. R. 2008. The Hedgehog protein family. *Genome Biol,* 9**,** 241.

BURNS, M., GAYNOR, K., OLM, V., MERCKEN, M., LAFRANCOIS, J., WANG, L., MATHEWS, P. M., NOBLE, W., MATSUOKA, Y. & DUFF, K. 2003. Presenilin redistribution associated with aberrant cholesterol transport enhances beta-amyloid production in vivo. *J Neurosci,* 23**,** 5645-9.

BUSH, A. I., PETTINGELL, W. H., JR., PARADIS, M. D. & TANZI, R. E. 1994a. Modulation of A beta adhesiveness and secretase site cleavage by zinc. *J Biol Chem,* 269**,** 12152-8.

BUSH, A. I., PETTINGELL, W. H., MULTHAUP, G., D PARADIS, M., VONSATTEL, J. P., GUSELLA, J. F., BEYREUTHER, K., MASTERS, C. L. & TANZI, R. E. 1994b. Rapid induction of Alzheimer A beta amyloid formation by zinc. *Science,* 265**,** 1464-7.

BUSQUE, S. M., KERSTETTER, J. E., GEIBEL, J. P. & INSOGNA, K. 2005. L-type amino acids stimulate gastric acid secretion by activation of the calcium-sensing receptor in parietal cells. *Am J Physiol Gastrointest Liver Physiol,* 289**,** G664-9.

BUTLER, J. D., VANIER, M. T. & PENTCHEV, P. G. 1993. Niemann-Pick C disease: cystine and lipids accumulate in the murine model of this lysosomal cholesterol lipidosis. *Biochem Biophys Res Commun,* 196**,** 154-9.

CALCRAFT, P. J., RUAS, M., PAN, Z., CHENG, X., ARREDOUANI, A., HAO, X., TANG, J., RIETDORF, K., TEBOUL, L., CHUANG, K. T., LIN, P., XIAO, R., WANG, C., ZHU, Y., LIN, Y., WYATT, C. N., PARRINGTON, J., MA, J., EVANS, A. M., GALIONE, A. & ZHU, M. X. 2009. NAADP mobilizes calcium from acidic organelles through two-pore channels. *Nature,* 459**,** 596-600.

CANFRAN-DUQUE, A., PASTOR, O., QUINTANA-PORTILLO, R., LERMA, M., DE LA PENA, G., MARTIN-HIDALGO, A., FERNANDEZ-HERNANDO, C., LASUNCION, M. A. & BUSTO, R. 2014. Curcumin promotes exosomes/microvesicles secretion that attenuates lysosomal cholesterol traffic impairment. *Mol Nutr Food Res,* 58**,** 687-97.

CARETTE, J. E., RAABEN, M., WONG, A. C., HERBERT, A. S., OBERNOSTERER, G., MULHERKAR, N., KUEHNE, A. I., KRANZUSCH, P. J., GRIFFIN, A. M., RUTHEL, G., DAL CIN, P., DYE, J. M., WHELAN, S. P., CHANDRAN, K. & BRUMMELKAMP, T. R. 2011. Ebola virus entry requires the cholesterol transporter Niemann-Pick C1. *Nature,* 477**,** 340-3.

CARINI, R., CASTINO, R., DE CESARIS, M. G., SPLENDORE, R., DEMOZ, M., ALBANO, E. & ISIDORO, C. 2004. Preconditioning-induced cytoprotection in hepatocytes requires Ca(2+)-dependent exocytosis of lysosomes. *J Cell Sci,* 117**,** 1065-77.

CARSTEA, E. D., MORRIS, J. A., COLEMAN, K. G., LOFTUS, S. K., ZHANG, D., CUMMINGS, C., GU, J., ROSENFELD, M. A., PAVAN, W. J., KRIZMAN, D. B., NAGLE, J., POLYMEROPOULOS, M. H., STURLEY, S. L., IOANNOU, Y. A., HIGGINS, M. E., COMLY, M., COONEY, A., BROWN, A., KANESKI, C. R., BLANCHETTE-MACKIE, E. J., DWYER, N. K., NEUFELD, E. B., CHANG, T. Y., LISCUM, L., STRAUSS, J. F., 3RD, OHNO, K., ZEIGLER, M., CARMI, R., SOKOL, J., MARKIE, D., O'NEILL, R. R., VAN DIGGELEN, O. P., ELLEDER, M., PATTERSON, M. C., BRADY, R. O., VANIER, M. T., PENTCHEV, P. G. & TAGLE, D. A. 1997. Niemann-Pick C1 disease gene: homology to mediators of cholesterol homeostasis. *Science,* 277**,** 228-31.

CARSTEA, E. D., POLYMEROPOULOS, M. H., PARKER, C. C., DETERA-WADLEIGH, S. D., O'NEILL, R. R., PATTERSON, M. C., GOLDIN, E., XIAO, H., STRAUB, R. E., VANIER, M. T. & ET AL. 1993. Linkage of Niemann-Pick disease type C to human chromosome 18. *Proc Natl Acad Sci U S A,* 90**,** 2002-4.

CHANDLER, R. J., WILLIAMS, I. M., GIBSON, A. L., DAVIDSON, C. D., INCAO, A. A., HUBBARD, B. T., PORTER, F. D., PAVAN, W. J. & VENDITTI, C. P. 2017. Systemic AAV9 gene therapy improves the lifespan of mice with Niemann-Pick disease, type C1. *Hum Mol Genet,* 26**,** 52-64.

CHAPEL, A., KIEFFER-JAQUINOD, S., SAGNE, C., VERDON, Q., IVALDI, C., MELLAL, M., THIRION, J., JADOT, M., BRULEY, C., GARIN, J., GASNIER, B. & JOURNET, A. 2013. An extended proteome map of the lysosomal membrane reveals novel potential transporters. *Mol Cell Proteomics,* 12**,** 1572-88.

CHEN, C. S., BACH, G. & PAGANO, R. E. 1998. Abnormal transport along the lysosomal pathway in mucolipidosis, type IV disease. *Proc Natl Acad Sci U S A,* 95**,** 6373-8.

CHEN, F. W., LI, C. & IOANNOU, Y. A. 2010. Cyclodextrin induces calcium-dependent lysosomal exocytosis. *PLoS One,* 5**,** e15054.

CHENG, N. H., PITTMAN, J. K., SHIGAKI, T., LACHMANSINGH, J., LECLERE, S., LAHNER, B., SALT, D. E. & HIRSCHI, K. D. 2005. Functional association of Arabidopsis CAX1 and CAX3 is required for normal growth and ion homeostasis. *Plant Physiol,* 138**,** 2048-60.

CHENG, X., ZHANG, X., YU, L. & XU, H. 2015. Calcium signaling in membrane repair. *Semin Cell Dev Biol,* 45**,** 24-31.

CHERYAN, M. 1980. Phytic acid interactions in food systems. *Crit Rev Food Sci Nutr,* 13**,** 297-335.

CHEVALLIER, J., CHAMOUN, Z., JIANG, G., PRESTWICH, G., SAKAI, N., MATILE, S., PARTON, R. G. & GRUENBERG, J. 2008. Lysobisphosphatidic acid controls endosomal cholesterol levels. *J Biol Chem,* 283**,** 27871-80.

CHIU, S. S., LUI, E., MAJEED, M., VISHWANATHA, J. K., RANJAN, A. P., MAITRA, A., PRAMANIK, D., SMITH, J. A. & HELSON, L. 2011. Differential distribution of intravenous curcumin formulations in the rat brain. *Anticancer Res,* 31**,** 907-11.

CHOI, H. Y., KARTEN, B., CHAN, T., VANCE, J. E., GREER, W. L., HEIDENREICH, R. A., GARVER, W. S. & FRANCIS, G. A. 2003. Impaired ABCA1-dependent lipid efflux and hypoalphalipoproteinemia in human Niemann-Pick type C disease. *J Biol Chem,* 278**,** 32569-77.

CHRISTENSEN, K. A., MYERS, J. T. & SWANSON, J. A. 2002. pH-dependent regulation of lysosomal calcium in macrophages. *J Cell Sci,* 115**,** 599-607.

CHURCHILL, G. C., OKADA, Y., THOMAS, J. M., GENAZZANI, A. A., PATEL, S. & GALIONE, A. 2002. NAADP mobilizes Ca(2+) from reserve granules, lysosome-related organelles, in sea urchin eggs. *Cell,* 111**,** 703-8.

CLAPHAM, D. E. 2007. Calcium signaling. *Cell,* 131**,** 1047-58.

COHEN, P. A. 2014. Hazards of hindsight--monitoring the safety of nutritional supplements. *N Engl J Med,* 370**,** 1277-80.

COLINA, C., CERVINO, V. & BENAIM, G. 2002. Ceramide and sphingosine have an antagonistic effect on the plasma-membrane Ca2+-ATPase from human erythrocytes. *Biochem J,* 362**,** 247-51.

CONN, S. J., GILLIHAM, M., ATHMAN, A., SCHREIBER, A. W., BAUMANN, U., MOLLER, I., CHENG, N. H., STANCOMBE, M. A., HIRSCHI, K. D., WEBB, A. A., BURTON, R., KAISER, B. N., TYERMAN, S. D. & LEIGH, R. A. 2011. Cell-specific vacuolar calcium storage mediated by CAX1 regulates apoplastic calcium concentration, gas exchange, and plant productivity in Arabidopsis. *Plant Cell,* 23**,** 240-57.

COOPER, G. M. 2000. *The Cell: A Molecular Approach*, ASM Press.

CORONA, C., PENSALFINI, A., FRAZZINI, V. & SENSI, S. L. 2011. New therapeutic targets in Alzheimer's disease: brain deregulation of calcium and zinc. *Cell Death Dis,* 2**,** e176.

COTE, M., MISASI, J., REN, T., BRUCHEZ, A., LEE, K., FILONE, C. M., HENSLEY, L., LI, Q., ORY, D., CHANDRAN, K. & CUNNINGHAM, J. 2011. Small molecule inhibitors reveal Niemann-Pick C1 is essential for Ebola virus infection. *Nature,* 477**,** 344-8.

COUSINS, R. J., LIUZZI, J. P. & LICHTEN, L. A. 2006. Mammalian zinc transport, trafficking, and signals. *J Biol Chem,* 281**,** 24085-9.

COX, T., LACHMANN, R., HOLLAK, C., AERTS, J., VAN WEELY, S., HREBICEK, M., PLATT, F., BUTTERS, T., DWEK, R., MOYSES, C., GOW, I., ELSTEIN, D. & ZIMRAN, A. 2000. Novel oral treatment of Gaucher's disease with N-butyldeoxynojirimycin (OGT 918) to decrease substrate biosynthesis. *Lancet,* 355**,** 1481-5.

COX, T. M. & CACHON-GONZALEZ, M. B. 2012. The cellular pathology of lysosomal diseases. *J Pathol,* 226**,** 241-54.

CROCKER, A. C. & FARBER, S. 1958. Niemann-Pick disease: a review of eighteen patients. *Medicine (Baltimore),* 37**,** 1-95.

CRUMLING, M. A., LIU, L., THOMAS, P. V., BENSON, J., KANICKI, A., KABARA, L., HALSEY, K., DOLAN, D. & DUNCAN, R. K. 2012. Hearing loss and hair cell death in mice given the cholesterol-chelating agent hydroxypropyl-beta-cyclodextrin. *PLoS One,* 7**,** e53280.

CUOGHI, B. & MOLA, L. 2007. Microglia of teleosts: facing a challenge in neurobiology. *Eur J Histochem,* 51**,** 231-40.

DANESE, A., PATERGNANI, S., BONORA, M., WIECKOWSKI, M. R., PREVIATI, M., GIORGI, C. & PINTON, P. 2017. Calcium regulates cell death in cancer: Roles of the mitochondria and mitochondria-associated membranes (MAMs). *Biochim Biophys Acta*.

DARFEUILLE-MICHAUD, A., BOUDEAU, J., BULOIS, P., NEUT, C., GLASSER, A. L., BARNICH, N., BRINGER, M. A., SWIDSINSKI, A., BEAUGERIE, L. & COLOMBEL, J. F. 2004. High prevalence of adherent-invasive Escherichia coli associated with ileal mucosa in Crohn's disease. *Gastroenterology,* 127**,** 412-21.

DARFEUILLE-MICHAUD, A., NEUT, C., BARNICH, N., LEDERMAN, E., DI MARTINO, P., DESREUMAUX, P., GAMBIEZ, L., JOLY, B., CORTOT, A. & COLOMBEL, J. F. 1998. Presence of adherent Escherichia coli strains in ileal mucosa of patients with Crohn's disease. *Gastroenterology,* 115**,** 1405-13.

DAVIDSON, C. D., ALI, N. F., MICSENYI, M. C., STEPHNEY, G., RENAULT, S., DOBRENIS, K., ORY, D. S., VANIER, M. T. & WALKLEY, S. U. 2009. Chronic cyclodextrin treatment of murine Niemann-Pick C disease ameliorates neuronal cholesterol and glycosphingolipid storage and disease progression. *PLoS One,* 4**,** e6951.

DAVIES, J. P., CHEN, F. W. & IOANNOU, Y. A. 2000. Transmembrane molecular pump activity of Niemann-Pick C1 protein. *Science,* 290**,** 2295-8.

DAVIES, K. J. 1987. Protein damage and degradation by oxygen radicals. I. general aspects. *J Biol Chem,* 262**,** 9895-901.

DAVIS, M. E. & BREWSTER, M. E. 2004. Cyclodextrin-based pharmaceutics: past, present and future. *Nat Rev Drug Discov,* 3**,** 1023-35.

DAWSON, G. 1972. Detection of glycosphingolipids in small samples of human tissue. *Ann Clin Lab Sci,* 2**,** 274-84.

DE DUVE, C. 1983. Lysosomes revisited. *Eur J Biochem,* 137**,** 391-7.

DEL PRINCIPE, D., GIARDINI, O., BALLATI, G. & TORRONI, A. 1971. [Coagulation inhibiting factor and platelet changes in a patient with Niemann-Pick disease]. *Haematologica,* 56**,** 36-48.

DELMAR, J. A., SU, C. C. & YU, E. W. 2013. Structural mechanisms of heavy-metal extrusion by the Cus efflux system. *Biometals,* 26**,** 593-607.

DENIS, V. & CYERT, M. S. 2002. Internal Ca(2+) release in yeast is triggered by hypertonic shock and mediated by a TRP channel homologue. *J Cell Biol,* 156**,** 29-34.

DENTON, R. M., RANDLE, P. J. & MARTIN, B. R. 1972. Stimulation by calcium ions of pyruvate dehydrogenase phosphate phosphatase. *Biochem J,* 128**,** 161-3.

DEXTER, D. T., CARAYON, A., JAVOY-AGID, F., AGID, Y., WELLS, F. R., DANIEL, S. E., LEES, A. J., JENNER, P. & MARSDEN, C. D. 1991. Alterations in the levels of iron, ferritin and other trace metals in

Parkinson's disease and other neurodegenerative diseases affecting the basal ganglia. *Brain,* 114 (Pt 4)**,** 1953-75.

DICZFALUSY, U. 2013. On the formation and possible biological role of 25-hydroxycholesterol. *Biochimie,* 95**,** 455-60.

DINELEY, K. E., RICHARDS, L. L., VOTYAKOVA, T. V. & REYNOLDS, I. J. 2005. Zinc causes loss of membrane potential and elevates reactive oxygen species in rat brain mitochondria. *Mitochondrion,* 5**,** 55-65.

DIVANGAHI, M., CHEN, M., GAN, H., DESJARDINS, D., HICKMAN, T. T., LEE, D. M., FORTUNE, S., BEHAR, S. M. & REMOLD, H. G. 2009. Mycobacterium tuberculosis evades macrophage defenses by inhibiting plasma membrane repair. *Nat Immunol,* 10**,** 899-906.

DONG, X. P., SHEN, D., WANG, X., DAWSON, T., LI, X., ZHANG, Q., CHENG, X., ZHANG, Y., WEISMAN, L. S., DELLING, M. & XU, H. 2010. PI(3,5)P(2) controls membrane trafficking by direct activation of mucolipin Ca(2+) release channels in the endolysosome. *Nat Commun,* 1**,** 38.

DRAPER, B. W., MORCOS, P. A. & KIMMEL, C. B. 2001. Inhibition of zebrafish fgf8 pre-mRNA splicing with morpholino oligos: a quantifiable method for gene knockdown. *Genesis,* 30**,** 154-6.

DUNN, K. W. & MAXFIELD, F. R. 1992. Delivery of ligands from sorting endosomes to late endosomes occurs by maturation of sorting endosomes. *J Cell Biol,* 117**,** 301-10.

EFTHYMIOU, A. G., STEINER, J., PAVAN, W. J., WINCOVITCH, S., LARSON, D. M., PORTER, F. D., RAO, M. S. & MALIK, N. 2015. Rescue of an in vitro neuron phenotype identified in Niemann-Pick disease, type C1 induced pluripotent stem cell-derived neurons by modulating the WNT pathway and calcium signaling. *Stem Cells Transl Med,* 4**,** 230-8.

EGAN, M. E., PEARSON, M., WEINER, S. A., RAJENDRAN, V., RUBIN, D., GLOCKNER-PAGEL, J., CANNY, S., DU, K., LUKACS, G. L. & CAPLAN, M. J. 2004. Curcumin, a major constituent of turmeric, corrects cystic fibrosis defects. *Science,* 304**,** 600-2.

EISEN, J. S. & SMITH, J. C. 2008. Controlling morpholino experiments: don't stop making antisense. *Development,* 135**,** 1735-43.

ELLEDER, M., JIRASEK, A., SMID, F., LEDVINOVA, J., BESLEY, G. T. & STOPEKOVA, M. 1984. Niemann-Pick disease type C with enhanced glycolipid storage. Report on further case of so-called lactosylceramidosis. *Virchows Arch A Pathol Anat Histopathol,* 402**,** 307-17.

ELLEDER, M. & SMID, F. 1985. Adrenal changes in Niemann-Pick disease: differences between sphingomyelinase deficiency and type C. *Acta Histochem,* 76**,** 163-76.

ELORANTA, J. J. & KULLAK-UBLICK, G. A. 2005. Coordinate transcriptional regulation of bile acid homeostasis and drug metabolism. *Arch Biochem Biophys,* 433**,** 397-412.

ERICKSON, R. P., GARVER, W. S., CAMARGO, F., HOSSAIN, G. S. & HEIDENREICH, R. A. 2000. Pharmacological and genetic modifications of somatic cholesterol do not substantially alter the course of CNS disease in Niemann-Pick C mice. *J Inherit Metab Dis,* 23**,** 54-62.

FENG, J., PETERSEN, C. D., COY, D. H., JIANG, J. K., THOMAS, C. J., POLLAK, M. R. & WANK, S. A. 2010. Calcium-sensing receptor is a physiologic multimodal chemosensor regulating gastric G-cell growth and gastrin secretion. *Proc Natl Acad Sci U S A,* 107**,** 17791-6.

FERRANTE, A., DE NUCCIO, C., PEPPONI, R., VISENTIN, S., MARTIRE, A., BERNARDO, A., MINGHETTI, L. & POPOLI, P. 2016. Stimulation of adenosine A2A receptors reduces intracellular cholesterol accumulation and rescues mitochondrial abnormalities in human neural cell models of Niemann-Pick C1. *Neuropharmacology,* 103**,** 155-62.

FINERAN, P., LLOYD-EVANS, E., LACK, N. A., PLATT, N., DAVIS, L. C., MORGAN, A. J., HOGLINGER, D., TATITURI, R. V., CLARK, S., WILLIAMS, I. M., TYNAN, P., AL EISA, N., NAZAROVA, E., WILLIAMS, A., GALIONE, A., ORY, D. S., BESRA, G. S., RUSSELL, D. G., BRENNER, M. B., SIM, E. & PLATT, F. M. 2016. Pathogenic mycobacteria achieve cellular persistence by inhibiting the Niemann-Pick Type C disease cellular pathway. *Wellcome Open Res,* 1**,** 18.

FLUEGEL, M. L., PARKER, T. J. & PALLANCK, L. J. 2006. Mutations of a Drosophila NPC1 gene confer sterol and ecdysone metabolic defects. *Genetics,* 172**,** 185-96.

FOSSALE, E., WOLF, P., ESPINOLA, J. A., LUBICZ-NAWROCKA, T., TEED, A. M., GAO, H., RIGAMONTI, D., CATTANEO, E., MACDONALD, M. E. & COTMAN, S. L. 2004. Membrane trafficking and mitochondrial abnormalities precede subunit c deposition in a cerebellar cell model of juvenile neuronal ceroid lipofuscinosis. *BMC Neurosci,* 5**,** 57.

FRAHER, D., SANIGORSKI, A., MELLETT, N. A., MEIKLE, P. J., SINCLAIR, A. J. & GIBERT, Y. 2016. Zebrafish Embryonic Lipidomic Analysis Reveals that the Yolk Cell Is Metabolically Active in Processing Lipid. *Cell Rep,* 14**,** 1317-29.

FREDERICKSON, C. J., SUH, S. W., SILVA, D., FREDERICKSON, C. J. & THOMPSON, R. B. 2000. Importance of zinc in the central nervous system: the zinc-containing neuron. *J Nutr,* 130**,** 1471s-83s.

FU, R., YANJANIN, N. M., BIANCONI, S., PAVAN, W. J. & PORTER, F. D. 2010. Oxidative stress in Niemann-Pick disease, type C. *Mol Genet Metab,* 101**,** 214-8.

FUKUDA, M. 1991. Lysosomal membrane glycoproteins. Structure, biosynthesis, and intracellular trafficking. *J Biol Chem,* 266**,** 21327-30.

GALIONE, A., CHUANG, K. T., FUNNELL, T. M., DAVIS, L. C., MORGAN, A. J., RUAS, M., PARRINGTON, J. & CHURCHILL, G. C. 2014. Synthesis of NAADP-AM as a membrane-permeant NAADP analog. *Cold Spring Harb Protoc,* 2014**,** pdb.prot076927.

GALIONE, A. & CHURCHILL, G. C. 2002. Interactions between calcium release pathways: multiple messengers and multiple stores. *Cell Calcium,* 32**,** 343-54.

GALLALA, H. D. & SANDHOFF, K. 2011. Biological function of the cellular lipid BMP-BMP as a key activator for cholesterol sorting and membrane digestion. *Neurochem Res,* 36**,** 1594-600.

GARCIA-ARRIBAS, A. B., ALONSO, A. & GONI, F. M. 2016. Cholesterol interactions with ceramide and sphingomyelin. *Chem Phys Lipids.*

GARCIA-ROBLES, A. A., COMPANY-ALBIR, M. J., MEGIAS-VERICAT, J. E., FERNANDEZ-MEGIA, M. J., PEREZ-MIRALLES, F. C., LOPEZ-BRIZ, E., ALCALA-VICENTE, C., GALEANO, I., CASANOVA, B. & POVEDA, J. L. 2016. Use of 2 hydroxypropyl-beta-cyclodextrin therapy in two adult Niemann Pick Type C patients. *J Neurol Sci,* 366**,** 65-7.

GARNER, B., HARVEY, D. J., ROYLE, L., FRISCHMANN, M., NIGON, F., CHAPMAN, M. J. & RUDD, P. M. 2001. Characterization of human apolipoprotein B100 oligosaccharides in LDL subfractions derived from normal and hyperlipidemic plasma: deficiency of alpha-N-acetylneuraminyllactosyl-ceramide in light and small dense LDL particles. *Glycobiology,* 11**,** 791-802.

GARY-BOBO, M., NIRDE, P., JEANJEAN, A., MORERE, A. & GARCIA, M. 2007. Mannose 6-phosphate receptor targeting and its applications in human diseases. *Curr Med Chem,* 14**,** 2945-53.

GEE, K. R., ZHOU, Z. L., TON-THAT, D., SENSI, S. L. & WEISS, J. H. 2002. Measuring zinc in living cells. A new generation of sensitive and selective fluorescent probes. *Cell Calcium,* 31**,** 245-51.

GEIBEL, J. P. & HEBERT, S. C. 2009. The functions and roles of the extracellular Ca2+-sensing receptor along the gastrointestinal tract. *Annu Rev Physiol,* 71**,** 205-17.

GERASIMENKO, J. V., TEPIKIN, A. V., PETERSEN, O. H. & GERASIMENKO, O. V. 1998. Calcium uptake via endocytosis with rapid release from acidifying endosomes. *Curr Biol,* 8**,** 1335-8.

GHOSHAL, K. & JACOB, S. T. 2001. Regulation of metallothionein gene expression. *Prog Nucleic Acid Res Mol Biol,* 66**,** 357-84.

GINZBURG, L. & FUTERMAN, A. H. 2005. Defective calcium homeostasis in the cerebellum in a mouse model of Niemann-Pick A disease. *J Neurochem,* 95**,** 1619-28.

GOLDIN, E., BLANCHETTE-MACKIE, E. J., DWYER, N. K., PENTCHEV, P. G. & BRADY, R. O. 1995. Cultured skin fibroblasts derived from patients with mucolipidosis 4 are auto-fluorescent. *Pediatr Res,* 37**,** 687-92.

GOLDSTEIN, J. L., ANDERSON, R. G. & BROWN, M. S. 1979. Coated pits, coated vesicles, and receptor-mediated endocytosis. *Nature,* 279**,** 679-85.

GONDRE-LEWIS, M. C., MCGLYNN, R. & WALKLEY, S. U. 2003. Cholesterol accumulation in NPC1-deficient neurons is ganglioside dependent. *Curr Biol,* 13**,** 1324-9.

GONG, Y., DUVVURI, M., DUNCAN, M. B., LIU, J. & KRISE, J. P. 2006. Niemann-Pick C1 protein facilitates the efflux of the anticancer drug daunorubicin from cells according to a novel vesicle-mediated pathway. *J Pharmacol Exp Ther,* 316**,** 242-7.

GRANT, B. D. & DONALDSON, J. G. 2009. Pathways and mechanisms of endocytic recycling. *Nat Rev Mol Cell Biol,* 10**,** 597-608.

GRASSL, G. A., VALDEZ, Y., BERGSTROM, K. S., VALLANCE, B. A. & FINLAY, B. B. 2008. Chronic enteric salmonella infection in mice leads to severe and persistent intestinal fibrosis. *Gastroenterology,* 134**,** 768-80.

GRIFFIN, L. D., GONG, W., VEROT, L. & MELLON, S. H. 2004. Niemann-Pick type C disease involves disrupted neurosteroidogenesis and responds to allopregnanolone. *Nat Med,* 10**,** 704-11.

GRIMM, C., JORS, S., SALDANHA, S. A., OBUKHOV, A. G., PAN, B., OSHIMA, K., CUAJUNGCO, M. P., CHASE, P., HODDER, P. & HELLER, S. 2010. Small molecule activators of TRPML3. *Chem Biol,* 17**,** 135-48.

GRUENBERG, J. 2001. The endocytic pathway: a mosaic of domains. *Nat Rev Mol Cell Biol,* 2**,** 721-30.

GRUPP, L., WOLBURG, H. & MACK, A. F. 2010. Astroglial structures in the zebrafish brain. *J Comp Neurol,* 518**,** 4277-87.

GUICCIARDI, M. E., LEIST, M. & GORES, G. J. 2004. Lysosomes in cell death. *Oncogene,* 23**,** 2881-90.

GUNTHER, L., BECK, R., XIONG, G., POTSCHKA, H., JAHN, K., BARTENSTEIN, P., BRANDT, T., DUTIA, M., DIETERICH, M., STRUPP, M., LA FOUGERE, C. & ZWERGAL, A. 2015. N-acetyl-L-leucine accelerates vestibular compensation after unilateral labyrinthectomy by action in the cerebellum and thalamus. *PLoS One,* 10**,** e0120891.

HAFNER, M., REZEN, T. & ROZMAN, D. 2011. Regulation of hepatic cytochromes p450 by lipids and cholesterol. *Curr Drug Metab,* 12**,** 173-85.

HANADA, K., NISHIJIMA, M., FUJITA, T. & KOBAYASHI, S. 2000. Specificity of inhibitors of serine palmitoyltransferase (SPT), a key enzyme in sphingolipid biosynthesis, in intact cells. A novel evaluation system using an SPT-defective mammalian cell mutant. *Biochem Pharmacol,* 59**,** 1211-6.

HANTKE, K. 2001. Bacterial zinc transporters and regulators. *Biometals,* 14**,** 239-49.

HARTMANN, J. & KONNERTH, A. 2005. Determinants of postsynaptic Ca2+ signaling in Purkinje neurons. *Cell Calcium,* 37**,** 459-66.

HEMSLEY, K. M. & HOPWOOD, J. J. 2010. Lessons learnt from animal models: pathophysiology of neuropathic lysosomal storage disorders. *J Inherit Metab Dis,* 33**,** 363-71.

HERBERT, A. S., DAVIDSON, C., KUEHNE, A. I., BAKKEN, R., BRAIGEN, S. Z., GUNN, K. E., WHELAN, S. P., BRUMMELKAMP, T. R., TWENHAFEL, N. A., CHANDRAN, K., WALKLEY, S. U. & DYE, J. M. 2015.

Niemann-pick C1 is essential for ebolavirus replication and pathogenesis in vivo. *MBio,* 6**,** e00565-15.

HIGASHI, Y., MURAYAMA, S., PENTCHEV, P. G. & SUZUKI, K. 1993. Cerebellar degeneration in the Niemann-Pick type C mouse. *Acta Neuropathol,* 85**,** 175-84.

HOGLINGER, D., HABERKANT, P., AGUILERA-ROMERO, A., RIEZMAN, H., PORTER, F. D., PLATT, F. M., GALIONE, A. & SCHULTZ, C. 2015. Intracellular sphingosine releases calcium from lysosomes. *Elife,* 4.

HOZUMI, I., HASEGAWA, T., HONDA, A., OZAWA, K., HAYASHI, Y., HASHIMOTO, K., YAMADA, M., KOUMURA, A., SAKURAI, T., KIMURA, A., TANAKA, Y., SATOH, M. & INUZUKA, T. 2011. Patterns of levels of biological metals in CSF differ among neurodegenerative diseases. *J Neurol Sci,* 303**,** 95-9.

HSU, H. J., HSIAO, P., KUO, M. W. & CHUNG, B. C. 2002. Expression of zebrafish cyp11a1 as a maternal transcript and in yolk syncytial layer. *Gene Expr Patterns,* 2**,** 219-22.

HU, Y. B., DAMMER, E. B., REN, R. J. & WANG, G. 2015. The endosomal-lysosomal system: from acidification and cargo sorting to neurodegeneration. *Transl Neurodegener,* 4**,** 18.

HUANG, X., ATWOOD, C. S., MOIR, R. D., HARTSHORN, M. A., VONSATTEL, J. P., TANZI, R. E. & BUSH, A. I. 1997. Zinc-induced Alzheimer's Abeta1-40 aggregation is mediated by conformational factors. *J Biol Chem,* 272**,** 26464-70.

HUANG, X., SUYAMA, K., BUCHANAN, J., ZHU, A. J. & SCOTT, M. P. 2005. A Drosophila model of the Niemann-Pick type C lysosome storage disease: dnpc1a is required for molting and sterol homeostasis. *Development,* 132**,** 5115-24.

HUI, L., GEIGER, N. H., BLOOR-YOUNG, D., CHURCHILL, G. C., GEIGER, J. D. & CHEN, X. 2015. Release of calcium from endolysosomes increases calcium influx through N-type calcium channels: Evidence for acidic store-operated calcium entry in neurons. *Cell Calcium,* 58**,** 617-27.

HUNG, Y. H., FAUX, N. G., KILLILEA, D. W., YANJANIN, N., FIRNKES, S., VOLITAKIS, I., GANIO, G., WALTERFANG, M., HASTINGS, C., PORTER, F. D., ORY, D. S. & BUSH, A. I. 2014. Altered transition metal homeostasis in Niemann-Pick disease, type C1. *Metallomics,* 6**,** 542-53.

HWANG, J. J., LEE, S. J., KIM, T. Y., CHO, J. H. & KOH, J. Y. 2008. Zinc and 4-hydroxy-2-nonenal mediate lysosomal membrane permeabilization induced by H2O2 in cultured hippocampal neurons. *J Neurosci,* 28**,** 3114-22.

IMRIE, J., DASGUPTA, S., BESLEY, G. T., HARRIS, C., HEPTINSTALL, L., KNIGHT, S., VANIER, M. T., FENSOM, A. H., WARD, C., JACKLIN, E., WHITEHOUSE, C. & WRAITH, J. E. 2007. The natural history of Niemann-Pick disease type C in the UK. *J Inherit Metab Dis,* 30**,** 51-9.

INFANTE, R. E., RADHAKRISHNAN, A., ABI-MOSLEH, L., KINCH, L. N., WANG, M. L., GRISHIN, N. V., GOLDSTEIN, J. L. & BROWN, M. S. 2008. Purified NPC1 protein: II. Localization of sterol binding to a 240-amino acid soluble luminal loop. *J Biol Chem,* 283**,** 1064-75.

IOANNOU, Y. A. 2005. Guilty until proven innocent: the case of NPC1 and cholesterol. *Trends Biochem Sci,* 30**,** 498-505.

IYENGAR, V., PULLAKHANDAM, R. & NAIR, K. M. 2010. Dietary ligands as determinants of iron-zinc interactions at the absorptive enterocyte. *J Food Sci,* 75**,** H260-4.

JAISWAL, J. K., ANDREWS, N. W. & SIMON, S. M. 2002. Membrane proximal lysosomes are the major vesicles responsible for calcium-dependent exocytosis in nonsecretory cells. *J Cell Biol,* 159**,** 625-35.

JALANKO, A. & BRAULKE, T. 2009. Neuronal ceroid lipofuscinoses. *Biochim Biophys Acta,* 1793**,** 697-709.

JEONG, J. Y., KWON, H. B., AHN, J. C., KANG, D., KWON, S. H., PARK, J. A. & KIM, K. W. 2008. Functional and developmental analysis of the blood-brain barrier in zebrafish. *Brain Res Bull,* 75**,** 619-28.

JEYAKUMAR, M., LEE, J. P., SIBSON, N. R., LOWE, J. P., STUCKEY, D. J., TESTER, K., FU, G., NEWLIN, R., SMITH, D. A., SNYDER, E. Y. & PLATT, F. M. 2009. Neural stem cell transplantation benefits a monogenic neurometabolic disorder during the symptomatic phase of disease. *Stem Cells,* 27**,** 2362-70.

JOLLIFFE, D. S. & SARKANY, I. 1983. Niemann-Pick type III and Crohn's disease. *J R Soc Med,* 76**,** 307-8.

JOUAVILLE, L. S., PINTON, P., BASTIANUTTO, C., RUTTER, G. A. & RIZZUTO, R. 1999. Regulation of mitochondrial ATP synthesis by calcium: evidence for a long-term metabolic priming. *Proc Natl Acad Sci U S A,* 96**,** 13807-12.

JOURGHANIAN, P., GHAFFARI, S., ARDJMAND, M., HAGHIGHAT, S. & MOHAMMADNEJAD, M. 2016. Sustained release Curcumin loaded Solid Lipid Nanoparticles. *Adv Pharm Bull,* 6**,** 17-21.

JOVIC, M., SHARMA, M., RAHAJENG, J. & CAPLAN, S. 2010. The early endosome: a busy sorting station for proteins at the crossroads. *Histol Histopathol,* 25**,** 99-112.

KABASHI, E., BRUSTEIN, E., CHAMPAGNE, N. & DRAPEAU, P. 2011. Zebrafish models for the functional genomics of neurogenetic disorders. *Biochim Biophys Acta,* 1812**,** 335-45.

KADAM, R. S., BOURNE, D. W. & KOMPELLA, U. B. 2012. Nano-advantage in enhanced drug delivery with biodegradable nanoparticles: contribution of reduced clearance. *Drug Metab Dispos,* 40**,** 1380-8.

KAGEDAL, K., ZHAO, M., SVENSSON, I. & BRUNK, U. T. 2001. Sphingosine-induced apoptosis is dependent on lysosomal proteases. *Biochem J,* 359**,** 335-43.

KARLSTAD, J., SUN, Y. & SINGH, B. B. 2012. Ca(2+) signaling: an outlook on the characterization of Ca(2+) channels and their importance in cellular functions. *Adv Exp Med Biol,* 740**,** 143-57.

KARTEN, B., PEAKE, K. B. & VANCE, J. E. 2009. Mechanisms and consequences of impaired lipid trafficking in Niemann-Pick type C1-deficient mammalian cells. *Biochim Biophys Acta,* 1791**,** 659-70.

KARTEN, B., VANCE, D. E., CAMPENOT, R. B. & VANCE, J. E. 2002. Cholesterol accumulates in cell bodies, but is decreased in distal axons, of Niemann-Pick C1-deficient neurons. *J Neurochem,* 83**,** 1154-63.

KARTEN, B., VANCE, D. E., CAMPENOT, R. B. & VANCE, J. E. 2003. Trafficking of cholesterol from cell bodies to distal axons in Niemann Pick C1-deficient neurons. *J Biol Chem,* 278**,** 4168-75.

KAUFMANN, A. M. & KRISE, J. P. 2008. Niemann-Pick C1 functions in regulating lysosomal amine content. *J Biol Chem,* 283**,** 24584-93.

KILPATRICK, B. S., EDEN, E. R., SCHAPIRA, A. H., FUTTER, C. E. & PATEL, S. 2013. Direct mobilisation of lysosomal Ca2+ triggers complex Ca2+ signals. *J Cell Sci,* 126**,** 60-6.

KIM, B. E., WANG, F., DUFNER-BEATTIE, J., ANDREWS, G. K., EIDE, D. J. & PETRIS, M. J. 2004. Zn2+-stimulated endocytosis of the mZIP4 zinc transporter regulates its location at the plasma membrane. *J Biol Chem,* 279**,** 4523-30.

KIM, H. R., LEE, G. H., HA, K. C., AHN, T., MOON, J. Y., LEE, B. J., CHO, S. G., KIM, S., SEO, Y. R., SHIN, Y. J., CHAE, S. W., REED, J. C. & CHAE, H. J. 2008. Bax Inhibitor-1 Is a pH-dependent regulator of Ca2+ channel activity in the endoplasmic reticulum. *J Biol Chem,* 283**,** 15946-55.

KIM, Y. H. & KOH, J. Y. 2002. The role of NADPH oxidase and neuronal nitric oxide synthase in zinc-induced poly(ADP-ribose) polymerase activation and cell death in cortical culture. *Exp Neurol,* 177**,** 407-18.

KIMMEL, C. B. 1993. Patterning the brain of the zebrafish embryo. *Annu Rev Neurosci,* 16**,** 707-32.

KIMMEL, C. B., BALLARD, W. W., KIMMEL, S. R., ULLMANN, B. & SCHILLING, T. F. 1995. Stages of embryonic development of the zebrafish. *Dev Dyn,* 203**,** 253-310.

KINANA, A. D., VARGIU, A. V. & NIKAIDO, H. 2013. Some ligands enhance the efflux of other ligands by the Escherichia coli multidrug pump AcrB. *Biochemistry,* 52**,** 8342-51.

KIRKEGAARD, T., GRAY, J., PRIESTMAN, D. A., WALLOM, K. L., ATKINS, J., OLSEN, O. D., KLEIN, A., DRNDARSKI, S., PETERSEN, N. H., INGEMANN, L., SMITH, D. A., MORRIS, L., BORNAES, C., JORGENSEN, S. H., WILLIAMS, I., HINSBY, A., ARENZ, C., BEGLEY, D., JAATTELA, M. & PLATT, F. M. 2016. Heat shock protein-based therapy as a potential candidate for treating the sphingolipidoses. *Sci Transl Med,* 8**,** 355ra118.

KIRKEGAARD, T., ROTH, A. G., PETERSEN, N. H., MAHALKA, A. K., OLSEN, O. D., MOILANEN, I., ZYLICZ, A., KNUDSEN, J., SANDHOFF, K., ARENZ, C., KINNUNEN, P. K., NYLANDSTED, J. & JAATTELA, M. 2010. Hsp70 stabilizes lysosomes and reverts Niemann-Pick disease-associated lysosomal pathology. *Nature,* 463**,** 549-53.

KISELYOV, K., CHEN, J., RBAIBI, Y., OBERDICK, D., TJON-KON-SANG, S., SHCHEYNIKOV, N., MUALLEM, S. & SOYOMBO, A. 2005. TRP-ML1 is a lysosomal monovalent cation channel that undergoes proteolytic cleavage. *J Biol Chem,* 280**,** 43218-23.

KISHIMOTO, Y., HIRAIWA, M. & O'BRIEN, J. S. 1992. Saposins: structure, function, distribution, and molecular genetics. *J Lipid Res,* 33**,** 1255-67.

KLINGER, M., FREISSMUTH, M. & NANOFF, C. 2002. Adenosine receptors: G protein-mediated signalling and the role of accessory proteins. *Cell Signal,* 14**,** 99-108.

KMA, L. 2014. Plant extracts and plant-derived compounds: promising players in a countermeasure strategy against radiological exposure. *Asian Pac J Cancer Prev,* 15**,** 2405-25.

KO, D. C., GORDON, M. D., JIN, J. Y. & SCOTT, M. P. 2001. Dynamic movements of organelles containing Niemann-Pick C1 protein: NPC1 involvement in late endocytic events. *Mol Biol Cell,* 12**,** 601-14.

KOBAYASHI, T., BEUCHAT, M. H., LINDSAY, M., FRIAS, S., PALMITER, R. D., SAKURABA, H., PARTON, R. G. & GRUENBERG, J. 1999. Late endosomal membranes rich in lysobisphosphatidic acid regulate cholesterol transport. *Nat Cell Biol,* 1**,** 113-8.

KOLTER, T. & SANDHOFF, K. 2005. Principles of lysosomal membrane digestion: stimulation of sphingolipid degradation by sphingolipid activator proteins and anionic lysosomal lipids. *Annu Rev Cell Dev Biol,* 21**,** 81-103.

KUPPERMAN, E., AN, S., OSBORNE, N., WALDRON, S. & STAINIER, D. Y. 2000. A sphingosine-1-phosphate receptor regulates cell migration during vertebrate heart development. *Nature,* 406**,** 192-5.

LACHMANN, R. H., TE VRUCHTE, D., LLOYD-EVANS, E., REINKENSMEIER, G., SILLENCE, D. J., FERNANDEZ-GUILLEN, L., DWEK, R. A., BUTTERS, T. D., COX, T. M. & PLATT, F. M. 2004. Treatment with miglustat reverses the lipid-trafficking defect in Niemann-Pick disease type C. *Neurobiol Dis,* 16**,** 654-8.

LAPAQUETTE, P., BRINGER, M. A. & DARFEUILLE-MICHAUD, A. 2012. Defects in autophagy favour adherent-invasive Escherichia coli persistence within macrophages leading to increased pro-inflammatory response. *Cell Microbiol,* 14**,** 791-807.

LEE, J. Y., COLE, T. B., PALMITER, R. D., SUH, S. W. & KOH, J. Y. 2002. Contribution by synaptic zinc to the gender-disparate plaque formation in human Swedish mutant APP transgenic mice. *Proc Natl Acad Sci U S A,* 99**,** 7705-10.

LI, X., WANG, J., COUTAVAS, E., SHI, H., HAO, Q. & BLOBEL, G. 2016. Structure of human Niemann-Pick C1 protein. *Proc Natl Acad Sci U S A,* 113**,** 8212-7.

LI, Y., CAM, J. & BU, G. 2001. Low-density lipoprotein receptor family: endocytosis and signal transduction. *Mol Neurobiol,* 23**,** 53-67.

LIESCHKE, G. J. & CURRIE, P. D. 2007. Animal models of human disease: zebrafish swim into view. *Nat Rev Genet,* 8**,** 353-67.

LIGHTLE, S., TOSHEVA, R., LEE, A., QUEEN-BAKER, J., BOYANOVSKY, B., SHEDLOFSKY, S. & NIKOLOVA-KARAKASHIAN, M. 2003. Elevation of ceramide in serum lipoproteins during acute phase response in humans and mice: role of serine-palmitoyl transferase. *Arch Biochem Biophys,* 419**,** 120-8.

LIM, J., LEE, H. K., YU, W. & AHMED, S. 2014. Light sheet fluorescence microscopy (LSFM): past, present and future. *Analyst,* 139**,** 4758-68.

LINKE, T., WILKENING, G., LANSMANN, S., MOCZALL, H., BARTELSEN, O., WEISGERBER, J. & SANDHOFF, K. 2001. Stimulation of acid sphingomyelinase activity by lysosomal lipids and sphingolipid activator proteins. *Biol Chem,* 382**,** 283-90.

LIU, A., LOU, H., ZHAO, L. & FAN, P. 2006. Validated LC/MS/MS assay for curcumin and tetrahydrocurcumin in rat plasma and application to pharmacokinetic study of phospholipid complex of curcumin. *J Pharm Biomed Anal,* 40**,** 720-7.

LIU, C. & HERMANN, T. E. 1978. Characterization of ionomycin as a calcium ionophore. *J Biol Chem,* 253**,** 5892-4.

LIU, J., LU, W., REIGADA, D., NGUYEN, J., LATIES, A. M. & MITCHELL, C. H. 2008. Restoration of lysosomal pH in RPE cells from cultured human and ABCA4(-/-) mice: pharmacologic approaches and functional recovery. *Invest Ophthalmol Vis Sci,* 49**,** 772-80.

LIU, Y., WU, Y. P., WADA, R., NEUFELD, E. B., MULLIN, K. A., HOWARD, A. C., PENTCHEV, P. G., VANIER, M. T., SUZUKI, K. & PROIA, R. L. 2000. Alleviation of neuronal ganglioside storage does not improve the clinical course of the Niemann-Pick C disease mouse. *Hum Mol Genet,* 9**,** 1087-92.

LIUZZI, J. P. & COUSINS, R. J. 2004. Mammalian zinc transporters. *Annu Rev Nutr,* 24**,** 151-72.

LIUZZI, J. P., GUO, L., YOO, C. & STEWART, T. S. 2014. Zinc and autophagy. *Biometals,* 27**,** 1087-96.

LLOYD, T. E. & TAYLOR, J. P. 2010. Flightless flies: Drosophila models of neuromuscular disease. *Ann N Y Acad Sci,* 1184**,** e1-20.

LLOYD-EVANS, E., MORGAN, A. J., HE, X., SMITH, D. A., ELLIOT-SMITH, E., SILLENCE, D. J., CHURCHILL, G. C., SCHUCHMAN, E. H., GALIONE, A. & PLATT, F. M. 2008. Niemann-Pick disease type C1 is a sphingosine storage disease that causes deregulation of lysosomal calcium. *Nat Med,* 14**,** 1247-55.

LLOYD-EVANS, E., PELLED, D., RIEBELING, C. & FUTERMAN, A. H. 2003. Lyso-glycosphingolipids mobilize calcium from brain microsomes via multiple mechanisms. *Biochem J,* 375**,** 561-5.

LLOYD-EVANS, E. & PLATT, F. M. 2010. Lipids on trial: the search for the offending metabolite in Niemann-Pick type C disease. *Traffic,* 11**,** 419-28.

LLOYD-EVANS, E., WALLER-EVANS, H., PETERNEVA, K. & PLATT, F. M. 2010. Endolysosomal calcium regulation and disease. *Biochem Soc Trans,* 38**,** 1458-64.

LOFTUS, S. K., ERICKSON, R. P., WALKLEY, S. U., BRYANT, M. A., INCAO, A., HEIDENREICH, R. A. & PAVAN, W. J. 2002. Rescue of neurodegeneration in Niemann-Pick C mice by a prion-promoter-driven Npc1 cDNA transgene. *Hum Mol Genet,* 11**,** 3107-14.

LOMOVSKAYA, O., WARREN, M. S., LEE, A., GALAZZO, J., FRONKO, R., LEE, M., BLAIS, J., CHO, D., CHAMBERLAND, S., RENAU, T., LEGER, R., HECKER, S., WATKINS, W., HOSHINO, K., ISHIDA, H. & LEE, V. J. 2001. Identification and characterization of inhibitors of multidrug resistance efflux pumps in Pseudomonas aeruginosa: novel agents for combination therapy. *Antimicrob Agents Chemother,* 45**,** 105-16.

LOPEZ, M. E., KLEIN, A. D., DIMBIL, U. J. & SCOTT, M. P. 2011. Anatomically defined neuron-based rescue of neurodegenerative Niemann-Pick type C disorder. *J Neurosci,* 31**,** 4367-78.

LOUWETTE, S., REGAL, L., WITTEVRONGEL, C., THYS, C., VANDEWEEGHDE, G., DECUYPER, E., LEEMANS, P., DE VOS, R., VAN GEET, C., JAEKEN, J. & FRESON, K. 2013. NPC1 defect results in abnormal platelet formation and function: studies in Niemann-Pick disease type C1 patients and zebrafish. *Hum Mol Genet,* 22**,** 61-73.

LU, F., LIANG, Q., ABI-MOSLEH, L., DAS, A., DE BRABANDER, J. K., GOLDSTEIN, J. L. & BROWN, M. S. 2015. Identification of NPC1 as the target of U18666A, an inhibitor of lysosomal cholesterol export and Ebola infection. *Elife,* 4.

LUZIO, J. P., BRIGHT, N. A. & PRYOR, P. R. 2007. The role of calcium and other ions in sorting and delivery in the late endocytic pathway. *Biochem Soc Trans,* 35**,** 1088-91.

LYSENG-WILLIAMSON, K. A. 2014. Miglustat: a review of its use in Niemann-Pick disease type C. *Drugs,* 74**,** 61-74.

MAARUP, T. J., CHEN, A. H., PORTER, F. D., FARHAT, N. Y., ORY, D. S., SIDHU, R., JIANG, X. & DICKSON, P. I. 2015. Intrathecal 2-hydroxypropyl-beta-cyclodextrin in a single patient with Niemann-Pick C1. *Mol Genet Metab,* 116**,** 75-9.

MACKIE, A. R., MACIERZANKA, A., AARAK, K., RIGBY, N. M., PARKER, R., CHANNELL, G. A., HARDING, S. E. & BAJKA, B. H. 2016. Sodium alginate decreases the permeability of intestinal mucus. *Food Hydrocoll,* 52**,** 749-755.

MAEKAWA, M., MISAWA, Y., SOTOURA, A., YAMAGUCHI, H., TOGAWA, M., OHNO, K., NITTONO, H., KAKIYAMA, G., IIDA, T., HOFMANN, A. F., GOTO, J., SHIMADA, M. & MANO, N. 2013. LC/ESI-MS/MS analysis of urinary 3beta-sulfooxy-7beta-N-acetylglucosaminyl-5-cholen-24-oic acid and its amides: new biomarkers for the detection of Niemann-Pick type C disease. *Steroids,* 78**,** 967-72.

MAEKAWA, M., SHIMADA, M., OHNO, K., TOGAWA, M., NITTONO, H., IIDA, T., HOFMANN, A. F., GOTO, J., YAMAGUCHI, H. & MANO, N. 2015. Focused metabolomics using liquid chromatography/electrospray ionization tandem mass spectrometry for analysis of urinary conjugated cholesterol metabolites from patients with Niemann-Pick disease type C and 3beta-hydroxysteroid dehydrogenase deficiency. *Ann Clin Biochem,* 52**,** 576-87.

MALAIYANDI, L. M., HONICK, A. S., RINTOUL, G. L., WANG, Q. J. & REYNOLDS, I. J. 2005. Zn2+ inhibits mitochondrial movement in neurons by phosphatidylinositol 3-kinase activation. *J Neurosci,* 25**,** 9507-14.

MALATHI, K., HIGAKI, K., TINKELENBERG, A. H., BALDERES, D. A., ALMANZAR-PARAMIO, D., WILCOX, L. J., ERDENIZ, N., REDICAN, F., PADAMSEE, M., LIU, Y., KHAN, S., ALCANTARA, F., CARSTEA, E. D., MORRIS, J. A. & STURLEY, S. L. 2004. Mutagenesis of the putative sterol-sensing domain of yeast Niemann Pick C-related protein reveals a primordial role in subcellular sphingolipid distribution. *J Cell Biol,* 164**,** 547-56.

MALNAR, M., HECIMOVIC, S., MATTSSON, N. & ZETTERBERG, H. 2014. Bidirectional links between Alzheimer's disease and Niemann-Pick type C disease. *Neurobiol Dis,* 72 Pt A**,** 37-47.

MANZONI, M., MONTI, E., BRESCIANI, R., BOZZATO, A., BARLATI, S., BASSI, M. T. & BORSANI, G. 2004. Overexpression of wild-type and mutant mucolipin proteins in mammalian cells: effects on the late endocytic compartment organization. *FEBS Lett,* 567**,** 219-24.

MARCHANT, J. S. & PATEL, S. 2013. Questioning regulation of two-pore channels by NAADP. *Messenger (Los Angel),* 2**,** 113-119.

MARET, W. & VALLEE, B. L. 1998. Thiolate ligands in metallothionein confer redox activity on zinc clusters. *Proc Natl Acad Sci U S A,* 95**,** 3478-82.

MATSUO, M., TOGAWA, M., HIRABARU, K., MOCHINAGA, S., NARITA, A., ADACHI, M., EGASHIRA, M., IRIE, T. & OHNO, K. 2013. Effects of cyclodextrin in two patients with Niemann-Pick Type C disease. *Mol Genet Metab,* 108**,** 76-81.

MAUE, R. A., BURGESS, R. W., WANG, B., WOOLEY, C. M., SEBURN, K. L., VANIER, M. T., ROGERS, M. A., CHANG, C. C., CHANG, T. Y., HARRIS, B. T., GRABER, D. J., PENATTI, C. A., PORTER, D. M., SZWERGOLD, B. S., HENDERSON, L. P., TOTENHAGEN, J. W., TROUARD, T. P., BORBON, I. A. & ERICKSON, R. P. 2012. A novel mouse model of Niemann-Pick type C disease carrying a D1005G-Npc1 mutation comparable to commonly observed human mutations. *Hum Mol Genet,* 21**,** 730-50.

MAXFIELD, F. R. 2014. Role of endosomes and lysosomes in human disease. *Cold Spring Harb Perspect Biol,* 6**,** a016931.

MAYOR, S. & PAGANO, R. E. 2007. Pathways of clathrin-independent endocytosis. *Nat Rev Mol Cell Biol,* 8**,** 603-12.

MAYRAN, N., PARTON, R. G. & GRUENBERG, J. 2003. Annexin II regulates multivesicular endosome biogenesis in the degradation pathway of animal cells. *Embo j,* 22**,** 3242-53.

MEDINA, D. L. & BALLABIO, A. 2015. Lysosomal calcium regulates autophagy. *Autophagy,* 11**,** 970-1.

MEIKLE, P. J., HOPWOOD, J. J., CLAGUE, A. E. & CAREY, W. F. 1999. Prevalence of lysosomal storage disorders. *Jama,* 281**,** 249-54.

MEKAHLI, D., BULTYNCK, G., PARYS, J. B., DE SMEDT, H. & MISSIAEN, L. 2011. Endoplasmic-reticulum calcium depletion and disease. *Cold Spring Harb Perspect Biol,* 3.

MELLMAN, I. 1996. Endocytosis and molecular sorting. *Annu Rev Cell Dev Biol,* 12**,** 575-625.

MICSENYI, M. C., SIKORA, J., STEPHNEY, G., DOBRENIS, K. & WALKLEY, S. U. 2013. Lysosomal membrane permeability stimulates protein aggregate formation in neurons of a lysosomal disease. *J Neurosci,* 33**,** 10815-27.

MIERSCH, S., ESPEY, M. G., CHAUBE, R., AKARCA, A., TWETEN, R., ANANVORANICH, S. & MUTUS, B. 2008. Plasma membrane cholesterol content affects nitric oxide diffusion dynamics and signaling. *J Biol Chem,* 283**,** 18513-21.

MILLARD, E. E., SRIVASTAVA, K., TRAUB, L. M., SCHAFFER, J. E. & ORY, D. S. 2000. Niemann-pick type C1 (NPC1) overexpression alters cellular cholesterol homeostasis. *J Biol Chem,* 275**,** 38445-51.

MINDELL, J. A. 2012. Lysosomal acidification mechanisms. *Annu Rev Physiol,* 74**,** 69-86.

MIYAKE, Y., KOZUTSUMI, Y., NAKAMURA, S., FUJITA, T. & KAWASAKI, T. 1995. Serine palmitoyltransferase is the primary target of a sphingosine-like immunosuppressant, ISP-1/myriocin. *Biochem Biophys Res Commun,* 211**,** 396-403.

MOCCHEGIANI, E., MALAVOLTA, M., COSTARELLI, L., GIACCONI, R., CIPRIANO, C., PIACENZA, F., TESEI, S., BASSO, A., PIERPAOLI, S. & LATTANZIO, F. 2010. Zinc, metallothioneins and immunosenescence. *Proc Nutr Soc,* 69**,** 290-9.

MOENS, C. B., DONN, T. M., WOLF-SAXON, E. R. & MA, T. P. 2008. Reverse genetics in zebrafish by TILLING. *Brief Funct Genomic Proteomic,* 7**,** 454-9.

MONROY, A., LITHGOW, G. J. & ALAVEZ, S. 2013. Curcumin and neurodegenerative diseases. *Biofactors,* 39**,** 122-32.

MORCOS, P. A., LI, Y. & JIANG, S. 2008. Vivo-Morpholinos: a non-peptide transporter delivers Morpholinos into a wide array of mouse tissues. *Biotechniques,* 45**,** 613-4, 616, 618 passim.

MORGAN, A. J., DAVIS, L. C. & GALIONE, A. 2015a. Imaging approaches to measuring lysosomal calcium. *Methods Cell Biol,* 126**,** 159-95.

MORGAN, A. J., DAVIS, L. C., RUAS, M. & GALIONE, A. 2015b. TPC: the NAADP discovery channel? *Biochem Soc Trans,* 43**,** 384-9.

MUNKACSI, A. B., PORTO, A. F. & STURLEY, S. L. 2007. Niemann-Pick type C disease proteins: orphan transporters or membrane rheostats? *Future Lipidol,* 2**,** 357-367.

NARITA, K., CHOUDHURY, A., DOBRENIS, K., SHARMA, D. K., HOLICKY, E. L., MARKS, D. L., WALKLEY, S. U. & PAGANO, R. E. 2005. Protein transduction of Rab9 in Niemann-Pick C cells reduces cholesterol storage. *Faseb j,* 19**,** 1558-60.

NASRA, M. M., KHIRI, H. M., HAZZAH, H. A. & ABDALLAH, O. Y. 2017. Formulation, in-vitro characterization and clinical evaluation of curcumin in-situ gel for treatment of periodontitis. *Drug Deliv,* 24**,** 133-142.

NAURECKIENE, S., SLEAT, D. E., LACKLAND, H., FENSOM, A., VANIER, M. T., WATTIAUX, R., JADOT, M. & LOBEL, P. 2000. Identification of HE1 as the second gene of Niemann-Pick C disease. *Science,* 290**,** 2298-301.

NAYLOR, E., ARREDOUANI, A., VASUDEVAN, S. R., LEWIS, A. M., PARKESH, R., MIZOTE, A., ROSEN, D., THOMAS, J. M., IZUMI, M., GANESAN, A., GALIONE, A. & CHURCHILL, G. C. 2009. Identification of a chemical probe for NAADP by virtual screening. *Nat Chem Biol,* 5**,** 220-6.

NEISS, W. F. 1984. A coat of glycoconjugates on the inner surface of the lysosomal membrane in the rat kidney. *Histochemistry,* 80**,** 603-8.

NEVILLE, D. C., COQUARD, V., PRIESTMAN, D. A., TE VRUCHTE, D. J., SILLENCE, D. J., DWEK, R. A., PLATT, F. M. & BUTTERS, T. D. 2004. Analysis of fluorescently labeled glycosphingolipid-derived oligosaccharides following ceramide glycanase digestion and anthranilic acid labeling. *Anal Biochem,* 331**,** 275-82.

NICOLI, E. R., AL EISA, N., CLUZEAU, C. V., WASSIF, C. A., GRAY, J., BURKERT, K. R., SMITH, D. A., MORRIS, L., COLOGNA, S. M., PEER, C. J., SISSUNG, T. M., USCATU, C. D., FIGG, W. D., PAVAN, W. J., VITE, C. H., PORTER, F. D. & PLATT, F. M. 2016. Defective Cytochrome P450-Catalysed Drug Metabolism in Niemann-Pick Type C Disease. *PLoS One,* 11**,** e0152007.

NOH, K. M., KIM, Y. H. & KOH, J. Y. 1999. Mediation by membrane protein kinase C of zinc-induced oxidative neuronal injury in mouse cortical cultures. *J Neurochem,* 72**,** 1609-16.

NYLANDSTED, J., GYRD-HANSEN, M., DANIELEWICZ, A., FEHRENBACHER, N., LADEMANN, U., HOYER-HANSEN, M., WEBER, E., MULTHOFF, G., ROHDE, M. & JAATTELA, M. 2004. Heat shock protein 70 promotes cell survival by inhibiting lysosomal membrane permeabilization. *J Exp Med,* 200**,** 425-35.

OTA, S., HISANO, Y., IKAWA, Y. & KAWAHARA, A. 2014. Multiple genome modifications by the CRISPR/Cas9 system in zebrafish. *Genes Cells,* 19**,** 555-64.

PADAMSEY, Z., MCGUINNESS, L., BARDO, S. J., REINHART, M., TONG, R., HEDEGAARD, A., HART, M. L. & EMPTAGE, N. J. 2017. Activity-Dependent Exocytosis of Lysosomes Regulates the Structural Plasticity of Dendritic Spines. *Neuron,* 93**,** 132-146.

PAK, J. E., EKENDE, E. N., KIFLE, E. G., O'CONNELL, J. D., 3RD, DE ANGELIS, F., TESSEMA, M. B., DERFOUFI, K. M., ROBLES-COLMENARES, Y., ROBBINS, R. A., GOORMAGHTIGH, E., VANDENBUSSCHE, G. & STROUD, R. M. 2013. Structures of intermediate transport states of ZneA, a Zn(II)/proton antiporter. *Proc Natl Acad Sci U S A,* 110**,** 18484-9.

PANARITI, A., MISEROCCHI, G. & RIVOLTA, I. 2012. The effect of nanoparticle uptake on cellular behavior: disrupting or enabling functions? *Nanotechnol Sci Appl,* 5**,** 87-100.

PANDEY, U. B. & NICHOLS, C. D. 2011. Human disease models in Drosophila melanogaster and the role of the fly in therapeutic drug discovery. *Pharmacol Rev,* 63**,** 411-36.

PANDEY, V., CHUANG, C. C., LEWIS, A. M., ALEY, P. K., BRAILOIU, E., DUN, N. J., CHURCHILL, G. C. & PATEL, S. 2009. Recruitment of NAADP-sensitive acidic Ca2+ stores by glutamate. *Biochem J,* 422**,** 503-12.

PARK, W. D., O'BRIEN, J. F., LUNDQUIST, P. A., KRAFT, D. L., VOCKLEY, C. W., KARNES, P. S., PATTERSON, M. C. & SNOW, K. 2003. Identification of 58 novel mutations in Niemann-Pick disease type C: correlation with biochemical phenotype and importance of PTC1-like domains in NPC1. *Hum Mutat,* 22**,** 313-25.

PARRA, J., KLEIN, A. D., CASTRO, J., MORALES, M. G., MOSQUEIRA, M., VALENCIA, I., CORTES, V., RIGOTTI, A. & ZANLUNGO, S. 2011. Npc1 deficiency in the C57BL/6J genetic background enhances Niemann-Pick disease type C spleen pathology. *Biochem Biophys Res Commun,* 413**,** 400-6.

PATEL, S. & CAI, X. 2015. Evolution of acidic Ca(2)(+) stores and their resident Ca(2)(+)-permeable channels. *Cell Calcium,* 57**,** 222-30.

PATEL, S., CHURCHILL, G. C., SHARP, T. & GALIONE, A. 2000. Widespread distribution of binding sites for the novel Ca2+-mobilizing messenger, nicotinic acid adenine dinucleotide phosphate, in the brain. *J Biol Chem,* 275**,** 36495-7.

PATEL, S. & DOCAMPO, R. 2010. Acidic calcium stores open for business: expanding the potential for intracellular Ca2+ signaling. *Trends Cell Biol,* 20**,** 277-86.

PATTERSON, M. C., DI BISCEGLIE, A. M., HIGGINS, J. J., ABEL, R. B., SCHIFFMANN, R., PARKER, C. C., ARGOFF, C. E., GREWAL, R. P., YU, K., PENTCHEV, P. G. & ET AL. 1993. The effect of cholesterol-lowering agents on hepatic and plasma cholesterol in Niemann-Pick disease type C. *Neurology,* 43**,** 61-4.

PATTERSON, M. C., HENDRIKSZ, C. J., WALTERFANG, M., SEDEL, F., VANIER, M. T. & WIJBURG, F. 2012. Recommendations for the diagnosis and management of Niemann-Pick disease type C: an update. *Mol Genet Metab,* 106**,** 330-44.

PATTERSON, M. C., VECCHIO, D., PRADY, H., ABEL, L. & WRAITH, J. E. 2007. Miglustat for treatment of Niemann-Pick C disease: a randomised controlled study. *Lancet Neurol,* 6**,** 765-72.

PCHITSKAYA, E., POPUGAEVA, E. & BEZPROZVANNY, I. 2017. Calcium signaling and molecular mechanisms underlying neurodegenerative diseases. *Cell Calcium*.

PENTCHEV, P. G., COMLY, M. E., KRUTH, H. S., VANIER, M. T., WENGER, D. A., PATEL, S. & BRADY, R. O. 1985. A defect in cholesterol esterification in Niemann-Pick disease (type C) patients. *Proc Natl Acad Sci U S A,* 82**,** 8247-51.

PETERSEN, N. H. & KIRKEGAARD, T. 2010. HSP70 and lysosomal storage disorders: novel therapeutic opportunities. *Biochem Soc Trans,* 38**,** 1479-83.

PITT, S. J., FUNNELL, T. M., SITSAPESAN, M., VENTURI, E., RIETDORF, K., RUAS, M., GANESAN, A., GOSAIN, R., CHURCHILL, G. C., ZHU, M. X., PARRINGTON, J., GALIONE, A. & SITSAPESAN, R. 2010. TPC2 is a novel NAADP-sensitive Ca2+ release channel, operating as a dual sensor of luminal pH and Ca2+. *J Biol Chem,* 285**,** 35039-46.

PITT, S. J., LAM, A. K., RIETDORF, K., GALIONE, A. & SITSAPESAN, R. 2014. Reconstituted human TPC1 is a proton-permeable ion channel and is activated by NAADP or Ca2+. *Sci Signal,* 7**,** ra46.

PITT, S. J., REILLY-O'DONNELL, B. & SITSAPESAN, R. 2016. Exploring the biophysical evidence that mammalian two-pore channels are NAADP-activated calcium-permeable channels. *J Physiol,* 594**,** 4171-9.

PIZZO, P., LISSANDRON, V., CAPITANIO, P. & POZZAN, T. 2011. Ca(2+) signalling in the Golgi apparatus. *Cell Calcium,* 50**,** 184-92.

PLATT, F. M., NEISES, G. R., DWEK, R. A. & BUTTERS, T. D. 1994. N-butyldeoxynojirimycin is a novel inhibitor of glycolipid biosynthesis. *J Biol Chem,* 269**,** 8362-5.

PONTIKIS, C. C., DAVIDSON, C. D., WALKLEY, S. U., PLATT, F. M. & BEGLEY, D. J. 2013. Cyclodextrin alleviates neuronal storage of cholesterol in Niemann-Pick C disease without evidence of detectable blood-brain barrier permeability. *J Inherit Metab Dis,* 36**,** 491-8.

PORTER, F. D., SCHERRER, D. E., LANIER, M. H., LANGMADE, S. J., MOLUGU, V., GALE, S. E., OLZESKI, D., SIDHU, R., DIETZEN, D. J., FU, R., WASSIF, C. A., YANJANIN, N. M., MARSO, S. P., HOUSE, J., VITE, C., SCHAFFER, J. E. & ORY, D. S. 2010. Cholesterol oxidation products are sensitive and specific blood-based biomarkers for Niemann-Pick C1 disease. *Sci Transl Med,* 2**,** 56ra81.

POTERYAEV, D., DATTA, S., ACKEMA, K., ZERIAL, M. & SPANG, A. 2010. Identification of the switch in early-to-late endosome transition. *Cell,* 141**,** 497-508.

PRAKASH, A., BHARTI, K. & MAJEED, A. B. 2015. Zinc: indications in brain disorders. *Fundam Clin Pharmacol,* 29**,** 131-49.

PRASAD, S., TYAGI, A. K. & AGGARWAL, B. B. 2014. Recent developments in delivery, bioavailability, absorption and metabolism of curcumin: the golden pigment from golden spice. *Cancer Res Treat,* 46**,** 2-18.

PRYOR, P. R., MULLOCK, B. M., BRIGHT, N. A., GRAY, S. R. & LUZIO, J. P. 2000. The role of intraorganellar Ca(2+) in late endosome-lysosome heterotypic fusion and in the reformation of lysosomes from hybrid organelles. *J Cell Biol,* 149**,** 1053-62.

PUERTOLLANO, R. & KISELYOV, K. 2009. TRPMLs: in sickness and in health. *Am J Physiol Renal Physiol,* 296**,** F1245-54.

PURI, V., WATANABE, R., DOMINGUEZ, M., SUN, X., WHEATLEY, C. L., MARKS, D. L. & PAGANO, R. E. 1999. Cholesterol modulates membrane traffic along the endocytic pathway in sphingolipid-storage diseases. *Nat Cell Biol,* 1**,** 386-8.

PURI, V., WATANABE, R., SINGH, R. D., DOMINGUEZ, M., BROWN, J. C., WHEATLEY, C. L., MARKS, D. L. & PAGANO, R. E. 2001. Clathrin-dependent and -independent internalization of plasma membrane sphingolipids initiates two Golgi targeting pathways. *J Cell Biol,* 154**,** 535-47.

QI, H. & SHUAI, J. 2016. Alzheimer's disease via enhanced calcium signaling caused by the decrease of endoplasmic reticulum-mitochondrial distance. *Med Hypotheses,* 89**,** 28-31.

REAGAN, J. W., JR., HUBBERT, M. L. & SHELNESS, G. S. 2000. Posttranslational regulation of acid sphingomyelinase in niemann-pick type C1 fibroblasts and free cholesterol-enriched chinese hamster ovary cells. *J Biol Chem,* 275**,** 38104-10.

REDDY, J. V., GANLEY, I. G. & PFEFFER, S. R. 2006. Clues to neuro-degeneration in Niemann-Pick type C disease from global gene expression profiling. *PLoS One,* 1**,** e19.

REITER, L. T., POTOCKI, L., CHIEN, S., GRIBSKOV, M. & BIER, E. 2001. A systematic analysis of human disease-associated gene sequences in Drosophila melanogaster. *Genome Res,* 11**,** 1114-25.

RENAU, T. E., LEGER, R., FLAMME, E. M., SANGALANG, J., SHE, M. W., YEN, R., GANNON, C. L., GRIFFITH, D., CHAMBERLAND, S., LOMOVSKAYA, O., HECKER, S. J., LEE, V. J., OHTA, T. & NAKAYAMA, K. 1999. Inhibitors of efflux pumps in Pseudomonas aeruginosa potentiate the activity of the fluoroquinolone antibacterial levofloxacin. *J Med Chem,* 42**,** 4928-31.

RIKKE, B. A., MURAKAMI, S. & JOHNSON, T. E. 2000. Paralogy and orthology of tyrosine kinases that can extend the life span of Caenorhabditis elegans. *Mol Biol Evol,* 17**,** 671-83.

RIZZUTO, R., DE STEFANI, D., RAFFAELLO, A. & MAMMUCARI, C. 2012. Mitochondria as sensors and regulators of calcium signalling. *Nat Rev Mol Cell Biol,* 13**,** 566-78.

RODRIGUEZ, A., WEBSTER, P., ORTEGO, J. & ANDREWS, N. W. 1997. Lysosomes behave as Ca2+-regulated exocytic vesicles in fibroblasts and epithelial cells. *J Cell Biol,* 137**,** 93-104.

RODRIGUEZ-LAFRASSE, C., ROUSSON, R., VALLA, S., ANTIGNAC, P., LOUISOT, P. & VANIER, M. T. 1997. Modulation of protein kinase C by endogenous sphingosine: inhibition of phorbol dibutyrate binding in Niemann-Pick C fibroblasts. *Biochem J,* 325 (Pt 3)**,** 787-91.

ROFF, C. F., GOLDIN, E., COMLY, M. E., COONEY, A., BROWN, A., VANIER, M. T., MILLER, S. P., BRADY, R. O. & PENTCHEV, P. G. 1991. Type C Niemann-Pick disease: use of hydrophobic amines to study defective cholesterol transport. *Dev Neurosci,* 13**,** 315-9.

RUSHTON, D. J., MATTIS, V. B., SVENDSEN, C. N., ALLEN, N. D. & KEMP, P. J. 2013. Stimulation of GABA-induced Ca2+ influx enhances maturation of human induced pluripotent stem cell-derived neurons. *PLoS One,* 8**,** e81031.

SAGER, J. J., BAI, Q. & BURTON, E. A. 2010. Transgenic zebrafish models of neurodegenerative diseases. *Brain Struct Funct,* 214**,** 285-302.

SALVIOLI, R., SCARPA, S., CIAFFONI, F., TATTI, M., RAMONI, C., VANIER, M. T. & VACCARO, A. M. 2004. Glucosylceramidase mass and subcellular localization are modulated by cholesterol in Niemann-Pick disease type C. *J Biol Chem,* 279**,** 17674-80.

SANDER, J. D., CADE, L., KHAYTER, C., REYON, D., PETERSON, R. T., JOUNG, J. K. & YEH, J. R. 2011. Targeted gene disruption in somatic zebrafish cells using engineered TALENs. *Nat Biotechnol.* United States.

SANDHOFF, K. & HARZER, K. 2013. Gangliosides and gangliosidoses: principles of molecular and metabolic pathogenesis. *J Neurosci,* 33**,** 10195-208.

SARKAR, S., CARROLL, B., BUGANIM, Y., MAETZEL, D., NG, A. H., CASSADY, J. P., COHEN, M. A., CHAKRABORTY, S., WANG, H., SPOONER, E., PLOEGH, H., GSPONER, J., KOROLCHUK, V. I. & JAENISCH, R. 2013. Impaired autophagy in the lipid-storage disorder Niemann-Pick type C1 disease. *Cell Rep,* 5**,** 1302-15.

SCHIEDER, M., ROTZER, K., BRUGGEMANN, A., BIEL, M. & WAHL-SCHOTT, C. A. 2010. Characterization of two-pore channel 2 (TPCN2)-mediated Ca2+ currents in isolated lysosomes. *J Biol Chem,* 285**,** 21219-22.

SCHUCHMAN, E. H. & WASSERSTEIN, M. P. 2016. Types A and B Niemann-Pick Disease. *Pediatr Endocrinol Rev,* 13 Suppl 1**,** 674-81.

SCHULZ, T. A. & PRINZ, W. A. 2007. Sterol transport in yeast and the oxysterol binding protein homologue (OSH) family. *Biochim Biophys Acta,* 1771**,** 769-80.

SCHUMACHER, A., STEINKE, P., BOHNERT, J. A., AKOVA, M., JONAS, D. & KERN, W. V. 2006. Effect of 1-(1-naphthylmethyl)-piperazine, a novel putative efflux pump inhibitor, on antimicrobial drug susceptibility in clinical isolates of Enterobacteriaceae other than Escherichia coli. *J Antimicrob Chemother,* 57**,** 344-8.

SCHWEND, T., LOUCKS, E. J., SNYDER, D. & AHLGREN, S. C. 2011. Requirement of Npc1 and availability of cholesterol for early embryonic cell movements in zebrafish. *J Lipid Res,* 52**,** 1328-44.

SCHWERD, T., PANDEY, S., YANG, H. T., BAGOLA, K., JAMESON, E., JUNG, J., LACHMANN, R. H., SHAH, N., PATEL, S. Y., BOOTH, C., RUNZ, H., DUKER, G., BETTELS, R., ROHRBACH, M., KUGATHASAN, S., CHAPEL, H., KESHAV, S., ELKADRI, A., PLATT, N., MUISE, A. M., KOLETZKO, S., XAVIER, R. J., MARQUARDT, T., POWRIE, F., WRAITH, J. E., GYRD-HANSEN, M., PLATT, F. M. & UHLIG, H. H. 2016. Impaired antibacterial autophagy links granulomatous intestinal inflammation in Niemann-Pick disease type C1 and XIAP deficiency with NOD2 variants in Crohn's disease. *Gut*.

SCOTT, C. & IOANNOU, Y. A. 2004. The NPC1 protein: structure implies function. *Biochim Biophys Acta,* 1685**,** 8-13.

SCRIVER, C. R. 1995. *The metabolic and molecular bases of inherited disease*, McGraw-Hill, Health Professions Division.

SENSI, S. L., TON-THAT, D., WEISS, J. H., ROTHE, A. & GEE, K. R. 2003. A new mitochondrial fluorescent zinc sensor. *Cell Calcium,* 34**,** 281-4.

SENSI, S. L., YIN, H. Z., CARRIEDO, S. G., RAO, S. S. & WEISS, J. H. 1999. Preferential Zn2+ influx through Ca2+-permeable AMPA/kainate channels triggers prolonged mitochondrial superoxide production. *Proc Natl Acad Sci U S A,* 96**,** 2414-9.

SENSI, S. L., YIN, H. Z. & WEISS, J. H. 2000. AMPA/kainate receptor-triggered Zn2+ entry into cortical neurons induces mitochondrial Zn2+ uptake and persistent mitochondrial dysfunction. *Eur J Neurosci,* 12**,** 3813-8.

SEVIN, M., LESCA, G., BAUMANN, N., MILLAT, G., LYON-CAEN, O., VANIER, M. T. & SEDEL, F. 2007. The adult form of Niemann-Pick disease type C. *Brain,* 130**,** 120-33.

SHABBIR, A., SHAHZAD, M., MASCI, P. & GOBE, G. C. 2014. Protective activity of medicinal plants and their isolated compounds against the toxic effects from the venom of Naja (cobra) species. *J Ethnopharmacol,* 157**,** 222-7.

SHACHAR, T., LO BIANCO, C., RECCHIA, A., WIESSNER, C., RAAS-ROTHSCHILD, A. & FUTERMAN, A. H. 2011. Lysosomal storage disorders and Parkinson's disease: Gaucher disease and beyond. *Mov Disord,* 26**,** 1593-604.

SHANMUGAM, M. K., RANE, G., KANCHI, M. M., ARFUSO, F., CHINNATHAMBI, A., ZAYED, M. E., ALHARBI, S. A., TAN, B. K., KUMAR, A. P. & SETHI, G. 2015. The multifaceted role of curcumin in cancer prevention and treatment. *Molecules,* 20**,** 2728-69.

SHARMA, D. K., BROWN, J. C., CHOUDHURY, A., PETERSON, T. E., HOLICKY, E., MARKS, D. L., SIMARI, R., PARTON, R. G. & PAGANO, R. E. 2004. Selective stimulation of caveolar endocytosis by glycosphingolipids and cholesterol. *Mol Biol Cell,* 15**,** 3114-22.

SHELINE, C. T., ZHU, J., ZHANG, W., SHI, C. & CAI, A. L. 2013. Mitochondrial inhibitor models of Huntington's disease and Parkinson's disease induce zinc accumulation and are attenuated by inhibition of zinc neurotoxicity in vitro or in vivo. *Neurodegener Dis,* 11**,** 49-58.

SHEN, D., WANG, X., LI, X., ZHANG, X., YAO, Z., DIBBLE, S., DONG, X. P., YU, T., LIEBERMAN, A. P., SHOWALTER, H. D. & XU, H. 2012. Lipid storage disorders block lysosomal trafficking by inhibiting a TRP channel and lysosomal calcium release. *Nat Commun,* 3**,** 731.

SHOBA, G., JOY, D., JOSEPH, T., MAJEED, M., RAJENDRAN, R. & SRINIVAS, P. S. 1998. Influence of piperine on the pharmacokinetics of curcumin in animals and human volunteers. *Planta Med,* 64**,** 353-6.

SINGH, R. D., LIU, Y., WHEATLEY, C. L., HOLICKY, E. L., MAKINO, A., MARKS, D. L., KOBAYASHI, T., SUBRAMANIAM, G., BITTMAN, R. & PAGANO, R. E. 2006. Caveolar endocytosis and microdomain association of a glycosphingolipid analog is dependent on its sphingosine stereochemistry. *J Biol Chem,* 281**,** 30660-8.

SINGH, R. D., PURI, V., VALIYAVEETTIL, J. T., MARKS, D. L., BITTMAN, R. & PAGANO, R. E. 2003. Selective caveolin-1-dependent endocytosis of glycosphingolipids. *Mol Biol Cell,* 14**,** 3254-65.

SLEAT, D. E., WISEMAN, J. A., EL-BANNA, M., PRICE, S. M., VEROT, L., SHEN, M. M., TINT, G. S., VANIER, M. T., WALKLEY, S. U. & LOBEL, P. 2004. Genetic evidence for nonredundant functional cooperativity between NPC1 and NPC2 in lipid transport. *Proc Natl Acad Sci U S A,* 101**,** 5886-91.

SNITSAREV, V., BUDDE, T., STRICKER, T. P., COX, J. M., KRUPA, D. J., GENG, L. & KAY, A. R. 2001. Fluorescent detection of Zn(2+)-rich vesicles with Zinquin: mechanism of action in lipid environments. *Biophys J,* 80**,** 1538-46.

SOMERS, K. L., BROWN, D. E., FULTON, R., SCHULTHEISS, P. C., HAMAR, D., SMITH, M. O., ALLISON, R., CONNALLY, H. E., JUST, C., MITCHELL, T. W., WENGER, D. A. & THRALL, M. A. 2001. Effects of dietary cholesterol restriction in a feline model of Niemann-Pick type C disease. *J Inherit Metab Dis,* 24**,** 427-36.

SPIEGEL, R., RAAS-ROTHSCHILD, A., REISH, O., REGEV, M., MEINER, V., BARGAL, R., SURY, V., MEIR, K., NADJARI, M., HERMANN, G., IANCU, T. C., SHALEV, S. A. & ZEIGLER, M. 2009. The clinical spectrum of fetal Niemann-Pick type C. *Am J Med Genet A,* 149a**,** 446-50.

STADTMAN, E. R. Oxidation of proteins by mixed-function oxidation systems: implication in protein turnover, ageing and neutrophil function. *Trends in Biochemical Sciences,* 11**,** 11-12.

STEIN, V. M., CROOKS, A., DING, W., PROCIUK, M., O'DONNELL, P., BRYAN, C., SIKORA, T., DINGEMANSE, J., VANIER, M. T., WALKLEY, S. U. & VITE, C. H. 2012. Miglustat improves purkinje cell survival and alters microglial phenotype in feline Niemann-Pick disease type C. *J Neuropathol Exp Neurol,* 71**,** 434-48.

STEVEN, L. C. & DRIVER, C. P. 2005. Niemann-pick disease type C and Crohn's disease. *Scott Med J,* 50**,** 80-1.

STORK, T., ENGELEN, D., KRUDEWIG, A., SILIES, M., BAINTON, R. J. & KLAMBT, C. 2008. Organization and function of the blood-brain barrier in Drosophila. *J Neurosci,* 28**,** 587-97.

STREHLER, E. E. 2015. Plasma membrane calcium ATPases: From generic Ca(2+) sump pumps to versatile systems for fine-tuning cellular Ca(2.). *Biochem Biophys Res Commun,* 460**,** 26-33.

STRUPP, M., TEUFEL, J., HABS, M., FEUERECKER, R., MUTH, C., VAN DE WARRENBURG, B. P., KLOPSTOCK, T. & FEIL, K. 2013. Effects of acetyl-DL-leucine in patients with cerebellar ataxia: a case series. *J Neurol,* 260**,** 2556-61.

SUN, X., MARKS, D. L., PARK, W. D., WHEATLEY, C. L., PURI, V., O'BRIEN, J. F., KRAFT, D. L., LUNDQUIST, P. A., PATTERSON, M. C., PAGANO, R. E. & SNOW, K. 2001. Niemann-Pick C variant detection by altered sphingolipid trafficking and correlation with mutations within a specific domain of NPC1. *Am J Hum Genet,* 68**,** 1361-72.

SUZUKI, J., KANEMARU, K., ISHII, K., OHKURA, M., OKUBO, Y. & IINO, M. 2014. Imaging intraorganellar Ca2+ at subcellular resolution using CEPIA. *Nat Commun,* 5**,** 4153.

SVAHN, A. J., GRAEBER, M. B., ELLETT, F., LIESCHKE, G. J., RINKWITZ, S., BENNETT, M. R. & BECKER, T. S. 2013. Development of ramified microglia from early macrophages in the zebrafish optic tectum. *Dev Neurobiol,* 73**,** 60-71.

SVENNERHOLM, L. 1976. Interaction of cholera toxin and ganglioside G(M1). *Adv Exp Med Biol,* 71**,** 191-204.

SYM, M., BASSON, M. & JOHNSON, C. 2000. A model for niemann-pick type C disease in the nematode Caenorhabditis elegans. *Curr Biol,* 10**,** 527-30.

TAKEDA, A. 2000. Movement of zinc and its functional significance in the brain. *Brain Res Brain Res Rev,* 34**,** 137-48.

TAMURA, H., TAKAHASHI, T., BAN, N., TORISU, H., NINOMIYA, H., TAKADA, G. & INAGAKI, N. 2006. Niemann-Pick type C disease: novel NPC1 mutations and characterization of the concomitant acid sphingomyelinase deficiency. *Mol Genet Metab,* 87**,** 113-21.

TAPPER, H. & SUNDLER, R. 1990. Role of lysosomal and cytosolic pH in the regulation of macrophage lysosomal enzyme secretion. *Biochem J,* 272**,** 407-14.

TE VRUCHTE, D., LLOYD-EVANS, E., VELDMAN, R. J., NEVILLE, D. C., DWEK, R. A., PLATT, F. M., VAN BLITTERSWIJK, W. J. & SILLENCE, D. J. 2004. Accumulation of glycosphingolipids in Niemann-Pick C disease disrupts endosomal transport. *J Biol Chem,* 279**,** 26167-75.

TERRY, R. D. & KATZMAN, R. 1983. Senile dementia of the Alzheimer type. *Ann Neurol,* 14**,** 497-506.

THEMAN, T. A. & COLLINS, M. T. 2009. The role of the calcium-sensing receptor in bone biology and pathophysiology. *Curr Pharm Biotechnol,* 10**,** 289-301.

TIKU, M. L., GUPTA, S. & DESHMUKH, D. R. 1999. Aggrecan degradation in chondrocytes is mediated by reactive oxygen species and protected by antioxidants. *Free Radic Res,* 30**,** 395-405.

TSAI, Y. M., CHIEN, C. F., LIN, L. C. & TSAI, T. H. 2011. Curcumin and its nano-formulation: the kinetics of tissue distribution and blood-brain barrier penetration. *Int J Pharm,* 416**,** 331-8.

TSENG, T. T., GRATWICK, K. S., KOLLMAN, J., PARK, D., NIES, D. H., GOFFEAU, A. & SAIER, M. H., JR. 1999. The RND permease superfamily: an ancient, ubiquitous and diverse family that includes human disease and development proteins. *J Mol Microbiol Biotechnol,* 1**,** 107-25.

TU, H., NELSON, O., BEZPROZVANNY, A., WANG, Z., LEE, S. F., HAO, Y. H., SERNEELS, L., DE STROOPER, B., YU, G. & BEZPROZVANNY, I. 2006. Presenilins form ER Ca2+ leak channels, a function disrupted by familial Alzheimer's disease-linked mutations. *Cell,* 126**,** 981-93.

URNOV, F. D., MILLER, J. C., LEE, Y. L., BEAUSEJOUR, C. M., ROCK, J. M., AUGUSTUS, S., JAMIESON, A. C., PORTEUS, M. H., GREGORY, P. D. & HOLMES, M. C. 2005. Highly efficient endogenous human gene correction using designed zinc-finger nucleases. *Nature,* 435**,** 646-51.

VALLEE, B. L. 1995. The function of metallothionein. *Neurochem Int,* 27**,** 23-33.

VALLEE, B. L. & FALCHUK, K. H. 1993. The biochemical basis of zinc physiology. *Physiol Rev,* 73**,** 79-118.

VANIER, M. T., RODRIGUEZ-LAFRASSE, C., ROUSSON, R., DUTHEL, S., HARZER, K., PENTCHEV, P. G., REVOL, A. & LOUISOT, P. 1991. Type C Niemann-Pick disease: biochemical aspects and phenotypic heterogeneity. *Dev Neurosci,* 13**,** 307-14.

VASSALLE, M. & LIN, C. I. 2004. Calcium overload and cardiac function. *J Biomed Sci,* 11**,** 542-65.

VAZQUEZ, M. C., DEL POZO, T., ROBLEDO, F. A., CARRASCO, G., PAVEZ, L., OLIVARES, F., GONZALEZ, M. & ZANLUNGO, S. 2011. Alteration of gene expression profile in Niemann-Pick type C mice correlates with tissue damage and oxidative stress. *PLoS One,* 6**,** e28777.

VAZQUEZ, M. C., MARTINEZ, P., ALVAREZ, A. R., GONZALEZ, M. & ZANLUNGO, S. 2012. Increased copper levels in in vitro and in vivo models of Niemann-Pick C disease. *Biometals,* 25**,** 777-86.

VENKATACHALAM, K., HOFMANN, T. & MONTELL, C. 2006. Lysosomal localization of TRPML3 depends on TRPML2 and the mucolipidosis-associated protein TRPML1. *J Biol Chem,* 281**,** 17517-27.

VETTORI, A., BERGAMIN, G., MORO, E., VAZZA, G., POLO, G., TISO, N., ARGENTON, F. & MOSTACCIUOLO, M. L. 2011. Developmental defects and neuromuscular alterations due to mitofusin 2 gene (MFN2) silencing in zebrafish: a new model for Charcot-Marie-Tooth type 2A neuropathy. *Neuromuscul Disord,* 21**,** 58-67.

VIBERT, N. & VIDAL, P. P. 2001. In vitro effects of acetyl-DL-leucine (tanganil) on central vestibular neurons and vestibulo-ocular networks of the guinea-pig. *Eur J Neurosci,* 13**,** 735-48.

VISENTIN, S., DE NUCCIO, C., BERNARDO, A., PEPPONI, R., FERRANTE, A., MINGHETTI, L. & POPOLI, P. 2013. The stimulation of adenosine A2A receptors ameliorates the pathological phenotype of fibroblasts from Niemann-Pick type C patients. *J Neurosci,* 33**,** 15388-93.

VITE, C. H., BAGEL, J. H., SWAIN, G. P., PROCIUK, M., SIKORA, T. U., STEIN, V. M., O'DONNELL, P., RUANE, T., WARD, S., CROOKS, A., LI, S., MAULDIN, E., STELLAR, S., DE MEULDER, M., KAO, M. L., ORY, D. S., DAVIDSON, C., VANIER, M. T. & WALKLEY, S. U. 2015. Intracisternal cyclodextrin prevents cerebellar dysfunction and Purkinje cell death in feline Niemann-Pick type C1 disease. *Sci Transl Med,* 7**,** 276ra26.

VITNER, E. B., PLATT, F. M. & FUTERMAN, A. H. 2010. Common and uncommon pathogenic cascades in lysosomal storage diseases. *J Biol Chem,* 285**,** 20423-7.

VOCKLEY, C.W. 2009. *FYI – Thinking about Experimental Therapies*, NNPDF,4th September 2017, http://nnpdf.org/issues-regarding-curcumin-therapy-for-npc/

VOLAK, L. P., GHIRMAI, S., CASHMAN, J. R. & COURT, M. H. 2008. Curcuminoids inhibit multiple human cytochromes P450, UDP-glucuronosyltransferase, and sulfotransferase enzymes, whereas piperine is a relatively selective CYP3A4 inhibitor. *Drug Metab Dispos,* 36**,** 1594-605.

WACHTER, R. M., ELSLIGER, M. A., KALLIO, K., HANSON, G. T. & REMINGTON, S. J. 1998. Structural basis of spectral shifts in the yellow-emission variants of green fluorescent protein. *Structure,* 6**,** 1267-77.

WAGER, K. & RUSSELL, C. 2013. Mitophagy and neurodegeneration: the zebrafish model system. *Autophagy,* 9**,** 1693-709.

WALKLEY, S. U. & SUZUKI, K. 2004. Consequences of NPC1 and NPC2 loss of function in mammalian neurons. *Biochim Biophys Acta,* 1685**,** 48-62.

WALTER, M., CHEN, F. W., TAMARI, F., WANG, R. & IOANNOU, Y. A. 2009. Endosomal lipid accumulation in NPC1 leads to inhibition of PKC, hypophosphorylation of vimentin and Rab9 entrapment. *Biol Cell,* 101**,** 141-52.

WANG, Z., TYMIANSKI, M., JONES, O. T. & NEDERGAARD, M. 1997. Impact of cytoplasmic calcium buffering on the spatial and temporal characteristics of intercellular calcium signals in astrocytes. *J Neurosci,* 17**,** 7359-71.

WARD, D. T., MUGHAL, M. Z., RANIERI, M., DVORAK-EWELL, M. M., VALENTI, G. & RICCARDI, D. 2013. Molecular and clinical analysis of a neonatal severe hyperparathyroidism case caused by a stop mutation in the calcium-sensing receptor extracellular domain representing in effect a human 'knockout'. *Eur J Endocrinol,* 169**,** K1-7.

WARD, S., O'DONNELL, P., FERNANDEZ, S. & VITE, C. H. 2010. 2-hydroxypropyl-beta-cyclodextrin raises hearing threshold in normal cats and in cats with Niemann-Pick type C disease. *Pediatr Res,* 68**,** 52-6.

WASSIF, C. A., CROSS, J. L., IBEN, J., SANCHEZ-PULIDO, L., COUGNOUX, A., PLATT, F. M., ORY, D. S., PONTING, C. P., BAILEY-WILSON, J. E., BIESECKER, L. G. & PORTER, F. D. 2016. High incidence of unrecognized visceral/neurological late-onset Niemann-Pick disease, type C1, predicted by analysis of massively parallel sequencing data sets. *Genet Med,* 18**,** 41-8.

WASSIF, C. A., VIED, D., TSOKOS, M., CONNOR, W. E., STEINER, R. D. & PORTER, F. D. 2002. Cholesterol storage defect in RSH/Smith-Lemli-Opitz syndrome fibroblasts. *Mol Genet Metab,* 75**,** 325-34.

WATARI, H., BLANCHETTE-MACKIE, E. J., DWYER, N. K., WATARI, M., BURD, C. G., PATEL, S., PENTCHEV, P. G. & STRAUSS, J. F., 3RD 2000. Determinants of NPC1 expression and action: key promoter regions, posttranscriptional control, and the importance of a "cysteine-rich" loop. *Exp Cell Res,* 259**,** 247-56.

WEBER, J. M., BRICHON, G., BODENNEC, J. & ZWINGELSTEIN, G. 2002. Palmitate and oleate metabolism of rainbow trout in vivo. *Comp Biochem Physiol A Mol Integr Physiol,* 131**,** 409-16.

WERNEBURG, N. W., GUICCIARDI, M. E., BRONK, S. F. & GORES, G. J. 2002. Tumor necrosis factor-alpha-associated lysosomal permeabilization is cathepsin B dependent. *Am J Physiol Gastrointest Liver Physiol,* 283**,** G947-56.

WILLIAMS, I. M., WALLOM, K. L., SMITH, D. A., AL EISA, N., SMITH, C. & PLATT, F. M. 2014. Improved neuroprotection using miglustat, curcumin and ibuprofen as a triple combination therapy in Niemann-Pick disease type C1 mice. *Neurobiol Dis,* 67**,** 9-17.

WISEMAN, H. & HALLIWELL, B. 1996. Damage to DNA by reactive oxygen and nitrogen species: role in inflammatory disease and progression to cancer. *Biochem J,* 313 (Pt 1)**,** 17-29.

XI, Y., NOBLE, S. & EKKER, M. 2011. Modeling neurodegeneration in zebrafish. *Curr Neurol Neurosci Rep,* 11**,** 274-82.

XU, J., TOOPS, K. A., DIAZ, F., CARVAJAL-GONZALEZ, J. M., GRAVOTTA, D., MAZZONI, F., SCHREINER, R., RODRIGUEZ-BOULAN, E. & LAKKARAJU, A. 2012a. Mechanism of polarized lysosome exocytosis in epithelial cells. *J Cell Sci,* 125**,** 5937-43.

XU, M., LIU, K., SWAROOP, M., PORTER, F. D., SIDHU, R., FIRNKES, S., ORY, D. S., MARUGAN, J. J., XIAO, J., SOUTHALL, N., PAVAN, W. J., DAVIDSON, C., WALKLEY, S. U., REMALEY, A. T., BAXA, U., SUN, W., MCKEW, J. C., AUSTIN, C. P. & ZHENG, W. 2012b. delta-Tocopherol reduces lipid accumulation in Niemann-Pick type C1 and Wolman cholesterol storage disorders. *J Biol Chem,* 287**,** 39349-60.

XU, M., LIU, K., SWAROOP, M., SUN, W., DEHDASHTI, S. J., MCKEW, J. C. & ZHENG, W. 2014. A phenotypic compound screening assay for lysosomal storage diseases. *J Biomol Screen,* 19**,** 168-75.

XU, X., YUAN, X., LI, N., DEWEY, W. L., LI, P. L. & ZHANG, F. 2016. Lysosomal cholesterol accumulation in macrophages leading to coronary atherosclerosis in CD38(-/-) mice. *J Cell Mol Med,* 20**,** 1001-13.

YAMAMOTO, T., TOKORO, T. & ETO, Y. 1994. The attenuated elevation of cytoplasmic calcium concentration following the uptake of low density lipoprotein in type C Niemann-Pick fibroblasts. *Biochem Biophys Res Commun,* 198**,** 438-44.

YAMAZAKI, T., CHANG, T. Y., HAASS, C. & IHARA, Y. 2001. Accumulation and aggregation of amyloid beta-protein in late endosomes of Niemann-pick type C cells. *J Biol Chem,* 276**,** 4454-60.

YANG, Z., LIU, N. & LIN, S. 2001. A zebrafish forebrain-specific zinc finger gene can induce ectopic dlx2 and dlx6 expression. *Dev Biol,* 231**,** 138-48.

YANO, S., BROWN, E. M. & CHATTOPADHYAY, N. 2004. Calcium-sensing receptor in the brain. *Cell Calcium,* 35**,** 257-64.

YAZAKI, I., TSURUGAYA, T., SANTELLA, L., CHUN, J. T., AMORE, G., KUSUNOKI, S., ASADA, A., TOGO, T. & AKASAKA, K. 2015. Ca(2)(+) influx-linked protein kinase C activity regulates the beta-catenin localization, micromere induction signalling and the oral-aboral axis formation in early sea urchin embryos. *Zygote,* 23**,** 426-46.

YERUSHALMI, B., SOKOL, R. J., NARKEWICZ, M. R., SMITH, D., ASHMEAD, J. W. & WENGER, D. A. 2002. Niemann-pick disease type C in neonatal cholestasis at a North American Center. *J Pediatr Gastroenterol Nutr,* 35**,** 44-50.

YOSHIDA, M. & MACKLIN, W. B. 2005. Oligodendrocyte development and myelination in GFP-transgenic zebrafish. *J Neurosci Res,* 81**,** 1-8.

ZEIDAN, Y. H. & HANNUN, Y. A. 2007. Activation of acid sphingomyelinase by protein kinase Cdelta-mediated phosphorylation. *J Biol Chem,* 282**,** 11549-61.

ZERVAS, M., SOMERS, K. L., THRALL, M. A. & WALKLEY, S. U. 2001. Critical role for glycosphingolipids in Niemann-Pick disease type C. *Curr Biol,* 11**,** 1283-7.

ZIDOVETZKI, R. & LEVITAN, I. 2007. Use of cyclodextrins to manipulate plasma membrane cholesterol content: evidence, misconceptions and control strategies. *Biochim Biophys Acta,* 1768**,** 1311-24.

ZONG, X., SCHIEDER, M., CUNY, H., FENSKE, S., GRUNER, C., ROTZER, K., GRIESBECK, O., HARZ, H., BIEL, M. & WAHL-SCHOTT, C. 2009. The two-pore channel TPCN2 mediates NAADP-dependent Ca(2+)-release from lysosomal stores. *Pflugers Arch,* 458**,** 891-9.